Purification of neuronal macromolecular complexes in the nematode *Caenorhabditis elegans*

Dissertation

zur Erlangung des Doktorgrades

der Naturwissenschaften

vorgelegt beim Fachbereich Biochemie, Chemie und Pharmazie

der Johann Wolfgang Goethe-Universität

in Frankfurt am Main

von

Florian Csintalan

aus Frankfurt am Main

Erklärung

Ich erkläre hiermit, dass ich mich bisher keiner Doktorprüfung unterzogen habe.

Lörrach, den ....

(Florian Csintalan)

Eidesstattliche Versicherung

Ich erkläre hiermit an Eides statt, dass ich die vorgelegte Dissertation über die

„**Purification of neuronal macromolecular complexes in the nematode *Caenorhabditis elegans*“**

selbständig angefertigt und mich anderer Hilfsmittel, als der in ihr angegebenen, nicht bedient habe, insbesondere, dass aus Schriften Entlehnungen, soweit sie in der Dissertation nicht ausdrücklich als solche mit Angabe der betreffenden Schrift bezeichnet sind, nicht stattgefunden haben.
Während der praktischen Arbeit und der Erstellung der Dissertation wurden die Grundsätze der guten wissenschaftlichen Praxis beachtet.

Lörrach, den ....

(Florian Csintalan)

Table of Content

1. Zusammenfassung/Summary 11

1.1. Zusammenfassung 11

1.2. Summary 16

2. Introduction 19

2.1. Synaptic Transmission 19

2.2. The Synapse 20

2.3. Presynaptic Structures 24

2.3.1. The active zone and the SNARE complex 24

2.3.2. The different stages of the SNARE complex life cycle 27

2.3.3. The synaptic vesicle 37

2.4. Purifications of synaptic proteins in other species 43

2.4.1. Purification of synaptic vesicles 43

2.4.2. Purification of presynaptic membranes 46

2.5. Advantages of Caenorhabditis elegans as neurological model organism 47

2.5.1. The nervous system of C. elegans 47

2.6. Aim of this thesis 49

3. Material and Methods 52

3.1. Materials 52

3.1.1. Chemicals 52

3.1.2. Buffers and Media 53

3.1.3. Plasmids 56

3.1.4. Strains 58

3.1.5. Antibodies 61

3.1.6. Oligonucleotides 61

3.1.7. Kits/Beads 66

3.1.8. Equipment 66

3.2. Worm methods 67

3.2.1. General C. elegans maintenance 67

3.2.2. Mos1 Single copy integration (MosSCI) 70

3.2.3. Biolistic Gene transformation 72
3.2.4. Aldicarb assay 74
3.2.5. Swimming assay 74
3.2.6. Genotyping of worms 75
3.3. Molecular Biology 75
3.3.1. Cloning 75
3.4. Biochemical methods 78
3.4.1. Purification of Tobacco Etch Virus protease 78
3.4.2. Tandem Affinity Purification of synaptic vesicles 81
3.4.3. Sucrose gradient purification of synaptic vesicle 83
3.4.4. One-Strep Purification of synaptic vesicles 84
3.4.5. Tandem affinity purification of SNARE complexes 84
3.4.6. Mass spectrometric analysis 85
3.4.7. Fast Protein Extract from C. elegans 86
3.4.8. SDS-PAGE, Western blotting and immuno detection 86
3.4.9. Stripping 87
3.4.10. Silver staining 87
4. Results 88
4.1. Synaptic vesicle purification 88
4.1.1. Design of SNG-1::TAP tag fusion protein for native vesicle purification 88
4.1.2. Application of Mos1 single copy integration to generate a low expression strain 89
4.1.3. Tandem affinity purification of C. elegans synaptic vesicles using TAP tagged synaptogyrin results in an insufficiently pure fraction for proteomic analysis 89
4.1.4. For further opimization of the synaptic vesicle purification several alterations of the strategy were tested 94
4.2. SNARE complex purification 102
4.2.1. The split TAP tag distributed to synaptobrevin and syntaxin (UNC-64) allowed purification of SNARE complexes 102
4.2.2. Mass spectrometry analyses of purified SNARE complex preparations identified numerous potential SNARE-associated proteins 118

4.2.3. Selected candidates were analyzed for potential roles in synaptic transmission by RNAi knock down followed by aldicarb assays 119
4.2.4. Localization studies with the help of promoter fusion or functional fusion constructs of frm-2, snap-29, mca-3 123
4.2.5. Phenotypic assessments of mca-3 mutants 127
5. Discussion 130
5.1. Synaptic vesicle purification in C. elegans is more complex than expected 130
5.1.1. Challenges during synaptic vesicle purification 131
5.2. SNARE complex purification allows new insights to the synaptic machinery 132
5.2.1. Understanding the transmission machinery 132
5.2.2. Proposed model of the SNARE/MCA-3 interaction 135
5.2.3. Drawbacks during SNARE complex purification 136
5.2.4. Improvements of purification 138
6. Supplements 140
7. References 148
8. List of Abbreviations 163

Table of figures

Figure 2.1 The contact between the pre- and postsynaptic cell including membranes and protein machineries is the synapse 21
Figure 2.2: The synaptic cleft is tightly organized by pre- and postsynaptic protein structures 23
Figure 2.3 The helical structure of the coiled SNARE complex 25
Figure 2.4 The SNARE complex docks the synaptic vesicle to the presynaptic membrane ... 27
Figure 2.5 The formation of a fusion pore is energetically driven by the coiling of the SNARE motifs 29
Figure 2.6 The SNARE subunits are recycled by the SNAP/NSF complex under ATP consumption 30
Figure 2.7 The synaptic vesicle cycle 38
Figure 2.8 The two models of synaptic vesicle fusion and recycling 40
Figure 2.9 The molecular model of synaptic vesicle 41
Figure 2.10 The nervous system of *C. elegans* 48
Figure 3.1 Three different liquid culture vessels for *C. elegans* breeding 68
Figure 3.2: The scheme of Mos1 Single copy integration. 71
Figure 3.3 The elution profiles of His-tagged Tobacco Etch Virus Protease showed a high amount of eluted protease after reaching the concentration of 200 mM imidazole 79
Figure 3.4 The highest concentrations of TEV were visible in fraction 17 to 24 80
Figure 3.5 A protease assay demonstrated the functionality of the purified TEV 81
Figure 4.1 The purification test demonstrated that tosyl-activated DynaBeads and Pierce Carboxyl beads have the strongest binding and elution capability 90
Figure 4.2 The tandem affinity purification showed a strong elution from IgG beads, but only a weak signal on calmodulin beads 91
Figure 4.3 The signals of the calmodulin beads after TEV digest showed low amount of digested and high amount of undigested SNG-1::TAP 92
Figure 4.4 The elution fractions from the CaM column of the SNG-1::TAP sample shows a diverse set of proteins 93
Figure 4.5 The CaM beads after purification displayed in addition to assumed proteins, proteins with unknown identity 94
Figure 4.6 A-C The elution from IgG beads seemed to be most efficacious at 150 mM sodium chloride concentration 95

Figure 4.7 The sucrose gradient fractionation revealed no enriched fractions 97
Figure 4.8 The FLAG antibody did not reveal specific bands 98
Figure 4.9 Only unintegrated strains showed a strep specific expression 99
Figure 4.10 The loaded One-Strep beads did not show specific bands during synaptic vesicles purification 99
Figure 4.11 The expression of SNT-1::OneStrep::FLAG was lower compared to SNG-1::OneStrep::FLAG 101
Figure 4.12 The *snb-1* and *unc-64* constructs were expressed 103
Figure 4.13 The UNC-64::CBP and ProtA::SNB-1 fusion constructs rescue genomic mutants to an almost wild type level 105
Figure 4.14 Purification of UNC-64::CBP via calmodulin beads caused co-purification of ProtA::SNB-1 107
Figure 4.15 Deoxycholate and Triton X-100 displayed the best solubilization results, but deoxycholate disabled TEV cleavage 108
Figure 4.16 After 150,000 g there is still an intense band in the supernatant, but previously pelleting proteins remained in the supernatant after Triton treatment. 109
Figure 4.17 The elution of SNB-1 by TEV cleavage was the most successful with solubilized samples from 100,000 g centrifugation step 110
Figure 4.18 The signals of the silver staining did not correspond to the differences observed in the western blot 112
Figure 4.19 The Tandem Affinity Purification was successful as shown by SNB-1 signal in the elution fraction 113
Figure 4.20 The calculation of the different sizes for SNARE complexes reflected the different purification steps 114
Figure 4.21 The strains ZX1586 (extrachr. array) and ZX1588 (integrated array) displayed a faint signal in the CaM bead elution fraction after tandem affinity purification 115
Figure 4.22 The elution in the microinjected (A) versus biolistic transformed strains (B) showed a successful purification for biolistic transformed strains 117
Figure 4.23 Knocking-down *mca-3* induced a resistance to aldicarb, whereas knocking-down *frm-2, snap-29, ekl-6, klb-8, mdh-2, pfk-2, piki-1* and *vamp-8* resulted in hypersensitivity 122
Figure 4.24 The FRM-2::GFP display a broad expression, not restricted to synapses or even neurons. 124

Figure 4.25 The SNAP::29 expression can be observed throughout the nematode. 125
Figure 4.26 A clear neuronal expression of the MCA-3B::GFP could be observed 126
Figure 4.27 Confocal analysis of MCA-3B::GFP and mCherry::SNB-1 displayed the difference between plasma membrane localization of MCA-3 and vesicle localization of SNB-1 127
Figure 4.28 The aldicarb assay did not show a rescue phenotype after injection of with *punc-17::mca-3* 128
Figure 4.29 The *punc-17::mca-3* partially rescues the mca-3 mutant in the swimming assay 129
Figure 5.1 Fluorescent image of KLP-8::GFP fusion 134
5.2 The MCA-3 has an important role in the functionality of Ca^{2+} induced vesicle fusion ... 136

Table of tables

Table 1 Chemicals 52
Table 2 MosSCI plasmids 56
Table 3 Synaptic Vesicle plasmids 56
Table 4 SNARE complex plasmids 57
Table 5 *C. elegans* strains 58
Table 6 Antibodies 61
Table 7 *sng-1* oligonucleotides 61
Table 8 *snb-1* oligonucleotides 63
Table 9 *unc-64* oligonucletides 64
Table 10 Oligonucleotides with diverse project contributions 65
Table 11 Selected proteins from SNARE purifications for analysis with possible function in synaptic transmission 119
Table 12 Excerpt of mass spectrometry results of CaM beads for SV purifications 140
Table 13 Mass spectrometric analysis of several SNARE complex purifications 141

1. Zusammenfassung/Summary

1.1. Zusammenfassung

Das Kernstück aller neuronalen Vorgänge ist die Synaptische Transmission. Sie besteht aus einer komplexen Abfolge von ineinandergreifenden Prozessen. Zwei wichtige dieser sind die Bindung von synaptischen Vesikeln (SV) an die präsynaptische Membran und die anschließende Fusion ihrer beider Membranen mittels des SNARE-Komplexes. Synaptische Vesikel sind neurotransmitter-gefüllte Membrankugeln mit einer Vielzahl von integralen und peripheren Proteinen. Die Funktionen der synaptischen Vesikel sind die Konzentration, Lagerung und Organisation der Neurotransmitter. Außerdem erlaubt der Aufbau der synaptischen Vesikel und ihre Interaktion mit anderen Proteinen eine regulierte Freisetzung ihrer enthaltenen Neurotransmitter. Der Hauptteil der synaptischen Vesikel entsteht entweder durch Clathrin-vermitteltetes Budding von Endosomen oder durch Recycling der Plasmamembran nach Vesikelfusion.

Der synaptische SNARE-Komplex ist ein Zusammenschluss von drei verschiedenen Proteinen: vesikuläres Synaptobrevin, präsynaptisches membrangebundenes Syntaxin und präsynaptisches membrangebundenes SNAP-25, die zusammen vier parallele α-Helices mit sechzehn gestapelten Ebenen mit interagierenden Seitenketten ergeben. Um zwei Membranen zu fusionieren muss die Abstoßungsenergie des Oberflächenwassers und die Abstoßungskraft der negativen Kopfgruppen der beiden Lipid-Doppelschichten überwunden werden.
Die Bildung eines coiled Coils aus den verschiedenen Untereinheiten des SNARE-Komplexes liefert die Energie für die Fusion der präsynaptischen Membran mit der synaptischen Vesikelmembran. Durch Interaktion mit anderen Proteinen, wie mUNC-18, mUNC-13 und Synaptotagmin reguliert die Bildung des coiled Coils. Die Bindung der synaptischen Vesikel und die Fusion mit der präsynaptischen Membran werden engmaschig kontrolliert, um die Spezifität der Neurotransmitterausschüttung zu gewährleisten.

Es wurden bereits viele Experimente, wie genetische Screenings und synaptische-Vesikel-Proteom-Analysen durchgeführt, um die Funktionen und Interaktionen der

diversen beteiligten Proteine zu bestimmen. Nichtsdestotrotz sind diese Prozesse und die Rollen von identifizierten Proteinen noch immer nicht abschließend geklärt.

Ziel dieser Arbeit war es zunächst mithilfe einer Tandem-Affinität-Aufreinigung (TAP) von synaptischen Vesikeln neue unbekannte Interaktionspartner zu finden und ihre Funktionen zu bestimmen. Dies sollte im nematodischen Modellorganismus *Caenorhabditis elegans* (*C. elegans*) durchgeführt werden. Da die zugrundeliegenden Mechanismen evolutionär konserviert sind, lassen sich durch Entdeckungen im Nematoden wichtige Rückschlüsse auf Vorgänge im menschlichen Nervensystem ziehen. Zwar existiert in *C. elegans* kein neuronenreiches Gewebe, wie in anderen Modellspezies, wie zum Beispiel Gehirne von Mäusen oder Ratten, es existieren jedoch vielfältige genetische Methoden in *C. elegans*, wie die Expression nach Mikroinjektion von Plasmiden, biolistische Transformation (Gene gun), Mos1 Single Copy Integration oder RNA Interferenz. Diese erlauben eine schnelle Erzeugung modifizierter Organismen und eine zügige Bestimmung der Funktion identifizierter Proteine.

Dazu wurde das integrale synaptische Vesikelprotein Synaptogyrin mit einem Tandem-Affinitäts-Aufreinigungs(TAP)-tag versehen. Der TAP-tag besteht aus einem ProteinA, das an IgG-Beads binden kann, einer Tobacco Etch Virus (TEV)-Protease-Schnittstelle zur Elution von den IgG-Beads und einem Calmodulin-Binde-Peptid (CBP), das mit Calmodulin-Beads interagiert. Die beiden Affinitätsaufreinigungsschritte werden nacheinander durchgeführt und erlauben eine hochspezifische native Aufreinigung von Proteinen bzw. Komplexen und ihren Interaktionspartnern. Dies sollte es erlauben intakte synaptische Vesikel in hoher Reinheit zu gewinnen. Bei erfolgreicher Aufreinigung kann man anschließend mit Hilfe massenspektrometrischer Methoden mit-aufgereinigte (co-purifizierte) Proteine identifizieren. Diese Kandidaten können nun mithilfe phenotypischer Experimente (Aldicarb- und Schwimmassay) auf ihren neuronalen Zusammenhang untersucht werden.

Durch eine Standardintegration via UV-Licht der getaggend Gene in das Genom kann es zu einer Überexpression des Proteins kommen. Diese Überexpression kann toxische oder dominant-negative Effekte haben, oder es kommt zu einer Fehlzuordnung der Proteine (missorting). Dies würde möglicherweise zur Identifikation von inkorrekten Interaktionspartnern führen oder den Aufreinigungserfolg unterbinden. Um diese Gefahr

zu reduzieren, wurde das Konstrukt in einfacher Ausführung mittels Mos1 single copy integration in das *C. elegans* Genom integriert.

Zwar gelang es in verschiedenen Aufreinigungen Synaptogyrin an die IgG-Beads zu binden und geringe Mengen zu eluieren, eine quantitative Elution konnte jedoch mithilfe der TEV-Protease nach der Bindung an IgG-Beads nicht erreicht werden. Aus diesem Grund wurde die Aufreinigungsstrategie im Laufe der Arbeit mehrfach modifiziert: die Verwendung von Magnetobeads, längere Linker-Sequenzen, Erhöhung von einer auf vier TEV-Schnittstellen (separiert widerum durch weitere Linkersequenzen), verschiedene NatriumChlorid-Konzentrationen (0 mM, 150 mM, 300 mM), Voraufreinigung der Vesikel durch einen Sucrosegradienten, andere Affinitätsaufreinigungsreste (OneStrep, FLAG, ProteinC) und Wechsel des Fusionsvesikelproteins auf Synaptotagmin. Auch diese Ansätze lieferten keine Verbesserung der Elution und so wurde dieses Projekt schlussendlich für ein erfolgversprechenderes Ziel, die SNARE-Komplex-Aufreinigung, aufgegeben. Abschließend betrachtet war vermutlich einer der Gründe für den fehlenden Erfolg der Vesikelaufreinigung der notwendige Verzicht auf Detergenz.

Das neue Ziel dieser Arbeit war es mithilfe der Tandem-Affinitäts-Aufreinigung neue unbekannte Interaktionspartner des SNARE-Komplexes zu identifizieren und ihre Rollen zu bestimmen. In dieser neuen Aufreinigungsstrategie konnte Detergenz verwendet werden, um den Komplex zu solubilisieren und für die Aufreinigung zugänglich zu machen. Um die Spezifität der Aufreinigung in Hinblick auf gebildete Komplexe – vesikuläres Synaptobrevin gebunden an Zielmembran-Synataxin und SNAP-25 – zu erhöhen, wurden die beiden SNARE-Untereinheiten Synaptobrevin (SNB-1 in *C. elegans*) mit ProteinA und TEV-Protease-Schnittstelle, und Syntaxin (UNC-64 in *C. elegans*) mit einem Calmodulin-Binde-Peptid separat verknüpft. Außerdem wurde mithilfe der Mos1 Single Copy Integration nur eine einfache Kopie in das Genom integriert, um oben genannte Fehlallokation zu vermeiden.

Das Anhängen von Affinitätsreinigungsresten an Proteine kann ihre Funktion beeinträchtigen und dies würde möglicherweise zur Identifizierung von falschen Interaktionspartnern führen oder die Aufreinigung unmöglich machen. So wurden in Stämmen mit mutierten SNARE-Untereinheiten die entsprechenden Fusionsproteine exprimiert, um ihre Funktionalität zu prüfen. Hierzu wurde ein Aldicarb Assay durchgeführt, der bei fehlerhaften synaptischen Proteinen Veränderungen im

Paralyseverlauf zeigt. Die mutierten Stämme, in denen zusätzlich Fusionsproteine exprimiert wurden, wiesen im Gegensatz zu den naiven mutierten Stämmen ein annäherndes Wildtyp-Verhalten auf.

Vor Beginn der eigentlichen Aufreinigung wurden verschiedene Detergenzien und Zentrifugationsschritte getestet, um eine Optimierung der Aufreinigungsstrategie zu erlangen. Es wurde das Detergenz Triton X-100 und eine differenzielle Zentrifugation mit finalem Schritt mit 150,000 g für eine Stunde als erfolgversprechendste Bedingungen identifiziert.
Um zu zeigen, dass die Aufreinigung des Komplexes prinzipiell funktioniert, wurde eine Aufreinigung mittels UNC-64::Calmodulin-Binde-Peptid durchgeführt. Die Analyse der Aufreinigung wies im Western Blot Signale von ProteinA::SNB-1 in der Elutionsfraktion auf und bewies, dass es möglich ist, eine SNARE-Untereinheit mithilfe der anderen aufzureinigen.

Mehrere vollständig durchgeführte Tandem-Affinitäts-Aufreinigungen zeigten im finalen Elutionsschritt ein SNG-1-Signal im Western blot und Protein Signale im Silver Stain. Diese positiven Elutionsproben wurden zusammen mit Wildtyp-Aufreinigungsproben als Negativkontrolle zur tandem-massenspektrometrischen Analyse an die verschiedenen Kooperationspartner Heinrich Heide (Labor Ilka Wittig, Frankfurt am Main), Ilka Wittig (Labor Ilka Wittig, Frankfurt am Main) und Uwe Plessmann (Labor Henning Urlaub, Göttingen) gesandt. Bei Beschränkung auf Datensätze, die SNARE-Proteine enthielten und Proteine, die nicht in Wildtyp-Proben auftauchten, wurden insgesamt 119 Proteine, inklusive der SNARE-Proteine RIC-4, SNAP-29, SNB-1, UNC-64, VTI-1, identifiziert.

Aus diesen Proteinen wurden Kandidaten zur weiteren Analyse ausgewählt, wenn sie in mindestens zwei SNARE-positiven MS-Analysen detektiert wurden oder bekannte neuronale Funktionen oder Homologien zu neuronalen Proteinen in anderen Spezies aufwiesen. Diese Kandidaten C33H5.8, *ekl-6*, F29G9.2, *frm-2*, *klp-8*, *mca-3*, *mdh-2*, *pfk-2*, *piki-1*, (*ric-4*,) *snap-29*, *tag-241*, *tax-6*, (*unc-64*,) *vamp-8*, *vha-10*, *vti-1*, W01B6.5, W09C3.1, Y116F11B.11 wurden mithilfe eines RNA Interferenz Knock-downs und anschließendem Aldicarb Assay auf ihre synaptische Funktionen untersucht. Die Behandlung mit ihrer spezifischen interferierenden RNA löste bei *mca-3* eine starke Resistenz gegenüber dem Acetylcholinesterase-Inhibitor Aldicarb aus – das für eine Hemmung der Acetylcholin-Ausschüttung durch *mca-3* Knock-down spricht. Während

frm-2, snap-29, ekl-6, klb-8, mdh-2, pfk-2, piki-1 und *vamp-8* in einer Hypersensitivität mündeten, das auf eine erhöhte Ausschüttung von Acetylcholin hinweist.

Die am stärksten auf aldicarb-reagierenden Gene *frm-2, snap-29* und *mca-3* wurden dahingehend untersucht, ob sie in Promoter- oder funktionalen Fusionskonstrukten eine Kolokalisation mit mCherry getaggten Synaptobrevin zeigten. Während FRM-2::GFP und SNAP-25::GFP keine neuronal-spezifischen Signale aufwiesen, konnte für MCA-3::YFP in regulären und in konfokalen Fluoreszenzmikroskopaufnahmen eine neuronale Expression nachgewiesen werden.

Um den synaptischen Charakter und die Funktionalität des MCA-3::YFP zu zeigen, wurde neben einem Aldicarb Assay, der keinen Rescue zeigte, ein Schwimm Assay durchgeführt. Hier wurden naive Stämme, die mutiertes *mca-3* enthielten, mit fusionskonstrukt-exprimierenden mutierten Stämmen und Wildtypstämmen auf ihr Verhalten in Flüssigkeit untersucht. Im Schwimm Assay konnte in den MCA-3::YFP-exprimierenden mutierten Stämmen eine partielle Wiederherstellung von Wildtypverhalten gezeigt werden.

Aufgrund unserer Daten sind wir überzeugt mit MCA-3 einen neuen Interaktionspartner des SNARE-Komplexes entdeckt zu haben. MCA-3 ist eine Plasmamembran Ca^{2+}-ATPase und wurde zwar mit neuronaler Expression, aber zunächst nur in ihrer Rolle in der Endozyose von spezifischen Filter-Zellen, den Coelomyzeten, gesehen. Ihre neue mutmaßliche Rolle ist die Senkung der Kalziumionenkonzentration am gebundenen SNARE-Komplex.

Da schon eine Interaktion von SNARE-Syntaxin mit Ca^{2+}-Kanälen gezeigt wurde, ist es nur verständlich mithilfe einer Interaktion auch Kalziumtransporter zu kolokalisieren um die Konzentration von Kalizumionen vor Ort auf ein Minimum zu senken. So wird die Konzentration schnell auf ein Nichterregungsmaß reduziert und ermöglicht neue gezielte Transmissionen.

1.2. **Summary**

The centerpiece of all neuronal processes is the synaptic transmission. It consists of a complex series of events. Two key elements are the binding of synaptic vesicles (SV) to the presynaptic membrane and the subsequent fusion of the two membranes. Synaptic vesicles are neurotransmitter-filled membranous spheres with many integral and peripheral proteins. The synaptic SNARE complex consists of three interacting proteins, which energize and regulate the fusion of the synaptic vesicle membrane with the presynaptic membrane. Both processes are closely orchestrated to ensure a specific release of neurotransmitter in the synaptic cleft. Already many experiments have been performed, such as genetic screens and proteome analysis of synaptic vesicle, to determine the functions and interactions of the various proteins involved. Nevertheless, these processes and the functions and roles of the identified proteins are still not fully elucidated. The aim of this thesis was initially applying a tandem affinity purification of synaptic vesicles to identify new unknown interaction partner of SV and to determine their role. This was supposed to be performed in the model organism *Caenorhabditis elegans*. The underlying mechanisms are conserved throughout the phylogentic tree and identified interaction partners will help to understand the processes in the mammalian brain. Although there is no neuron-rich tissue in C. elegans as in other model organisms, the diverse genetic methods allows a rapid creation of modified organisms and a prompt determination of the function of identified proteins.

The integral SV protein synaptogyrin has been fused to a tandem affinity purification (TAP) tag. The TAP-tag consists of a ProteinA, a TEV protease cleavage site and a calmodulin binding peptide. Both affinity purification steps are performed sequentially and allow a highly specific native purification of proteins and their interaction partners. To reduce the risk of false localization and thereby incorrect interaction partners the Mos1 single copy integration (MosSCI) was used to incorporate the construct into the C. elegans genome. Due to technical difficulties related to the elution step using the TEV protease, the purification strategy was modified several times during the course of this thesis and then finally abandoned for a more promising project, the SNARE complex

purification. In conclusion, one of the reasons of failure of the vesicle purification was the necessary lack of detergent.

The amended aim of this thesis has been the tandem affinity purification of detergent solubilized SNARE complex to identify new unknown interaction partner and to determine their role. In order to increase the specificity of the purification, in terms of formed complexes, the two SNARE subunits were separately fused to different affinity tags: synaptobrevin (SNB-1 in C. elegans) to ProteinA and a TEV protease cleavage site, and Syntaxin (UNC-64 in C. elegans) to a calmodulin binding peptide. In order to avoid the above mentioned misallocation MosSCI was again used for integration. As the modifications of the proteins could impair their function and lead to false interaction partners, their functionality was tested. For this purpose, the corresponding fusion constructs were expressed in strains with mutated snb1 and unc-64. Non-functional synaptic proteins display an altered course of paralysis in an aldicarb assay. The fusion proteins which were expressed in their respective mutant strains displayed a near to wild-type behavior in contrast to the naive mutant strains. To demonstrate the proof of principle of complex purification a purification utilizing UNC-64::calmodulin binding peptide was conducted. The analysis of the elution fraction in a western blot showed signals of Protein A::SNB-1 and underlined the possibility of complex purification.

Multiple tandem affinity purifications demonstrated SNG-1 signals in Western blot analysis and complex sets of proteins in the final elution step in a silver staining of SDS-PAGEs. Final elution samples with signals in western blot and/or silver staining were sent with negative control (wild-type purification samples) for tandem mass spectrometric analysis to various cooperation partners: Heinrich Heide (Wittig lab, Frankfurt) Ilka Wittig (Wittig lab, Frankfurt am Main) and Uwe Plessmann (Urlaub lab, Göttingen). 119 proteins were identified (including RIC 4, SNAP-29, SNB-1, UNC-64, VTI-1), which appeared only in data sets with SNARE proteins and did not appear in wild-type samples. If proteins were detected in at least two SNARE positive MS analysis and had known neural functions or homologies to neuronal proteins in other species, they were selected for further analysis. These candidates C33H5.8, ekl-6, F29G9.2, frm-2, klp-8, mca-3, mdh-2, pfk-2, piki-1, (ric-4) snap-29, tag-241, tax-6, (unc-64), vamp-8, vha-10, vti-1, W01B6.5, W09C3.1, Y116F11B.11 were knocked down by RNAi and tested for synaptic function in a following aldicarb assay. The treatment with their specific

interfering RNA resulted for mca-3 in a strong resistance to aldicarb, while frm-2, snap-29, ekl-6, klb-8, mdh-2, pfk-2, piki-1 and vamp-8 resulted in hypersensitivity. The most responsive genes frm-2, snap-29 and mca-3 were examined, whether they displayed a co-localization together with mCherry tagged synaptobrevin in promoter fusion constructs or functional fusion constructs. In regular and confocal fluorescence microscopy images only MCA-3::YFP demonstrated neuronal expression.

In order to substantiate the synaptic nature and functionality of the MCA-3::YFP, among others, a swimming assay was performed. Here, fusion construct expressing strains, which contained mutated mca-3, were compared with untreated mutant strains and wild-type strains according to their behavior in liquid media. In this swimming assay a partial restoration of wild-type behavior was shown in the MCA-3::YFP expressing mutant strains. Based on these data, we discovered with MCA-3 a new interaction partner of the SNARE complex. MCA-3 is a plasma membrane Ca2+-ATPase and was indeed seen with neuronal expression, but initially only in their role in the endocytosis of specific filter cells (coelomycetes). Its new putative role is the reduction of Ca2+ concentration at the bound SNARE complex. Since an interaction of syntaxin with Ca2+ channels has been demonstrated, it would be comprehensible to reduce the local concentration of Ca2+ to a minimum by tethering Ca2+ transporters to the SNARE complex.

2. Introduction

2.1. Synaptic Transmission

Chemical synaptic transmission is a series of events underlying the transmission of a neurotransmitter signal from a neuron to a recipient cell (Südhof, 2004). This essential process has received a lot of attention in the past decades, culminating in the Nobel Prize in Physiology or Medicine being awarded in 2013 to Thomas Südhof, Randy Schekman and James Rothman "*for their discoveries of machinery regulating vesicle traffic, a major transport system in our cells"*(Nobelprize.org, 2013).

This transmission happens via a multitude of sequential steps by a highly complex intertwining machinery: Upon the arrival of an action potential at the presynaptic membrane voltage-gated-calcium (Ca^{2+})-channels open and a local rise of Ca^{2+} concentration leads to a conformational change of the synaptic vesicle protein synaptotagmin (Archer, 2002; Hui et al., 2011; Betke et al., 2012; Krishnakumar et al., 2013). This change allows the partially coiled SNARE complex to coil completely and the free energy associated with this process is used to overcome the energy barrier between the synaptic vesicle and presynaptic plasma membrane lipids and induce mixing of the two membranes, followed by opening of a fusion pore (Sabatini and Refer, 1996; Südhof, 2004). This fusion leads to a secretion of the vesicle content into the synaptic cleft. There are two kinds of vesicles transmitting a signal to other cells: synaptic vesicles (SV) which are filled with neurotransmitters such as acetylcholine, glutamate and GABA or dense core vesicles (DCV) which contain neuropeptides. The diameter of synaptic vesicles varies between species and cell type, but is approximately 29 – 60 nm (Takamori et al., 2006; Alabi and Tsien, 2013; Kim et al., 2000; Stigloher et al., 2011; Stevens et al., 2012; Kittelmann et al., 2013). They were discovered as clear particles in the electron microscope (EM) – in contrast to dense core vesicles (DCV) which have an electron-dense appearance (Robertis and Franchi, 1956; Grey, 1963; Hoover et al., 2014; Grabner et al., 2006). DCVs are widely distributed in the cytosol, but although they differ in some characteristics, like content and recycling ability, both vesicles secrete their content via the same exocytosis machinery (Park and Kim, 2009). (The structure and generation of synaptic vesicles is discussed in chapter 2.3.3). Tarr et al. demonstrated in frog

neuromuscular junctions (NMJ) that only a small fraction of SV are released upon arrival of an action potential (350 released vesicles compared to 14,000 – 28,000 docked vesicles) (Tarr et al., 2013, Meriney and Dittrich, 2013). Transmitter release is the result of a multitude of inputs and interactions between different incoming and possible opposing electrical signals, second messenger levels and the protein network responsible for secretion (Betke et al., 2012). After the transmitter is released into the synaptic cleft it diffuses to the postsynaptic membrane and binds to neurotransmitter specific receptors.

2.2. **The Synapse**

The site of synaptic transmission is the synapse. Its basic composition is a) the presynaptic membrane with the SNAP-25/syntaxin acceptor complexes, formed by the SNARE proteins SNAP-25 and syntaxin (the SNAP-25/syntaxin acceptor complex and its components are described in chapter 2.3.2.1) and docked synaptic vesicles at the active zone, b) the synaptic cleft, which is the interspace between the neurotransmitter secreting neuron and the recipient cell and c) the postsynaptic membrane, which is the location of transmitter binding (compare Figure 2.1).

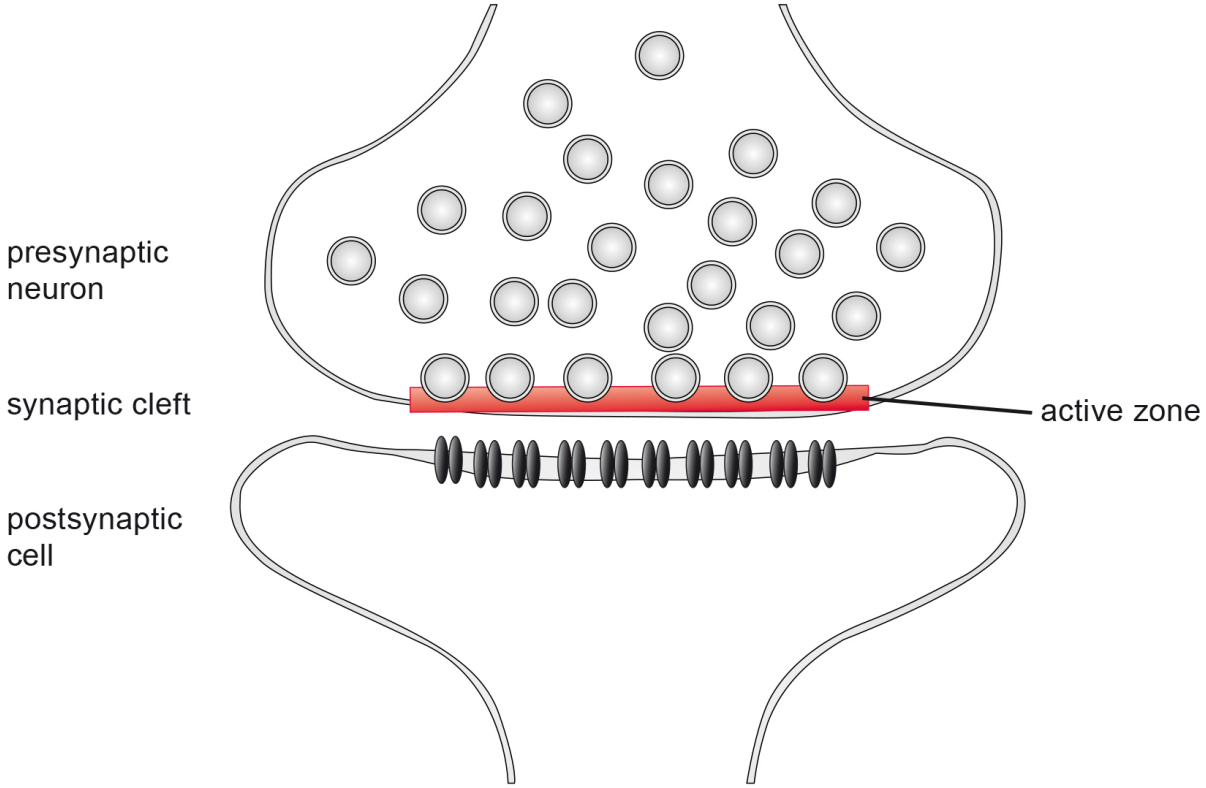

Figure 2.1 The contact between the pre- and postsynaptic cell including membranes and protein machineries is the synapse The synaptic vesicles (grey spheres) are transported to the active zone (red line), where they first dock and later fuse with the presynaptic membrane to release neurotransmitter into the synaptic cleft. The neurotransmitter diffuses to the opposite membrane and binds to receptors (black dimers). Adapted from Südhof et al. (Südhof, 2012).

For more information of the presynaptic membrane see chapter 2.3.1.

Structural proteins, such as neurexins/neuroligin complexes, cadherins, members of the immunoglobulin superfamily, and Ephrin B and Ephrin B receptors are responsible for the formation, specificity and localization of the synapse (High et al., 2015; Frei et al., 2014; Tanaka et al., 2012). Neurexins and neuroligins are believed to be the most important class for transsynaptic adhesion and facilitating specificity (Südhof et al., 2008). Both molecules interact via their extracellular domain, whereas their intracellular domains are involved in regulatory processes. To allow the specificity for the generation of hundreds of different synapses a large number of variants is required. This is based on genetic, transcriptional and translational isoforms (Yang et al., 2014). Neurexin1β and neuroligin complexes form heterotetrameric sheets (heterotetramer in which two Nrx1β protomers bind to a NL1 homodimer), whereas α-neurexins form heteromorphic structures with unknown function (Tanaka et al., 2012). Cadherins are transmembrane proteins depending on Ca^{2+} for adhesion, which share a specific cadherin motif at their extracellular domain. In synapses the synaptic adhesion is mediated by the puncta adherentia, a special form of cadherin *trans*-interaction between pre- and postsynaptic membranes. Cadherins are not only responsible for simple cell-cell adhesion, but can serve as recognition molecules via the subtype specificity of different cadherins (Hirano and Takeichi, 2012). In vertebrate brain N-cadherin is thought to be the major synaptic cadherin (Hirano and Takeichi, 2012), whereas in *C. elegans* FMI-1 (FLAMINGO/STAN cadherin) seems to be the most important synaptic cadherin since a mutation leads to defects in synaptogenesis (Pettitt, 2005). The other major adhesion molecules responsible for synaptic formation and recognition are members of the immunoglobulin superfamily (IgSF). They are called synaptic cell adhesion molecules (SynCAM) and share an amino-terminal signal peptide, three extracellular Ig domains, a transmembrane region and a short carboxy-terminal tail (Biederer et al., 2002; Frei et al., 2014). These proteins are N-glycosylated and show in addition to their adhesive properties modulatory effects on signal cascades and are scaffolding partners for receptor proteins (Beesley et al., 2014b)(Figure 2.2). IgSF11 the member of the immunoglobulin superfamily binds at the postsynaptic membrane the scaffolding protein PSD-95 which binds to the N-methyl-D-aspartate (NMDA) and the α-amino-3-hydroxy-5-methyl-4-isoxazolepropionic acid (AMPA) glutamate receptor (Jang et al., 2015). The neuroplastin Np65, another member of the IgSF, induces clustering of $GABA_A$ receptors at the postsynaptic membrane

(Beesley et al., 2014a). Both mechanisms result in the accumulation of receptor at the synapse.

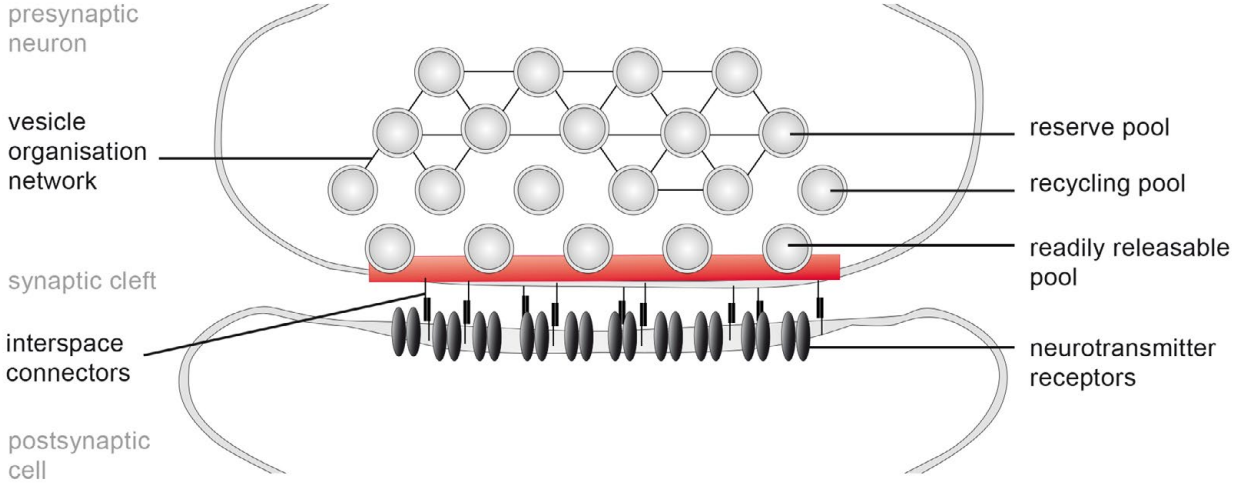

Figure 2.2: The synaptic cleft is tightly organized by pre- and postsynaptic protein structures The two membranes are linked and regulated by a complex protein-protein network. Binding to a proteinaceous network of actin filaments and the protein synapsin the presynaptic membrane differentiates between distinct vesicle pools (vesicle organization network)(Denker and Rizzoli, 2010; Fernández-Busnadiego et al., 2010). The docked vesicles represent the readily releasable pool, the loose vesicles the recycling pool and the filament-connected vesicles the reserve pool. Interspace connectors allow concentrating receptor and auxiliary proteins to sites of neurotransmitter secretion. Adapted from Denker et al. 2010, Fernández-Busnadiego et al. 2010 and High et al. 2015 (Denker and Rizzoli, 2010; Fernández-Busnadiego et al., 2010; High et al., 2015).

Ephrin B and Erythropoietin-producing hepatocellular carcinoma (Eph) receptor form together tetrameric ring-like complexes, which induce and maintain cell adhesive responses at excitatory synapses. The function of Ephrin B and Eph receptor includes the regulation of receptor trafficking which determines the synaptic class (neurotransmitter specific) and are responsible for the generation of synapses (Sloniowski and Ethell, 2012).

Neurotransmitter-receptors, which are named according to their ligand, are classified into two families: ionotropic and metabotropic receptors. The binding of acetylcholine to the nicotinic acetylcholine receptor (nAChR), as an example for an ionotropic receptor, induces the opening of the sodium channel. The influx of sodium ions into the cell leads to an activating depolarization (nAChR) (Miledi, 1960; Curtis and Ryall, 1964; Sakmann et al., 1983). As another example for an ionotropic receptor the $GABA_A$ receptor increases upon binding to GABA the permeability to chloride ions. The increased

chloride influx leads to an inhibitory hyperpolarization of the postsynaptic membrane (Akabas, 2004; Cesca et al., 2010). The activation of a metabotropic receptor influences the second messenger signaling cascades resulting in a slower but longer response in the postsynaptic cell. Most metabotropic receptors, except receptor tyrosine kinases (Purcell and Carew, 2003), are G protein coupled receptors (GPCRs)(Betke et al., 2012). Ligand-mediated GPCR activation results in the interaction of associated G proteins with different enzymes to generate a signaling cascade (Betke et al., 2012). For example, activation of the metabotropic glutamate receptor stimulates the enzyme phospholipase C, which generates the second messenger inositol triphosphate and diacylglycerol resulting in the opening of intracellular calcium channels, in addition to other effects (Wisden and Seeburg, 1993; Hollmann and Heinemann, 1994; Beqollari and Kammermeier, 2013). Another example is the $GABA_B$ receptor-induced inhibition of adenylate cyclase leading to the reduction of PKA activity which inhibits Ca^{2+} signals (Diamond and Huxley, 1968; Kantamneni, 2015). The metabotropic equivalent of the nicotinic acetylcholine receptor is the muscarinic AChR (Curtis and Ryall, 1964).

2.3. **Presynaptic Structures**

2.3.1. The active zone and the SNARE complex

The fusion of a vesicle and a membrane is a commonly used mechanism throughout the cell e.g. in ER-Golgi trafficking, endocytic vesicle-lysosome fusion, and secretion processes (Nobelprize.org, 2013). To fuse two membranes, the repulsion energy of the surface water and the repulsion force of the negative head groups of the lipid membrane (30-60 kcal/mol) of the two lipid bilayers need to be overcome (Kozlovsky and Kozlov, 2002). This energy and the pulling force is provided by the formation of a coiled-coil (or zippering) of four parallel α-helices with 16 stacked layers of interacting side chains - the SNARE complex (Sutton et al., 1998; Fasshauer et al., 2002; Cohen and Melikyan, 2004). The coiling α-helices are called the SNARE motif, a stretch of 60 - 70 amino acids with a heptad repeat (Figure 2.3). A heptad repeat is a pattern of seven hydrophobic and polar amino acids: hydrophobic, polar, polar, hydrophobic, charged, polar, and charged commonly found in coiled coils. Analysis of the amino acid sequence of the SNARE family among different species and compartments showed that all SNARE motifs form

hydrophobic layers – with one exception in the zero layer. Here three glutamine (Q) residues meet one arginine (R) residue e.g. SNAP-25 provides two helices with one Q-residue each, syntaxin one Q and synaptobrevin the R residue (Figure 2.3) (Fasshauer et al., 1998b; Fasshauer and Margittai, 2004; Antonin et al., 2002).

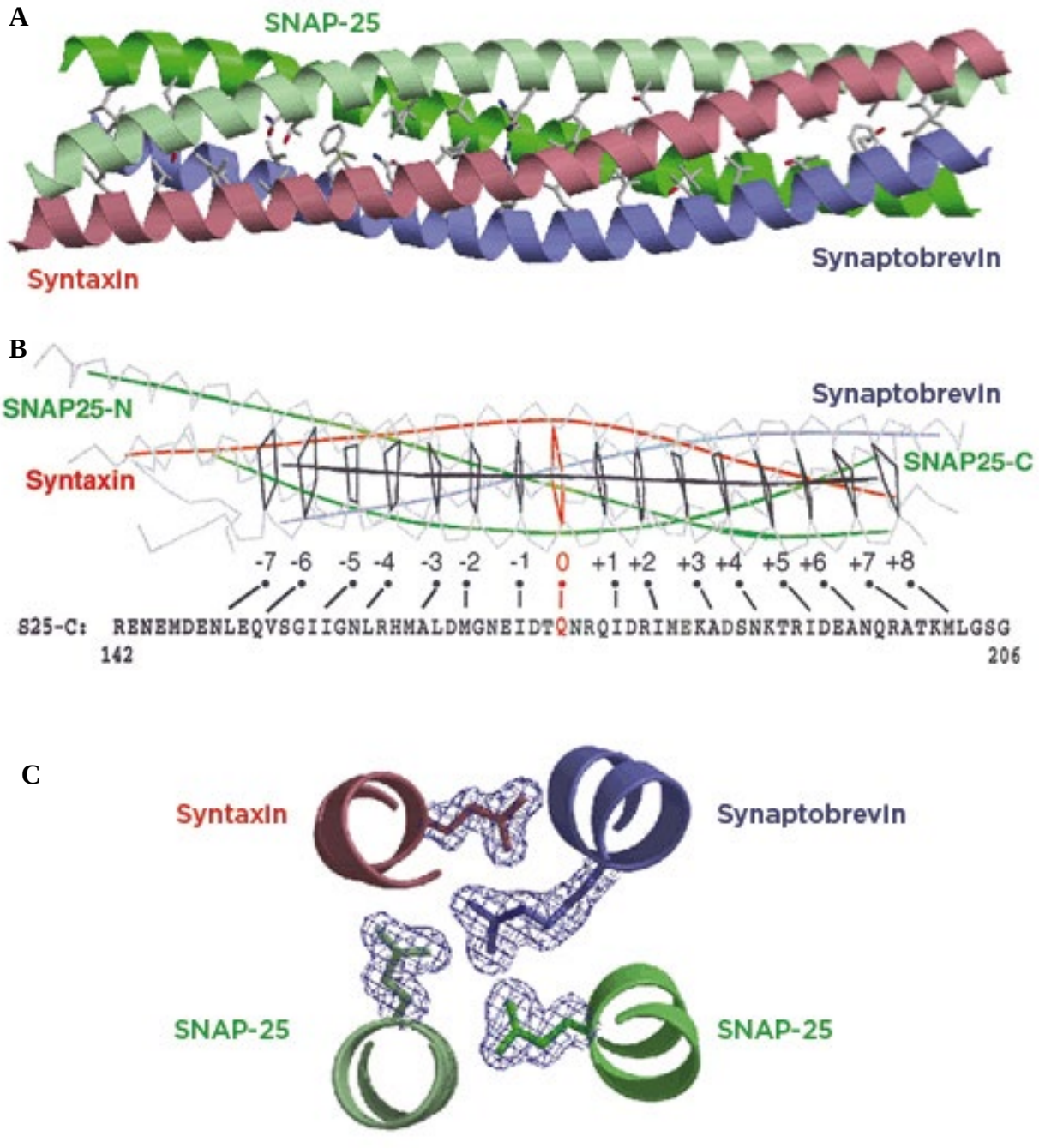

Figure 2.3 The helical structure of the coiled SNARE complex A The SNARE complex is formed by the coiling of the four SNARE motifs of the three SNARE subunits. The R-SNARE synaptobrevin is represented in blue, syntaxin in red and the two coils of SNAP-25 in green. **B** Structure of the four helix bundle and the zero-layer. The amino acid sequence originated from

SNAP-25 **C** The hydrophilic central zero layer is formed by three glutamine residues (syntaxin in red and SNAP-25 in green) and the arginine residue (synaptobrevin in blue) Taken with modifications from Antonin et al. and Chen et al. (Chen et al., 2001; Antonin et al., 2002).

During synaptic vesicle fusion synaptobrevin and syntaxin provide one SNARE motif each and SNAP-25 two (Fasshauer et al., 2002). In other vesicle fusion reaction each SNARE motif can originate from a different protein. Since this complex was first discovered in 1993 for being involved in the interaction with N-ethylmaleimide sensitive factor (NSF) forming a 20 S complex by Söllner et al. (Söllner et al., 1993a) the name "**S**oluble **N**SF **A**ttachment protein **re**ceptor" SNARE was defined. α-SNAP and NSF separate the SNARE complex into its subunits under ATP consumption (Barnard et al., 1996; Littleton et al., 2001; Zhao et al., 2015)(Figure 2.6).

The pulling force between the two membranes is provided by the anchoring of the SNARE complex subunits to the synaptic vesicle and presynaptic plasma membrane. Vesicular synaptobrevin and presynaptic membrane syntaxin comprise a single C-terminal transmembrane domain, whereas presynaptic membrane SNAP-25 has a palmitoyl side chain in the center of the molecule (Hess et al., 1992)(Figure 2.4).

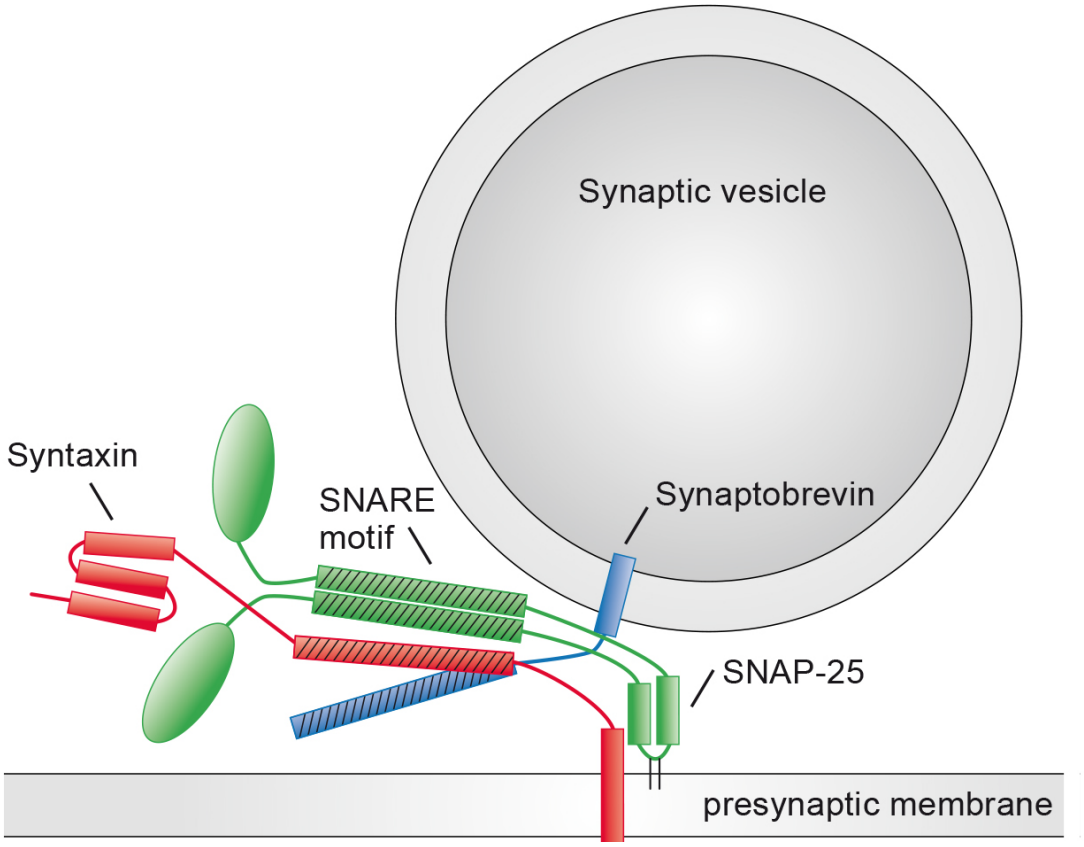

Figure 2.4 The SNARE complex docks the synaptic vesicle to the presynaptic membrane The different subunits form a complex by intertwining their α-helices. The binding of synaptobrevin (in blue) to syntaxin (in red) and SNAP-25 (in green) brings the two membranes in close proximity. The parallel cylindrical rods in the center of each protein (dashed) represent the different α-helical SNARE motifs of the subunits. The full coiling of these different SNARE proteins provides the energy to overcome the repulsion force. The three parallel helices at the end of syntaxin represent the H_{abc}-helices responsible for the regulation of SNARE complex formation.

2.3.2. The different stages of the SNARE complex life cycle

The life cycle of the SNARE complex consists of five different stages (closely reflected by the different stages of the synaptic vesicle cycle; chapter 2.3.3; Figure 2.7):

1) **Formation of a binary SNAP-25/syntaxin acceptor complex**: SNARE complex formation starts with a slow and rate limiting step by formation of the SNAP-25/syntaxin acceptor complex by the two target membrane SNAREs syntaxin and SNAP-25 (Fasshauer and Margittai, 2004; Dun and Duncan, 2010). This SNAP-25/syntaxin acceptor complex consists finally of three Q-SNARE motifs (Q_{abc}) ready to bind the missing R-SNARE synaptobrevin. The SNAP-25/syntaxin acceptor complex is stabilized and prepared for synaptobrevin binding by the Sec/mUNC-18 proteins (Bryant and James, 2001; Peng and Gallwitz 2002)(see chapter 2.3.2.1.4.1).

2) **Formation of a loose *trans*-SNARE complex or docking**: The SNAP-25/syntaxin acceptor complex binds the vesicular synaptobrevin and forms a loose ternary complex (Söllner et al., 1993b; Fasshauer et al., 1998a; Fiebig et al., 1999).
3) **Transformation to a ready-to-react state or primed state**: The H_{abc} domain of syntaxin interacts tightly with the loose-*trans*-SNARE complex and prevents full entry of synaptobrevin which results in a blocked coiling. The Sec/mUNC-18 protein binds to the closed form and together with mUNC-13 pulls back the H_{abc} domain of syntaxin and opens syntaxin. This opening allows the full entry of synaptobrevin into the *trans*-SNARE complex (Richmond et al., 2001; Südhof and Rothman, 2009; Rathore et al., 2010; Ma et al., 2013). Complexin induces the N-terminal assembly of the four SNARE motifs and clamps them to a half zippered fusion competent state, hallmark of the ready-to-react state (Archer, 2002; Hobson et al., 2011). McEvans et al. speculate that parts of the regulation of primed vesicles is achieved by a steady state of blocked vesicles to ready-to-react vesicles. Tomosyn blocks priming and membrane fusion by displaying partial homology to synaptobrevin and intercalating partially into the acceptor complex rendering it inaccessible (McEwen et al., 2006).
4) **Fusion**: The rise in Ca^{2+}-concentration due to an action potential induces a conformational change in synaptotagmin, a synaptic vesicle protein, which pulls the fusion competent SNARE complex away from clamping complexin and allows a full zippering (Söllner and Rothman, 1994; Südhof, 1995; Mochida et al., 1996; Hobson et al., 2011; Krishnakumar et al., 2013). The zippering pulls the two membranes together and in the first 100 to 200 ms a nascent fusion pore of ~ 2 nm is formed. The content of the synaptic vesicle is released even before appreciable dilation of the pore occurs (Bruns and Jahn, 1995; Shi et al., 2012). The full fusion model: As the fusion pore expands, the vesicle membrane fuses with the target membrane and *cis*-SNARE complexes remain at the presynaptic membrane (Figure 2.5)(Shi et al., 2012)(for the two models of neurotransmitter release compare Figure 2.8). The kiss-and-run model: the fusion pore opens only for a short period of time, releases neurotransmitter via the fusion pose and keeps its primary constitution (Südhof, 2004; Alabi and Tsien, 2013).

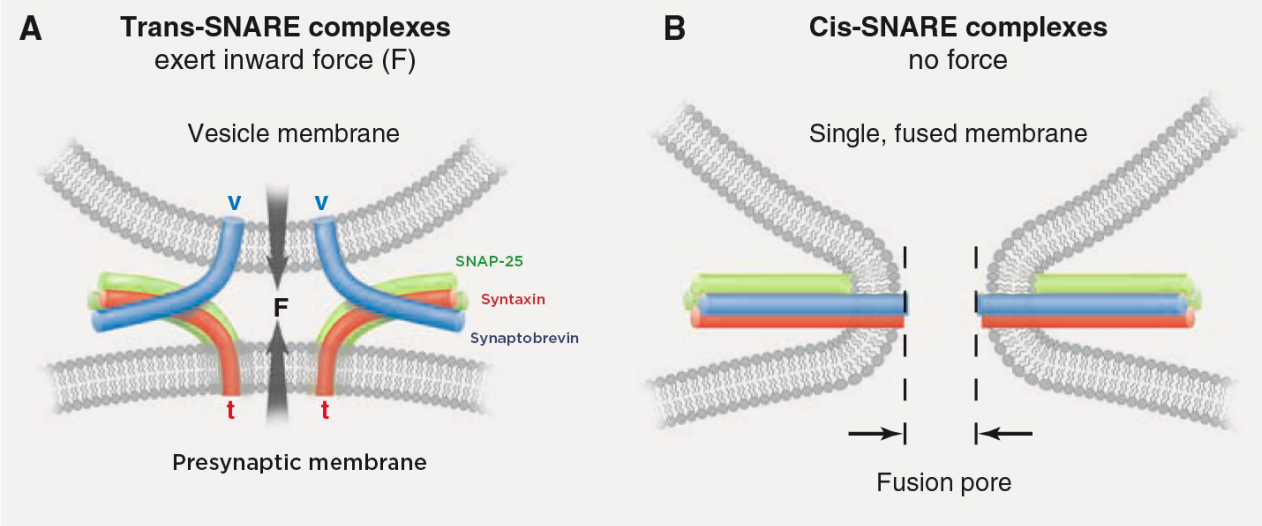

Figure 2.5 The formation of a fusion pore is energetically driven by the coiling of the SNARE motifs A The coiling of the *trans*-SNARE complex overcomes the repulsive force and pulls the two membranes together. A fusion pore opens and neurotransmitter is secreted into the synaptic cleft. **B** After formation of the fusion the low energy *cis*-SNARE complexes remain in the target membrane. v vesicle membrane, t target membrane. Taken with modifications from Südhof et al. 2009 (Südhof and Rothman, 2009)

The synchronization and timing of the fusion and the resulting neurotransmitter secretion is the key for signal transduction between neurons (Brose et al., 1992).

5) **Recycling of *cis*-complexes:** The formation of the hydrophobic layers (SNARE complex zippering/coiling) generates a lot of free energy which is invested in the fusion of the two repulsing membranes. In a later step this energy needs to be reinvested for the disassembly of the three intertwined SNARE proteins. First, up to four α-SNAP proteins bind the *cis*-SNARE complex. The α-SNAP/*cis*-SNARE complex interacts with NSF to bind and fasten the overall complex. The consumption of ATPs induces a torque to untangle the *cis*-SNARE complex which results in free SNARE subunits (Zhao et al., 2015).

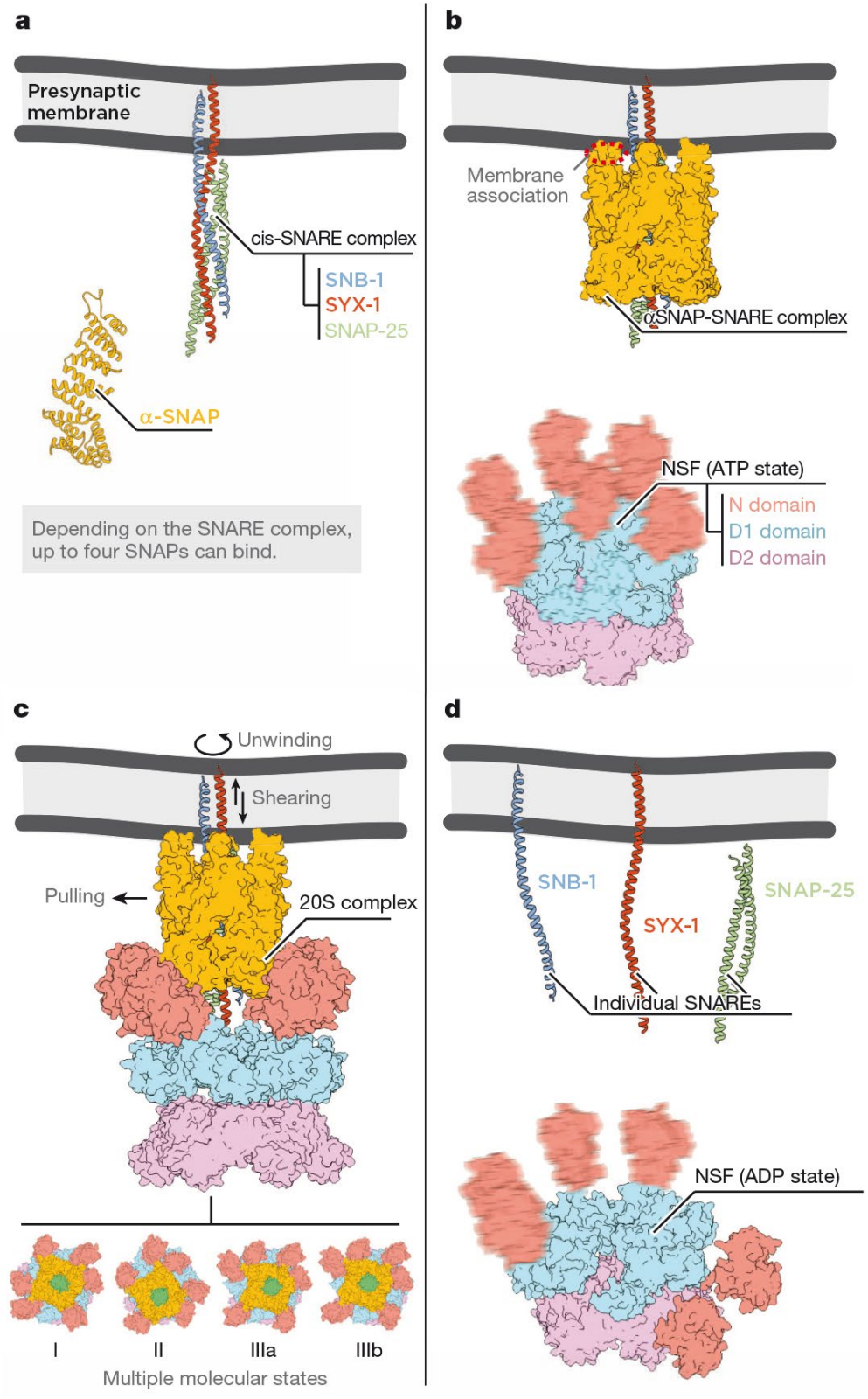

Figure 2.6 The SNARE subunits are recycled by the SNAP/NSF complex under ATP consumption A Up to four α-SNAP subunits bind to the *cis*-SNARE complex. **B** α-SNAP binds to the presynaptic membrane and prepares the complex for NSF interaction. **C** ATP consumption induces four different conformational states which unwind the zippered SNARE proteins **D** The reaction results in free SNARE subunits which are ready for another cycle of membrane fusion. Taken with modifications from Zhao et al. 2015 (Zhao et al., 2015).

The information of on how many copies of SNARE complexes are involved in the vesicle docking is inconclusive (Hua and Scheller, 2001; Keller et al., 2004; Montecucco et al., 2005): In recent publications van den Bogaart et al. describe one SNARE complex being sufficient for membrane fusion (van den Bogaart et al., 2010), whereas according to Shi et al. an efficient release requires three or more complexes (Shi et al., 2012). Fluorescent lifetime imaging microscopy and photoactivatable localization microscopy showed a clustering of SNAP-25/syntaxin acceptor complexes to small patches of 50 nm to allow a cooperative docking (Dun and Duncan, 2010; Rickman et al., 2010; Sieber et al., 2007).
In *C. elegans* the three SNAREs are *snb-1* (synaptobrevin homologue), *unc-64* (syntaxin homologue) and *ric-4* (SNAP-25 homologue). Their importance for formation and function of the SNARE complex is reflected by the lethality of the *unc-64* and *snb-1* null-alleles. A null allele of *ric-4* could not be isolated yet (Barclay et al., 2012). All loss of function (l-o-f) mutations result, due to their impaired exocytosis, in a resistance to cholinesterase inhibitors (RIC) phenotype (compare aldicarb assay chapter 3.2.4).

2.3.2.1. SNARE proteins

For a better understanding of the SNARE complex and its different roles an overview of the different participating proteins is given.

2.3.2.1.1. Synaptobrevin

Synaptobrevin (also known as **v**esicle **a**ssociated **m**embrane **p**rotein, VAMP, SNB-1 in *C. elegans*) is not only one of the most abundant proteins in the brain and within the synaptic vesicle (Walch-Solimena et al., 1995; Takamori et al., 2006), but is one of the three subunits of the SNARE complex with a size of 18,000 Dalton. Baumert and coworkers discovered synaptobrevin in 1989 during immunogold labeling of rat brain homogenate as protein co-migrating with synaptic vesicles (Baumert et al., 1989). Trimble et al. revealed three characteristic domains in synaptobrevin: a proline-rich amino terminus (*C. elegans* SNB-1 contains only two proline-residues at the N-terminus), a highly charged internal region, and a hydrophobic carboxyl-terminal transmembrane domain (Trimble et al., 1988). Synaptobrevin contains a single SNARE motif, which provides the arginine residue in the zero layer of the coiled SNARE motif (R-SNARE) (Bock et al., 2001). Fasshauer et al. and Weniger et al. discovered that first syntaxin and

SNAP-25 interact and form the SNAP-25/syntaxin acceptor complex. Subsequently, synaptobrevin binds the complex and docks the synaptic vesicle to the target membrane (Fasshauer and Margittai, 2004; Weninger et al., 2008). The transmembrane domain of synaptobrevin is not only important for the function of the SNARE complexes (Shi et al., 2012), but its transmembrane domain seems to be sufficient for fusion events (Bowen and Brunger, 2006). During further analysis of the SNARE complex assembly Fasshauer et al. showed that N-terminal truncation of SNB-1 did not show a reduction of SNARE complex formation (Fasshauer and Margittai, 2004). According to the full fusion model (versus Kiss-and-run)(Wang et al., 2003)(compare chapter 2.3.3) synaptobrevin is at the presynaptic membrane after membrane fusion and α-SNAP and NSF mediated recovery. Synaptobrevin will be recovered for SVs either by endosome generating endocytosis (Watanabe et al., 2013) or clathrin-mediated endocytosis (Watanabe et al., 2014); compare chapter 2.3.3) (Südhof, 2004). Surprisingly, the localization of synaptobrevin at the plasma membrane is around 30% shown by a GFP fused synaptobrevin (Dittman and Kaplan, 2006). Presynaptic surface synaptobrevin is in equilibrium with non-synaptic axonal surface synaptobrevin and alterations in secretion result in a change of this steady state (Dittman and Kaplan, 2006).

2.3.2.1.2. UNC-64/syntaxin

The structure of syntaxin (UNC-64 in *C. elegans*) can be divided into four domains: 1) The N-terminus with three alpha helices (H_a, H_b and H_b; or altogether H_{abc}), 2) A linker region with 44 AA, 3) the SNARE motif responsible for the SNARE complex formation, and 4) the transmembrane region for anchoring syntaxin in the presynaptic membrane (Dulubova et al., 1999). The N-terminus of syntaxin is known to interact with synaptotagmin, a synaptic vesicle protein, and the modulator proteins mUnc-13 and mUnc-18 (Dulubova et al., 1999; Toonen and Verhage, 2003).

Syntaxin has two conformations: open and closed with each conformation being important for the different steps of SV fusion. The closed conformation is composed of the three N-terminal helices, the linker region and the N-terminal half of the SNARE motif (Dulubova et al., 1999).

Hata et al. co-purified mUNC-18 together with a GST-syntaxin fusion, demonstrating the strong interaction between both proteins (Hata et al., 1993). mUNC-18 binds the closed

N-terminus of syntaxin (Dulubova et al., 2003; Toonen and Verhage, 2003; Weimer et al., 2003) and locks the partially coiled SNARE complex (McEwen et al., 2006; Gracheva et al., 2010). After a Ca^{2+} burst mUNC-13 replaces mUNC-18 from syntaxin-interaction and changes the conformation to an "open" syntaxin. This exposes the syntaxin helix fully to synaptobrevin and allows a complete zippering of syntaxin (Dulubova et al., 1999; Richmond et al., 2001; Fasshauer and Margittai, 2004; Stevens et al., 2005; Hammarlund et al., 2007; Barclay et al., 2012; Betke et al., 2012). In *C. elegans* the syntaxin orthologue is called UNC-64 – a relation to the **UNC**oordinated phenotype of strains with a mutated gene (Brenner, 1974; Saifee et al., 1998).

2.3.2.1.3. RIC-4/SNAP-25

SNAP-25 stands for **S**y**N**aptosomal-**A**ssociated **P**rotein of 25 kDa. SNAP-25 can be partitioned into three regions: an unstructured linker region not taking part in complex formation, but anchoring SNAP-25 via a palmitoyl side chain to the plasma membrane, as well as an N-terminal and a C-terminal SNARE motif responsible for SNARE complex formation during exocytosis (Hess et al., 1992; Fasshauer et al., 1998a; Sutton et al., 1998). Binary complexes of syntaxin and SNAP-25 form the already mentioned SNAP-25/syntaxin acceptor complex with 17 surface salt bridges. The functional importance of the C-terminal SNARE motif was shown by Chen et al.. The authors removed the C-terminal SNARE motif by treatment with Botulinum toxin. Even though they still detected assembled SNARE complexes, exocytosis was completely inhibited until administration of recombinant SNAP-25 SNARE motif (Chen et al., 2001).

CD analysis showed that the C-terminal SNARE motif undergoes a structural change upon binding to syntaxin (Fasshauer et al., 1997; Fasshauer and Margittai, 2004), which seems to be the rate limiting step for synaptobrevin binding.

The *C. elegans* orthologue to SNAP-25 has been named RIC-4, as a mutation renders the nematode **R**esistant to **I**nhibitors of **C**holinesterase as shown in an Aldicarb assay (as described in chapter 3.2.4)(Nguyen et al., 1995).

2.3.2.1.4. SNARE interaction partners

As the discovery of new interaction partners of the SNARE complex is the aim of this thesis, a selection of established interaction partners is introduced.

2.3.2.1.4.1. Sec1/mUNC-18/UNC-18 proteins

The Sec1/mUNC-18 proteins (SM proteins) are a highly conserved gene family (around 1800 nucleotides) related to vesicle trafficking and fusion. It was demonstrated by Archer et al. that *in vitro* SNARE proteins (SNAP-25, syntaxin, synaptobrevin) in high concentrations are sufficient for fusion of two membranes (Archer, 2002), but *in vivo* with its lower concentrations of SNARE the vesicle fusion depends also on SM proteins (Verhage et al., 2000; Südhof and Rothman, 2009; Shen et al., 2015). Prior to exocytosis the SM protein folds into an arch like structure binding first activating/opening syntaxin and later binding to the fully formed SNARE complex catalyzing its zippering (Südhof and Rothman, 2009; Rathore et al., 2010). A uniform role of the SM proteins is unknown (Toonen and Verhage, 2003; Südhof and Rothman, 2009): One proposed role of the SM proteins is embracing the three helices of the H_{abc} and one helix of the SNARE domain which holds syntaxin in a closed position and inhibits the SNARE coiling (Hata et al., 1993; Toonen and Verhage, 2003; Südhof and Rothman, 2009). But deletion of SM proteins does not lead to an increase of exocytosis - it reduces transmission to a larger extent than synaptobrevin removal (Schoch et al., 2001). This indicated the existence of a second, fusion inducing, role of SM proteins. A possible mechanism is the interaction with the H_{abc} domain, leading to a loosening of the SNAP-25/syntaxin acceptor complex for synaptobrevin intercalation (Bryant and James, 2001; Peng and Gallwitz 2002; Weimer et al., 2003; Rathore et al., 2010). Mutagenesis studies revealed that mUNC-18 binding sites are on R and Q-SNAREs hinting to a uniform SNARE interaction (Dulubova et al., 2007). A different role of SM proteins was proposed by Südhof and Rothman. They suggested the positive effect of SM proteins for synaptic fusion by forcing the SNAREs into a specific conformation, inducing ring-like arrangements and removing *trans*-SNARE complexes from the potential contact point of the two membranes (Südhof and Rothman, 2009; Dulubova et al., 2007; Rathore et al., 2010). The name mUNC-18 originates from its severe locomotory defect (**unc**oordinated) discovered in *C. elegans* and its **m**ammalian homologue (Brenner, 1974; Hata et al., 1993).

2.3.2.1.4.2. Complexin

Four domains have been identified in complexin influencing exocytosis: a) the central helix with a SNARE motif, b) the N- and c) C-terminal domains which promote fusion,

and d) the accessory helix which binds assembled SNARE complexes and inhibits fusion (Weninger, 2011). The role of complexin is still unclear due to the diverse set of knock-out phenotypes. *In vitro* the addition of complexin arrests fusion of SNARE loaded liposomes at the step of hemi fusion (Schaub et al., 2006), but deletion of complexin in mice decreases synaptic transmission (Xue et al., 2010). The complexin accessory and central helix has a high affinity to assembled SNAREs, which reflects a role after docking (Barclay et al., 2012) or an accelerating role in exocytosis via *trans*-SNARE complex stabilization (Archer, 2002). The complexin knock-out has the same phenotype as synaptotagmin deletion (reduction of synchronous, but not of asynchronous release and PSPs), so complexin presumably activates the SNARE complex via synaptotagmin interaction (Reim et al., 2001). A different role proposed by Li et al. is that complexin first facilitates the zippering by activating the N-terminal assembly, then clamping it to a half-zippered fusion incompetent state by blocking the C-terminal assembly (Li et al., 2011).

2.3.2.1.4.3. Tomosyn

Tomosyn, a protein of 130 kDa, consists of an N-terminal domain with WD40 repeats and a C-terminus similar to the SNARE motif of synaptobrevin (Hatsuzawa et al., 2003). This SNARE motif can form a four helix bundle with syntaxin and SNAP-25, competing with synaptobrevin (Hatsuzawa et al., 2003; McEwen et al., 2006), and thus blocking fusion events. The importance of the presence of full-length tomosyn was shown in a tomosyn knock-down by Burdina et al. in 2011. These authors demonstrated that neither expression of N- or C-terminal domains alone, nor coexpression of these fragments displayed the same phenotype as expression of the full length tomosyn (negatively regulating synaptic transmission)(Burdina et al., 2011). Tomosyn deletion leads to an increased exocytosis, more primed vesicles and a higher abundance of UNC-13 (McEwen et al., 2006). It was speculated by McEwan et al. that the amount of primed vesicles is regulated by a steady state between SNARE complexes either blocked by tomosyn or opened by UNC-13 (McEwen et al., 2006).

2.3.2.1.5. mUNC-13/UNC-13

UNC-13 plays an essential role in the preparation of SNARE complexes for priming and thus also for fusion of synaptic vesicles. The deletion of UNC-13 leads to a strong

reduction of synaptic transmission and highly reduced readily releasable pool (RRP) (the different vesicle pools are described in chapter 2.3.3)(Aravamudan et al., 1999; Richmond et al., 2001; Weimer et al., 2006). UNC-13 interacts with the H_{abc} domain of syntaxin, removes UNC-18 binding to the closed form of syntaxin and allows a transformation to an open conformation of syntaxin (Richmond and Broadie, 2002; McEwen et al., 2006). *C. elegans unc-13* mutants exhibit highly reduced exocytosis rates and therefore display a RIC phenotype (Miller et al., 1996). The opening role of UNC-13 to the syntaxin/UNC-64 complex could be demonstrated in *C. elegans:* the synaptic transmission deficient UNC-13 knock-out displayed synaptic transmission after introduction of a constitutively open form of UNC-64 (Dulubova et al., 1999; Richmond et al., 2001; Hammarlund et al., 2007). Interestingly, Madison et al. could demonstrate that mutated UNC-13, which could not interact with syntaxin, still allowed priming, but abolished normal synaptic fusion (Madison et al., 2005; McEwen et al., 2006). So the sole role of UNC-13 for priming is still debated.

2.3.3. The synaptic vesicle

The synaptic vesicle (SV) is a neurotransmitter filled membranous sphere with a diameter of 29 - 60 nm, depending on the species and the neuron type (whereas Kittelmann et al. found during their analysis of around 25,000 SVs uniform vesicle sizes of 33 – 34 nm; personal communication with Alexander Gottschalk) (Hu et al., 2008; Qu et al., 2009; Stigloher et al., 2011; Stevens et al., 2012; Kittelmann et al., 2013) containing a multitude of integral and peripheral proteins (Takamori et al., 2006; Alabi and Tsien, 2013). Synaptic vesicle functions are concentrating, storing, and organizing neurotransmitters as well as enabling their regulated secretion. The synaptic vesicles are generated either via clathrin mediated budding from endosomes (these endosomes originate from endocytosis of presynaptic plasma membrane (Watanabe et al., 2014)(Figure 2.7) or by direct recycling from the plasma membrane after SV/plasma membrane fusion (Rey et al., 2015). Malfunctional and lost synaptic vesicle proteins are replenished via the endoplasmatic reticulum and the *trans* Golgi network. The vesicles are refilled with their appropriate cargo via transporters like vesicular acetylcholine transporter or GABA transporter. The vesicle organization differentiates between three distinct vesicle pools: the readily releasable pool (RRP) a small pool of around 1 – 2 % physically docked vesicles at the active zone, a recycling pool with around 10 - 20 % vesicles to replenish the RRP and a large reserve pool representing 80 – 90 % of vesicles for filling up losses in the recycling pool (Rizzoli and Betz, 2005; Denker and Rizzoli, 2010; Denker et al., 2011). The different pools are classified according to their stimulation response: The readily releasable pool vesicles secrete their cargo instantly after a brief Ca^{2+}influx, under mild stimulation. The recycling pool refreshes the RRP and mobilizes upon physiological stimulation and whereas the reserve pool is only released after strong or high frequency stimulation (Fernández-Busnadiego et al., 2010; Denker and Rizzoli, 2010).

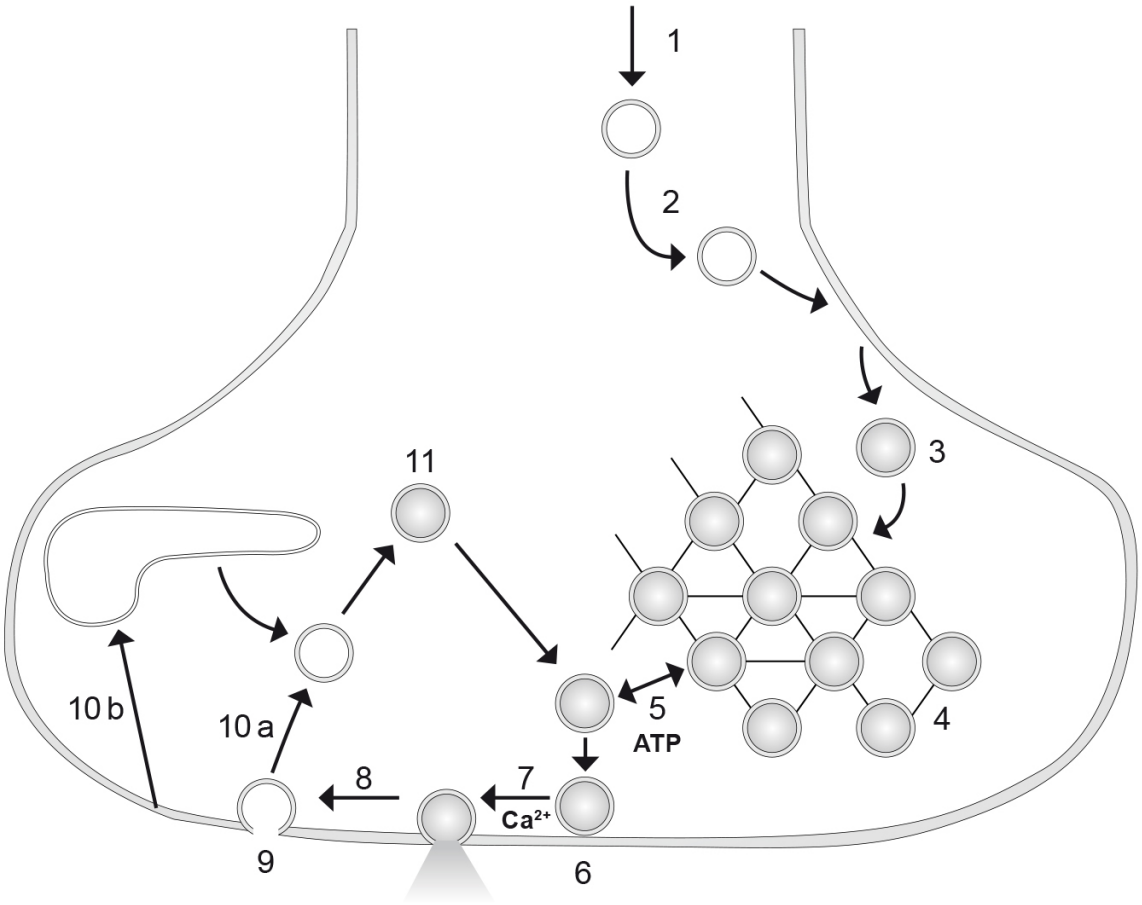

Figure 2.7 The synaptic vesicle cycle After synthesis in the soma, synaptic vesicle precursors are transported via motor proteins to the synapse (1), followed by a maturation step in which vesicle proteins, specific lipids and neurotransmitter accumulate via intervesicle fusion events and endocytosis (2 to 3), and binding to the actin cytoskeleton representing the reserve pool (4). Removal of the vesicle from the reserve pool necessitates ATP (5). Docking and priming to the AZ membrane require formation of the *trans*-SNARE complex (6) and allow, after a rise in Ca^{2+}-concentration, the opening of the fusion pore (7) and the release of the vesicle content into the synaptic cleft (8). After exocytosis the empty vesicle (9) is recycled either by single vesicle recycling (10a) (Rey et al., 2015) or (10b) via the endosomal pathway via endocytosis and clathrin mediated budding (Watanabe et al., 2013; Watanabe et al., 2014). The neurotransmitter are refilled by corresponding transport proteins powered by a proton gradient (11). Adapted from Lin et al. 2000 (Richard C. Lin and Richard H. Scheller, 2000)

Synaptic vesicles in the reserve pool cannot traverse freely in the presynaptic cytosol, but are tightly linked to the actin cytoskeleton via synapsin. A release into the RRP requires ATP and synapsin phosphorylation (Richard C. Lin and Richard H. Scheller, 2000; Denker et al., 2011). Analysis of high resolution electron microscopy images revealed, that the vesicles in the RRP are docked at a very low or no measureable distance to the presynaptic membrane (Verhage et al., 2000; Denker et al., 2011; Rey et al., 2015). This

electron dense area is called the active zone (see Figure 2.2)(Weimer et al., 2003; Fernández-Busnadiego et al., 2010).

As already mentioned in chapter 2.1: To render a synaptic vesicle fusion competent two important-steps can be distinguished: first docking, followed by a priming step. Docking is a protein mediated binding of the vesicle to the presynaptic membrane and priming via transformational changes prepares the vesicle to release its content upon Ca^{2+} influx (Weimer et al., 2003; Südhof, 2004)(compare chapter 2.3.21)). Two models of the opening of the fusion pore (compare chapter 2.3.1) are discussed: 1) full collapse fusion (FF), in which the vesicle passes completely into the presynaptic plasma membrane or the 2) the kiss-and-run model (KR), in which the fusion pore is only opened for a fraction of time and is resealed later on (Figure 2.8A). The FF requires the former vesicle membrane with the different synaptic vesicle proteins to be endocytosed with the help of actin and dynamin (Watanabe et al., 2013)(Figure 2.8B). After a kiss-and-run (KR) process all the vesicle proteins (except fusion complex proteins) remain on the vesicle and the vesicle detaches from the presynaptic membrane (Südhof, 2004; Alabi and Tsien, 2013). In both mechanisms the newly formed vesicles are filled with protons by the vesicular ATPase for an electrochemical potential to power the neurotransmitter transport into the vesicle. Vesicles after FF require fusion with endosomes to obtain essential SV proteins (Südhof, 2004). The model of kiss-and-run is still debated. On the one hand the work of Watanabe et al. shows the ultrafast invagination of endosomes (50 ms) and clathrin-mediated SV generation (5 - 6 seconds after stimulation) rendering the rather slow process of kiss-and-run unlikely. The authors could not observe any “kiss-and-run vesicles”, but admit the difficulty of discovering 2 nm fusion pores in 40 nm thick slices (Watanabe et al., 2013; Watanabe et al., 2014). On the other hand Bretou et al. demonstrated in gut neuroendocrine tumor cells the role of Cdc42, a Rho GTPase, as a regulator of membrane tension regulating the fusion manner between full fusion and kiss-and-run. The authors speculate a Cdc42-regulated pore opening according to the cargo (Bretou et al., 2014). And even Watanbe speculate about the possibility of a parallel kiss-and-run for plasma membrane recovery demands (Watanabe, 2015).

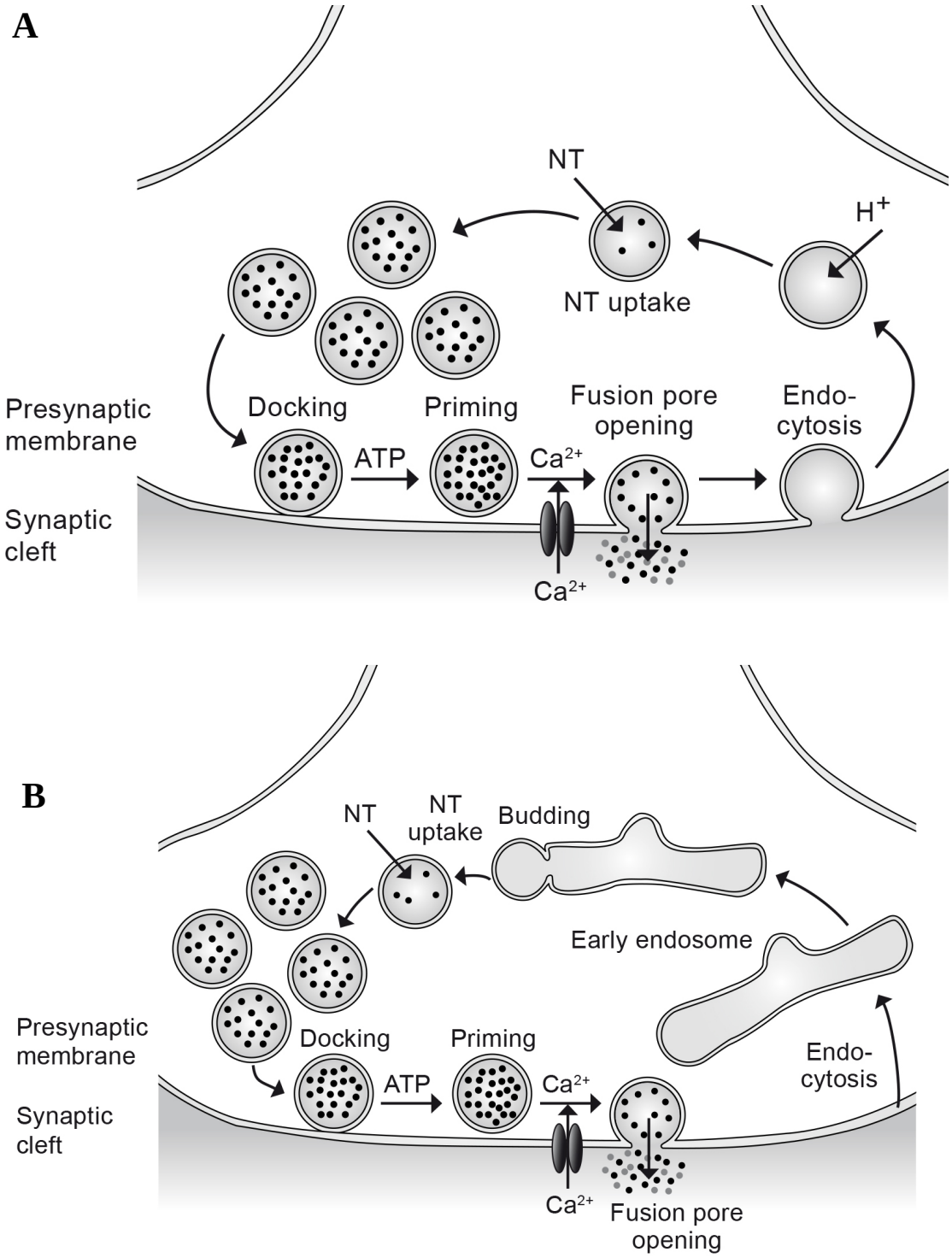

Figure 2.8 The two models of synaptic vesicle fusion and recycling A In the vesicle reuse or the "kiss-and-run" model the fusion pore opens only for a short period of time and keeps its primary constitution. B The vesicle undergoes a full collapse and the vesicle proteome and lipidome mix with the presynaptic membrane. After endocytosis of an endosome a recycling step via the clathrin-mediated budding resupplies the vesicle with the appropriate proteins and lipids. Taken with modifications from Südhof 2004 (Südhof, 2004).

The synaptic vesicle proteins fulfill different functions throughout the SV life cycle (Figure 2.7): transport to the synapse, interaction with the cytoskeleton/vesicle organization network, acidification, neurotransmitter uptake, docking, priming, exo- and endocytosis and vesicle recycling. A large amount of data has been accumulated to identify and characterize proteins associated with these processes (Baumert et al., 1989; Bennett et al., 1992; Lin and Scheller, 2000; Südhof, 2004; Burré et al., 2006; Takamori et al., 2006; Boyken et al., 2013). In addition, several proteome analyses have been performed to identify SV proteins and proteins involved in SV mechanisms (Morciano et al., 2005; Blondeau et al., 2004; Burré et al., 2006; Takamori et al., 2006).

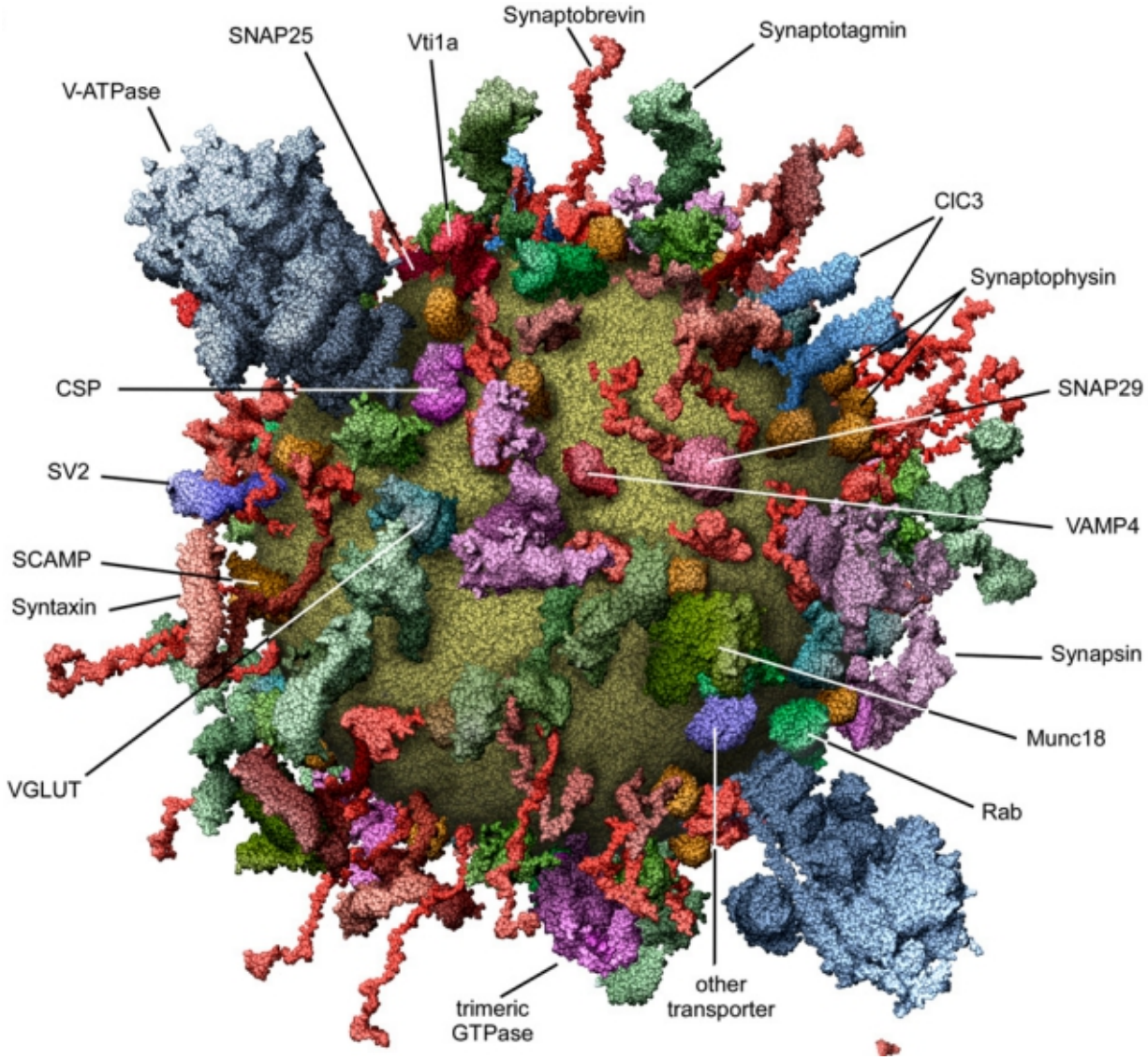

Figure 2.9 The molecular model of synaptic vesicle The model is based on the space filling models of the appropriate proteins and lipids with approximately 2/3 of the abundant proteins. The model visualizes the high protein content and complex nature of the synaptic vesicle. Taken from Takamori et al. 2006 (Takamori et al., 2006)

The importance of identification of interaction partners of the synaptic vesicle/SNARE machinery is still high (Morciano et al., 2005). Analyzing these complexes in *C. elegans* would not only allow us to identify new candidates, but draw conclusions of their function and possible mode of action.

2.3.3.1. Synaptic Vesicle Proteins

Although many proteins are essential during the SV life cycle, a focus is set on some proteins according to their importance in this work.

2.3.3.1.1. Synaptobrevin

Synaptobrevin has already been described in chapter 2.3.2.1.1.

2.3.3.1.2. Tetraspan vesicle membrane proteins

Tetraspan vesicle membrane proteins can be grouped into physins, gyrins and secretory carrier-associated membrane proteins (Hübner et al., 2002). As synaptophysin is absent in *C. elegans* neurons and its orthologue synaptogyrin (SNG-1) is expressed in all GABAergic neurons and presumably in all other neurons (Nonet, 1999; Abraham et al., 2011) its regulatory function is probably assigned to synaptogyrin (Nonet, 1999; Hübner et al., 2002; Abraham et al., 2011). Although this protein family is, after synaptobrevin, one of the most abundant synaptic vesicle proteins (7 % of SV protein consist of synaptophysin)(Takamori et al., 2006; McMahon et al., 1996), a deletion of synaptophysins in mice and synaptogyrin (SNG-1) in *C. elegans* does not lead to any lethal effects (Eshkind and Leube, 1995; McMahon et al., 1996; Abraham et al., 2006); Abraham et al., 2011). The precise role of synaptophysin and synaptogyrin is still under debate (Edelmann et al., 1995; Abraham et al., 2011). Edelmann et al. propose a regulatory role of the tetraspan vesicle membrane protein: it antagonizes the syntaxin-interaction of synaptobrevin which results in an inhibited exocytosis (Edelmann et al., 1995). However, Abraham et al. could not determine a singular function which can be addressed to synaptogyrin - even after broad analysis of the function of SNG-1 in *C. elegans*. Experimental data show that up or down regulation resulted in a similarly altered response in drug assays (Abraham et al., 2011).

2.3.3.1.3. Synaptotagmin

100 µs after the arrival of an action potential neurotransmitters are secreted into the synaptic cleft (Südhof, 2004). This is the result of a ready-to-react state of the SNARE complex of the readily releasable pool (see chapter 2.3.1) The high energy state of the primed SNARE complex requires a proper control mechanism (Kozlovsky and Kozlov, 2002), because an uncontrolled secretion of neurotransmitter would render regular neuronal function impossible (Brose et al., 1992). This regulation and synchronization is achieved by Ca^{2+} induced conformational changes of the synaptic vesicle protein synaptotagmin. Synaptotagmins are a family of calcium binding proteins, characterized by two cytoplasmic domains: C2A and C2B (Hui et al., 2011; Betke et al., 2012). After docking of SV to the presynaptic membrane the half-zippered *cis*-SNARE complex is formed by arresting the SNARE zippering with the help of an accessory helix of complexin (see chapter 2.3.2.1.4.2)(Hobson et al., 2011; Krishnakumar et al., 2013). The binding of synaptotagmin to the partially formed complexin-SNARE-complex is mediated by an interaction with SNAP-25 (Wang et al., 2014). Upon a rise in the Ca^{2+}-concentration synaptotagmin changes its conformation and inserts itself into the nearest lipid bilayer. Thereby synaptotagmin pulls the complexin clamp off the SNARE complex and allows the full zippering of the SNARE complex (Krishnakumar et al., 2013). In addition to the release of the SNARE complex the interaction of synaptotagmin with the presynaptic membrane induces a positive curvature “below” the SNARE complex and reduces the distance and energy barrier between the two membranes even more (Martens et al., 2007). The importance of this protein is shown by its null mutants in *C. elegans.* These animals are slow growing, small, severely uncoordinated and **r**esistant **i**n **c**holinesterase inhibitors (RIC) (Barclay et al., 2012).

2.4. Purifications of synaptic proteins in other species

2.4.1. Purification of synaptic vesicles

Many examples of purifications of synaptic proteins in different species have already been reported:

An enrichment of the active zone of marine ray with microbeads has been performed already in 1982 (Miljanich et al., 1982). Rabbit anti-SV serum was added to prepurified

synaptosomes, followed by incubation with polyacrylamide beads coated with anti-rabbit antibodies. After lysis of the bound synaptosomes the putative presynaptic plasma membrane was obtained and analyzed. In the light of the past 30 years, the analysis of synaptosome lysate is quite up-to date as many other groups still apply similar purification approaches (Takamori et al., 2006; Morciano et al., 2009).

A different purification procedure used a cation exchange to extract and identify the 39 kDa subunit of the vacuolar H^+-ATPase (Siebert et al., 1994). Rat brain synaptic plasma membranes were treated with Triton X-100 to generate a crude extract of synaptosomal fractions. This extract was enriched by a passage of a cation exchange column at pH 5.5. This was followed by a carbohydrate binding lentil-lectine column purification step. An interaction or tethering of the 39 kDa subunit of the vacuolar H^+-ATPase to synaptophysin has been discovered. Siebert et al. used detergent for solubilization and enrichment of a synaptic vesicle plasma membrane protein.

The rat synaptic vesicle proteome has been analyzed by the laboratories of Prof. Volknandt and Prof. Zimmermann. Rat brains were extracted and homogenized. The homogenate was differentially centrifuged and prepurified using a Percoll gradient to generate synaptosomes. The synaptosomes were osmotically lyzed and SVs were concentrated with the help of a sucrose gradient and magnetic beads coated with antibodies against synaptic vesicle glycoprotein 2. The obtained SV proteins were analyzed via three different methods: A) The proteins were analyzed after detergent elution via two dimensional BAC (benzyl dimethyl-n-hexadecylammonium chloride)/SDS (Sodium DodecylSulphate) gel electrophoresis followed by MALDI (Matrix assisted laser desorption ionization)-TOF (Time of flight)/mass spectrometry (MS) (Morciano et al., 2005). B) After detergent solubilization the proteins were analyzed via three different PAGE systems: SDS-PAGE followed by ESI (Electrospray ionization)/MS, two dimensionally SDS/SDS followed by MALDI-TOF/MS and two dimensional BAC/SDS gel electrophoresis followed by MALDI-TOF/MS (Burré et al., 2006) and C) Different magnetobeads and the SV protein elution from beads was combined with a phase separation based on the behavior of Triton X-114 and PEG-6000 combined with detergent and application of methanol/chloroform (Burré et al., 2007). The authors discovered a large number of proteins in the synaptic vesicles, displaying the different SV species and corresponding proteins. Interestingly the different gel analyses discovered, in addition to mutual findings, a different subset of proteins. Only 19% of all

185 novel proteins were discovered in each purification setting. Increasing this set of purification methods 240 proteins related to the active zone were discovered using the docked vesicle pool from 2005 by Morciano et al. but applying 1d SDS PAGE and ESI/MS (Morciano et al., 2009).

In 2006 Takamori et al. analyzed a rather crude purification of SVs analog to purification methods from 1976 or 1983 respectively (Nagy et al., 1976; Huttner et al., 1983) and therefore called the publication "Molecular Anatomy of a Trafficking Organelle" (Takamori et al., 2006). Rat brains were homogenized and differentially centrifuged to generate synaptosomes (in contrast to Percoll prepurifications by Miljanich, Burré and Morciano) (Miljanich et al., 1982; Burré et al., 2006; Morciano et al., 2009). These synaptosomes were osmotically lyzed and the lysate was centrifuged. The resuspended pellet was applied to a glucose gradient and the SV containing zone was addressed to a size exclusion chromatography. The fraction with vesicles between 40 – 50 nm was collected and analyzed applying 16-BAC/SDS and as well as a simple SDS analysis followed by liquid chromatography-tandem mass spectrometry (LC-MS/MS) analysis (Takamori et al., 2006).

They identified 410 different proteins with more than 80 different integral proteins, while only around 40 of these were known as SV residents, resulting in a huge set of newly identified proteins (Takamori et al., 2006). Next to SNARE proteins a multitude of Rab proteins was discovered. Rab proteins are small monomeric GTPases commonly responsible for organelle sorting. In addition, they discovered peripheral proteins not obviously linked to SV function e.g. signaling pathways, cytoskeleton proteins, metabolic enzymes and chaperones. Interestingly, they also discovered RNA processing and ribosomal proteins (Takamori et al., 2006), which could hint to a stronger link and interaction of synaptic vesicles to protein synthesis at the synapse (Martin et al., 1998; Rolls, 2002). If the high complexity of the discovered proteins is based on the sensitive detection arrangement or heterogeneity of the vesicle sample, due to the lack of an SV specific immunological purification step, is at debate. In their work Takamori et al. quantified the abundance of some of the known proteins via western or dot blot analysis and analyzed the protein/lipid and protein/protein ratio proposing a model for a synaptic vesicle (Figure 2.9). The presence of SNAP-25 and syntaxin on the vesicle is not commented by the authors, but could either be an artifact due to rather crude purification (syntaxin and SNAP-25 on a vesicle would interact with synaptobrevin and would

probably form an cis-SNARE complex) or non-specifically incorporated during endocytosis.

2.4.2. Purification of presynaptic membranes

Boyken at al. isolated synaptic vesicles which were docked to the presynaptic membrane. Synaptosomes were prepared by homogenization, differential centrifugation and a Ficoll gradient. These synaptosomes were briefly treated with trypsin to remove postsynaptic membranes. The treated synaptosomes were osmotically lysed and the docked synaptic vesicles were separated from free ones by a sucrose gradient. In a next step beads coated with antibodies against synaptophysin were used to generate a purified SV fraction. The docked and undocked SV fractions were analyzed and 493 proteins were identified. In a second step the microbeads were not covered with anti-synaptophysin, but with antibodies either against VGLUT1 or VGAT for differentiation between glutamatergic and GABAergic docked SV. The samples were labeled with isobaric tags according to their species and then MS analyzed. Hereby comparisons and quantification of the docked to undocked proteomes and the difference between the different neuron species were performed (Boyken et al., 2013). The most abundant set of proteins in the docked fraction remains the synaptic vesicle proteins – surprisingly the presynaptic plasma membrane SNAREs syntaxin and SNAP-25 were only 3- to 6-fold enriched compared to undocked vesicles. In addition, Boyken et al. discovered only small differences between glutamatergic and GABAergic vesicles, demonstrating the identical sorting, docking and fusion machinery. Although several purifications already analyzed the vesicle proteome 30 uncharacterized proteins were identified in this recent work, and new insights of the small differences between glutamatergic and GABAergic docking complexes were gained.

In all mentioned systems a tissue of high neuron content resulting in a large quantity and concentration of synaptic vesicles and docking complexes could be used and thus differential centrifugation steps and single step purifications with antibody coated beads could be applied.

2.5. **Advantages of *Caenorhabditis elegans* as neurological model organism**

The maintenance of *C. elegans* has many advantages: It is non-pathogenic, has a invariant cell number and fate, a small size (1 mm), a short life span (3 days), is self-fertilizing and can be frozen. A multitude of powerful genetic and transgenic strategies are available (including simple gene transfer by strain crossing) and allows easy handling (Berezikov et al., 2004; Evans, 2006; Schafer, 2006; Stiernagle, 2006; Barclay et al., 2012). The maintenance of *C. elegans* has not changed since the first publication of Sydney Brenner (Brenner, 1974). Especially in the field of neurobiology this nematode has been widely used. Inducing mutations in a genetic screen allowed the identification and mapping of genes with implications in the nervous system (Brenner, 1974). With the help of electron micrographs of 50 nm slices and the resulting images a full neuronal connectome and their respective locations within the nematode body could be identified. On this basis all 302 neurons and their resulting connections could be reconstructed in a wiring diagram (Sulston et al., 1983; White et al., 1986). This wiring diagram has been recently updated with a more comprehensive and sophisticated analysis (Varshney et al., 2011). It could be demonstrated that many genes in the neurological context are highly conserved (Kenyon, 1988; Bergmann, 1998; Richmond, 2006). Many neuronal genes, like the already mentioned SNARE interaction partner mUNC-13 and mUNC-18, were discovered as **unc**oordinated mutants in *C. elegans* (Brenner, 1974; Hata et al., 1993; Brose et al., 2000). Mutations and alterations in the expression of neuronal proteins can be analyzed and characterized by an ever-expanding number of simple phenotypic assays (Mahoney et al., 2006). The existence of males as carrier of a specific genetic allele allows the simple combination of two traits in the cross-progeny (Edgley et al., 2006).

2.5.1. The nervous system of C. elegans

The nervous system follows a simple bilaterally symmetric body plan with 302 neurons for the hermaphrodite (the male, 383). Almost all *C. elegans* neurons display a simple monopolar or sometimes a bipolar morphology with mostly unbranched processes. These processes follow nearly identical trajectories in each animal with most neurons being arranged in a series of fiber bundles along the hypodermal ridges. Each neuron was systematically named according to its location and function. The neurons were classified into 118 different classes, with 1 to 13 neurons in each class – being coupled to anterior

and posterior ganglions (White et al., 1976). The center of the nervous system, comprising around half of the neurons, is the nerve ring. As this nerve ring, surrounded by the central neuropil, contains the processes of almost all interneurons and the axons of most of the sensory neurons, it can be called the brain of *C. elegans* (White et al., 1986). The muscles in the head are connected to the motor neurons of the nerve ring, whereas the muscles in the remainder of the body are innerved by a set of motor neurons in a longitudal fiber bundle - the ventral nerve cord (White et al., 1976). Alongside this ventral cord many cell bodies of excitatory and inhibitory motoneurons are positioned which innervate the dorsal and ventral muscle cells (McIntire et al., 1997)

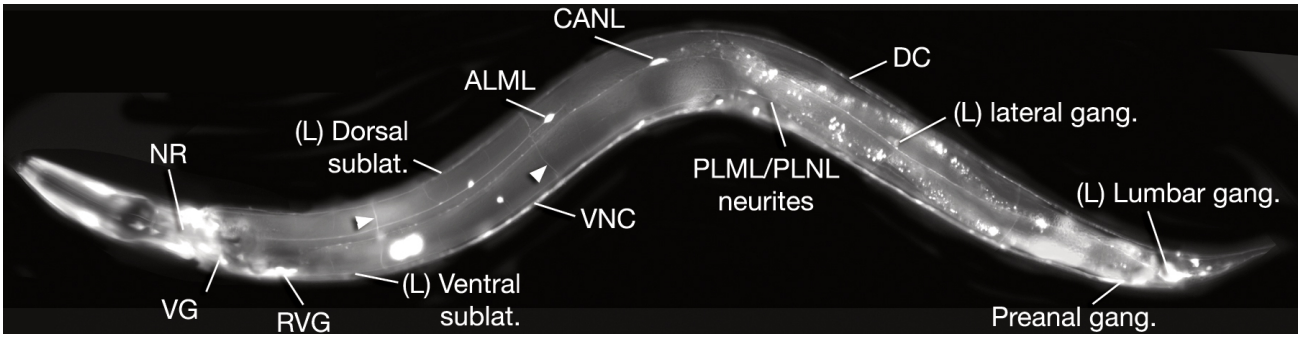

Figure 2.10 The nervous system of *C. elegans* The nervous system of *C. elegans* comprehends 302 neurons and spans the whole body. The nerve ring (NR), which encircles the pharynx, is a complex circuitry of different interconnecting neurons governing most aspects of behavior. The nerve ring is connected to several head ganglia including the retrovesicular ganglion (RVG) and ventral ganglion (VG). The sublateral cords (dorsal and ventral) lie inside a thin layer of hypodermis adjacent to body wall muscles. The ventral nerve cord (VNC) bundles a large number of motoneurons neurons controlling the undulatory locomotion. The dorsal cord (DC), located in the dorsal hypodermal ridge, consists of motor neuron axons originating from their soma in the VNC via commissures (arrowheads) to innervate muscles on the dorsal side. ALM and PLM are the lateral touch receptor neurons (ALM in the anterior part, PLM in the posterior part), which run on the peripheral side of the hypodermis. The canal-associated neurons (CAN) run close to the seam and the excretory canal between the hypodermis and pseudocoelom. The second largest collection (after the nerve ring) of neuronal cell bodies can be found in the tail ganglia, including the lumbar ganglion and the preanal ganglion. Magnification, 400x. Strain marker: *unc-119*::GFP. (Strain source: CGC.) Taken from WormAtlas.org (Altun et al., 2011).

The neurons can be classified in addition to their functions: sensory receptor neurons, motoneurons and interneurons. Sensory neurons can be recognized by their sensilla facing to the environment or inside of the worm. An exception are the Mec neurons, which employ mechanosensitve dendrites for information collection. Interneurons are diverse in their organization but are by definition positioned between sensory and

motoneurons. They sometimes exhibit processes with a larger diameter and unusual increase number of synaptic connections. All neurons, which are not classified as sensory neurons or motoneurons are interneurons. Each motoneuron connects only to a specific muscle population forming a neuromuscular junction. *C. elegans* neurons are often highly connected, and in its entirety, the nervous system contains around 5000 synapses, 2000 neuromuscular junctions and 600 gap junctions (White et al., 1986). At these synapses almost all known vertebrate neurotransmitters are utilized, a multitude of conserved, as well as invertebrate-specific neuropeptides (Brownlee and Fairweather, 1999). Despite its rather simple nervous system, complex behaviors like adaption to environmental changes, tactile behaviors, a mating behavior, and even simple forms of learning can be observed in *C. elegans* (Bono, 2003; Bono and Villu Maricq, 2005; Giles et al., 2005).The highest concentration of synapses is found in the nerve ring, as well as in the ventral and dorsal cords. Synapses are generally *en passent*, i.e. formed along the neurite between adjacent processes where pre-synaptic specializations are found. These synapses are characterized by an electron-rich presynaptic density around 50 nm wide and 100 to 400 nm long (see active zone, Figure 2.1) with docked synaptic vesicles (Weimer, 2003; Jin, 2005; Margeta et al., 2008). Electron microscopic analysis of synapses displayed little or no specialization at the area of connection. So unlike in vertebrates, proximity seems to be the major determinant of synaptic communication and the synaptic cleft generally appears, with an exception to pre and post-synaptic densities, as a regular membrane of the axon (Altun and Hall D.H, 2011).

2.6. **Aim of this thesis**

The aim of this thesis has been the purification of synaptic vesicles from the nematode *C. elegans* to identify novel proteins involved in SV biogenesis, membrane fusion and recycling. As the work of Burré et al., Morciano et al., Boyken et al. and Takamori et al. demonstrated there is still a high need in the understanding of the SV proteome and the corresponding machinery (Burré et al., 2006; Boyken et al., 2013; Takamori et al., 2006; Morciano et al., 2009). The purification of synaptic complexes could be performed by differential centrifugation and in some cases in combination with single step immunological purification steps (Burré et al., 2006; Boyken et al., 2013; Miljanich et al., 1982; Takamori et al., 2006; Morciano et al., 2009). This was possible due to the high

abundance of neuronal macromolecular complexes in the brain (8.7% of the SV proteins corresponds to synaptobrevin, Walch-Solimena et al., 1995; 1 % of the total brain protein relates to syntaxin and SNAP-25, Walch-Solimena et al., 1995; Jahn and Scheller, 2006). The identification of proteins by single step pull-down or co-immunoprecipitations is prone to a high number of false positives and thus we propose that a high purity identification should be followed by an assessment of the discovered protein would allow a better understanding of the underlying machinery.

We decided to use the model organisms *Caenorhabditis elegans* as the genes involved in neurotransmission are highly conserved (Richmond et al., 2006) and the versatile genetic tools, simple behavioral tests and transparent body structure would allow a purification and identification followed by the function characterization of neuronal proteins. We believe these qualities outweigh the disadvantage of the non-existence of neuronal tissue like a brain. To compensate this lack, a high affinity purification strategy – the tandem affinity purification (TAP) method – has been applied. The Tandem affinity purification is a highly specific purification method with changing purification moieties with affinities in the nanomolar range (Stofko-Hahn et al., 1992; Rigaut et al., 1999; Puig et al., 2001, Yang et al., 2003). TAP allows the purification of low abundant proteins and avoid the detection of unspecific targets (Rigaut et al., 1999; Puig et al., 2001). This specific tag combination has been used successfully for natively expressed targets in a complex mixture of proteins in yeast (Rigaut et al., 1999; Puig et al., 2001) and in *C. elegans* (Gottschalk et al., 2005). After purification of SVs the proteome and associated proteins were supposed to be analyzed by mass spectrometry and newly identified proteins functionally characterized by genetic manipulation and behavioral tests.

During the course of this thesis the aim shifted due to technical difficulties from the identification of synaptic vesicle interaction partners to the purification of the closely related SNARE complex followed by the identification and characterization of unknown interaction partners. What has been true for SV purification similarly applies for SNARE complex purification: The fusion machinery is not completely resolved (Boyken et al., 2013) and the machinery is highly conserved (Kenyon, 1988; Bergmann, 1998; Richmond, 2006). The purification of the SNARE complex should identify (by mass spectrometric analysis) proteins which were supposed to be knocked-down via RNA interference and analyzed for the behavioral/transmissional impact. Positive candidates

should now be further analyzed for their synaptic localization by GFP fusion constructs and verified for their synaptic context in further behavioral tests.

3. Material and Methods

3.1. Materials

3.1.1. Chemicals

Table 1 Chemicals

Chemical	Manufacturer
2-Mercaptoethanol	Carl Roth
Acetic acid	Carl Roth
Acetone	Carl Roth
Adenosine triphosphate (ATP)	Fermentas
Agarose	Carl Roth
Agar Agar	AppliChem
Ampicillin	Carl Roth
Antifoam 204	Sigma Aldrich
Ammonium Peroxodisulfate (APS)	Carl Roth
Biotin	Carl Roth
Bovine serum albumin (BSA)	Fermentas
Brij 35	Carl Roth
Brilliant blue G250	Carl Roth
Bromophenol blue	Sigma
Calcium chloride ($CaCl_2$)	Carl Roth
Cholesterol	Carl Roth
Coomassie	Carl Roth
Deoxycholate	Carl Roth
Desthiobiotin	Carl Roth
Dimethylsulfoxide (DMSO)	Carl Roth
Di-potassium hydrogen phosphate	Carl Roth
Disodium carbonate (Na_2CO_3)	Carl Roth
Disodium hydrogen phosphate	Carl Roth
Dithiotreitol (DTT)	Carl Roth
Eriochromblack T	Carl Roth
Ethanol	Carl Roth
Ethidium bromide	Carl Roth
Ethylendiamine tetra acetate (EDTA)	Carl Roth
Formaldehyde	Carl Roth
GeneRuler 1kB plus	Fermentas
GeneRuler mix	Fermentas
Glycerin	Carl Roth
Guanidine Hydrochloride	Carl Roth
Halocarbon oil	Halocarbon
Hydrochloric acid	Carl Roth
Hydrogen peroxide	Carl Roth
Hydroxyphenyl azobenzoeic acid (HABA)	Sigma Aldrich
Imidazole	Carl Roth
Isopropanol	Carl Roth
Luminol	Carl Roth
Magnesium acetate	Carl Roth
Magnesium chloride	Carl Roth
Magnesium sulphate	Carl Roth
Methanol	Carl Roth
Milk powder	Carl Roth
Nystatin	Sigma Aldrich
Octylglycopyranoside	Carl Roth
Page Blue protein staining solution	Fermentas
P-coumaric acid	Carl Roth
Phenol chloroform isoamyl alcohol (25:24:1)	Carl Roth
Phenylmethylsulfonylfluorid (PMSF)	Sigma Aldrich
Polyethylenglycol (PEG)	Carl Roth
Ponceau S	Carl Roth
Potassium actetate	Carl Roth
Potassium chloride	Carl Roth
Potassium citrate	Carl Roth
Potassium dihydrogen phosphate	Carl Roth
Potassium Hexacyanoferrat (III)	Merck
Prestained Protein Marker	Fermentas
Complete Protease Inhibitor EDTA free	Roche
Rotiphorese Gel 30	Carl Roth
Rubidium chloride	Carl Roth
Sigmacote	Sigma Aldrich
Silvernitrate ($AgNO_3$)	Carl Roth
Sodium acetat	Carl Roth
Sodium azide (NaN_3)	Carl Roth

Chemical	Manufacturer
Sodium chloride	Carl Roth
Sodium dihydrogen phosphate	Carl Roth
Sodium dodecylsulphate (SDS)	Carl Roth
Sodium hydroxide	Carl Roth
Sodium hypochloride 12 %	Carl Roth
Sodium Thiosulfate Pentahydrate	Carl Roth
Spermidine	Carl Roth
Streptomycin	Carl Roth
Sucrose	Südzucker
Tetramethylethylenediamine (TEMED)	Carl Roth

Chemical	Manufacturer
Trichloro acetic acid (TCA)	Carl Roth
Tris(hydroxymethyl)-aminomethan (TRIS)	Carl Roth
Triton X-100	Carl Roth
Trypton/Pepton	Carl Roth
Tween-20	Carl Roth
Urea	Carl Roth
Xylenecyanole	Carl Roth
Yeast extract	Carl Roth
Zellutrans Roth dialysis tube	Carl Roth

3.1.2. Buffers and Media

10 X Injection Buffer
200 mM KPO4
30 mM Potassium Citrate
20 % Polyethylene glycol

10 X PCR Buffer
100 mM Tris/HCl pH 8,3
500 mM KCl
15 mM MgCl 2
0.001 % Gelatin

10 – 15 % Resolving Gel
10 – 15 % acryl-bisacrylamide mix
375 mM Tris (pH 8.8)
0.1 % SDS
0.1 % ammonium persulfate
0.04 % (v/v) TEMED

4 % Stacking Gel
4 % acryl-bisacrylamide mix
187.5 mM Tris (pH 6.8)
0.1 % SDS
0.1 % ammonium persulfate
0.1 % (v/v) TEMED

6 X Laemmli
12 % (w/v) SDS (sodium dodecyl sulfate)
0.6 g/l bromophenol blue
47 % (v/v) glycerol
60 mM Tris 0.5M pH6.8

Bleach solution
0,5 M NaOH
3.6 % Sodium hypochlorite

Calmodulin Binding Buffer
50 mM Tris pH 8.0
150 mM NaCl
1 mM Mg Acetate
1 mM Imidazole
1 mM DTT
0.5 mM PMSF
2 mM CaCl
(0.05 % (v/v) Trition X-100)* *according to the purification strategy

Calmodulin Elution Buffer
50 mM Tris pH 8.0
150 mM NaCl
1 mM Mg Acetate
1 mM Imidazole
1 mM DTT
0.5 mM PMSF
4 mM EDTA
4 mM EGTA
(0.05 % (v/v) Trition X-100)* *according to the purification strategy

DNA loading dye
40 % (w/v) Sucrose
0.25 % Bromophenol blue
0.25 % Xylenecyanol
In 6 X TAE

Elisa Substrate Buffer (ESB)
80 mM Tris pH 6.8
2 % SDS
10 % Glycerol
1.5 % DTT
0.1 mg/ml Bromophenol blue

High growth media (HGM) Agar
2 % Peptone,
51mM NaCL
25mM KPO4
5mg/l Cholesterol
1mM CaCl2
1mM MgSO4
2.5 % Agar

IPP 150
50 mM Tris pH 8.0
150 mM NaCl
1 mM DTT
0.5 mM PMSF
(0.05 % (v/v) Trition X-100)* *according to the purification strategy

Lysogeny Broth (LB) agar
1 % (w/v) Trypton/Pepton
0.5 % Yeast extract
172 mM NaCl
1.5 % Agar Agar

Lysogeny Broth (LB) medium
1 % (w/v) Trypton/Pepton
0.5 % Yeast extract
172 mM NaCl

M9 Buffer
20 mM KH2PO4
40 mM Na2HPO4
85 mM NaCl
1 mM MgSO4

Nematode growth media (NGM)
0.25 % Peptone,
51 mM NaCL
25 mM KPO4
5 mg/l Cholesterol
1 mM CaCl2
1 mM MgSO4
1.7 % Agar

Potassium Citrate pH 6.0 (1 M)
2 % (w/v) Citric acid monohydrate
29.3 % (w/v) K3Citrate Monohydrate

Resuspension buffer
20 mM Tris-Cl pH 8
100 mM NaCl
5 mM Imidazole (500mM for elution)
10 mM β-Mercaptoethanol

S basal
100 mM NaCl,
0.1 % (w/v) K2 HPO4
0.6% (w/v) KH2PO4
5 mg/l cholesterol

SDS Running buffer
190 mM Glycine
25 mM Tris pH 8.6
0.1 % SDS (w/v)

Single Worm/ Egg Lysis Buffer (SEWLB)
10 mM Tris pH 8.3
50 mM KCl
2.5 mM MgCl2
0.45 % Tween-20
0.05 % Gelatin

S-medium
S-Basal plus:
1% (v/v) 1 M Potassium citrate
1% (v/v) Trace metal solution
3 mM CaCl2
3 mM MgSO4

Strep buffer
50 mM Tris/HCl pH 8,
150 mM NaCl,
2.5 mM EDTA
2.5 mM EGTA
1 mM DTT
0.5 mM PMSF
Roche Complete

Strep elution buffer
50 mM Tris/HCl pH 8
150 mM NaCl
2.5 mM EDTA
2.5 mM EGTA
1mM DTT
0.5 mM PMSF
2 mM Biotin, (244.3 g/mol, 5 µL of 40 mM stock)
3 mM Desthiobiotin (214 g/mol, 5 µL of 60 mM)

Stripping buffer
100 mM 2-Mercaptoethanol
2 % SDS
62.5 mM Tris pH 6.7

Tris Acetic acid EDTA (TAE) Buffer
40 mM Tris
20 mM Acetic acid
1 mM EDTA

Tris Buffered Saline (TBS)
50 mM Tris pH 7.5
150 mM NaCl

TBS-T
50 mM Tris pH 7.5
150 mM NaCl
0.05 % (v/v) Triton X-100

TEV Cleavage Buffer
50 mM Tris pH 8.0
150 mM NaCl
0.5 mM EDTA
1 mM DTT
(0.05 % (v/v) Triton X-100)* *according to the purification strategy

Trace metal solution
5 mM disodium EDTA
2.5 mM FeSO4 •7 H2O
1.5 mM MnCl2•4 H2O
1.2 mM ZnSO4 •7 H2O
0.1 mM CuSO4 •5 H2O

Transfer Buffer
25 mM Tris pH 8.3
150 mM Glycine,
20 % (v/v) Methanol
0.037 % (w/v) SDS

3.1.3. Plasmids

Table 2 MosSCI plasmids

Name	Backbone	Inserted Sequence	Origin
pCFJ151		ttTi5605	CFJ (Frøkjær-Jensen et al., 2008)
pCFJ90		p*myo-2*::mCherry	CFJ (Frøkjær-Jensen et al., 2008)
pCFJ104		p*myo-3*::mCherry	CFJ (Frøkjær-Jensen et al., 2008)
pCFJ350		ttTi5605	CFJ (Frøkjær-Jensen et al., 2012)
pCFJ352		ttTI4348	CFJ (Frøkjær-Jensen et al., 2012)
pCFJ601		p*eft-3*::Mos1 transposase	CFJ (Frøkjær-Jensen et al., 2012)
pGH8		p*rab-3*::mCherry	CFJ (Frøkjær-Jensen et al., 2012)
pJL43		p*glh-2*::Mos1 transposase	CFJ (Frøkjær-Jensen et al., 2012)
pMA122		p*eel-1* negative selection marker	CFJ (Frøkjær-Jensen et al., 2012)
CFJ Christian Froekjaer-Jensen			

Table 3 Synaptic Vesicle plasmids

Name	Backbone	Inserted Sequence	Origin
pESG-IBA168		One-Strep::FLAG	IBA lifesciences GmbH
	pUC19	p*sng-1::sng-1*::CBP::4xTEV::ProtA	YF
	pCFJ151	p*sng-1::sng-1*::CBP::4xTEV::ProtA	FC
pFC14	pCFJ151	*psng-1::sng-1*::8xG4S::CBP::4xTEV::ProtA	FC
pFC15	pCFJ151	p*sng-1::sng-1*::8xG4S::StrepOne::ProteinC	FC
pFC16	pCFJ151	p*sng-1::sng-1*::8xG4S::StrepOne::FLAG	FC
pFC17	pCFJ151	p*snt-1::snt-1*::OneStrep::FLAG	FC
pFC18	pCFJ151	p*sng-1::sng-1*::8xG4S::StrepOne::FLAG	FC
pFC19	pCFJ151	p*snt-1::snt-1*::OneStrep::FLAG	FC
CFJ Christian Froekjaer-Jensen, YF Yvonne Füll			

Table 4 SNARE complex plasmids

Name	Backbone	Inserted Sequence	Origin	Comment
pMH421	pTX21	truncated *unc-64*	MH	Always open UNC-64 (Hammarlund et al., 2007)
pTX21	unknown	full size *unc-64*	MN	(Nonet et al., 1999)
pCS55	unknown	*punc-17*::ChR2::YFP:: *unc-54* 3'UTR	CS	target vector for *mca-3* cloning (Schultheis et al., 2011)
pFC01	pUC19	p*snb-1::*ProtA::2xTEV::*snb-1::*Bicis::*unc-64* (trunc)::CBP::*unc-54* 3'UTR	FC	truncated *unc*-64 (always open) originating from pMH421
pFC02	pCFJ350	p*snb-1::*ProtA::2xTEV::*snb-1*::Bicis::*unc-64* (trunc)::CBP::*unc-54* 3'UTR	FC	Left-right orientation
pFC03	pCFJ350	p*snb-1::*ProtA::2xTEV::*snb-1*::Bicis::*unc-64* (trunc)::CBP::*unc-54* 3'UTR	FC	Right-left orientation (Frøkjær-Jensen et al., 2012)
pFC04	pUC19	p*unc-64*(2.3kB)::*unc-64*::CBP::*unc-54* 3'UTR	FC	*unc-64* sequence origin Mike Nonet plasmid pTX21
pFC05	pUC19	p*snb-1::*ProtA::2xTEV::*snb-1*::Bicis::*unc-64*::CBP::*unc-54* 3'UTR	FC	
pFC06	pCFJ350	p*snb-1::*ProtA::2xTEV::*snb-1*::Bicis::*unc-64*::CBP::*unc-54* 3'UTR	FC	Left-right orientation (Frøkjær-Jensen et al., 2012)
pFC07	pCFJ350	p*snb-1::*ProtA::2xTEV::*snb-1*::Bicis::*unc-64*::CBP::*unc-54* 3'UTR	FC	Right-left orientation
pFC08	pCFJ352	p*unc-64*(2.3kB)::*unc-64*::CBP::*unc-54* 3'UTR	FC	
pFC11	pUC19	p*rab-3*::*unc-64*a::CBP::*unc-54* 3'UTR	FC	
pFC12	pCFJ352	p*rab-3*::*unc-64*a::CBP:: *unc-54* 3'UTR	FC	
pFC21	pUC57	*mca-3b* cDNA	Genewiz	
pFC22	pCS55	p*unc*-17::*mca-3b* cDNA::YFP::*unc-54* 3'UTR]	FC	
pFC23	pUC19	p*snb-1*::mCherry::*snb-1::unc-54* 3'UTR	FC	
pFC24	L4440	L4440; *vti-1* coding region: 10-867	FC	L4440 was a gift from the Andrew Fire *C. elegans* Vector Kit (Addgene plasmid # 1654)
Originator of the plasmids are: CFJ Christian Froekjaer-Jensen, CS Christian Schultheis, MH Marc Hammarlund, MN Mike Nonet, FC Florian Csintalan				

3.1.4. Strains

C. elegans

Table 5 *C. elegans* strains

Name	**Genetic background**	**Transgene or description**	**Prod./ user**
EG6699	*ttTi5605 II; unc-119(ed3) III*	*oxEx1578 (eft-3p::GFP; Cbr-unc-119)*	CFJ (Frøkjær-Jensen et al., 2012)
GS2526	*arIs37 I [myo-3p::ssGFP + dpy-20(+)] I; mca-3(ar492) dpy-20(e1282) IV*	asIs37 encodes a secreted GFP, which would end in coelomocytes, but due to the *mca-3* mutation is localized in the pseudocoelom	GS (Bednarek et al., 2007)
NM467	*snb-1(md247) V*	Reduction of function mutation of *snb-1* (insertion of cgctatcgtcgtcattctta in exon 2)	NM (Nonet et al., 1998)
NM534	*snb-1(js17) V.*	Reduction of function (Substitution from a g to a in exon 2(L62F))	NM (Nonet et al., 1998)
NM547	*unc-64(js21) III.*	Reduction of function mutation of *unc-64* (Substitution from c to t in exon 7 (A241V))	NM (Nonet et al., 1998)
NM979	*unc-64(js115)/bli-5(e518) III*	Loss of function mutation of *unc-64* (substitution c to t in exon 3 (Q71Stop))	NM (Nonet et al., 1998)
NM1081	*snb-1(js124)/dpy-11(e224) unc-68(r1158) V*	Loss of function mutation of *snb-1* (substitution g to a in exon 2 (Q50Stop))	NM (Nonet et al., 1998)
ZX687	*EG4322 ttTi5605 II; unc-119(ed3) III*	*zxIs67[C.br. unc-119(+); psng-1::sng-1::TAP,4xTEV] II*	FC
ZX697	*EG4322 ttTi5605 II; unc-119(ed3) III*	*zxIs68[C.br. unc-119(+); psng-1::sng-1::TAP,4xTEV] II*	FC
ZX786	*EG4322 ttTi5605 II; unc-119(ed3) III*	*zxIs76[C.br. unc-119(+) ; psng-1::sng-1::TAP 8x SG4 4xTEV] II*	FC
ZX787	*EG4322 ttTi5605 II; unc-119(ed3) III*	*zxIs77[C.br. unc-119(+); psng-1::sng-1::TAP 8x SG4 4xTEV] II*	FC
ZX1105	*EG4322 ttTi5605 II; unc-119(ed3) III*	*zxIs69[MosSCI sng-1::OneStrep::FLAG] II*	FC
ZX1106	*EG4322 ttTi5605 II; unc-119(ed3) III*	*zxIs70[MosSCI sng-1::OneStrep::FLAG] II*	FC
ZX1585	*ttTi5605 II; unc-119(ed3) III*	*zxEx10[pFC06: pCFJ350 back bone; psnb-1::ProtA::2xTEV::snb-1::Bicis::unc-64::CBP::unc-54 3'UTR 7.5 ng/µL; pmyo-2::mCherry 1.25 ng/µL]*	FC
ZX1586	*ttTi5605 II; unc-119(ed3) III*	*zxEx11[pFC06: pCFJ350 back bone; psnb-1::ProtA::2xTEV::snb-1::Bicis::unc-64::CBP::unc-54 3'UTR 25ng/µL; pmyo-2::mCherry]*	FC
ZX1587	*ttTi5605 II; unc-119(ed3) III*	*zxEx12[pFC01: pCFJ350 back bone; psnb-1::ProtA::2xTEV::snb-1::Bicis::trunc(pMH421) unc-64::CBP::unc-54 3'UTR 25 ng/µL; pmyo-2::mCherry]*	FC

ZX1588	*ttTi5605 II; unc-119(ed3) III*	*zxIs72[bomb pFC07: pCFJ350 back bone; psnb-1::ProtA::2xTEV:::snb-1::Bicis::unc-64::CBP::unc-54 3'UTR* , Cbr *unc-119 Line 9.3]*	FC
ZX1589	*ttTi5605 II; unc-119(ed3) III*	*zxIs73[bomb pFC07: pCFJ350 back bone; psnb-1::ProtA::2xTEV::snb-1::Bicis::unc-64::CBP::unc-54 3'UTR Line 10.4]*	FC
ZX1590	*ttTi5605 II; unc-119(ed3) III*	*zxIs74[bomb pFC07: pCFJ350 back bone; psnb-1::ProtA::2xTEV::snb-1::Bicis::unc-64::CBP::unc-54 3'UTR Line 10.8]*	FC
ZX1591	*ttTi5605 II; unc-119(ed3) III*	*zxIs75 [bomb pFC07: pCFJ350 back bone; psnb-1::ProtA::2xTEV::snb-1::Bicis::unc-64::CBP::unc-54 3'UTR Line 12.4]*	FC
ZX1592	*ttTi5605 II; unc-119(ed3) III*	*zxIs71[psnb-1::ProtA::2xTEV::snb-1::Bicis::unc-64::CBP::unc-54 3'UTR, Cbr unc-119]*	FC
ZX1682	*arIs37 I [myo-3p::ssGFP + dpy-20(+)] I; mca-3(ar492) dpy-20(e1282) IV*	*zxIs6[punc-17::chop-2(H134R)::yfp;lin-15+] V (GS2526 crossed with zxIS6 (ZX460))*	FC
ZX1683	*N2*	*zxEx13[punc-17::mca-3b cDNA::YFP; psnb-1::mCherry::snb-1]*	FC
ZX1684	*N2*	*zxEx14 [punc-17::mca-3 b cDNA::YFP; psnb-1::mCherry::snb-1]*	FC
ZX1685	*N2*	*zxEx15 [pW01B6.5::W01B6.5::GFP; psnb-1::mCherry::snb-1]*	FC
ZX1686	*EG6699 (ttTi5605 II; unc-119(ed3) III)*	*zxEx16 [pfrm-2::frm-2::GFP; psnb-1::mCherry::snb-1; unc-119 nat]*	FC
ZX1687	*EG6699 (ttTi5605 II; unc-119(ed3) III)*	*zxEx17[pSNAP-29::SNAP-29::GFP unc-119-Nat; psnb-1::mCherry::snb-1]*	FC
ZX1688	*EG6699 (ttTi5605 II; unc-119(ed3) III)*	*zxEx18[pSNAP-29::SNAP-29::GFP unc-119-Nat; psnb-1::mCherry::snb-1]*	FC
ZX1689	*zx1682 (arIs37[pmyo-3::ssGFP ; dpy-20(+)]I; mca-3(ar492); dpy-20(e1282)IV; zxIs6[punc-17::ChR2(H134R)::YFP; lin-15+]V)*	*zxEx19[punc-17::mca-3b cDNA::YFP; psnb-1::mCherry::snb-1]*	FC
Originators are: GS and *ar* Greenwald lab, NM Nonet lab; FC Florian Csintalan and CFJ Christian Froekjaer-Jensen			

Integrated arrays

Name	**Integration Method**	**Genetic name**	**Resp. Strain**
zxIs67	MosSCI	*zxIs67[C.br. unc-119(+);psng-1::sng-1::TAP,4xTEV] II*	ZX687
zxIs68	MosSCI	*zxIs68[C.br. unc-119(+);psng-1::sng-1::TAP,4xTEV] II*	ZX697
zxIs69	MosSCI	*zxIs69[MosSCI sng-1::OneStrep::FLAG; Cbr unc-119] II*	ZX1105
zxIs70	MosSCI	*zxIs70[MosSCI sng-1::OneStrep::FLAG; Cbr unc-119] II*	ZX1106
zxIs71	MosSCI	*zxIs71[psnb-1::ProtA::2xTEV::snb-1::Bicis::unc-64::CBP::unc-54 3'UTR, Cbr unc-119] III*	ZX1592

zxIs72	bombardment	*zxIs72[bomb pFC07: pCFJ350 back bone; psnb-1::ProtA::2xTEV:::snb-1::Bicis::unc-64::CBP::unc-54 3'UTR; CBr unc-119; Line 9.3]*	ZX1588
zxIs73	bombardment	*zxIs73[bomb pFC07: pCFJ350 back bone; psnb-1::ProtA::2xTEV:::snb-1::Bicis::unc-64::CBP::unc-54 3'UTR; CBr unc-119; Line 10.4]*	ZX1589
zxIs74	bombardment	*zxIs74[bomb pFC07: pCFJ350 back bone; psnb-1::ProtA::2xTEV:::snb-1::Bicis::unc-64::CBP::unc-54 3'UTR; CBr unc-119; Line 10.8]*	ZX1590
zxIs75	bombardment	*zxIs75[bomb pFC07: pCFJ350 back bone; psnb-1::ProtA::2xTEV:::snb-1::Bicis::unc-64::CBP::unc-54 3'UTR; CBr unc-119; Line 12.4]*	ZX1591
zxIs76	MosSCI	*zxIs76 [C.br. unc-119(+);psng-1::sng-1::TAP,4xTEV, 8xG4S] II*	ZX786
zxIs77	MosSCI	*zxIs77 [C.br. unc-119(+);psng-1::sng-1::TAP,4xTEV, 8xG4S] II*	ZX787

Extrachromosomal Arrays

Name	**Genetic name**	**Injected DNA (ng/µL)**	**Marker DNA (ng/µL)**	**Resp. Strain**
zxEx10	zxEx10[p*snb-1*::ProtA::2xTEV:.*snb-1*::Bicis::*unc-64*::CBP::*unc-54* 3'UTR]	pFC06 (pCFJ350 back bone; p*snb-1*::ProtA::2xTEV::*snb-1*::Bicis::*unc-64*::CBP::*unc-54* 3'UTR) 25 ng/µL	pCFJ90 (pmyo-2::mCherry) 1.25 ng/µL	ZX1585
zxEx11	zxEx11[p*snb-1*::ProtA::2xTEV:.*snb-1*::Bicis::*unc-64*::CBP::*unc-54* 3'UTR]	pFC06 (pCFJ350 back bone; p*snb-1*::ProtA:2xTEV::*snb-1*::Bicis::*unc-64*::CBP::*unc-54* 3'UTR) 7.5 ng/µL	pCFJ90 (pmyo-2::mCherry) 1.25 ng/µL	ZX1586
zxEx12	zxEx12[p*snb-1*::ProtA::::2xTEV:.*snb-1*::Bicis::trunc(pMH421) *unc-64*::CBP::*unc-54* 3'UTR]	pFC01 (pCFJ350 back bone; p*snb-1*::ProtA::::2xTEV:.*snb-1*::Bicis::trunc(pMH421) *unc-64*::CBP::unc-54 3'UTR) 25 ng/µL	pCFJ90 (pmyo-2::mCherry) 1.25 ng/µL	ZX1587
zxEx13	*zxEx13[punc-17::mca-3b cDNA::YFP; psnb-1::mCherry::snb-1]*	plasmid pFC22 (p*unc*-17::mca-3b cDNA::YFP) 15 ng/µL; pFC23 (p*snb-1*::mCherry::s*nb-1*) 30 ng/µL	pCFJ90 (pmyo-2::mCherry) 1.25 ng/µL	ZX1683
zxEx14	*zxEx14 [punc-17::mca-3 b cDNA::YFP; psnb-1::mCherry::snb-1]*	*pFC22 (punc-17::mca-3 b cDNA::YFP) 15ng/µL; pFC23 (psnb-1::mCherry::snb-1) 30ng/µL*	pCFJ90 (pmyo-2::mCherry) 1.25 ng/µL	ZX1684
zxEx15	*zxEx15 [pW01B6.5::W01B6.5::GFP; psnb-1::mCherry::snb-1]*	*pFC25 (pW01B6.5::W01B6.5::GFP) 10 ng/µL; pFC23 (psnb-1::mCherry::snb-1) 30ng/µL*	pCFJ90 (pmyo-2::mCherry) 1.25 ng/µL	ZX1685
zxEx16	*zxEx16 [pfrm-2::frm-2::GFP; psnb-1::mCherry::snb-1; unc-119 nat]*	Fosmid WRM0612A_C12 *(pfrm-2::frm-2::GFP unc-119-Nat) 15ng/µL; pFC23 (psnb-1::mCherry::snb-1) 30ng/µL*	pCFJ90 (pmyo-2::mCherry) 1.25 ng/µL	ZX1686
zxEx17	*zxEx17[pSNAP-29::SNP-29::GFP unc-119-Nat; psnb-1::mCherry::snb-1]*	Fosmid WRM0641C_A06: *(pSNAP-29::SNP-29::GFP unc-119-Nat) 15ng/µL; pFC23 (psnb-1::mCherry::snb-1) 30ng/µL*	pCFJ90 (pmyo-2::mCherry) 1.25 ng/µL	ZX1687
zxEx18	*zxEx18[pSNAP-29::SNP-29::GFP unc-119-Nat; psnb-1::mCherry::snb-1]*	Fosmid WRM0641C_A06: *pSNAP-29::SNAP-29::GFP unc-119-Nat 15ng/µL; pFC23 (psnb-1::mCherry::snb-1) 30ng/µL*	pCFJ90 (pmyo-2::mCherry) 1.25 ng/µL	ZX1688
zxEx19	*zxEx19[punc-17::mca-3b cDNA::YFP; psnb-*	*pFC22 (punc-17::mca-3b cDNA::YFP) 15 ng/µL; pFC23(psnb-*	pCFJ90 (pmyo-2::mCherry) 1.25	ZX1689

	1::mCherry::snb-1]	*1::mCherry::snb-1) 30 ng/µL*	ng/µL	

***E. coli* strains**

K12	Standard growing strain, was used for feeding during bioreactor incubation, all other *E. coli* subtypes derive from this parent
DH5α	Standard transformation strain for high copy number of plasmids
OP50	Uracil requiring mutant, for better observation of nematodes on plate *(Brenner, 1974))*
HB101	Subtype of K-12, was used for thicker bacterial lawn during propagation
BL21	Transformation strain for high expression of proteins

3.1.5. Antibodies

Table 6 Antibodies

Name	**Epitope**	**Working concentr.**	**Host**	**Manufacturer**
Anti-CBP (a00635)	CBP	1:100	mouse	Genscipt
Anti-FLAG (F3165)	FLAG	1:100	mouse	Sigma Aldrich
Anti-mouse-HRP (62-6520)	Mouse	1:10000	goat	Life technologies
Anti-Strep-HRP	Steptavidin	1:100	rabbit	Pierce
Anti-TAP (CAB1001)	TAP	1:100	rabbit	Pierce
PAP	ProtA	1:1000	mouse	Sigma Aldrich
SB1	SNB-1	1:100	mouse	DSHB (Mike Nonet)(Hadwiger G et al., 2010)
Anti-rabbit-HRP	Rabbit	1:10000	goat	Sigma Aldrich

3.1.6. Oligonucleotides

Oligonucleotides used during experiments for synaptic vesicle purification

Table 7 *sng-1* oligonucleotides

Name	**Sequence**	**Length**	**Comment**
CBP test fw	CCGTCTCAGCAGCCAACC	18	
CF419	CAATTCATCCCGGTTTCTGT	20	Mos1 integration test, created by Christian Froekjaer-Jensen (Frøkjær-Jensen et al., 2008)
FC001 fw	CACTCAGTCGGAAGGATATGG	21	*sng-1* end of coding region
FC002 rev	AAATCGGGAGGCGAACCTAAC	21	3' genomic integration site
FC003 fw	GACTCGAGCAAATCGACAAC	20	Alternative for oGF419
FC004 rev	TAGGGTGCAGACAGAATAGG	20	Alternative for GF419
FC005 fw	CCTCCACCTCAATCCTCATAC	21	100 bp upstream of *sng-1*

Name	Sequence	Length	Comment
			stop codon
FC006 rev	GTTTGCGTGTTCTCCCATTC	20	3’ genomic integration site
FC007 fw	GGCGGAGGGTCAGGGGTACCGTCCGGAGGT GGAGGGAGT	39	Glycine serine linker
FC008 rev	TTTCCATGGATACCGGGTACGCTCCGCCTCCA CCTGACCC	40	Glycine serine linker
FC009 fw	GCCTTTGGCGAACAAGTACC	20	Transposase seq
FC010 rev	TGTGGATTCCACGCCAGTAG	20	Transposase seq
FC011 fw	CCTTTGGCGAACAAGTACC	19	Transposase seq
FC012 rev	TCCCATCGAAGCGAATAGG	19	Transposase seq
FC013 rev	TACATAACCTTCGGGCATGG	20	50 bp 3’ of TAP tag stop codon
FC014 rev	GTAATCCCAGCAGCTGTTAC	20	*unc-54* 3’ UTR
FC015 rev	TCCACGGCTTCATCGTGTTG	20	pCFJ151 *unc-119* p*sng-1*::*sng-1*-4xTEV-5xSG4::*unc-54*-3'UTR
FC016 fw	GCAAAGTTGTGGGCATGAAGAG	22	Gen. DNA after Integration *sng-1*-4xTEV-5xSG4
FC017 rev	TTAAAGCGGTTGGCTGCTGAG	21	Gen. DNA after Integration *sng-1*-4xTEV-5xSG4
FC018 fw	GTCCAAATTATCCGCCTTCG	20	product (Seq)
FC019 fw	GGCTTAACTATGCGGCATCA	20	pFC17 sequencing (MosSCI *snt-1*::OneStrep:FLAG)
FC020 rev	GCTCAATGGCATACACTTGG	20	*snt-1* sequencing
FC021 fw	CCAAGTGTATGCCATTGAGC	20	*snt-1* sequencing
FC022 rev	ACCACCACCAGATGACAAAG	20	*snt-1* sequencing
FC023 fw	CTTTGTCATCTGGTGGTGGT	20	*snt-1* sequencing
FC024 rev	CAGAGCAACAACGACAAAGG	20	*snt-1* sequencing
FC025 fw	CCTTTGTCGTTGTTGCTCTG	20	*snt-1* sequencing
FC026 rev	GAGAACGACGAAGACTTGAC	20	*snt-1* sequencing
FC027 fw	GTCAAGTCTTCGTCGTTCTC	20	*snt-1* sequencing
FC028 rev	CACAACAAAGCCGACTACTC	20	*snt-1* sequencing
FC029 fw	CACTCCCTCCACCTCCTC	18	test for correct linker
FC030 rev	GAGGAGGTGGAGGGAGTG	18	test for correct linker
KasI p*sng-1* fw	ATTGGCGCCGAGAGCGTGTTCCTGTTTAG	29	
KpnI p*sng-1* rev	GATGGTACCGCTAAAATAAAAGAAATATAGA GGAT	35	
oAG30	GTGTCTTGTAGTTCCCGT	18	94 bp 3' of TAP tag stop codon, created by Alexander Gottschalk
oAG31	GCGGATGACCAGCGGTATCCATGGAAAAGA GAAGA	35	Glycine serine linker start of TAP tag, created by Alexander Gottschalk
oCF419	TCTGGCTCTGCTTCTTCGTT	20	Mos-1 Integration test primer, created by Christian Froekjaer-Jensen (Frøkjær-Jensenet al., 2008)
V2 fw	ATCCCCGGGATTGGCCAAAGGACCCAAAGGT	112	ProteinC::StrepII tag

Name	Sequence	Length	Comment
	ATGTTTAAATGTGATCTAGATCACATTTGCTAAATGTGATCTAGATCACATTTATTTTCAGGAGGACCCTTGGAGGGTAC		integration
V2 rev	CTCCAAGGGTCCTCCTGAAAATAAATGTGATCTAGATCACATTTAGCAAATGTGATCTAGATCACATTTAAACATACCTTTGGGTCCTTTGGCCAATCCCGGG	104	ProteinC::StrepII tag integration
YF10	CTTTCCTGTACATAACCTTCG	21	50 bp 3' of TAP tag stop codon, created by Yvonne Füll

SNARE complex purification

Table 8 *snb-1* oligonucleotides

Name	Sequence	Length
350xpFC05infuf	CACCGTACGTCTCGAGGTACCGCTGAAATCTAGGATTAC	39
350xpFC05infur	TGGATCCAGATATCCAAACAGTTATGTTTGGTATATTGGG	40
352xpFC04 inf f	GTCTCGAGGAATTCCCTCGAGTAGATCAAACGTTTTTTTTC	41
352xpFC04 inf r	GGCCTTGACTAGAGGAAACAGTTATGTTTGGTATATTGGG	40
AvrII-ProtA-snb-1	GGGCCTAGGGGTACCGCTGAAATCTAGG	28
js124 test fw	CGGATAAGACCATCTTGACG	20
js124 test rev	ATCCGGGACAAAGGTCGTG	19
pCFJ350::ProtA-Snb-1-1	CGTGCCTCCATCTTCATAC	19
pCFJ350::ProtA-Snb-1-2	AGGTTCTCGGCATGGTACGG	20
pCFJ350::ProtA-Snb-1-3	TCCGACATTGTTGCCCATAG	20
pCFJ350::ProtA-Snb-1-4	GAAATAGAGATGCGCGTAGG	20
pCFJ350::ProtA-Snb-1-5	CCGAAAGTAGACGCGAATTG	20
pCFJ350::ProtA-Snb-1-6	CGCGATAAGCTGCGTGATCC	20
SbfI-ProtA-snb-1	CCCCTGCAGGCCTTGACAGTTTTGAGTTTTCAAC	34
snb1 fw neu	GGAACCTGCAGGGGTACCGCTGAAATCTAGG	31

Name	**Sequence**	**Length**
snb-1 test fw	CCCGGAAATTTACCCATTAG	20

Table 9 *unc-64* oligonucletides

Name	Sequence	Length
BamHI *unc-64* rv	CATAGGATCCCGCAATGCCAGGAATATACTGAATG	35
BamHI peft-3 rev	CCCGGATCCTGAGCAAAGTGTTTCCCAAC	29
BamHI-CBP	TTTAGGATCCTATGGTGGCGGAGGGTCTGGTG	32
BamHI-*unc-64* R	GCCGGATCCCGCAATGCCAGGAATATACTGAATG	34
HindIII peft-3	GCCGAAGCTTGCACCTTTGGTCTTTTATTG	30
infu prab-3::*unc-64*::CBP f2	ATTTTCCTAGAAGCTATGGCATGCAAAAGCTAGCCG	36
infu prab-3::unc64::CBP r2	CCAAGCTTGCATGCCAAACAGTTATGTTTGGTATATTGGG	40
infus p*unc-64* 3kb;;*unc-64* new 1	TACCGCATCAGGCGCCGGTGCTTGCGTATTTGGAGCAG	38
infusion p*unc-64*,*unc-64* fw new	TACCGCATCAGGCGCCGGTGCTTGCGTATTTGGAGCAG	38
Infusion *unc-64* fw	TACCGCATCAGGCGCCGCCGCTCTAGAACTAGTGGATCC	39
Infusion *unc-64* rev	CGCCACCATAGGATCCAATGCCAGGAATATACTGAATGAGC	41
js115 test fw	CGCAAATTCTATGACCAATCACAC	24
js115 test fw v2	GCAGGTTGAAGAGATTCG (js115 WT (Pair)	18
js115 test rev	CCTAAGCCTAAGCCTAACTC	20
KasI prab-3 fw	GAGAGGCGCCGTATAGAAAAGTTGATCTTCAG	32
KasI punc64 2.3 kb fw	GTTCGGCGCCCTCGAGTAGATCAAACGTTTTTTTTC	36
KpnI prab-3 rev	CTCTGGTACCAAACTTGTCATCTGAAAATAGG	32
KpnI *unc-64* exon1 fw	GAAGGTACCATGACTAAGGACAGGTGAGTC	30

Name	Sequence	Length
KpnI *unc-64* fw	GAAGGTACCATGGCATGCAAAAGCTAGCCG	30
Kpni *unc-64* rev	GCCGGTACCGGAATGCCAGGAATATACTGAATG	33
KpnI-*unc-64*aF	GTTGGCCATGGATGGCATGCAAAAGCTAGCCG	32
MscI *unc-64*	GGCGTTGGCCAGAATGCCAGGAATATACTGAATG	34
MscI *unc-64*	GGCGTTGGCCAGAATGCCAGGAATATACTGAATG	34
NheI punc64 unc64 r	CAAAACAAACGCTAGCCGATATTG	24
NheI *unc-64* fw	CAAAACAAACGCTAGCCGATATTG	24
PstI-*unc-64* fw	GAACTGCAGATGGCATGCAAAAGCTAGCCG	30
unc-64 CBP infusion fw	AGTAGGATGAGACACCATGGCATGCAAAAGCTAGCCG	37
unc-64 CBP infusion rev	CCAAGCTTGCATGCCGTAGGAAACAGTTATGTTTGG	36
unc-64 fw exon1	GAAGGTACATGACTAAGGACAGGTGAGTC	29
unc-64 seq.10	AAGTATCGTAGGCAGGTAGG (Sequencing Primer)	20
unc-64 test fw	GGCTTCGTTTCTCTGTGG	18
unc-64 test fw	GGCTTCGTTTCTCTGTGG	18
unc-64.Seq.1	CAGCTGCCAGACACATTTTC (Sequencing Primer)	20
unc-64.Seq.2	ACAGCAATGACGATGACGAG (Sequencing Primer)	20
unc-64.Seq.3	GAGCCACAGAGAAACGAAGC (Sequencing Primer)	20
unc-64.Seq.4	CGCAGCACATTTCTGTATGG (Sequencing Primer)	20
unc-64.Seq.5	GGTTGGTGGTGAGTGAACAG (Sequencing Primer)	20
unc-64.Seq.6	CTTTATGCTTCCGGCTCGTA (Sequencing Primer)	20
unc-64.seq.7	TACCGCTGTCTCATCCTAC (Sequencing Primer)	19
unc-64.seq.8	AGCGAAGGCTACAGTAAGTC (Sequencing Primer)	20
unc-64.seq.9	CGCTTAGGCTCAGGTTTAGG (Sequencing Primer)	20
*unc-64*CBPinf f3	GGAAACTGCTGTACCTGCAGATGGCATGCAAAAGCTAGCCG	41
unc64CBPinf f4	GGAAACTGCTGTACCTGCAGATGACTAAGGACAGGTGAGTC	41
*unc-64*CBPinf r3	ATTACGCCAAGCTTGCATGCAAACAGTTATGTTTGGTATATTGGG	45
XhoI-*unc-64*	GGCCCTCGAGACTTTCCATCAAAATCTCTTTC	32
XhoI-*unc-64*	GGCCCTCGAGACTTTCCATCAAAATCTCTTTC	32

Table 10 Oligonucleotides with diverse project contributions

Name	**Sequence**	**Length**
PmeI-CBP	CCCGTTTAAACTCATCAAAGTGCCCCGGAGGATGA	35

Pst Bicis rev new	CTCTCTGCAGGTACAGCAGTTTCCCTGAA	29
PstI 3'UTR rev	GGCTGCAGGTAGGAAACAGTTATGTTTGG	29
PstI Bicis rev	TGACTGCAGTGTCTCATCCTACTTTCACC	29
PstI-CBP rev	CTACTGCAGGTTAAAGTGCCCCGGAGGATGAG	32
SbfI 3'UTR	AACCTGCAGGGTCCAATTACTCTTCAACATCCC	33
SbfI Bicis	GGCCTGCAGGGTACAACTAGTAAGAGCTC	29
SbfI-Stop-CBP	ACCTGCAGGTTAAAGTGCCCCGGAGGATGAGATT	34
SphI 3'UTR	GGCATGCGTAGGAAACAGTTATGTTTGG	28
XhoI Bicis	CCTGCTCGAGGTACAGCAGTTTCCCTGAA	29

3.1.7. Kits/Beads

Name	**Manufacturer**
Carboxylactivated Magnetobeads	Pierce
Calmodulin Sepharose beads	GE health care
Gel/PCR DNA Fragments Extraction Kit	Avagene life sciences
In-Fusion PCR Cloning System	Clontech
IgG Agarose beads	Sigma
MyOne Dynabeads (Magnetobeads)	ThermoFisher Scientific
NucleoBond PC 100	Macherey-Nagel
NucleoSpin Plasmid Kit	Macherey-Nagel
Strep-Tactin Superflow	IBA GmbH
Rotiprep Mini Plasmid Kit	Carl-Roth

3.1.8. Equipment

Description	**Name**	**Manufacturer**
Air filter	Acro® 50 Vent Devices with Emflon® II Membrane	Pall Corporation
Agarose gel chamber	Sunrise	Life technology
Bunsen burner	Tipe 1010	Usebeck
Cameras	Powershot G9	Canon
Centrifuges	Biofuge Pico	Heraeus
Centrifuges	Centrifuge Pico 17	Heraeus
Centrifuges	Centrifuge 5415 R	Eppendorf
Centrifuges	Centrifuge 5810 R	Eppendorf
Centrifuges	Microcentrifuge	Carl Roth
Centrifuges	Rotanta	Hettich
Columns	Mobicols	Mobitec
ddH_2O equipment	Milli-Q Plus	Millipore
Electrophoresis chamber, horizontal	Varia 1	Carl Roth

Electrophoresis chamber, vertical	SDS-PAGE apparatus	Phase
Gel documentation system	Dark Hood 40, Canon EOS 1000D	Biostep
Heat block	Digital dry bath	Labnet
Head-over tail rotor		VWR
Incubator	3015	GFL
Incubator	Kelvitron T	Heraeus
Incubator	Unitron	Heraeus
Incubator	Vinothek	Liebherr
Incubator	InforsHT	Ecotron
Lamps	HBO 100	Osram
Magnetic stirrer	Stuart CB162	Bibby Scientific
Micromanipulator	MMJ rechts with 1/2"-Klammer	Märzhäuser
Micropipette puller	Model P-97	Sutter
Microscopes	Axio Observer	Zeiss
Microscopes	Leica MZ 16F	Leica
Microscopes	SMZ645	Nikon
Microwave oven	CC 6459	Cybercom
pH meter	Cyberscan pH 510	Eutech
Photometer	Jenway	Genova
Pipette Helper	Pipettus	Hirschmann
Power supplies	Enduro^{TM} Power Supplies 300V	Labnet
Power supplies	Standard Power Pack P25	Biometra
Shaker, Horizontal	WT16	Biometra
Thermal cycler	MyCycler Personal Thermal Cycler	Bio-Rad
Thermal cycler	T1 Thermocycler	Biometra
Vortexer	Vortex Genie 2	Scientific Industries
Weighing machines	Analysewaage 770	Kern
Weighing machines	Emb 600-2	Kern
Weighing machines	Adventurer Pro	Ohaus
Western blot	Semi-Dry Pro	Phase

3.2. **Worm methods**

3.2.1. General C. elegans maintenance

Worms were grown on 6 or 10 cm Nematode growth media (NGM) dishes with a dry OP50 lawn. If the worms were supposed to grow to higher density the media were changed to high growth media (HGM). The worms were kept at 16 °C for long term storage, at 20 °C for standard conditions and 25 °C for faster growth (Stiernagle et al., 2006).

Liquid cultures of worms were grown with the help of a 5 L flask (filled with up to2 L) or two bioreactors (5 and 10 L) (compare Figure 3.1) following the protocol of Stiernagle et al. from wormbook.org (Stiernagle et al., 2006).

Figure 3.1 Three different liquid culture vessels for *C. elegans* breeding. The different containers were used for large scale breeding of nematodes. The first reactor could hold up to 10 L of S medium, the smaller contained up to 6 L and the 5 L flask could be filled with up to 2 L medium.

Small adaptations to the Stiernagl liquid culture protocol with respect to the use of bioreactors were applied. For 10 L liquid culture around 100 HGM plates covered with *C. elegans* (around 10 g of *C. elegans*) were washed with sterile S buffer into the fermenter (for the smaller volumes the respective amounts needs to be adapted). The *E. coli* lawn should be almost consumed and no contaminations should be visible. Clean air was added by the ventilation valve via a sterile air filter (Acro® 50 Vent Device) and the mechanical stirrer was set to 80 turns a minute. All steps until final harvest were performed under maximal sterile conditions (e.g. feeding and sample removal with open flame). After adding the nematodes to the 10 L fermenter 5 g of *E. coli* pellet was added (self-made OP50 or commercial K12, pellet was “pipettable”). On day 2 10 g of bacteria and on day 4 another 35 g of *E. coli* pellet was added. As the starting material and the growth according to the phenotype influenced the consumption of bacteria alterations of feeding amount and time according to the turbidity of the culture liquid have been made (too much bacteria seem to be toxic). The turbidity was assessed by regular sampling of the liquid culture and observation under the microscope. Over the course of one week the worms were allowed to multiply. After one week the

liquid was transferred into two 5 L buckets which were placed in an ice bath (~0 °C) to allow the worms to settle to the ground and reduce number the centrifugation rounds. All further steps were performed at 0 – 4 °C to increase the pelleting property of the nematodes. After 15 – 20 min the supernatant was removed and the concentrated worms were centrifuged once at 1000 g for 10 min (in 50 mL falcon tubes in an Eppendorf tabletop centrifuge 5810 R). The supernatant was removed and the worm pellet was resuspended in nine volumes M-9 buffer (e. g. 5 mL worm and 45 mL M-9 buffer) and again centrifuged for 10 min at 1000 g. The pellet was again resuspended in nine volumes of M-9 and applied to the same amount of 60 % sucrose solution (25 mL suspension and 25 mL sucrose solution). This suspension was centrifuged at 1000 g for 5 min. The upper layer containing the adult worms without eggs and *E. coli* was removed and resuspended again in nine volumes of M-9 buffer to dilute the mildly toxic sucrose. The pellet was now resuspended in 0.5 volumes of M-9 (e. g. 5 mL plus 2.5 mL M-9) and the suspension was dripped into liquid nitrogen. The resulting worm beads were transferred into 50 mL falcon tubes and stored at -80 °C for long term storage (CAVE: the lid should have been punctured to avoid explosions in the freezer). One bioreactor run with one week duration and 10 L volume resulted regularly in 25 – 50 g of worms. But as the feeding and sampling procedure could only be performed in a less than sterile fashion contaminations occurred from time to time.

During the course of this thesis the standard of large-scale breeding went from 5 L shaking flask to 10 L culture and finally to egg plates.

The eggplates were prepare according to Hochbaum et al. (Hochbaum et al., 2010). In short, around 100 10 cm NGM plates were prepared previously and set aside. The yolks of 10 chicken eggs were transferred into a sterile 500 mL flask and filled up with LB medium to 400 mL volume. This solution was shaken thoroughly and transferred to a 60 °C water bath for 1 h (to inactive lysozyme). After the solution cooled down to room temperature 100 mL of OP50 culture was added, carefully mixed and 5 mL of this suspension was transferred to each NGM plate. To inoculate the 100 egg plates the worms from ten 10 cm overgrown plates (HGM plates or previously prepared egg plates covered with *C elegans*) were washed off and bleached to obtain sterile eggs (Protocol 4 of (Stiernagle et al., 2006)). After incubation at 20 °C for about one week the worms were washed off the plates and treated in the same way as described before following the removal from the bioreactor (cooling, several centrifugation steps, sucrose gradient cleaning and final liquid nitrogen freezing). A separating funnel was an important tool for pre-separating adult alive worms from egg matter, *E.*

coli, *C. elegans* eggs and dead worms prior to the first centrifugation step. The use of egg plates allowed the preparation of up to 100 g of adult worms with 100 egg plates, with less risk of contamination (starting sample was per se sterile; contamination of one plate was not transferred) and labor.

3.2.2. Mos1 Single copy integration (MosSCI)

The composition of synaptic vesicle proteins as well as of the secretion machinery is tightly regulated. Overexpression of key proteins in this processes could lead not only to an enrichment in the protein processing organelles and therefore to purification of wrong interaction partners, but to an alteration of structure and mode of action. For example an excess of syntaxin inhibited *snb-1* binding and therefore blocked exocytosis (Fasshauer and Margittai, 2004). The standard integration protocol, with array formation after injection followed by UV irradiation for double strand break induction, would result in large copy numbers (arrays after microinjection contain around 80 to 300 copies of the injected plasmid) (Praitis et al., 2001). But to ensure a close-to-native expression pattern and abundance it is of interest to obtain low copy numbers. One method for a low-copy number-integration is the Mos1 Single copy integration (MosSCI) (Frøkjær-Jensen et al., 2008) and (Frøkjær-Jensen et al., 2012). Here the sequence of interest is integrated with a help double strand break induced by the excision of a Mos1 site. This is performed by an introduced Mos1 transposase and a homologous recombination event combines the appropriate adjacent flanking sequences (compare Figure 3.2).

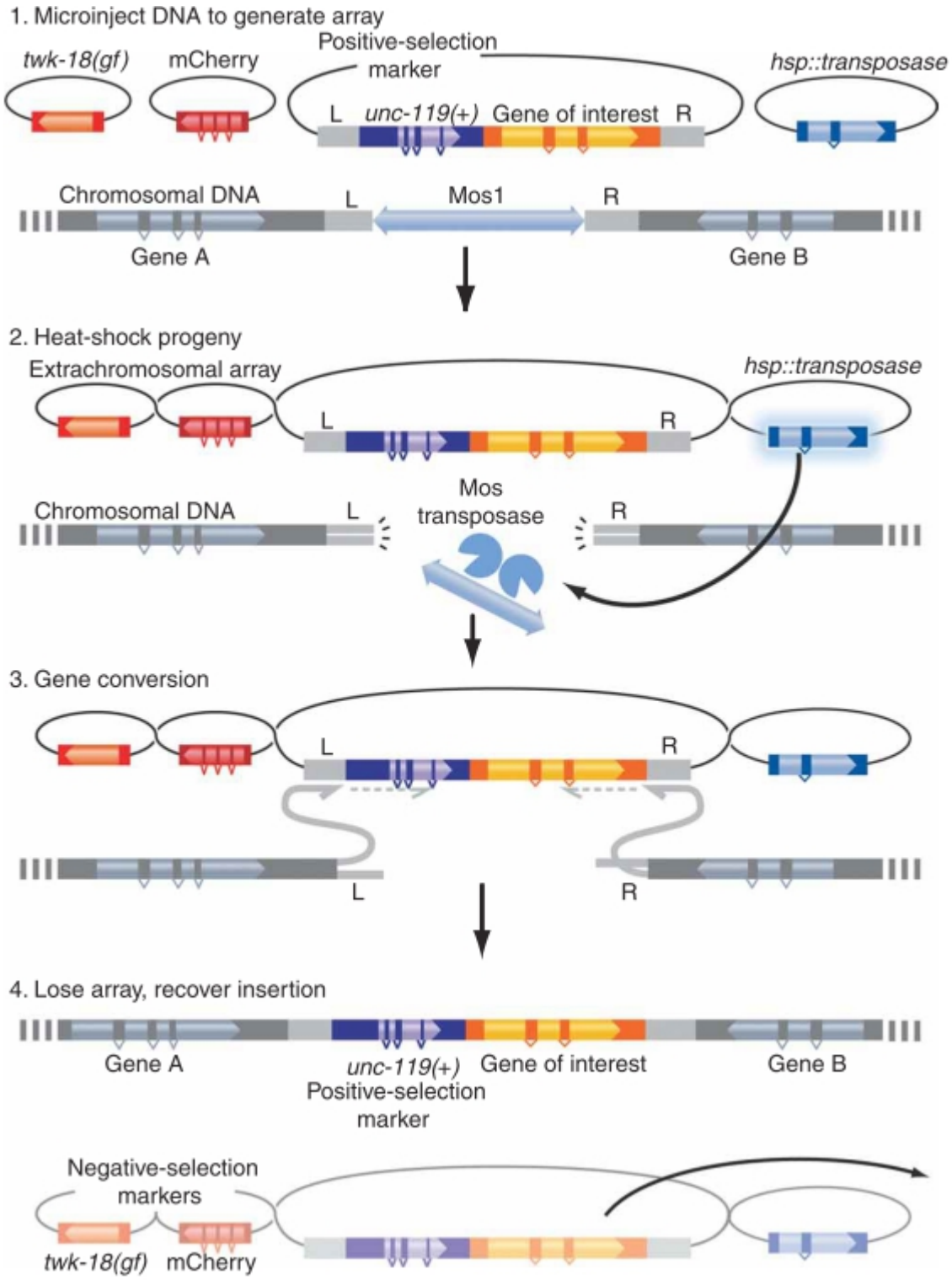

Figure 3.2: The scheme of Mos1 Single copy integration. A combination of plasmids containing the transposase, for induction of strand breaks, the region of interest for homologous recombination and mCherry reporter to verify finally the absence of extrachromosomal arrays. Taken from Frøkjær-Jensen et al., 2008 (Frøkjær-Jensen et al., 2008)

The integration site is determined by the used strain and the appropriate vector, as there are MosSCI strains for chromosome I, II, IV and X (Frøkjær-Jensen et al., 2012). The protocol of the integration

of synaptic vesicle proteins was performed according to the protocol of Frøkjær-Jensen from 2008 (Frøkjær-Jensen et al., 2008) and for construction of strains for the SNARE complex purification the protocol from 2012 (Frøkjær-Jensen et al., 2012) was used.

In short, around 30 animals of the *unc-119* deletion strain EG6699 strain were injected with 50 ng/µL target vector, 50 ng/µL pJL43.1 (Transposase), 10 ng/µL pGH8 (prab-3::mCherry), 1.25 ng/µL pCHJ90 (pmyo-2::mCherry), 5 ng/µL pCHJ104 (pmyo-3::mCherry) and 10 ng/µL pMA122 (toxic *eel-1* under heat shock promoter). The high concentration technique combined with the toxic *eel-1* was applied to positively select the loss of extra chromosomal arrays by heat induced toxic *eel-1).*

After injection the animals were allowed to recover overnight at 16 °C and the following day the plates were transferred to the 25 °C incubator. Here, they were left for starvation as the *unc-119* negative phenotypes will not form Dauer larvae and starve (long term surviving Dauer larval stage with reduced metabolism requires the *unc-119* gene). Surviving worms had either being transiently transformed or could have integrated the *unc-119* rescue. To discriminate between these possibilities the worms were incubated for 2 h at 34 °C to induce the heat shock and kill worms with remaining arrays. Animals which survived the heat shock had an *unc-119* rescue, but no toxic *eel-1* present, which hinted due to the lack of an array to a positive integration event. These surviving animals were analyzed for remaining fluorescence marker, which would indicate to a remaining array. In case of missing fluorescence and wild type behavior (lack of *unc-119* phenotype) they were transferred to a single plate. After several days the positive integration was confirmed by genotyping via polymerase chain reaction (PCR).

3.2.3. Biolistic Gene transformation

A different method of integrating artificial DNA into the nematode genome in a low copy number is the biolistic gene transformation or “gene gun”. Gold microparticles are coated with DNA and shot into the nematode body with the help of helium pressure. The gold particles introduce double strand breaks by shear force, which are repaired with plasmid DNA as template. Utilizing *unc-119* deletion worms and *unc-119* injection marker allowed easy identification of transformants and similar selection techniques to the MosSCI were applied. Due to the rather easy experimental setting it is easy to transform a multitude of different constructs and worms (Wilm et al., 1999; Praitis et al., 2001; Berezikov et al., 2004).

The transformation was performed twice: the first transformation was performed in the lab of Ekkehard Schulze in Freiburg and the second “gene shooting” was made in the lab of Enrico Schleiff

in Frankfurt. Both times the micro-particle bombardment of *unc-119* mutants was performed with the PDS-1000/He with Hepta adapter from Bio-Rad. First, we prepared the gold beads: 15 mg of 1 µm gold beads were transferred into a siliconized reaction tube and 1 mL of 70 % (highest grade) Ethanol was added. Now the suspension was vortexed for 5 min, tube was set on the bench to settle for 15 min, briefly spun (3 - 5 s) in a microcentrifuge and the supernatant was removed. The pellet was now washed 3 times with 1 mL ddH_2O, including vortexing for 1 min and brief centrifugation (3 - 5 s). The pellet was now treated with 250 µL 50 % glycerol. These beads can be stored at RT for 2 weeks. The coating with DNA was performed by vortexing the prepared beads (in 50% glycerol) for 5 min. 110 µL of the gold particles were aliquoted (for 10 bombardments, incl. 10 % loss) in a siliconized reaction tube. The beads were now vortexed for 1 min, 11 µL of plasmid pFC07 with a concentration of 950 ng/µL was added, 1 min of vortexed and 110 µL of 2.5 M $CaCl_2$ was added, 1 min vortexed, 44 µL 0.1 M Spermidine (highest quality and freshly prepared) was added and again vortexed for 1 min. After all additions the suspension was again vortexed for 3 min. Now the beads were allowed to settle and were spun briefly to remove the supernatant. The beads were then again resuspended in 330 µL 70 % ethanol (highest grade) with a pipette. The suspension was spun again and the supernatant removed. The coated microparticles were now treated with 110 µL of 100 % ethanol (water free) and vortexed for at least 3 min. Clumps of beads require to be dispersed by pipetting. 10 µL of gold beads were placed on macrocarriers/macrocarrier holder in the central region of each macrocarrier. The macrocarrier should be placed in a way to allow a fast drying of the ethanol.

unc-119 nematodes were cultured on egg plates (Berezikov et al., 2004; Hochbaum et al., 2010). The worms were washed several times to remove any debris or contamination of *E. coli*. 50 µL of highly packed *unc-119* worms were pipetted onto a refrigerated 9 cm NGM plate in a monolayer on a 2 cm *E. coli* spot (a yellow cut tip was used for pupating). The worms were now bombarded with gap distance of ¼ inch, a vacuum of 100 mbar, a 1350 psi rupture disc. Bombarded worms were allowed to recover for one hour and then washed from the plate with M9 buffer and divided among 20 × 10 cm NGM plates seeded with a lawn of OP50. The progeny of bombarded nematodes were starved for one to two weeks, because *unc-119* mutant animals do not form Dauer larvae and will not survive. From each plate with wild type phenotype 10 to 15 animals were singled out and checked for appearance of *unc-119* phenotypes hinting to array formation and not integration. This protocol was developed by Praitis et al. (Praitis et al., 2001) and modified by Ekkehard Schulze.

3.2.4. Aldicarb assay

The use of acetylcholine as a neurotransmitter is highly conserved throughout evolution. Nematodes like *C. elegans* use this neurotransmitter to stimulate muscle contraction. Exposing the worm to an acetylcholine esterase inhibitor like aldicarb increases the steady-state acetylcholine concentration at the neuromuscular junction (NMJ), driving all muscles to contract and leaving the nematode paralyzed. This dynamic process can be used to analyze functionality of the synaptic transmission machinery (Mahoney et al., 2006). As the gradual accumulation of acetylcholine, followed by paralysis is time dependent – a change of the response time (faster or slower) caused by a mutation would uncover which part of transmission machinery is affected. Mutations in proteins responsible for exocytosis lead to reduced secretion and therefore a longer period to accumulate acetylcholine for the complete paralysis (resistant to inhibitors of cholinesterase, RIC, e.g. the SNAP-25 homologue RIC-4). Conversely, a mutation in the regulatory/inhibitory system lead to constant secretion of acetylcholine and paralysis would occur earlier (hypersensitive to inhibitors of cholinesterase, HIC).
In this work two different aldicarb assays were applied. First, a time course experiment was performed. 25 animals were placed on a 25 mm NGM plate with 1 or 2 mM aldicarb. Every 20 min to 30 min the ratio of completely paralyzed worms per plate was determined, following gentle touches to the head of the animal, using a platinum wire pick.
The other assay was performed after neuronal RNAi knock-out of different target proteins. Here, 4 times 25 worms were placed in a well of a 24 well plate containing 1 mM aldicarb. After 100 min the ratio of mobile worms was quantified. For equal humidity for all wells only the outer wells were used. Due to the complexity of this experiment and the resulting chance of errors the tests were performed in quadruplicates (Vashlishan et al., 2008) and several candidates with altered aldicarb response could be detected.

3.2.5. Swimming assay

As any major disturbance of the neuronal and/or motor neuron network results in altered locomotion, counting of body thrashes in liquid media is used to identify mutations in the synaptic transmission apparatus (Kraemer et al., 2003). For a swimming assay 10 animals were placed in 200 µL liquid M9 in a 24 well plate well prefilled with NGM and allowed to settle for 1 min. Now the well was recorded for 1 min and 10 s and the trashes for all animals were scored for 1 min.

3.2.6. Genotyping of worms

Genotyping was used for the validation of integration and crossing success. Ten worms were put into a PCR tube containing 25 µL single egg worm lysis buffer (SEWLB; incl. proteinase K). Now the tubes were transferred for 15 min into the -80°C freezer to disrupt the worm cuticula and their cells. The nematodes were incubated for 1 h at 60 h to allow proteinase K to digest all proteins and finally for 95 °C for 5 min to denature the protease (avoidance of the digest of the subsequently added polymerase). The lysate can be used as the template for a PCR reaction. 2.5 µL of this solution is enough for a 20 µL reaction. In a next step single animals were analyzed with 2.5 µL buffer to validate the result and to make sure the entire population carries the sequence of interest.

3.3. **Molecular Biology**

3.3.1. Cloning

All cloning was performed via standard molecular biology techniques.
Some preparations were more complex and require explanation:
pFC01 (pUC19::p*snb-1*::ProtA::2xTEV::*snb-1*::Bicis::*unc-64a*::CBP::*unc-54* 3’ UTR): pUC19 was opened using KpnI and BamHI. The synaptobrevin promoter sequence of plasmid pSB103 (Mike Nonet, Nonet et al., 1998) was amplified using the following primers CCGGCGGTACCGCT-GAAATCTAGGATTACAGTA and CCGGCGGATCCGTCGTCAAGATGGTCTTATCCG. After ligation and reopening with BamHI and PstI the coding region and 3’UTR was inserted with the help of pSB103 and the primers CCGGCGGATCCGACGCTCAAGGAGATGCCGGC and CCGGCCTGCAGCTGAAAAGACCAGGCCCACTAA. The resulting plasmid was digested with BamHI and the N-TAP insert pBS1761 from Puig et al. (Puig et al., 2001) was amplified by using the following primers: CCGGCGGATCCATGGCAGGCCTTGCGCAA and CCGGCGGATCCTGACCCTCCGCCACCGGACCCTCCGCCACCAGACCCTCCGCCACCAA-GTGCCCCGGAGGATGA. The reverse primer introduced a 4x Glycine Serine linker to reduce a possible impact of the fusion construct. The plasmid was digested with StuI and DraIII to remove almost all of the TAP tag, but keep the G4S linker. The pBS1761 was used to create a ProtA-TEV sequence with these primers: GGCCCAGGCCTTGCGCAACACGA and CGGGCCACCAAGT-GCGCCCTGGAAGTACAGGTTCTCTGAACCTAGTTCACCTTGAAAATATAA. The second primer allowed us to introduce a second TEV site to improve the cleavage probability during purification. Then, the 3’UTR was removed by digestion with PstI and PshAI. The *snb-1* backbone

incl. promoter and N-terminal ProtA was generated by Alexander Gottschalk. An trans splice acceptor site was created originating from the plasmid pEntry(polycys)GFP (SL2; a gift from Mario de Bono, MRC Laboratory of Molecular Biology, Cambridge, UK) using the oligonucleotides Bicis fw neu: GTACAACTAGTAAGAGCTCAAGG and PstI Bicis rev new CTCTCTGCAGGTACAGCAGTTTCCCTGAA. This plasmid was called pUC19::p*snb-1*::ProtA::TEV::*snb-1*::bicis.

For the *unc-64* construct the CBP was modified: The plasmid pBS1479 was opened by PciI and NcoI digest and two annealed oligos: TGGTGGCGGAGGGTCTGGTGGCGGAGGGTC-CGGTGGCGGAGGGTCAGGGGTACCGGTATC and CATGGATACCGGTACCCCT-GACCCTCCGCCACCGGACCCTCCGCCACCAGACCCTCCGCCACCACATG were inserted. This was performed by Alexander Gottschalk. This plasmid was again opened by KpnI and NcoI digest and two annealed oligos: 5xG4S fw: CGTCCGGAGGTGGAGGGAGTGGCGGTGGC-GGATCTGGCGGGGGAGGGAGCGGGGGAGGAGGGTCAGGTGGAGGCGGAGC and 5xG4S rev CATGGCTCCGCCTCCACCTGACCCTCCTCCCCCGCTCCCTCCCCCGCCAGATC-CGCCACCGCCACTCCCTCCACCTCCGGACGGTAC were ligated into the vector to generate an 8xG4S linker. This template was amplified using primers BamHI CBP fw TTTAGGATCCT-ATGGTGGCGGAGGGTCTGGTG and SbfI Stop CBP: ACCTGCAGGTTAAAGTGCCCCGGAG-GATGAGATT. Digesting the amplificon and a pUC19 with BamHI and SbfI rendered them ligation competent and introduced a stop codon at the 3' end of CBP. The plasmid was opened with SphI and SbfI and *unc-54* 3'UTR from the Fire lab vector pPD95.75 was amplified using the primers SbfI 3'UTR AACCTGCAGGGTCCAATTACTCTTCAACATCCC and SphI 3'UTR neu GGCATGCGTAGGAAACAGTTATGTTTGG. The vector was digested with KasI, treated with Klenow and was then digested with BamHI resulting in a semi-blunt vector. The truncated *unc-64* was amplified using KpnI syx-1 fw GAAGGTACCATGGCATGCAAAAGCTAGCCG and BamHI syx-1a rev GCCGGATCCCGCAATGCCAGGAATATACTGAATG and pMH421 as a template. Then, the fragment was digested with BamHI and ligated into the semi-blunt vector.

The truncated *unc-64*a::CBP::*unc-54* 3'UTR template was amplified with two infusion primers using the infusion cloning technology from Clonetech: *unc-64* CBP infusion fw AGTAGGATGAGACACCATGGCATGCAAAAGCTAGCCG and *unc-64* CBP infusion rev CCAAGCTTGCATGCCGTAGGAAACAGTTATGTTTGG. The previously described plasmid was opened with SphI and the trunc *unc-64*::CBP::3'UTR was inoculated together.

pFC02 and pFC03: pFC01 was double digested with PvuI and SphI and blunted with T4 DNA polymerase. The pCFL350 was blunted after XhoI and SbfI digest. The ligation of both blunt end vectors resulted in plasmids with both orientations pFC02 (Left-right) and pFC03 (right left).

pFC04: a 2.3 kB 5' UTR was amplified using KasI p*unc-64* 2.3 fw and BamHI p*unc-64* 2.3 rev, and genomic DNA as template cloning it into pUC19::prab-3::*unc-64*a::3'UTR after KasI and BamHi digest.

pFC05 exchanging the truncated *unc-64* in the pFC01 with the full size *unc-64* amplified from pTX21 using KpnI *unc-64* exon 1fw and KpnI *unc-64* rev.

pFC06 and pFC07: pFC05 (The pUC19 p*snb-1*::ProtA::TEV::*snb-1*::Bicis::*unc-64*a::CBP::3'UTR) was now double digested with PvuI and SphI and blunted with T4 DNA polymerase, MosSCI vector pCFJ350 was treated with XhoI and SbfI and followed by a T4 DNA polymerase blunting step. The blunt end ligation resulted in both oriented inserts pFC06 and pFC07 coded the SNARE construct on the complementary strand compared to *C. Br. unc-119* (+)(results in a higher *unc-119* rescue probability; personal communication with Knudra Transgenics, Murray, Utah USA)

pFC08: pFC04 was double digested with KasI and BsiEI and blunted with T4 DNA polymerase. The pCFJ352 was opened with KpnI and blunted with T4 DNA polymerase. Both constructs were adjoined with the help of T4 DNA ligase.

pFC22: As the MCA-3 isoform b and d were identified in the mass spectrometry the fluorescence of one of these isoforms should be analyzed. As the coding transcript of isoform b was already at least 20 kB long, the cDNA of *mca-3* b (3.7 kB) was commercially synthesized (Genewiz Inc., South Plainfield, NJ;USA) and cloned into pCS55 [*punc-17*::ChR2::YFP::3'UTR] after removal of ChR2 by KpnI and NheI. This was done by infusion primer: mca-3 cDNA fw AGGACCCTTGGCTAG-CATGCCCGAATATGGTGCATC and mca-3 cDNA rev TGGTGGCGGCCGCGGGT-ACCGTCACGTGAGCAACAGAAACTGG and infusion cloning by Clonetech.

pFC23 (pUC19::p*snb-1*::mCherry::*snb-1*::3'UTR): The plasmid of Alexander Gottschalk pUC19-SNB-1-N-ProtA-2xTEV was digested with StuI and DraIII. The mCherry was amplified using infusion primers inf mCherry fw: CGGATCCATGGCAGGCCTATGGTCTCAAAGGGTGAAGA and inf mCherry rev: CAGACCCTCCGCCACCAAGTGTATACAATTCATCCATGCCACC with pCFJ104 (pmyo-3::mCherry) removing the stop codon from the end. The sequences were ligated using the infusion cloning kit from Clonetech.

pFC24 (L4440::*vti-1* seq.): The plasmid L4440 was double digested with HindIII and KpnI. The coding region of bp 10-867 was amplified using the primer inf vti fw 3 ATTCGATATCAAG-CTTAATCGGCAACAGTTGAGC and inf vti rev 3: TATAGGGCGAATTGGGTACCTTGG-

CGGTTGTAAATGGG using a template prepared by using a nested primer pair. These primer nest vti-1 fw CCACCTATCAGGTTCCATTTCC and nest vti rev: GTGGGTCCTAACGATCAGTTTG were applied to N2 genomic sequence as template.
The infusion amplificon and the cut vector were adjoined using the infusion cloning kit.

3.4. **Biochemical methods**

3.4.1. Purification of Tobacco Etch Virus protease

The imidazole side chain of the histidine shows a high affinity for chelated metals. A nickel ion is complexed by an immobilized chelating agent at the surface of sepharose beads (immobilized metal ion affinity chromatography, IMAC). During purification the His tag with its fusion protein is retained at the column and can be extracted from contaminating proteins of the lysis solution. After appropriate washing steps imidazole was administered to the washing solution and competed with the his-tag for the nickel ion eluting the clean fusion construct.
In cooperation with Orla Slattery form the Pos lab (Goethe University Frankfurt) the tobacco etch virus protease was prepared for further use. Some bacteria were transferred of a frozen perm culture (in a BL21 strain) with the plasmid pRK508TEV into 200 mL LB media (100 µg/mL Amp and 35 µg/ mL Chloramphenicol). The culture was incubated for 6 h at 37°C and then added to 2 L LB for an OD 600 nm of 0.1. Now the 2 L culture was incubated at 37°C until OD reached 0.2 to 0.3 (~1 h) and transferred to a 25°C incubator until OD reached 0.7-0.8. IPTG was added to a final concentration of 0.4 mM to induce the production of the TEV protease. After incubation for 4 h at 25°C the cells were harvested in a centrifugation step with 6000 rpm for 20 min at 4°C. The cells were resuspended in cold resuspension buffer (60 mL) and incubated with 30 mg Lysozyme for 30 min at 4°C. Now the cells were treated with 10 s ultrasound and 10 s rest on ice cycles. This was repeated for each liter liquid culture 8-10 times. After one round of ultracentrifugation for 1 h with 45,000 g the supernatant was used for the Ni-NTA purification. A Ni-NTA column was equilibrated with 4 volumes of degassed resuspension buffer and loaded supernatant onto Ni-NTA column with 0.4 mL/min (Flow rate 0.3). The wash was continued until no protein could be detected (base line). Now TEV was eluted with a continuous gradient ranging from 5 mM to 500 mM imidazole (see Figure 3.3). To each fraction 50 % glycerol and 5 mM DTT was added and frozen in the -80°C freezer for long term storage and use.

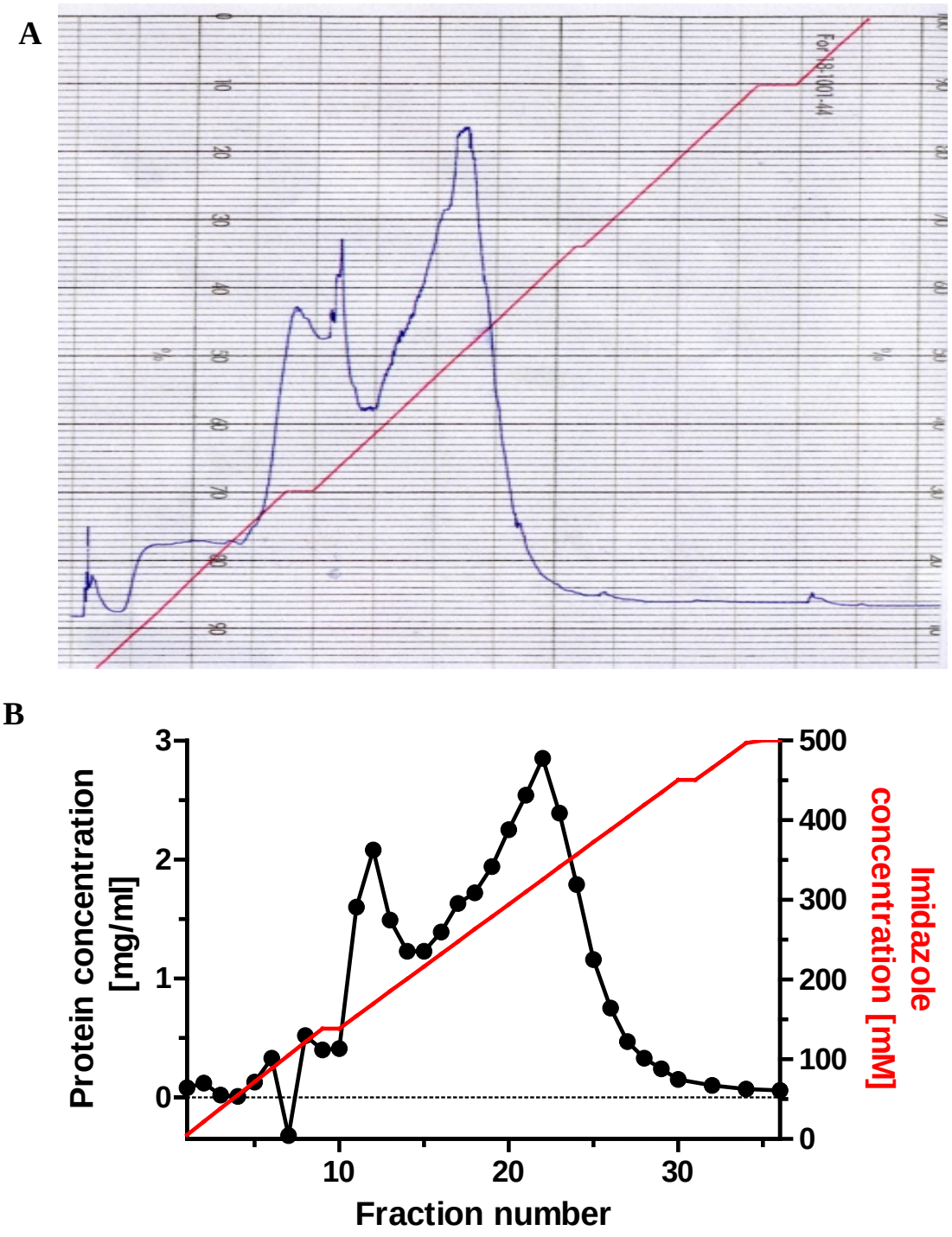

Figure 3.3 The elution profiles of His-tagged Tobacco Etch Virus Protease showed a high amount of eluted protease after reaching the concentration of 200 mM imidazole The profile shows the UV absorption at 280 nm in relation to the ratio of low imidazole solution (5 mM) to high imidazole solution (500 mM). The start of the red graph shows 100% solution A and 0 % solution B and finally 0 % solution A and 100 % solution B. You can see a first elution at 30 % B and the start of a second peak at 40 % is visible B. **B** The elution profile according to the calculated protein content.

All fractions with higher protein content of 1.5 mg/mL were analyzed via SDS Page (11, 12, 17-24). The purity in samples from fraction 17 was much cleaner, but even if the TEV protease is dominating the fractions, there are still many other proteins.

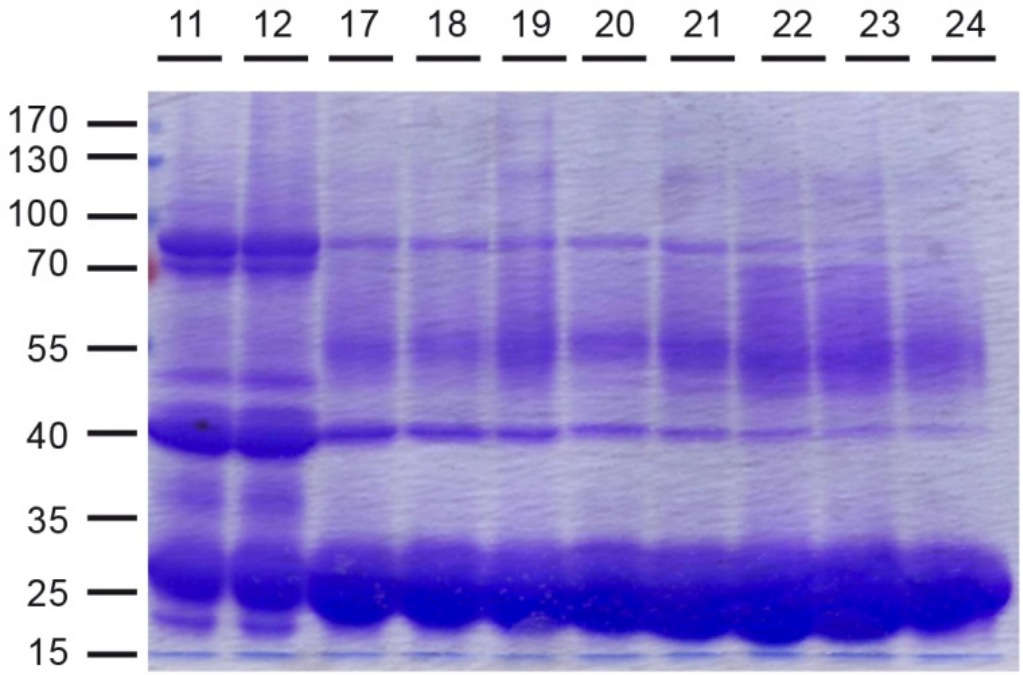

Figure 3.4 The highest concentrations of TEV were visible in fraction 17 to 24 TEV protease runs at 25 to 27 kDa. The numbers on the left indicate the molecular size in kDa and the numbers at the top the fraction number. A clear difference in the purity of the samples 11 and 12 and 17 to 24 can be seen.

After pooling fractions 17 to 24 Orla Slaterly of the Pos lab performed a size exclusion chromatography (gel filtration). The column contains porous beads which all molecules penetrate according to their volume (size). If a molecule is small it enters rather deep and has a longer route till elution. If the molecule is rather big it does not enter the beads and therefore pass the column rather fast (Eisenstein, 2006). After cleaning the TEV protease from contaminants a functionality test was performed. In cooperation with Victoria Decker a protease assay was performed with 1.5 µg substrate and 1 h of incubation at 4 °C with different concentrations and origins of TEV protease. The substrate was a gift by Markus Becker of the Tampé group.

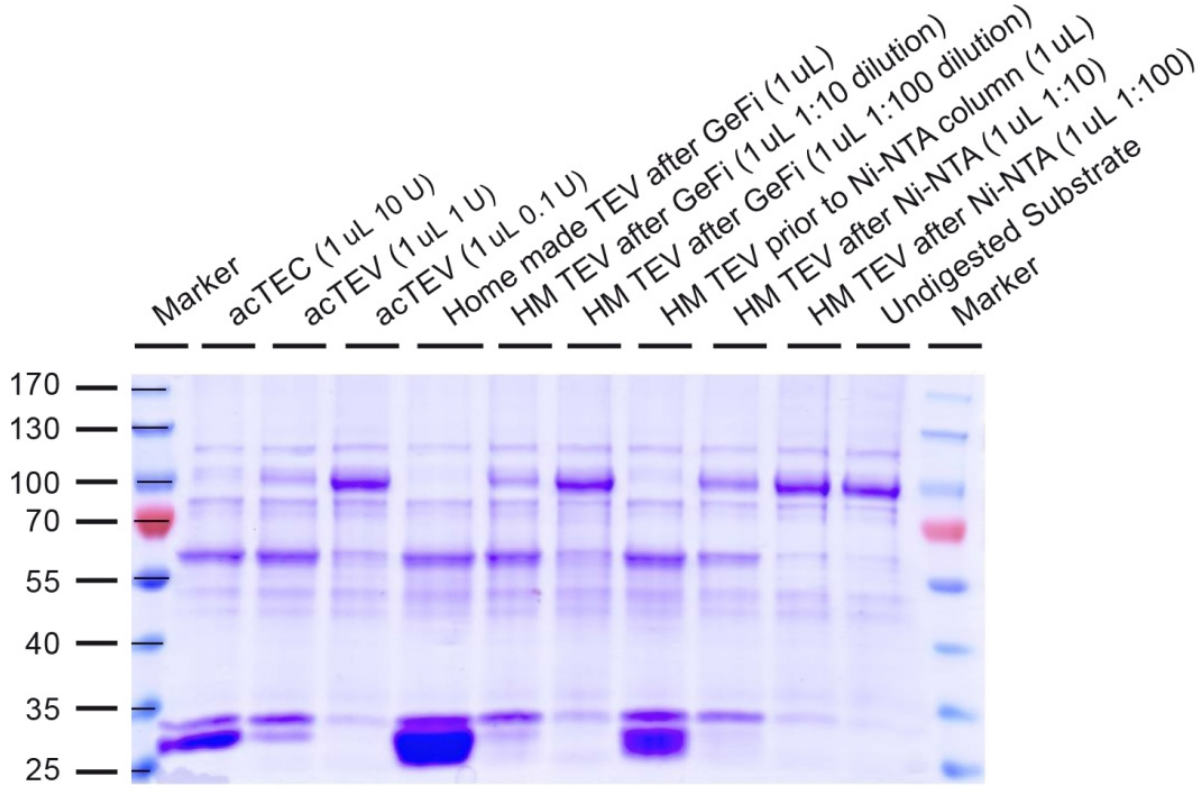

Figure 3.5 A protease assay demonstrated the functionality of the purified TEV To prove the functionality and purity of the TEV protease a digest assay has been performed. The TEV after gel filtration (column 5) showed the highest content and the best digestion result. Even with this high amount of TEV protease no other contaminating bands were visible.

The Home made TEV after Gel filtration was used in all of the following tandem affinity purifications.

3.4.2. Tandem Affinity Purification of synaptic vesicles

The TAP tag consists of two sequential purification tags: the Protein A of *Staphylococcus aureus* and two tobacco etch virus (TEV) cleavage sites at the N-terminus of SNB-1 and the Calmodulin binding peptide at the C-terminus of UNC-64 (Rigaut et al., 1999; Puig et al., 2001). The tagging of two complex partners and the change of the affinity matrix allowed purifying of only formed complexes and reducing the background to a minimum. Gottschalk et al. had shown that tandem affinity purification can be used to isolate integral membrane proteins (Gottschalk et al., 2005). Many other groups performed successful purifications in other species and could identify interaction partners (Rigaut et al., 1999; Puig et al., 2001; Li et al., 2004; Gloeckner and Boldt, 2009; Rohila et al., 2009; Völkel et al., 2010). The tandem affinity purification is preferable to the heterologous expression system, as the protein-protein interactions are most likely reflecting the in-vivo situation

(Puig et al., 2001; Gottschalk et al., 2005). The successful use of the antibody coated magnetobeads to purify SV and docked vesicles was shown by Burré et al. (Burré et al., 2006) and Morciano et al. (Morciano et al., 2005; Morciano et al., 2009).

For the purification of synaptic vesicles the standard TAP protocol needed to be modified. No detergent could be used and the IgG agarose and CaM Sepharose beads were exchanged to IgG coupled IgG magneto beads and CaM coupled magneto beads – previous experiments by Yvonne Füll and Yolanda Martinez-Fernandez showed a reduced elution using sepharose beads, probably due to sieving effects of the gravity flow technique. Coupling was performed one day in advance to avoid degradation of the coupled proteins (IgG and CaM). 5 mL 200 µL beads corresponding to 5 mg beads for coupling with 20 µg ligand were used for each preparation. The beads were washed 3 times with 15 mL coupling buffer and resuspended with 2.5 mL of coupling buffer. Now 6 mL of hIgG solution (Sigma) dissolved in coupling buffer (60 µg protein) was added. The beads were then mixed thoroughly, but foaming was avoided. 4.2 mL ammonium sulfate solution was added and put in the 37°C incubator O/N in a head over tail rotor. The beads were now washed three times with 15 mL 0.5 % BSA in 50 mM Tris pH 7.4 and the final washing step was kept for 1 h at 37 °C. The same protocol was used for the CaM beads, but was started one day later due to time shift. 55 g of worm suspension (corresponding to around 37 of worm pellet) were ground under liquid nitrogen until a fine powder resulted (portions of around 20 g were ground for 1 h). The powder was now slowly thawed on ice. 110 mL of lysis buffer (containing 3 Roche complete) were added and the solution was homogenized via a tight fitting glass tissue homogenizer (Kontes, New Jersey) on ice with 40 strokes. The homogenate was spun for 10 min at 1,000 g (3,000 rpm in an SS-34 rotor) to remove the first part insoluble material. The supernatant was set aside and the pellet was resuspended with 35 mL of lysis buffer dounced once more 40 times and again centrifuged. The supernatants were combined centrifuged for 30 min at 30,000 g (20,000 rpm in a Ti70 rotor). After centrifugation, the (fatty) top layer (containing lipids, personal communication with Alexander Gottschalk) was removed and the clear interphase (around 200 mL) was incubated with the prepared IgG magneto beads ON at 4°C in a head over tail rotor. The next morning the slurry was transferred bit by bit into 15 mL falcon tube positioned in a magnetic rack for at least 3 min. The resulting supernatant was applied to another 15 mL falcon tube in a magnetic rack to decrease the loss of magneto beads during collection. The magneto beads were concentrated in the first 15 mL falcon and washed with 15 times 10 mL IPP150 and 2 times 10 mL TEV cleavage buffer to remove the protease inhibitors. Again, two 15 mL falcons were used to avoid loss. The magnetobeads were resuspended in 5 mL of TEV cleavage buffer and 150 µL of TEV protease (Homemade and commercial turbo-TEV protease)

were added. The suspension was incubated in a head of tail rotor for ON at 16 °C. The liquid was transferred into 2 mL reaction tube in a magnetic rack and after 3 min of incubation the supernatant was removed. To the supernatant 12.5 µL of 1 M $CaCl_2$ (to compensate to EGTA and increase the Ca concentration to 2 mM), 5 µL of1 M Imidazole, 5 µL of1 M Mg acetate and 5 µL of 1 M DTT was added. The CaM magneto beads were washed with 3 x 3 mL Calmodulin Binding Buffer and the supernatant was added to the CaM magnetobeads and incubated for 4 h at 4 °C in a head over tail rotor. The CaM beads were now washed with 15 times 10 mL Calmodulin Binding Buffer and eluted with 10 times 100 µL Calmodulin buffer.

3.4.3. Sucrose gradient purification of synaptic vesicle

Different groups successfully used a gradient pre-purification step prior to magneto bead treatment for the preparation of synaptic vesicles (Morciano et al., 2005; Burré et al., 2006; Burré et al., 2007; Morciano et al., 2009; Boyken et al., 2013). Synaptic vesicles bound to membrane debris or vesicle pool compartments could reduce the accessibility of the TEV cleavage sites and thus reduce the protease activity. To improve the elution after IgG binding a sucrose gradient can be applied to separate free vesicles from membrane or compartment bound vesicles (personal communication with Sandhya Padmanabhan Koushika, Koushika Lab, Bangalore, India).

5 g of worm suspension corresponding to 3.3 g worm pellet were ground and 20 mL homogenization buffer was added. This suspension was homogenized via a tight fitting glass tissue homogenizer (Kontes, New Jersey) with 40 strokes –all steps were conducted at 4 °C. The supernatant was centrifuged at 50,000 g (26,000 rpm in a 70 ti rotor) for 40 min to clear the suspension from debris and heavy membrane fractions. The supernatant was again centrifuged at 175,000 g (50,000 rpm in 70 ti rotor) for 150 min to pellet the synaptic vesicles. The final pellet was resuspended in 1 mL homogenization buffer to obtain a suspension with a high concentration of synaptic vesicles.

The sucrose gradient had been prepared in advance with four different layers of sucrose concentration: 5 mL of 0.1 M, 5 mL of 0.6 M, 15 mL of 1 M and 5 mL of 1.5 M sucrose solution resulting in 30 mL. The vesicle suspension was carefully loaded onto the sucrose gradient and centrifuged at 60,000 g (22,000 rpm in a SW32 rotor) for 120 min. 1 mL fractions were collected and analyzed via SDS-PAGE and western blotting.

3.4.4. One-Strep Purification of synaptic vesicles

The One-STrEP™ protocol of the IBA GmbH was applied with minor modifications (IBA GmbH, 2008)

0.5 g of worms (corresponding to 3,3 g of worms) were thoroughly ground under liquid nitrogen and thawed after addition of 1.5 mL of Strep Buffer. The suspension was dounced 40 times with a tight fitting glass tissue homogenizer (Kontes, New Jersey) and the homogenate was centrifuged for 30 min with 50,000 g at 4°C (30,000 rpm in a TLA 55 rotor). During centrifugation the One-Strep beads were prepared. 40 µL of slurry corresponding to 2 mg of beads were washed 3 times with Strep buffer. After centrifugation the supernatant was added to beads in a 2 mL Eppendorf cup and incubated for 4 h in a head over tail rotor at 4 °C. The suspension was transferred into a filter column and allowed to empty by gravitational force. The beads were washed 5 times with 200 µL Strep buffer. 50 µL Strep elution buffer were added, incubated in a head over tail rotor for 1 h at 4 °C and the elution was collected. Now another 50 µL of Strep elution buffer was added and incubated for 2 h at 4 °C in a head over tail rotor with following collecting. The samples were analyzed via a SDS-PAGE and a western blot.

3.4.5. Tandem affinity purification of SNARE complexes

The tandem affinity purification was used as described in Gottschalk et al. (Gottschalk et al., 2005) with some minor modifications.

60 g of worm suspension (corresponding to 40 g worm pellet) were thoroughly ground under liquid nitrogen (~ 3 h). The powder was slowly thawed and 150 mL IPP150 (50 mM Tris pH 8, 150 mM NaCl, 3 tablets Roche complete w/o EDTA, 1 mM DTT, 0.5 mM PMSF) were added to the powder. The suspension was dounced 40 times with a tight fitting glass tissue homogenizer (Kontes, New Jersey) and the homogenate was centrifuged for 10 min with 3,000 g at 4 °C (3,800 rpm in tabletop Eppendorf centrifuge 5810 R). The supernatant was put aside and the pellet resuspended in 45 mL IPP150, again dounced and centrifuged. All supernatants were combined and centrifuged at 150,000 g for 1 h at 4 °C. All pellets were resuspended in 15 mL IPP150 incl. 1 % Triton. The solution was incubated head over tail for 1 h and dialyzed with 3 times 5 L of IPP150 with 0.05 %. The solution was incubated with washed 500 µL IgG Agarose bead slurry for 6 h. The beads were loaded into 10 Mobicol columns. The columns were washed thoroughly with 150 mL IPP150 including DTT and PMSF. Then, the buffer was changed/the beads washed with 50 mL TEV cleavage buffer (TCB). The last milliliter of TCB was used to transfer the beads to a 2 mL Eppendorf cup and was filled up to 2 mL. 25 µL (500 U) of commercial TEV and 25 µL homemade

TEV were added to the cup and incubated overnight at 16 °C in a head over tail rotor. The beads were collected by filtration columns (Mobicols; MobiTec GmbH) and centrifugation (100 g for 1 min at 4 °C). Unspecific protein on the beads was removed with additional 2.5 mL Calmodulin Binding Buffer. 2.5 mmol $CaCl_2$ were added to the Eluate (2 mM for binding and 0.5 mM for compensating 0.5 mM EDTA) (5 µL of 1 M $CaCl_2$). Then 500 µL of Calmodulin beads were added to the Eluate and incubated for 4 h at 4°C. The liquid was distributed into 5 Mobicols and the beads were washed with 30 mL Calmodulin Binding Buffer each. Now the complex was eluated in 100 µL fractions each separately collected and then pooled according to the fraction count.

Each fraction of 500 µL was precipitated with 125 µL trichloroacetic acid (TCA), incubated on ice for 10 min and spun for 5 min at around 16,000 g (14,000 rpm in a microcentrifuge). The supernatant was removed leaving the pellet intact and washed twice with 200 µL ice cold acetone (5 min at around 16,000 g). The pellet was dried at the heating block at 95 °C for 5 to 10 min. The pellet was resuspended in 25 µL 1 X Laemmli buffer and boiled for 10 min at 95 °C. If the dye turned yellow 0,5µL of 0.5 M Tris pH 6.8 was added to buffer residual protons from TCA. The fractions were analyzed by western blot, silver stain and mass spectrometry.

3.4.6. Mass spectrometric analysis

The protein sample preparation and mass spectrometric analyses were performed by Heirich Heide and Ilka Wittig both from the department of Functional Proteomics at the Faculty of Medicine of the Goethe University in Frankfurt am Main and Uwe Plessmann from the Urlaub Mass Spectrometry Research Group at the Max-Planck-Institute for Biophysical Chemistry in Göttingen. The protein samples were digested by trypsin (sequencing grade, Promega) in 50 mM ammonium hydrogen carbonate solution for 16 h. The resulting peptides were dried, resolved in a solution of 1 % acetonitrile and 0.5 % formic acid. The solution was loaded onto a C18 reversed-phase precolumn (Zorbax 300SB-C18, Agilent Technologies) and the peptides were separated by an in-house packed 3 µm Reprosil C18 resin (Dr. Maisch GmbH) picotip emitter tip (diameter 75 µm, 10 cm long, New Objective, Woburn, USA) by gradients from 5 % to 50 % acetonitrile with 0.1 % formic acid for 60 min with an Agilent 1200 nano-high-performance liquid chromatography (HPLC) system. The hydrophilic gradient was followed by a washout phase for the hydrophobic residues applying 90 % acetonitrile, 0.1 % formic acid and column equilibration with 5 % acetonitrile, 0.1 % formic acid for 15 min. The liquid chromatography-electron spray ionization tandem mass spectrometry (LC-ESI-MS/MS) was performed on an Orbitrap XL mass spectrometer (Thermo Scientific). The resulting MS data was recorded by data-dependent acquisition top 10 method selecting the most abundant

precursor ions in positive mode, analyzed via the Mascot program Max Quant and different databases: uniprot *Caenorhabditis elegans* (Heirich Heide and Ilka Wittig), ws240 (most current worm peptide database from wormbase.org at that moment) and deposited sequences of the fusion constructs (Uwe Plessmann).

3.4.7. Fast Protein Extract from C. elegans

For small amounts of protein for an SDS PAGE, the following protocol was used. Worms were grown on one small NGM dish (6 cm), cultivated until short of all bacteria being consumed, were washed with cold M9 into a reaction tube and briefly spun down for 1 min with 1000 g at 4 °C. The pellet was washed with M9 until the supernatant was clear. The supernatant was removed, 30 µL of ESB was added and immediately heated to 100 °C for 3 min. 30 µL of glass beads were added and vortexed for 2 min. Another 70 µL ESB was added, heated up to 100 °C for 1 min and spun shortly. 5 to 20 µL were used for SDS PAGE analysis.

3.4.8. SDS-PAGE, Western blotting and immuno detection

The polyacrylamide gel electrophoresis (PAGE) can be used to separate protein samples according to their size. Proteins migrate in a polyacrylamide matrix at a specific speed according to the mesh size of the matrix, their molecular weight, the structure and electrical charge. Sodium dodecyl sulfate (SDS) binds to the protein backbone and introduces a charge according to the protein weight and destroys any secondary structures. Application of DTT or beta-mercaptoethanol and heating up to 95 °C destroys all disulfide bonds and only linearized subunits enter the acryl amide matrix.

First, the gel apparatus was assembled and the separating gel was filled into the gel chamber. The liquid was overlayered with isopropanol and allowed to solidify. The isopropanol was discarded and the chamber was washed few times to remove residual alcohol. Now the stacking gel was combined and poured into the chamber. The comb was inserted and the gel was allowed to polymerize. After the introduction of the different samples in the different wells an electrical voltage of 25 to 200 V was applied. The use of bromophenol blue in the samples buffer visualized the progression of electrophoresis.

After separation the gel was addressed either to a Coomassie stain or silver stain, in which all proteins are visualized without identification or a western blot. Here, the separated proteins were transferred unto a nitrocellulose membrane for later immuno detection. The gel, 6 sheets of 3 mm filter paper and the nitrocellulose were incubated for 10 min in transfer buffer. Then 3 layers of

3 mm filter paper, the gel, the membrane and again 3 layers was placed on the semidry blotting chamber. The lid was closed and a current of 0.8 mA/cm^2 for 90 min was applied. After blotting the membrane was washed 3 times 1 min with water and treated with Ponceau S staining solution. Hereby, the successful protein transfer was tested. The staining was removed by several washes with TBS-T. Now the membrane was blocked by application of 5 % milk in TBS-T. The first antibody was applied for one hour at RT in 5 % milk/TBS-T, then the membrane was washed three times 5 min with TBS-T. Then nitrocellulose was incubated with the secondary antibody for one hour at RT in 5 % milk/TBS-T and again washed three times with TBS-T for 5 min. Finally, the membrane was addressed to a chemiluminescence reaction with the help of the horseradish peroxidase at the Fc terminus of the secondary antibody. The ECL solution was layered onto the membrane and the emerging photons were documented by a CCD camera.

3.4.9. Stripping

The antibody labeled blot was applied with stripping buffer for 30 min at 50 °C. The membrane was washed 5 times 5 min with TBS-T and olfactory tested for residual sulfuric compounds. The blot was now blocked again with 5 % milk in TBS-T for 1 h at room temperature and could be labeled with new antibodies.

3.4.10. Silver staining

The gel was fixed by treatment for at least one hour best ON with 50 % methanol, 12 % acetic acid, 0.5 mL/l 37 % formaldehyde solution. The gel was now washed three times for 20 min with 50 % ethanol and treated with 0.2 g/l $Na_2S_2O_3$ 5 H_2O for one minute. The gel was washed 3 times 20 s with H_2O and treated for 20 min with a 2 g/l $AgNO_3$ and 0.75 mL/l 37 % HCOH solution. Now the gel was washed three times for 20 s with distilled water. Development was induced by application of a solution containing 60 g/l Na_2CO_3, 0.5 mL/l 37% formaldehyde and 4 mg/l $Na_2S_2O_3$ 5 H_2O for 10 min. After complete staining the gel was washed twice with water for 2 min and stopped by 50 % methanol and 12 % acetic acid for 10 min. For long term storage the stain was now washed with 50 % methanol for at least 20 min and dried on a drying rack.

4. Results

4.1. Synaptic vesicle purification

4.1.1. Design of SNG-1::TAP tag fusion protein for native vesicle purification

The identification of interaction partners of the synaptic vesicle proteins has been successfully performed by several other groups (as discussed in chapter 2.4) (Miljanich et al., 1982; Takamori et al., 2006; Burré et al., 2007; Morciano et al., 2009). These groups discovered many unknown proteins, but the functional characterization of identified proteins remain tedious. The purification of SV proteins of the nematode *C. elegans* would allow, with its corresponding genetic and behavioral tools, a faster determination of a neuronal role of discovered proteins. Further explorations of the role of unknown interaction partners could elucidate the conserved transport and regulatory machinery. The purification of an intact organelle should discover these interaction partners. In our lab several unsuccessful trials with TAP tagged synaptobrevin-1 (SNB-1) with the expression as extrachromosomal arrays and integrated array have been performed – especially eluting the synaptic vesicles from purification beads turned out to be difficult. In this thesis different modifications of the initial purification method were performed:

a) **Utilization of a low copy synaptic vesicle protein**
b) **Mos1 single copy integration**
c) **Introduction of additional TEV cleavage sites**
d) **Extension of the linker region**

a) The intention behind utilizing synaptogyrin (SNG-1), a synaptic vesicle protein with a low copy number, instead of SNB-1, the most abundant vesicle protein, was to reduce the binding sites of a vesicle to the IgG bead. Takamori et al. detected two copies of SNG-1 on each vesicle compared to SNB-1 with 70 copies (Takamori et al., 2006). As the TEV digest is a rate limiting step and an efficiency of 100 % is never reached (Arnau et al., 2006; Gloeckner and Boldt, 2009), undigested ProtA-SNB-1 would adhere to the IgG beads inhibiting elution. Therefore, reducing the binding sites should improve the elution in an incomplete cleavage situation.

b) To generate a more natural expression pattern (including a reduced expression) and to avoid purification of false interaction partners due to mislocalization, the Mos1 single copy integration strategy was applied (for details see chapter 3.2.2 and next paragraph)(Frøkjær-Jensen et al., 2008; Frøkjær-Jensen et al., 2012).

c) The introduction of more cleavage sites by Yvonne Füll in our lab was supposed to increase the linker size and to improve digestion of the construct.
d) As described by Takamori et al. the synaptic vesicle contains a large quantity of proteins with a multitude of surface domains (Figure 2.9) (Takamori et al., 2006), which might be a reason for a steric interference. The extension of the linker region making the tag longer should make it more accessible for interactions and cleaving enzymes improving further purification steps.

SNG-1::8XG_4S::CBP::4x(G_4S::TEV)::G_4S::ProtA

The final SNG-1 fusion design showed an elongation between SNG-1 and CBP and G4S-linkers in combination to additional cleavage sites. The G_4S-linker between SNG-1 and CBP was introduced to increase the interaction of CBP with calmodulin beads; the insertion of several TEV cleavage sites with G_4S linker had the aim to improve the cleavage probability.

4.1.2. Application of Mos1 single copy integration to generate a low expression strain

The Mos1 Single copy integration (MosSCI) from the Jorgensen lab was not only used as a fast integration method to avoid problems with mosaicisms and transmission rates (Yochem, 2003), but in addition it induced a native expression with only one copy – reflecting the natural expression rate (Frøkjær-Jensen et al., 2008; Frøkjær-Jensen et al., 2012). High-copy transgenes are often down-regulated by transgene silencing and are subject to misrouting (Praitis et al., 2001; Frøkjær-Jensen et al., 2008). The successful injection was demonstrated by an *unc-119* rescue phenotype (compare chapter 3.2.2).

4.1.3. Tandem affinity purification of C. elegans synaptic vesicles using TAP tagged synaptogyrin results in an insufficiently pure fraction for proteomic analysis

To maximize the amount of transgenic worms a liquid bioreactor was utilized (compare chapter 3.2.1). To test different immobilization techniques and bead materials the abundance of the TAP signal after application of an anti-TAP antibody was compared. The different samples contained either beads with a carboxyl-residue from Chemicell, Dynal, and Pierce, or tosyl-residue beads from Dynal. The coupling of the carboxyl magneto beads to IgG required 1-Ethyl-3-(3-dimethylaminopropyl) carbodiimide (EDC). The tosyl beads do not need to be chemically activated since the tosyl beads react with amino groups autonomously. The different beads displayed a variety

of binding capabilities (compare Figure 4.1), with tosyl-residue DynaBeads showing the most promising results.

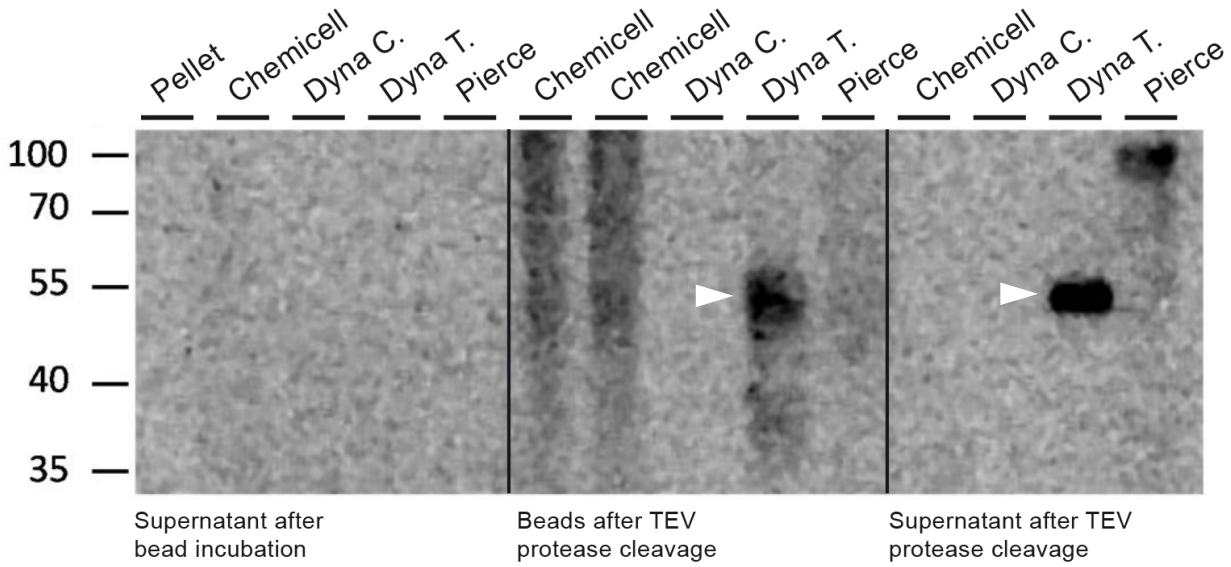

Figure 4.1 The purification test demonstrated that tosyl-activated DynaBeads and Pierce Carboxyl beads have the strongest binding and elution capability Four different kinds of beads according to manufacturer and coupling strategy were tested. Chemicell: Chemicell beads with carboxyl residue, Dyna C.: DynaBeads with carboxyl residue, Dyna T: DynaBeads tosyl-activated and Pierce: Pierce Beads with carboxyl residue. The beads tosyl DynaBeads and Pierce carboxyl beads showed the signal with the highest intensity. The band at around 50 kDa (white arrowhead) probably reflects SNG-1::TEV (TAP after cleavage). A second Chemicell lane was used in the beads after TEV samples as the loading seemed incomplete. Antibody: Anti-TAP (Pierce).

SNG-1 has a molecular weight of 35 kDa and fusion of TAP with SNG-1 resulted in a calculated size of 53 kDa. In Figure 4.1 two characteristic signals were detected: at around 50 kDa the beads and the supernatant of Dyna beads probably representing a cleaved SNG-1 (according to following experiments) and at the supernatant of Pierce beads a signal at 90 kDa displaying probably a possibly uncleaved SNG-1::TAP. The uncleaved version could be an artifact due to transfer of magneto beads the supernatant and the subsequent TCA precipitation. In the experiment the DynaBeads with Tosyl coupling and Pierce carboxyl beads showed the highest binding capacity, whereas the DynaBeads seemed to be the most promising bead/coupling strategy. Using these beads for a tandem purification a signal at 65 kDa and 35 kDa could be detected for the DynaBeads and a weak signal at 40 kDa for the Pierce beads (Figure 4.2). The combination of both samples and the application to calmodulin beads (commercial sepharose CaM beads, Sigma Aldrich) did not show any purification success since the flow through showed the same signal as the IgG elution sample. Still a rather faint band at 55 kDa could be detected in the CaM bead sample after elution (Figure 4.2).

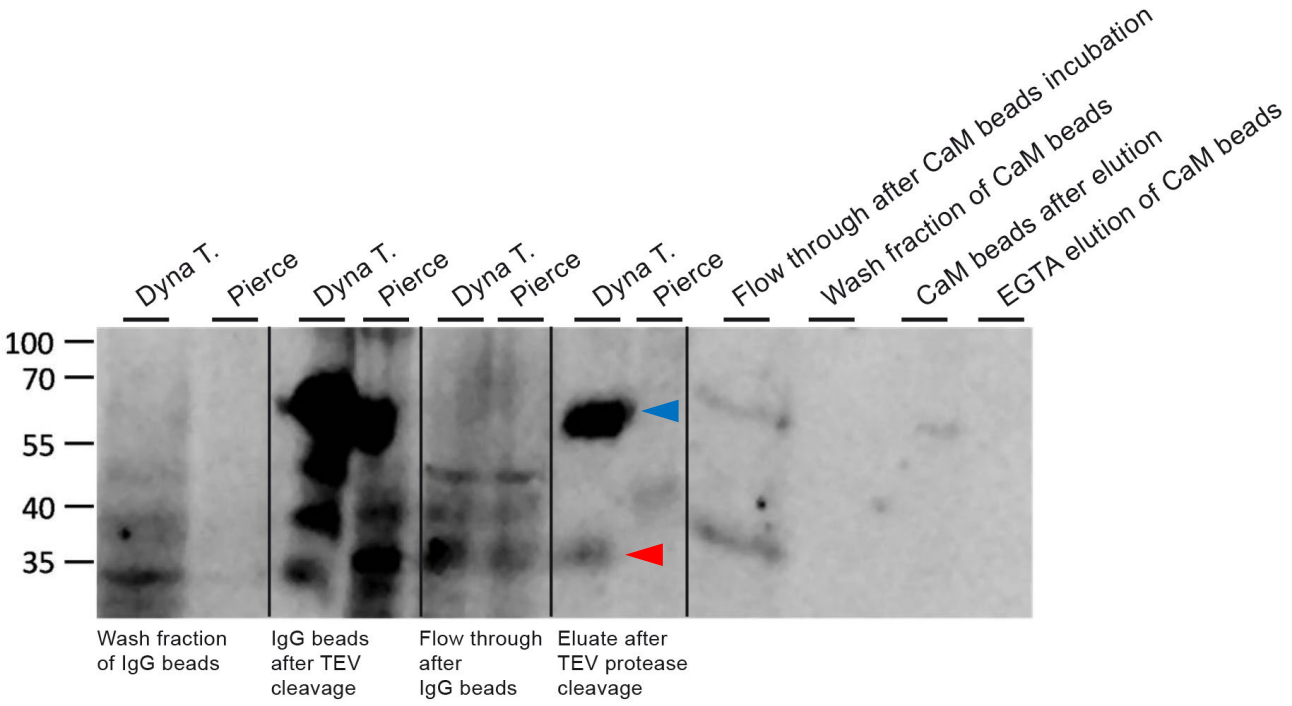

Figure 4.2 The tandem affinity purification showed a strong elution from IgG beads, but only a weak signal on calmodulin beads Dyna T: DynaBeads tosyl-activated and Pierce: Pierce Beads with carboxyl residue. A tandem affinity purification was performed utilizing the Dyna and Pierce magnetobeads of the previous experiment. The eluate of DynaBeads showed a strong signal at 65 kDa (blue arrowhead) corresponding to uncleaved SNG-1::TAP and a weak signal at 35 kDa (red arrowhead) corresponding to cleaved SNG-1. The flow through showed a rather similar signal distribution and a faint band at the eluated CaM beads at 55 kDa. Antibody: Anti-TAP (Pierce).

After these results only tosyl DynaBeads were used for the following experiments. Even an elution could be detected; the flow through sample showed a large concentration of unbound cleaved and uncleaved SNG-1. Thus, it was speculated that this was the result of the inaccessibility of the calmodulin binding peptide during purification and therefore the linker between SNG-1 and CBP was elongated (see chapter 4.1.1d)). To determine the functionality of sepharose beads CaM sepharose beads were tested in comparison to CaM magneto beads (Figure 4.3).

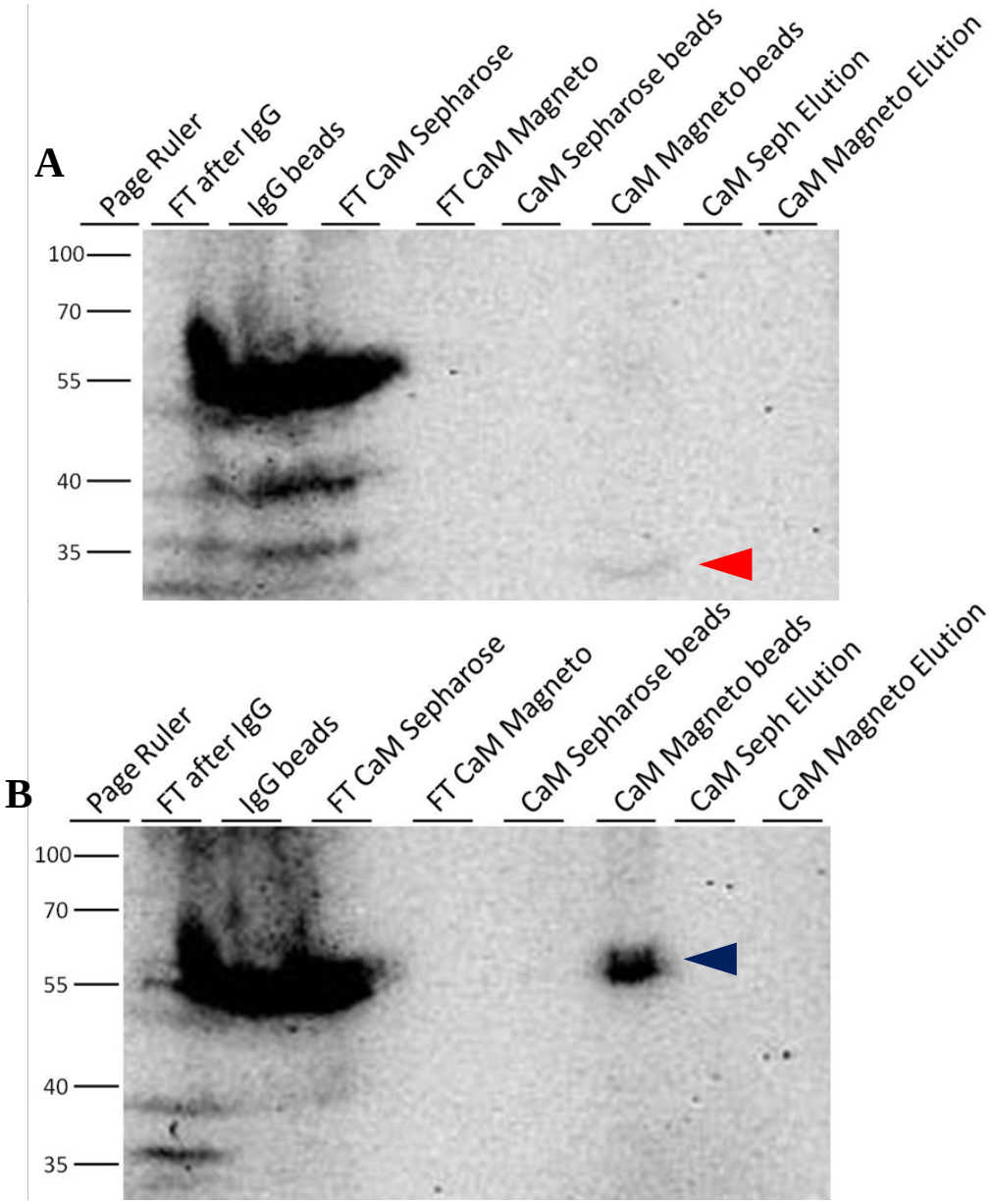

Figure 4.3 The signals of the calmodulin beads after TEV digest showed low amount of digested and high amount of undigested SNG-1::TAP Tandem affinity purification was performed to test the extended linker and compare the two different types of CaM beads. **A** The application of anti-TAP antibody showed a weak signal of cleaved SNG-1 on the magneto beads (~ 35 kDa; red arrowhead). **B** After stripping and incubation with the PAP complex the magnetobead sample after TEV incubation showed a strong signal for uncleaved SNG-1::TAP (~ 55 kDa; blue arrowhead. FT flow through; CaM calmodulin; Seph sepharose. Antibodies A: Anti-TAP antibody (Pierce); B peroxidase antiperoxidase complex (PAP; Sigma). FT Flow through, IgG immunoglobulin G, CaM calmodulin, TEV tobacco etch virus protease.

The comparison of CaM sepharose beads and CaM magneto beads showed a major difference in protein binding capabilities. Magneto beads displayed a weak but detectable signal for cleaved SNG-1 and a strong band for uncleaved SNG-1::TAP (Figure 4.3). Unfortunately, the precipitation of the elution samples did not show any of the mentioned signals. In a purification following the same protocol, no protein bands could be detected in a western blot, possibly due to technical

difficulties during the blotting. Addressing a silver staining with the remaining elution fractions displayed numerous proteins (Figure 4.4). One prominent band at around 20 kDa reflected probably CaM (compare Figure 4.4 and Figure 4.6).

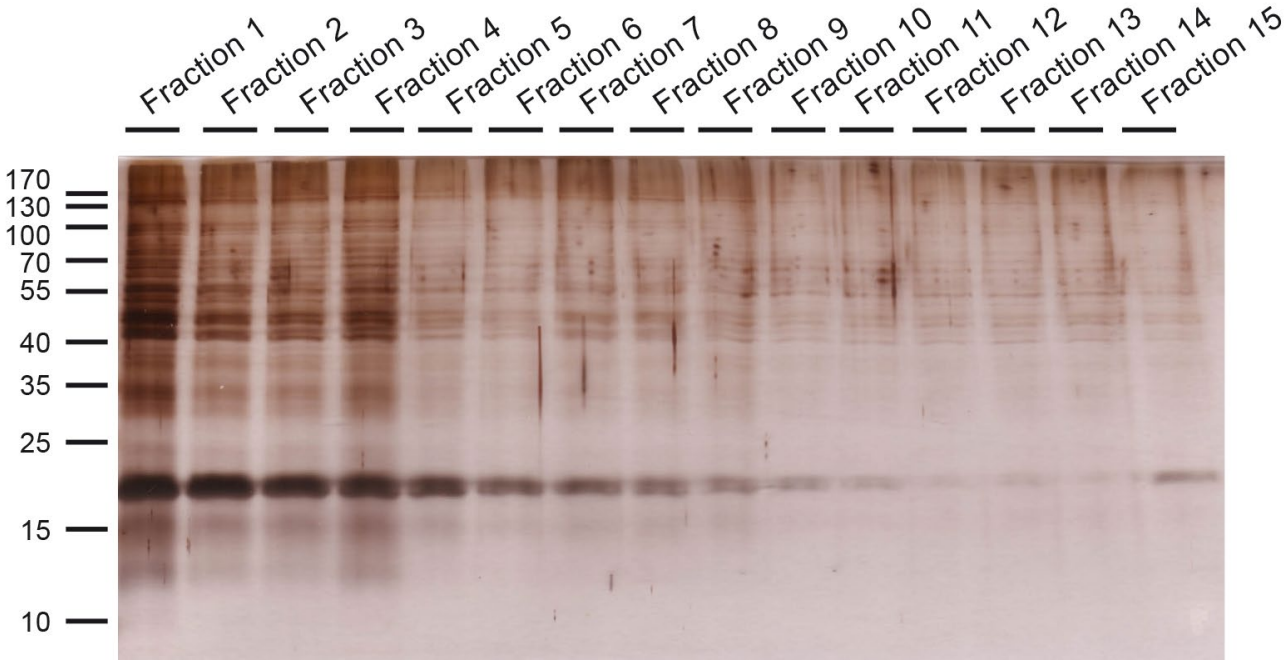

Figure 4.4 The elution fractions from the CaM column of the SNG-1::TAP sample shows a diverse set of proteins The elution fractions of a tandem affinity purification (second step, CaM columns) were analyzed by SDS PAGE and silver staining. The different elution fractions showed a comparable set of proteins with descending intensity. A prominent band at 20 kDa was visible.

The mass spectrometric analysis of the samples (Yates lab, The Scripps Research Institute, La Jolla, California, USA) did not detect SNG-1, SNB-1 or any obvious synaptic vesicle protein. Analysis of a combination of the different fractions did not reveal any positive immuno blot signal.

In a different purification the elution from IgG beads showed proteins, but no elution of material from CaM beads could be detected. Analyzing the CaM beads via silver staining showed possible SNG-1 bands, presumably CaM bands (same height as loaded CaM beads) and other potentially interesting proteins bands (Figure 4.5).

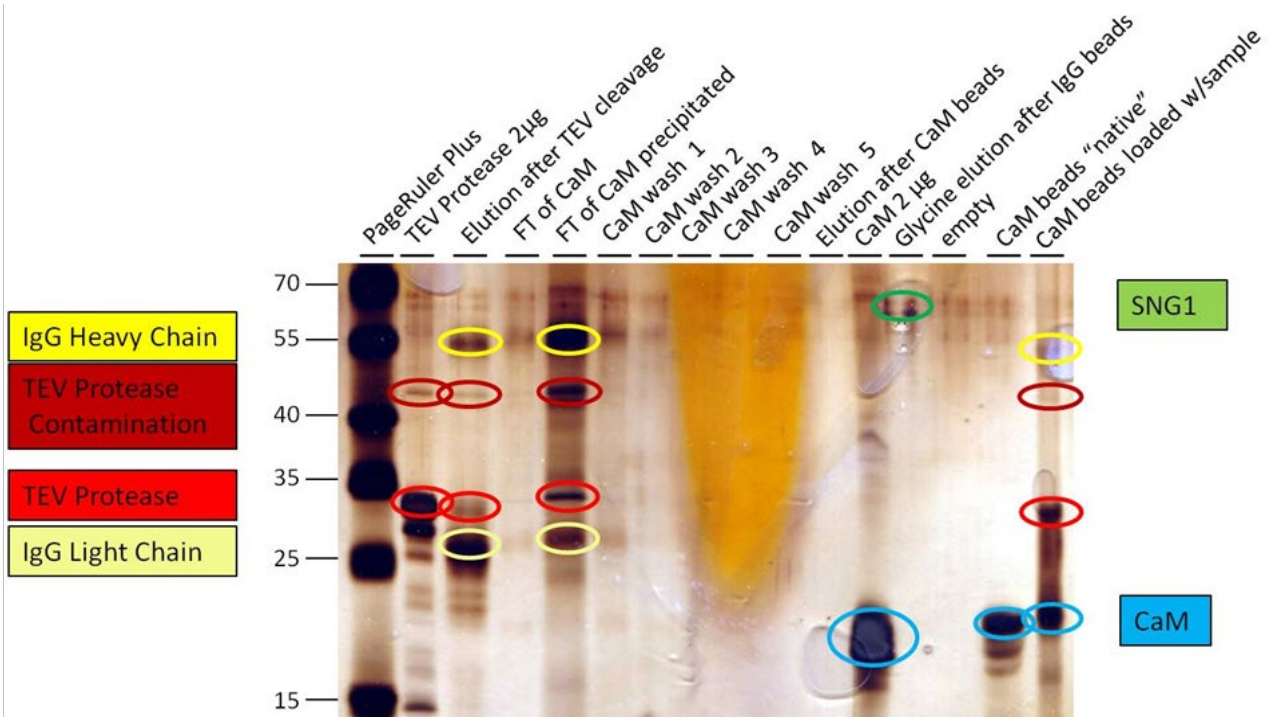

Figure 4.5 The CaM beads after purification displayed in addition to assumed proteins, proteins with unknown identity The CaM beads retained a diverse set of proteins with a possible SNG-1. Yellow circles correspond probably to IgG chains; red circles probably to TEV Protease and TEV contamination; blue circles assumed to represent calmodulin, and the green circle possibly to SNG-1. FT Flow through, CaM calmodulin, IgG immunoglobulin G, TEV tobacco etch virus protease. Silver staining of SDS PAGE, wash 1 – 5 corresponds to the different wash fractions, CaM beads "native" corresponds to unloaded CaM beads.

The CaM bead sample was analyzed by tandem mass spectrometry by Uwe Plessmann in the Urlaub lab in Göttingen (MPIBPC). However, despite detection of some neuronal proteins (e.g. SNG-1, SNB-1 and SNT-1) more than 1100 proteins were identified, leaving the significance of this data rather doubious.

4.1.4. For further opimization of the synaptic vesicle purification several alterations of the strategy were tested

1) **Different sodium chloride concentrations:**

   The sodium chloride concentration during purifcation was gererally at 150 mM to preserve the integrity of the vesicle. But as the digest seems to be the rate limiting step concentrations of no NaCl, 150 mM or 300 mM were tested to allow changes in the conformation or to induce ruptures of possibly formed synaptosomes and possibly allow a more efficient TEV cleavage. The samples treated with 150 mM NaCl during purification displayed the band with the highest intesity, yet no quantiativly digest was observeable (by reduction of TAP intensity before and after TEV digest) in any of the three concentrations (Figure 4.6).

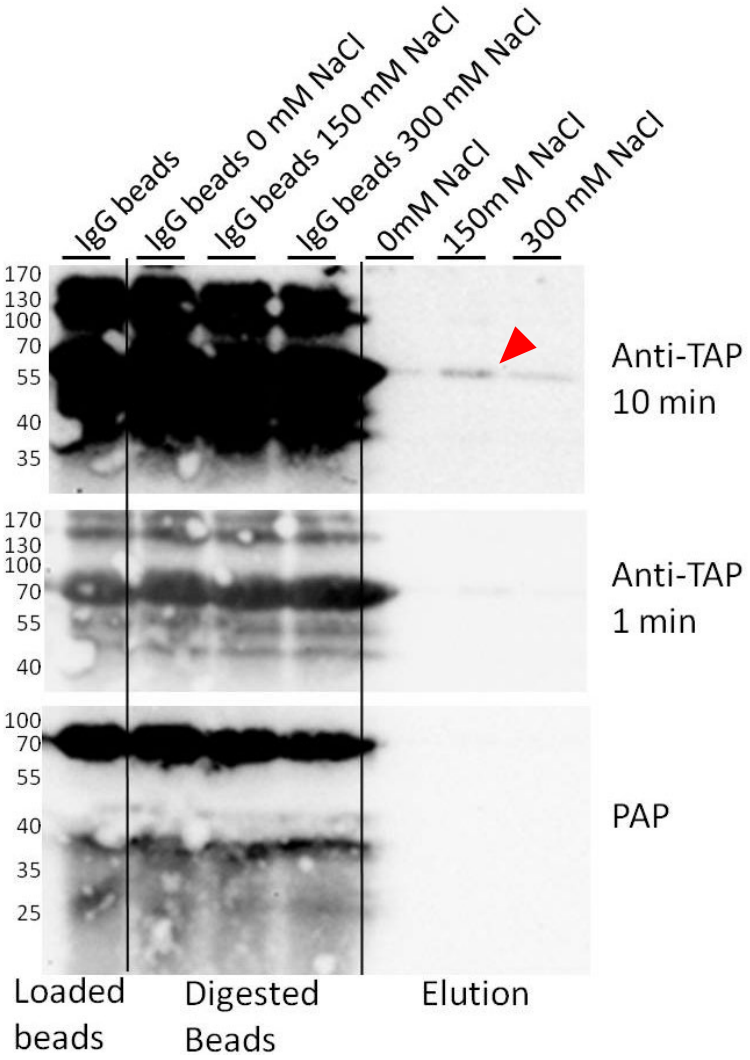

Figure 4.6 A-C The elution from IgG beads seemed to be most efficacious at 150 mM sodium chloride concentration The loaded beads represent the washed beads loaded with the synaptic vesicle suspension after centrifugation. Three different concentrations 0 mM, 150 mM and 300 mM NaCl were used during 16 h TEV cleavage. The digested bead samples represent the beads after washing and digest with the different salt concentrations. The elution is the elution fraction after 16 h of digest. Here the fraction corresponding to the 150 mM NaCl concentration displayed the most intense elution band (red arrowhead). The bead samples seem to retain the same intensity of undigested TAP in comparison to the loaded beads despite extensive TEV digest. The western blot after anti-TAP antibody imaging was stripped and retreated with PAP complex.

2) Prepurifcation with glucose gradient centrifugation

Several other labs successfully generated synaptic vesicle samples by using rat or mouse brains. As working with *C. elegans* does not allow fractionation of neuronal tissue, concentration of vesicular organelles from the crude extract could be beneficial for the first steps of purification. Crude synaptosomes and other contaminating tissue could be removed and would allow a more targeted purification. A sucrose gradient for isolation of SVs was

used (personal communication with Sandhya Padmanabhan Koushika, Koushika Lab, Bangalore, India) (compare methods chapter 3.4.3). The crude homogentate was loaded onto a tube with a discontinous gradient of four different sucrose concentrations (0.1 M, 0.6 M, 1 M, 1.5 M). After centrifugation for two hours the gradient was fractioned and obtained samples were analyzed for the TAP signal in a western blot.

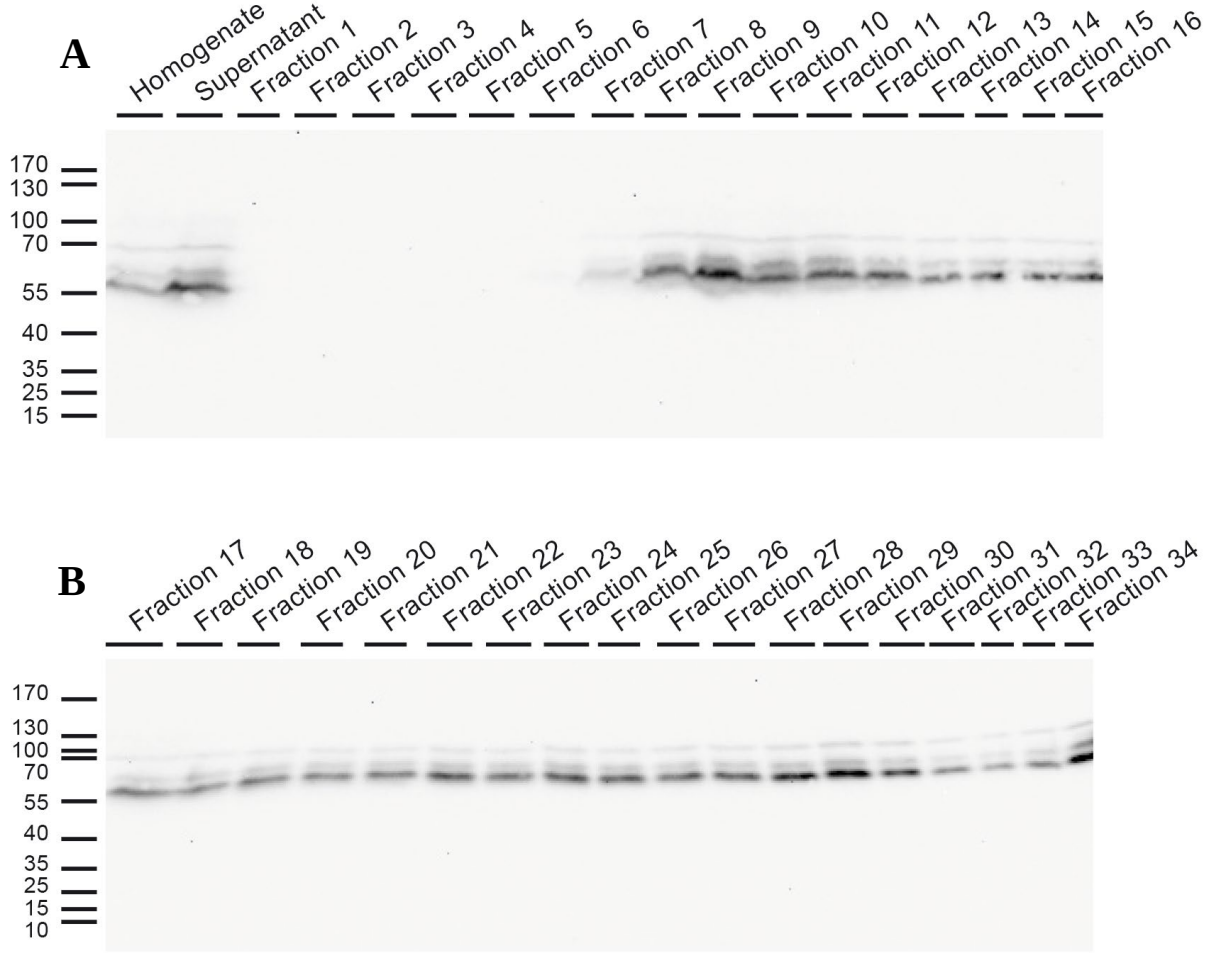

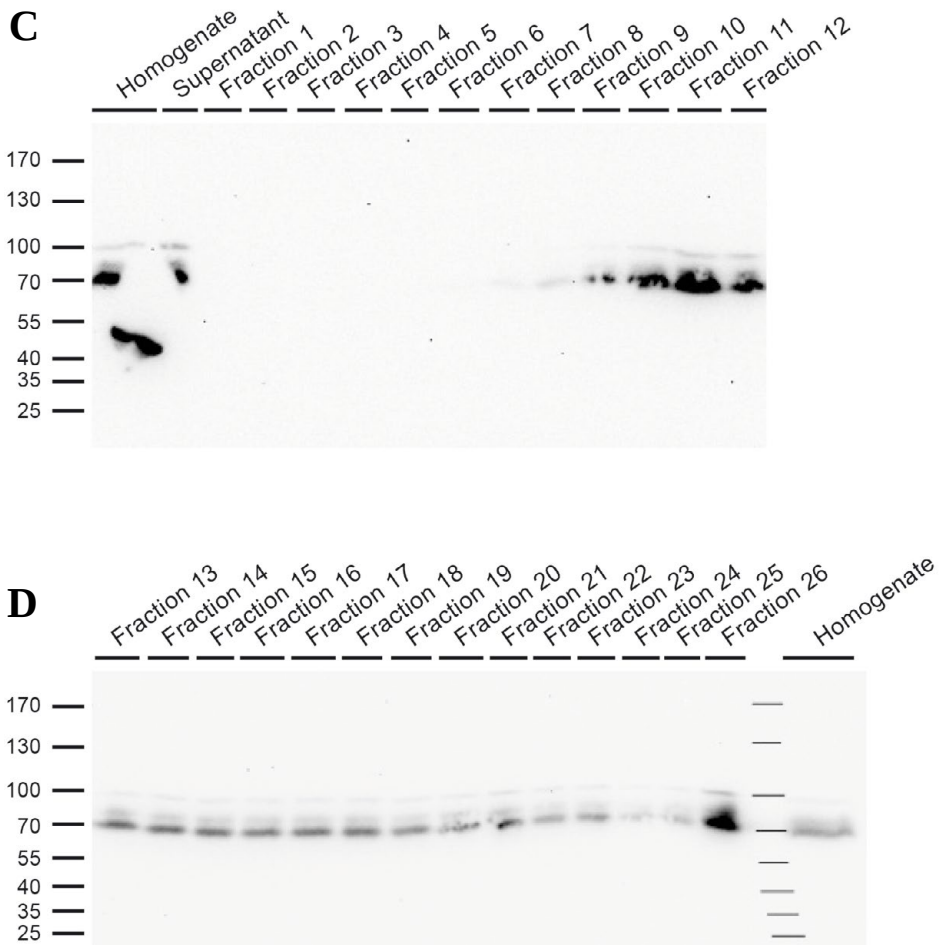

Figure 4.7 The sucrose gradient fractionation revealed no enriched fractions The western blot reflected the different fractions obtained in two different sucrose gradient purifications (A/B and C/D). In both experiments no clear enrichment was visible (fractions with almost no signal in contrast to fractions with an intense signal). The signals in C and D could hint a fractionation to the fractions 9 to 12 and to fraction 29, but the comparison of the homogenate demonstrated that the fractions 9 to 12 correspond to fraction 13 to 23. The different fraction numbers originate from different fraction volumes. Antibody: PAP (Sigma).

Unfortunately all fractions showed signals for the TAP tag and therefore the desired preconcentration could not be accomplished (Figure 4.7).

3) Introduction of a new tandem strategy: StrepOne::FLAG

Due to the incomplete cleavage despite protease treatment for 16 h and the restriction of protease inhibitor usage during TEV digest, the TEV cleavage is regarded as an unfavorable elution mechanism (Arnau et al., 2006). In an alternative purification strategy the affinity purification step involving protease cleavage was exchanged to a metabolite based binding and elution (Gloeckner and Boldt, 2009). The Strep tag principle is based on Biotin-Streptavidin binding which is the strongest known noncovalent binding in nature (K_d: Biotin/Streptavidin 10 pM, Calmodulin/CBP 1 nM, IgG/Protein A 50nM)(Gloeckner and

Boldt, 2009). Binding of the streptavidin fusion protein to biotin beads is released via biotin in the elution buffer. The FLAG affinity tag utilizes an artificial octapeptide (DYKDDDDK) which binds to anti-FLAG antibodies coupled to magneto beads. Both tags do not use calcium in the elution buffer and therefore should not possibly interfere with the calcium sensing synaptotagmin (chapter 2.3.3.1.3).

p*sng-1::sng-1::*8xG4S::OneStrep::FLAG

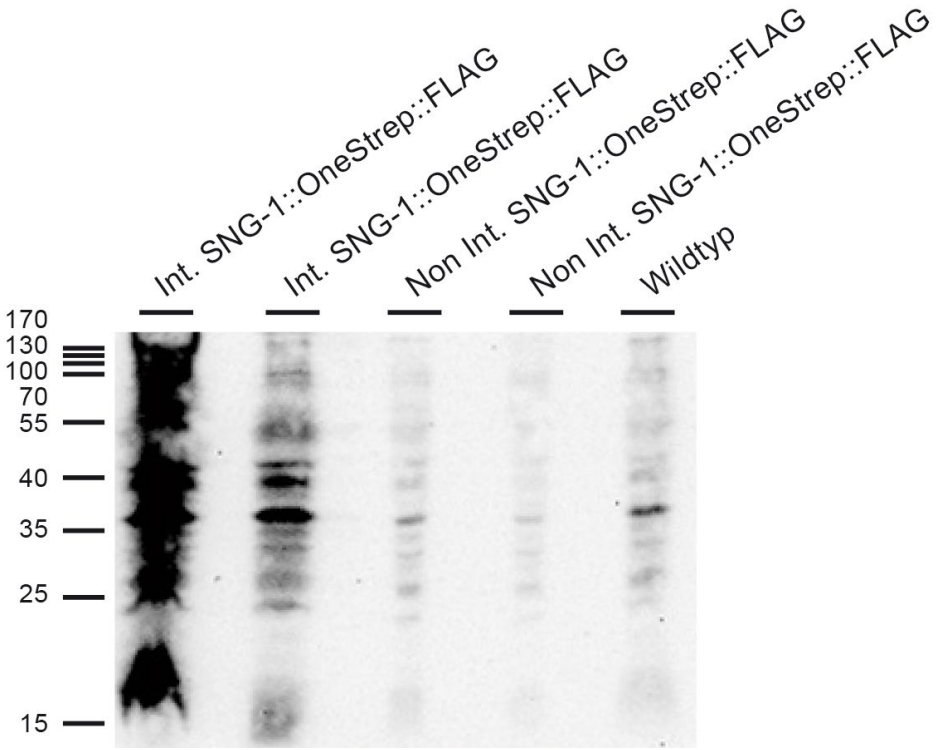

Figure 4.8 The FLAG antibody did not reveal specific bands The different strains were applied for a SDS-PAGE and western blot analysis using the fast protein extract protocol. The integrated SNG-1::One-Strep::FLAG (ZX1105), Integrated SNG-1::OneStrep::FLAG (ZX1106), Extrachromosomal SNG-1::OneStrep::FLAG and Extrachromosomal SNT-1::OneStrep::FLAG (N2) did not show any specific band which was not observable in the wild type (N2). Antibody: anti-FLAG (Sigma Aldrich).

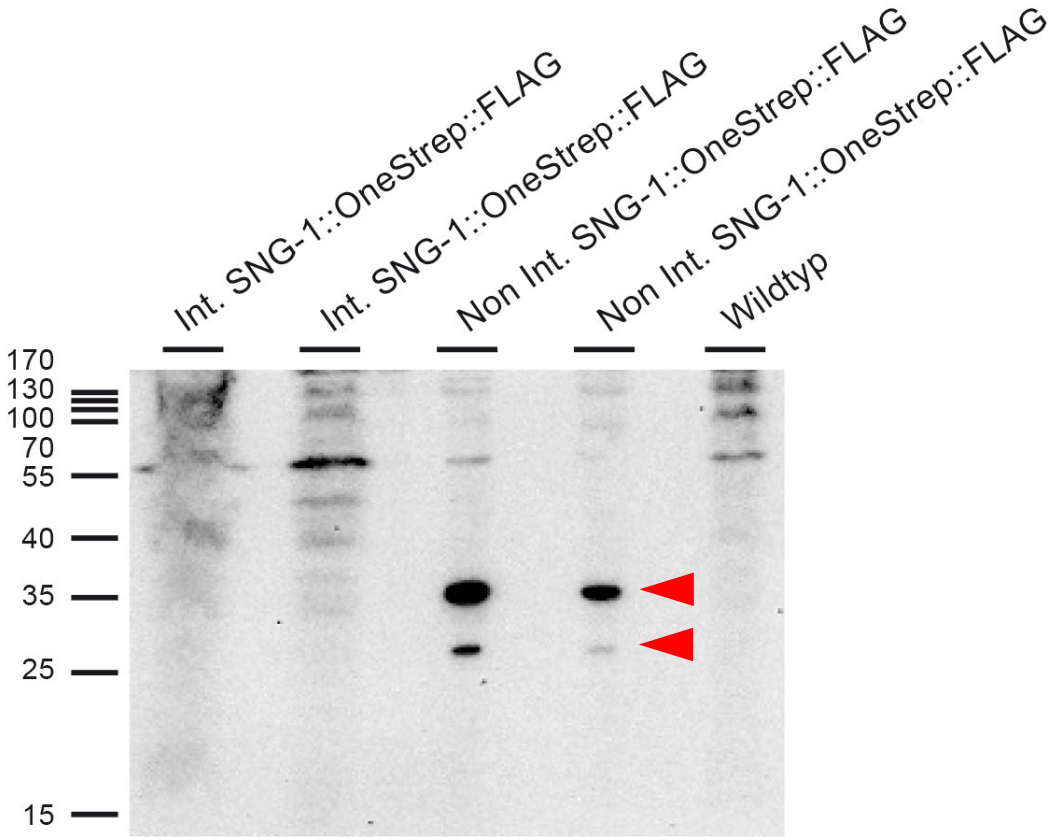

Figure 4.9 Only unintegrated strains showed a strep specific expression The Integrated SNG-1::One-Strep::FLAG (ZX1105) and integrated SNG-1::OneStrep::FLAG (ZX1106) showed a similar western blot pattern compared to wild type (N2), whereas extrachromosomal SNG-1::OneStrep::FLAG and extrachromosomal SNT-1::OneStrep::FLAG displayed two bands at 25 kDa and 35 kDa (red arrowheads) which could not be detected in the wild type. Antibody: Anti-Strep-HRP (Pierce).

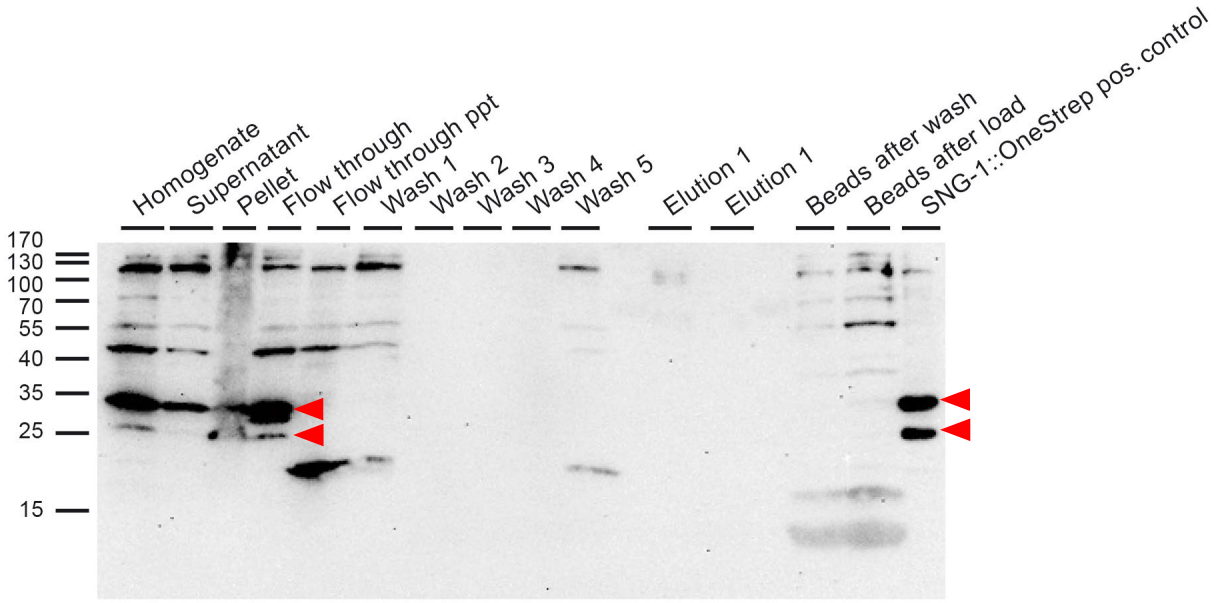

Figure 4.10 The loaded One-Strep beads did not show specific bands during synaptic vesicles purification Immunoblotting of OneStrep purification utilizing a strain with extrachromosomal expressed

SNG-1::OneStrep::FLAG. The Anti-Step Antibody displayed several background signals (compare wild type sample in Figure 4.9). The probably characteristic pattern at 35 kDa and 25 kDa (red arrowheads) was lost during loading of the biotin beads. ppt = precipitated Antibody: Anti-Strep-HRP (Pierce).

In the previous experiment the strain with extrachromosomal expressing SNG-1::OneStrep::FLAG showed more characteristic bands than integrated strains, therefore this strain was used for an OneStrep purification to proof the functionality of the concept. Unfortunately the western blot signal did not indicate any enrichment of specific protein during strep purification (with western blot signal in integrated strains); instead, a complete loss of signal was observed during washing of the biotin beads.

4) Using SNT-1 as a protein target

As an alternative to SNG-1::StrepOne::FLAG, an SV protein with higher intrinsic expression level was used. Synaptotagmin with 15 copies per synaptic vesicle in rodents (as assumed by Takamori et al., 2006) was selected as a synaptic vesicle fusion protein. The fusion protein had the following design:

p*snt-1::snt-1*::8xG4S::StrepOne::FLAG

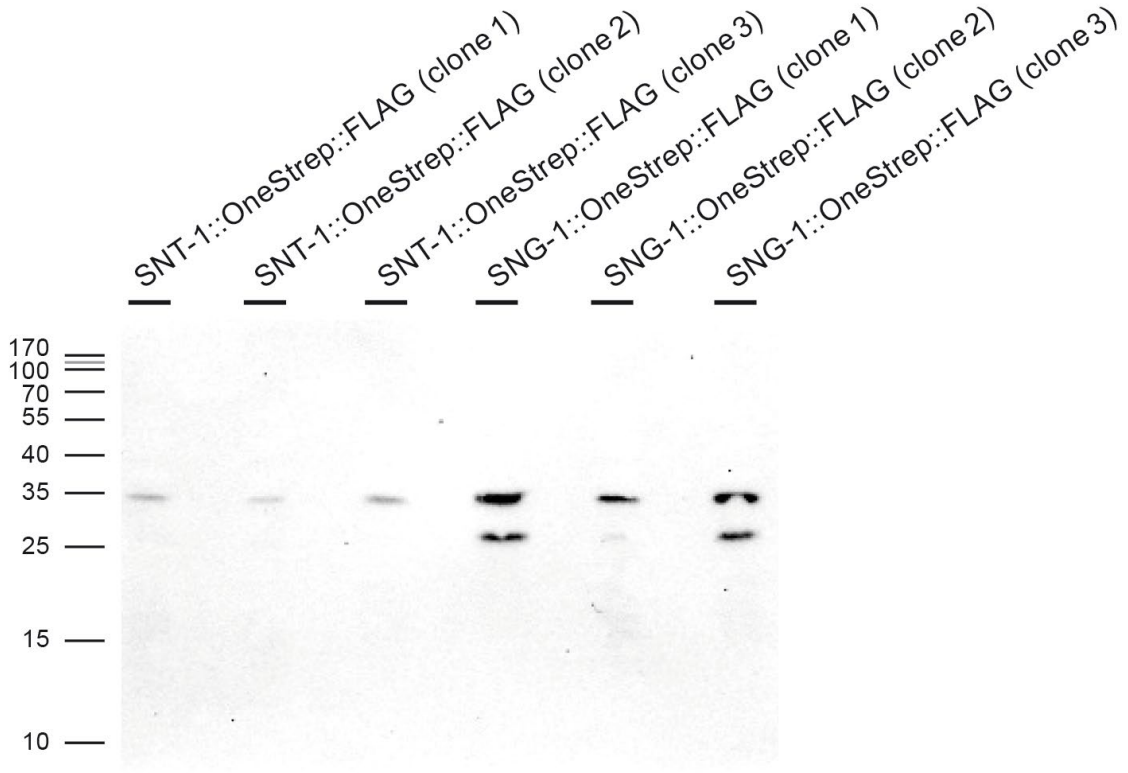

Figure 4.11 The expression of SNT-1::OneStrep::FLAG was lower compared to SNG-1::OneStrep::FLAG The immunoblotting of fast protein extract samples of strains expressing extrachromosomal SNT-1::OneStrep::FLAG displayed bands with low intensity and less intense than SNG-1::OneStrep::FLAG samples (extrachromosomal expression). Antibody: Anti-Strep-HRP (Pierce).

However SNT-1::Strep displayed a lower expression in comparison to SNG-1::Strep (both extrachromosomal arrays) and a rather weak signal in western blots. As the first step purificaiton with biotin beads did not show an enrichment for SNG-1::OneStrep::FLAG and the integration of *sng-1*::OneStrep::FLAG reduced the signal below the detection rate, the purification with SNT-1::OneStrep::FLAG was not pursued.

Following these unproductive attempts, the project was finally concluded.

4.2. SNARE complex purification

Even though the purification of synaptic vesicle proteins did not produce satisfying results, synaptic proteins and its interaction partners remain an attactive target for an elucidation of the underlying mechanisms, which are conserved through out the phylogentic tree (Jahn and Südhof, 1994; Richmond et al., 2002). Several mechanisms of SV docking/ priming, SNARE and SV recycling are still not fully understood (Boyken et al., 2013) and the role of discovered interaction partners remain elusive (Morciano et al., 2005; Burré et al., 2006; Burré et al., 2007; Takamori et al. 2006). Interactions partners of the transmission machinery in mammals were previously discoved by pull-down experiments (compare chapter 2.4) whereas interaction partners in *C. elegans* were identified by phenotypic/behavioral alterations after knocking down of genes by mutagenic compounds or RNA interference (RNAi) (Brenner, 1974; Miller et al., 1996; Kamath and Ahringer, 2003; Rual et al., 2004; Sieburth et al., 2005; Mahoney et al., 2006; Vashlishan et al., 2008; Nix et al., 2014; Wabnig et al., 2015). Several advantages compared to the purification of synaptic vesicles are at hand: the SNARE complex proteins are the most abundant proteins in neuronal matter (Walch-Solimena et al., 1995), the subunits present strong interactions during SNARE complex formation and would allow the usage of detergents during purification.

4.2.1. The split TAP tag distributed to synaptobrevin and syntaxin (UNC-64) allowed purification of SNARE complexes

The purification strategy was based on a split TAP-tag – here the one tag is fused to one subunit of the complex and the other tag is linked to a different subunit. In this work the ProteinA (ProtA) and several TEV protease cleavage sites were N-terminally linked to synaptobrevin and the calmodulin binding peptide (CBP) was C-terminally fused to syntaxin. The strong interaction of synaptobrevin with syntaxin (or UNC–64 in *C. elegans*) allowed after the formation of a *cis*- or *trans*-SNARE complex a sequential purification to pull-down the complex with its adhered interaction partners. *snb-1* is encoded on chromosome V and *unc-64* on chromosome III, respectively. A bicistronic sequence between *gpd-2* and *gpd-3* described by Mario deBono was used to facilitate the expression of both fusion constructs in one vector (personal communication of Alexander Gottschalk with Mario de Bono).

The resulting construct had the following design:

p*snb-1*::ProtA::TEV::G$_4$S::TEV::*snb-1*::Bicis::*unc-64*::CBP::*unc-54* 3'UTR

This sequence represents an 11 kb long DNA fragment, which was cloned into a 7 kb MosSCI vector resulting in a final 18 kb vector (compare cloning strategy in chapter 3.3.1). According to the wormbuilder homepage by Christian Frøkjær-Jensen MosSCI should be possible with vectors up to 16 kb (Christian Frøkjær-Jensen). Although the injection and the *unc-119* rescue succeeded we could not observe an integration event (for several months) and started therefore an alternative way of low copy integration. The biolistic transformation with micro particle bombardment allowed a low copy integration of the fusion construct (Praitis et al., 2001; Berezikov et al., 2004) (see method chapter 3.2.3).

The first test of expression included an immunoblot analysis of microinjected and bombarded strains (Figure 4.12).

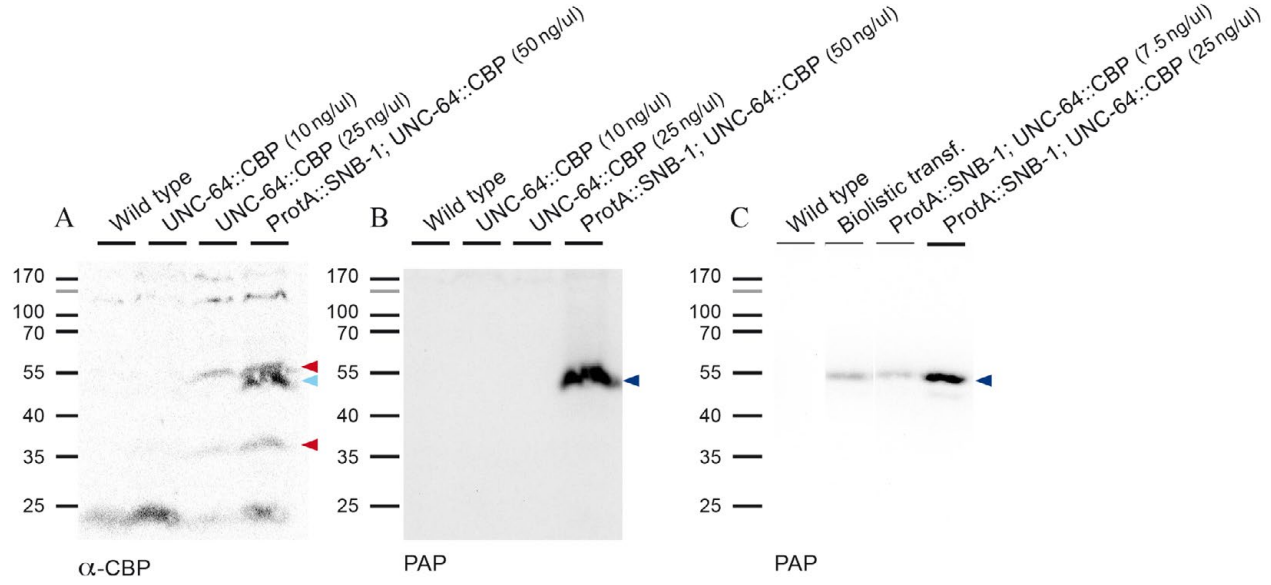

Figure 4.12 The *snb-1* and *unc-64* constructs were expressed A) Application of anti-CBP antibody displayed two characteristic bands (red arrow head), which could not be detected in the wild type sample. Another band (light blue arrowhead) right below the upper band in the bicistronic construct (ProtA::SNB-1; UNC-64::CBP) resembles the ProtA band in B. No CBP-bands could be detected in lane 2 B) Re-probing after stripping of the blot in A with peroxidase anti-peroxidase complex (PAP; probing for ProtA tags) showed only one band for SNB-1 (dark blue arrowhead). C) A new blot using PAP (Sigma) showed one single band, with higher concentration two bands (dark blue arrowhead). Different intensities for bombardment and microinjected strains could be observed. (The plasmid concentration in the injection mix for extrachromosomal array formation is indicated). Wild type samples are N2 fast protein extracts.

Both constructs could be detected on the protein level, even if the CBP signal was rather weak (compare Figure 4.12A red arrows). The CBP signals in Figure 4.12A were only visible in lane 3 and 4 (p*rab-3*::UNC-64::CBP; p*snb-1*::ProtA::SNB-1::Bicis::UNC-64::CBP), possibly due to the low binding capacity of the antibody or overall low concentration of UNC-64. The concentration of UNC-64 in lane has been only one third of lane 3 and could therefore be the reason for no CBP signal in this lane (longer exposure or digital enhancements only increased the background). The CBP band in lane 4 is slightly above the background ProtA signal of the ProtA::SNB-1 and can only be identified in correlation to the previous lane (lane 3). The ProtA band interacted with the CBP antibody due to interaction with any crystallizable fragment (F_c) of immunoglobulin G (basis of the first purification step and the functioning of the PAP antibody). UNC-64::CBP has a calculated size of 40 kDa, but could be detected at 35 and 55 kDa.

To prove the presence and functionality of both fusion-proteins rescue experiments with two corresponding reduction of function (r-o-f) mutant strains were performed: Strain NM467 is a *snb-1* mutant allele (*md247*), and strain NM547 is an *unc-64* mutant allele (*js21*).

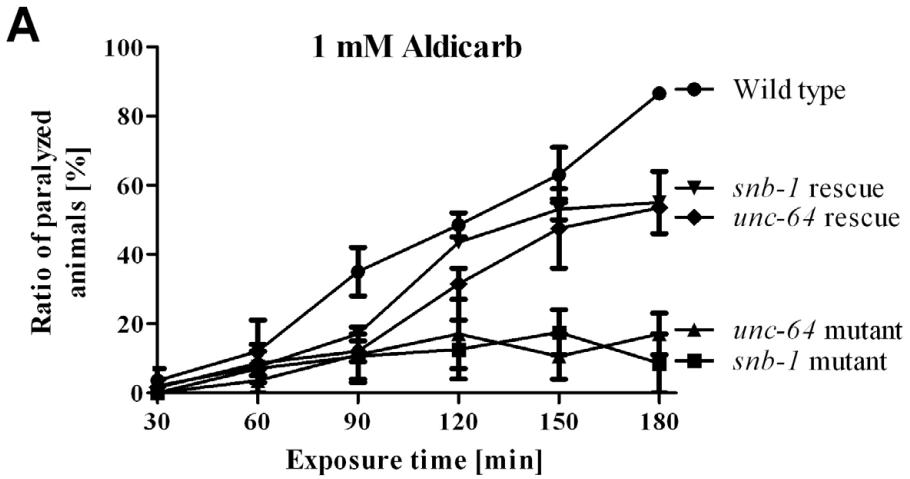

Time [min]	WT vs *snb-1* mut.	WT vs *unc-64* mut.	WT vs *snb-1* resc.	WT vs *unc-64* resc.	*snb-1* mut. vs *snb-1* resc.	*unc-64* mut. vs *unc-64* resc.
30	ns	ns	ns	ns	ns	ns
60	ns	ns	ns	ns	ns	ns
90	*	*	ns	ns	ns	ns
120	***	**	ns	ns	**	ns
150	***	***	ns	ns	**	***
180	***	***	**	**	***	***

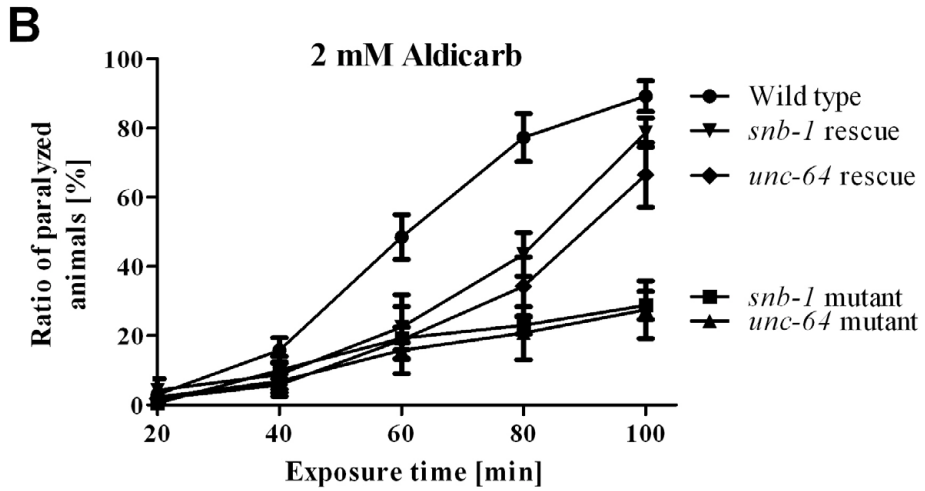

Time [min]	WT vs *snb-1* mut.	WT vs *unc-64* mut.	WT vs *snb-1* rescue	WT vs *unc-64* rescue	*snb-1* mut. vs *snb-1* rescue	*unc-64* mut. vs *unc-64* rescue
20	ns	ns	ns	ns	ns	ns
40	ns	ns	ns	ns	ns	ns
60	**	***	**	**	ns	ns
80	***	***	***	***	ns	ns
100	***	***	ns	*	***	***

Figure 4.13 The UNC-64::CBP and ProtA::SNB-1 fusion constructs rescue genomic mutants to an almost wild type level A The effect of 1 mM (N = 2, 25 animals each) or **B** 2 mM Aldicarb over time (N = 4,

25 animals each). Aldicarb has almost no effect on NM467 and NM547, whereas with wild type (N2) animals a paralysis of up to 85 % was reached. The expression the fusion proteins via the microinjected tandem plasmid (pFC06; p*snb-1*::ProtA::TEV::G4S::TEV::*snb-1*::Bicis::*unc-64*::CBP::*unc-54* 3'UTR) resulted in a higher paralysis rate proving a rescuing effect of the construct. The tables display the 2-way analysis of variance (ANOVA) (Bonferroni posttests) for the difference at each time point. *: $p < 0.05$; **: $p < 0.01$; ***: $p \leq 0.001$. (mut.: mutant; resc.: rescue; ns: not significant).

Aldicarb as a cholinesterase inhibitor induces paralysis at a certain time point, due to the accumulation of acetylcholine in the synaptic cleft. If the secretion machinery of acetylcholine is compromised, for example by disruptions of the synaptic vesicle fusion, the critical acetylcholine concentration for paralysis will be reached at a delayed time point (Mahoney et al., 2006). If the introduced SNB-1 or UNC-64 can compensate the mutated versions the paralysis happens as fast as in wild type animals. Microinjection of the bicistronic vector FC06 (p*snb-1*::ProtA::TEV::G4S::TEV::*snb-1*::Bicis::*unc-64*::CBP::*unc-54* 3'UTR) and subsequent isolation of F2 generation transgenic animals allowed a partial but statistically significant rescue of the aldicarb resistant phenotype of the SNARE protein mutants, which demonstrates that the ProtA::SNB-1 and UNC-64::CBP proteins are at least partly functional (Figure 4.13). The reduced rescue could be explained by mosaic expression of the extrachromosomal array and/or partial disturbance of protein function by the covalently attached tags (see discussion in chapter 5.2) (Yochem, 2003; Frøkjær-Jensen et al., 2008).

4.2.1.1. Utilization of the CaM tag revealed α-SNB-1 positive bands in the elution

A simple proof of UNC-64::CBPs ability for SNARE complex formation was demonstrated by a single step CaM purification in which a strong ProtA::SNB-1 signal could be detected in the elution fraction (Figure 4.14).

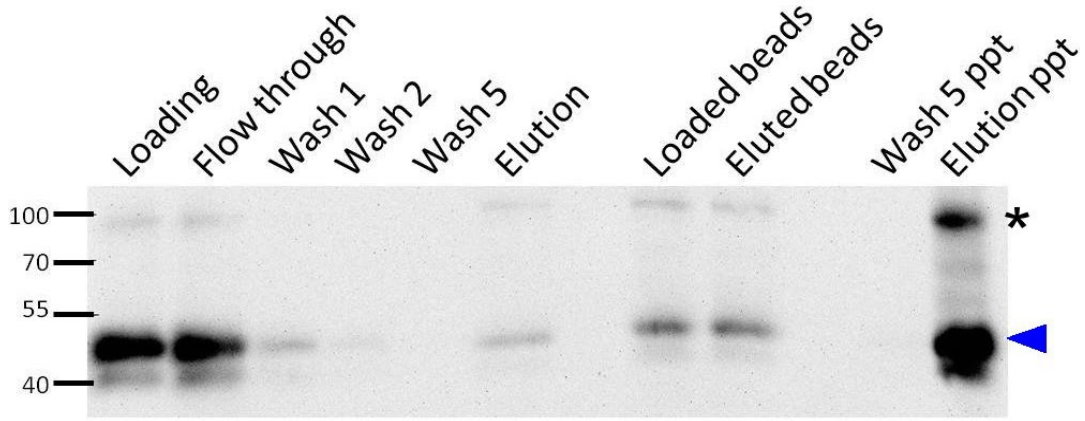

Figure 4.14 Purification of UNC-64::CBP via calmodulin beads caused co-purification of ProtA::SNB-1
Two prominent bands at 45 kDa (blue arrow head) representing ProtA::SNB-1 and a 100 kDa signal (black asterisks) possibly reflecting SNARE complexes containing ProtA::SNB-1. ppt = precipitated. Antibody: peroxidase anti-peroxidase complex (PAP, Sigma).

In the flow through significant amounts of ProtA::SNB-1 could be detected, probably representing SNB-1 protein that is not incorporated in SNARE complexes or UNC-64/SNB-1 subcomplexes, and which could originate from synaptic vesicles or plasma membrane (Dittman and Kaplan, 2006). The fact that ProtA::SNB-1 could be detected in the elution fractions after multiple washing steps supports three important conclusions: a) UNC-64::CBP was expressed via the bicistronic vector, b) the CaM-CBP purification step worked and c) the pull-down of UNC-64 resulted in a co-purification of SNB-1. Interestingly, a second strong signal arose at around 100 kDa, possibly reflecting mature SNARE complexes, resistant to SDS treatment (ProtA::SNB-1: 34 kDa, UNC-64::CBP: 40 kDa and RIC-4: 23 kDa) (Fasshauer et al., 2002).

The purification and the related washing steps are prone to inducing loss of interesting SNARE complex interaction partners. The purification of membrane protein complexes requires optimization of the solubilization process. Thus, diverse detergents were tested in this work. The samples were analyzed for ProtA-SNB-1 after detergent extraction. Frozen worms (ZX1585; expressing p*snb-1*::ProtA::TEV::G4S::TEV::*snb-1*::Bicis::*unc-64*::CBP::*unc-54* 3'UTR) were ground and homogenized. The homogenate was distributed in six parts and each sample was treated with detergent (except negative control) and centrifuged at 150,000 g for one hour. Now the supernatant was analyzed via SDS-PAGE and western blot. If the protein is properly solubilized it would correspond to a distinct signal in the supernatant (Figure 4.15A).

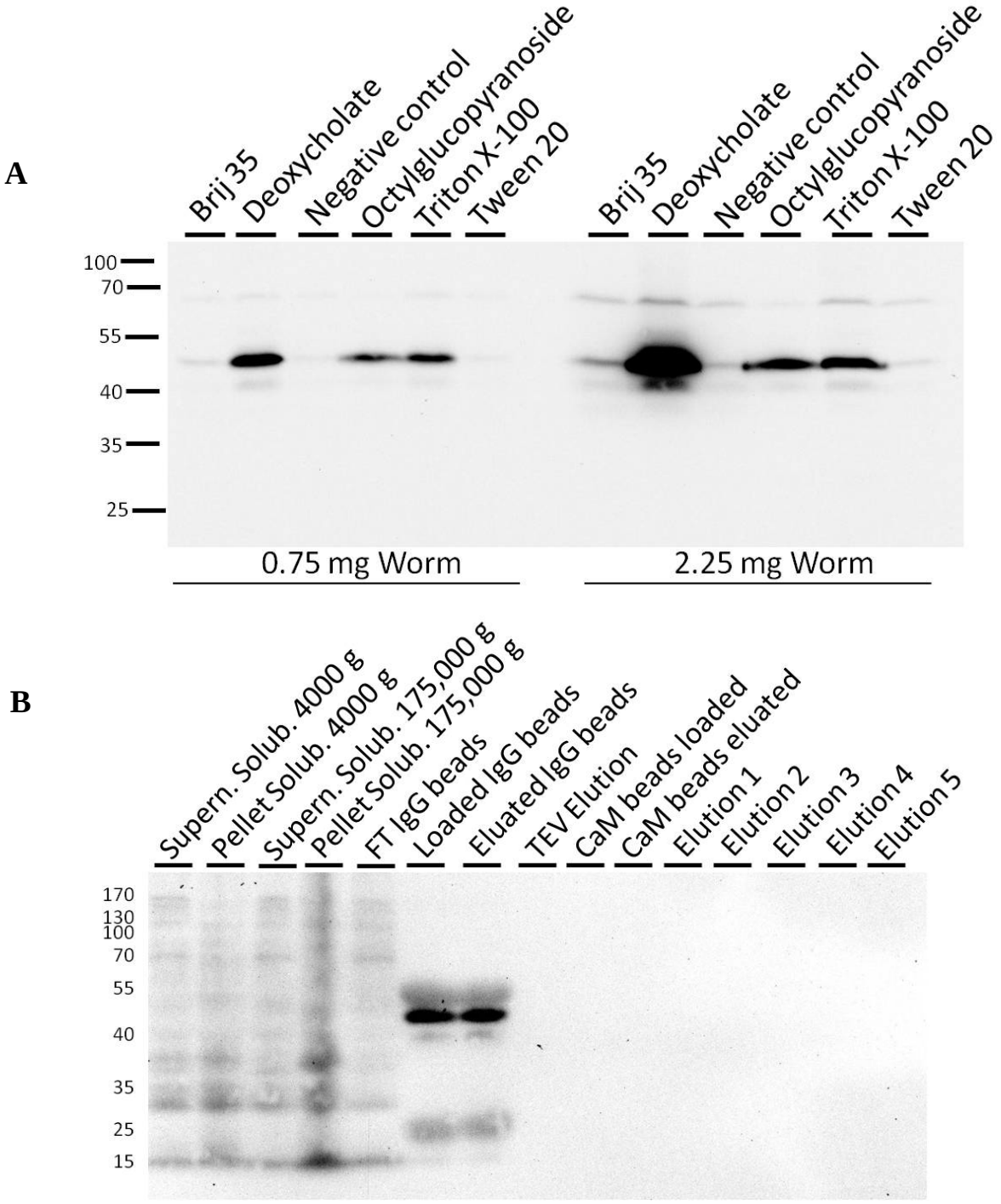

Figure 4.15 Deoxycholate and Triton X-100 displayed the best solubilization results, but deoxycholate disabled TEV cleavage A) Worm homogenate was separated and treated with five different detergents. Deoxycholate led to the highest amount of solubilized protein (though pellets were not analyzed here), followed by octyl-glucopyranoside and Triton X-100. The weight correspond to the dry weight of worm pellet (Antibody: PAP, Sigma) B) Tandem purification of SNARE complex indicating that TEV cleavage of ProtA::SNB-1 was blocked by deoxycholate. FT Flow through, IgG immunoglobulin G, CaM calmodulin, TEV tobacco etch virus protease. Antibody: anti-SNB-1(SB1, DSHB).

Deoxycholate displayed the strongest signal after detergent treatment in the supernatant (Figure 4.15A). Using deoxycholate in a tandem purification interfered with the TEV cleavage (Figure

4.15B) as SNB-1 did not elute from the IgG beads. Neither a reduction of size and signal strength nor an elution of SNB-1 could be detected. Further purifications were performed with Triton X-100 – a detergent successfully used in several purifications of neuronal membrane proteins (Brose et al., 1992; Söllner et al., 1993a; Siebert et al., 1994; Polanowska et al., 2004; Gottschalk et al., 2005).

For each membrane protein complex the solubilization procedure and differential centrifugation must be optimized. Thus the effects of stepwise increases of centrifugation force and solubilization with Triton X-100 on the presence and abundance of ProtA::SNB-1 in the soluble fraction were tested.

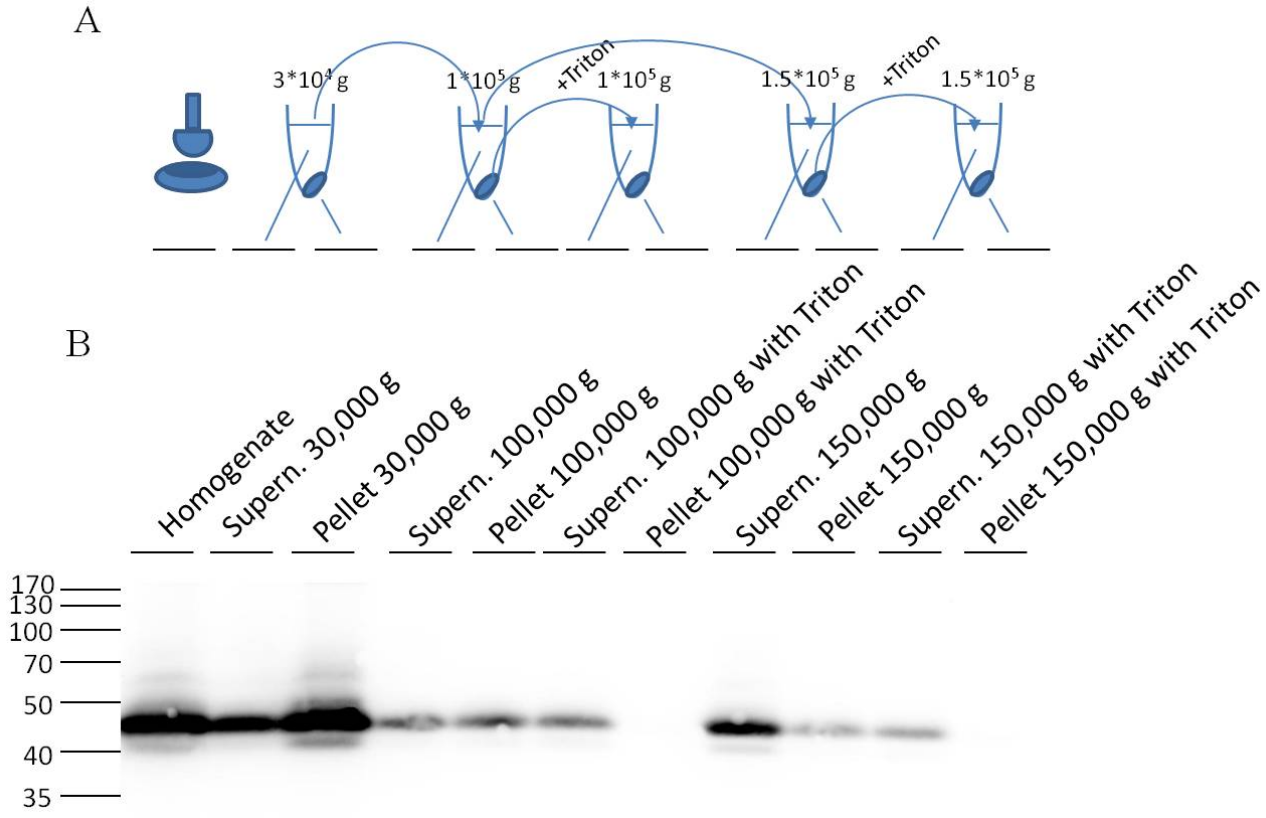

Figure 4.16 After 150,000 g there is still an intense band in the supernatant, but previously pelleting proteins remained in the supernatant after Triton treatment.A To determine the best centrifugation strategy a differential centrifugation with pellet solubilization and further centrifugation was performed. The experiment was supposed to show, if and at which centrifugational speed the SNB-1 pellet and if Triton solubilization was successful. The supernatant of the 30,000 g centrifugation step was recentrifuged at 100,000 g. The supernatant was again spun with 150,000 g, but the pellet was solubilized with Triton X-100 and then centrifuged with 100,000 g. The pellet of the 150,000 g supernatant was treated with Triton X-100 and spun at 150,000 g. **B** The pellet of the first fraction contained the highest amount of ProtA-SNB-1. The application of Triton X-100 in both pellet fractions (100,000 g and 150,000 g) resulted in solubilized SNB-1, which did not pelleted anymore. An intense SNB-1 signal could be detected in the supernatant after 150,000 g without detergent. Antibody: anti-SNB-1(SB1, DSHB).

In Figure 4. a high amount of SNB-1 was bound in the first crude pellets. Surprisingly, an intense SNB-1 band remained in the supernatant after 150,000 g. This is irregular, because any membrane proteins should pellet at this centrifugational force. An explanation could be the fatty top layer which forms during 150,000 g centrifugation steps (compare chapter 3.4.2). SNB-1 protein could be detected in the two pellets, until these were treated with Triton X-100. These solubilized SNB-1 proteins remained in the supernatant even with a high centrifugation force. This experiment revealed the importance of the solubilization of the different pellets (30,000 g to 150,000 g) as a crucial amount of SNB-1 can be detected in all pellets (compare chapter 3.4.5). But as already seen in Figure 4.15 and in the synaptic vesicle purification part, the presence of SNB-1 after solubilization could not be the only indicator of a successful purification and the subsequent TEV cleavage needed to be confirmed.

The obtained samples and the Triton solubilization were therefore tested for their eligibility during TEV cleavage and elution.

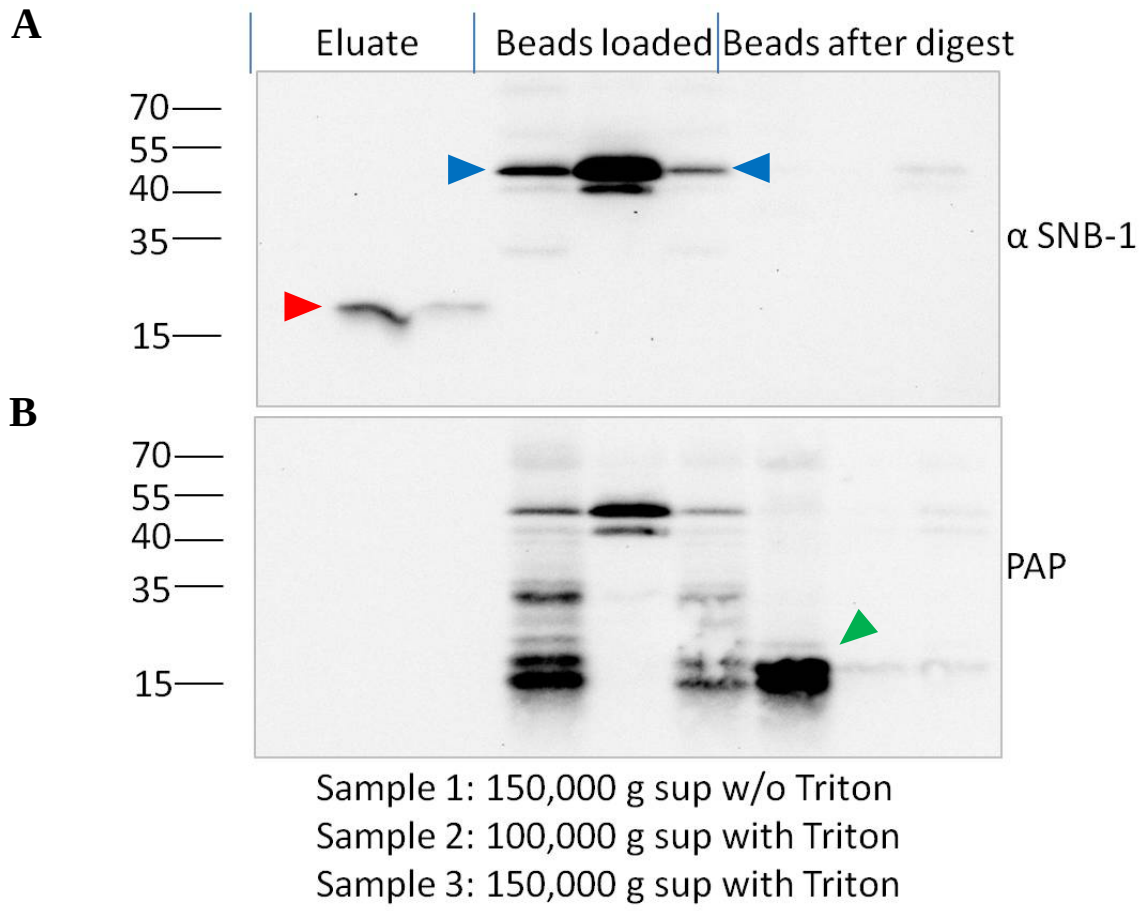

Figure 4.17 The elution of SNB-1 by TEV cleavage was the most successful with solubilized samples from 100,000 g centrifugation step A Three different samples with confirmed ProtA::SNB-1 in the supernatant from the previous experiment were incubated with IgG beads and after intense washing steps treated with TEV. The Western blot of the IgG purification of ProtA::SNB-1 fusion showed different cleavage and loading successes respective to their centrifugation speed during preparation. All samples showed a

SNB-1 band at around 55 kDa at the loaded beads (blue arrowheads). The most intense SNB-1 signal in the eluate was visible in the 100,000 g Triton sample (red arrowhead). **B** Application of the PAP after stripping showed several bands in the 150,000 g supernatant sample without detergent (probably reflecting degraded protein). The same sample showed in addition an intense ProtA signal after TEV cleavage on the eluated beads (green arrowhead). Antibodies in A: anti-SNB-1(SB1, DSHB), B: peroxidase antiperoxidase complex (PAP, Sigma).

Three samples of the previous experiment (150,000 g without Triton, 100,000 g with Triton and 150,000 g with Triton, compare Figure 4.) were addressed to the first purification step of the tandem affinity: the IgG purification. Here, the ProtA::SNB-1 fusion protein interacts with the Fc part of the Immunoglobulin G coupled to beads and is, after intense washing, eluated by the TEV protease cleavage, which removed the ProtA from the SNB-1. The different centrifugation samples showed a clear change in the signal comparing the SNB-1/PAP signals, prior and after TEV treatment (Figure 4.17). All samples showed a complete loss of its 50 kDa band after TEV treatment (except a faint band at the 150,000 g Triton sample after digest). An intense band at 15 kDa of the 150,000 g sample after digest can be observed, probably reflecting cleaved ProtA signal. Interestingly, no SNB-1 signal was detectable in the eluate of this sample, which could hint to background protease activity. The 100,000 g Triton sample interestingly lost almost the complete signal for the 50 kDa band during TEV digest (beads loaded versus beads after digest) and only a minor band for ProtA was detectable on the beads after digest, but it resulted in the highest elution signal. The different samples during the IgG purification of ProtA::SNB-1 fusion protein revealed that the most intense band in the elution corresponds to the samples treated with Triton and therefore confirmed Triton as the correct detergent.

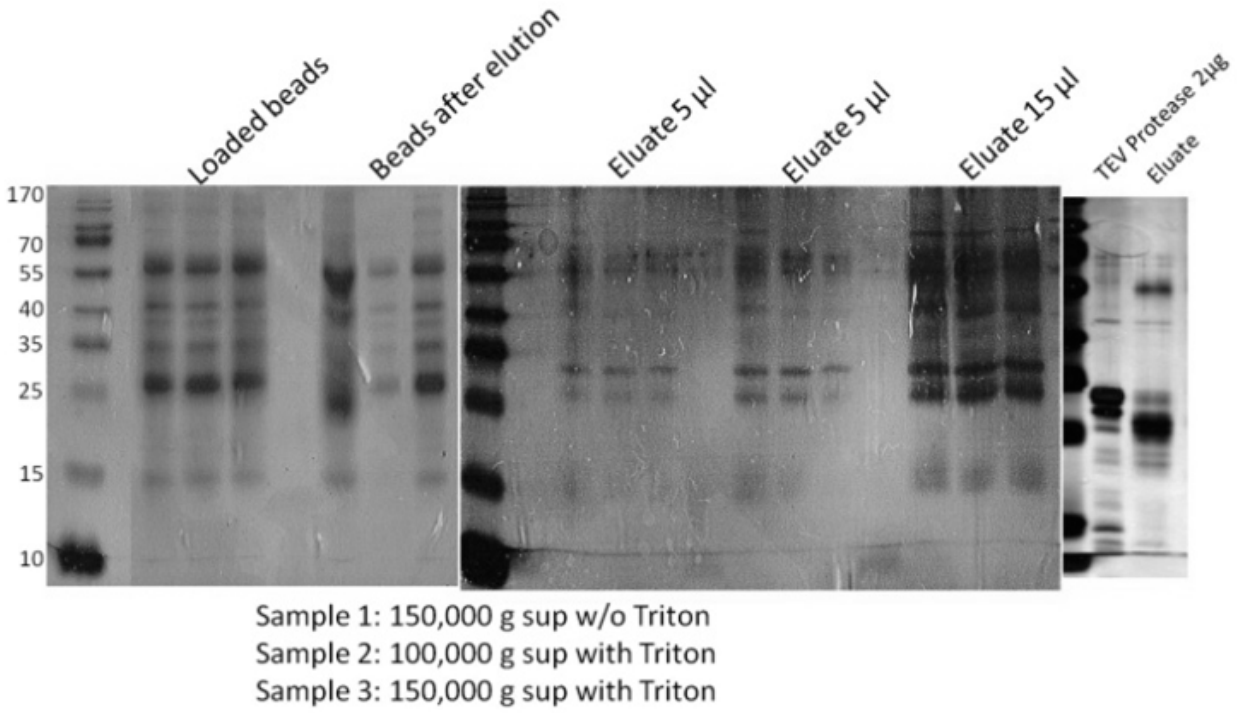

Figure 4.18 The signals of the silver staining did not correspond to the differences observed in the western blot The comparison of the different samples from the previous experiment displayed a more even pattern than in the western blot. Three different SDS PAGE with silver stain protein detections were analyzed: the beads, different concentrations of elution fractions and to compare the elution with TEV protease a sample of commercial TEV protease and additional analysis of the elution sample (100,000 g w/Triton). There is a clear difference between the TEV protease pattern to the eluate pattern.

The analysis of the previously generated eluate displayed a more or less evenly distributing of proteins. This reflects the need for the next purification step to generate highly pure samples. Still this simple purification revealed how complex the sample generation can be and how crucial the evaluation of the purification strategy is.

As the transient overexpression of proteins can lead to misrouting and wrong interactions, the next step was the generation of an integrated transgenic line expressing ProtA::SNB-1 and UNC-64::CBP via biolistic transformation, in collaboration with Ekkehard Schulze, Baumeister Lab, University of Freiburg (ZX1588; zxIs72 [bomb pFC07: pCFJ350 back bone; p*snb-1*::ProtA::2xTEV:::*snb-1*::Bicis::*unc-64*::CBP::*unc-54* 3'UTR, , Cbr *unc-119* Line 9.3]).
The transformed animals were selected as described (compare chapter 3.2.3) and bred to obtain large quantities with the help of egg plates (compare chapter 3.2.1). The obtained worms underwent the whole course of tandem affinity purification and the respective samples were analyzed via SDS-PAGE and western blotting. In addition to the biolistic transformed worms, we generated with the help of Knudra (Knudra Transgenics, Murray, Utah USA) MosSingle copy integrated

lines (MosSCI, compare chapter 3.2.2 and chapter 4.1.2)(ZX1592; zxIs71 [p*snb-1*::ProtA::2xTEV::*snb-1*::Bicis::*unc-64*::CBP::*unc-54* 3'UTR, Cbr *unc-119*]). Large quantities were bred and a whole course of tandem affinity purification was performed (Figure 4.19).

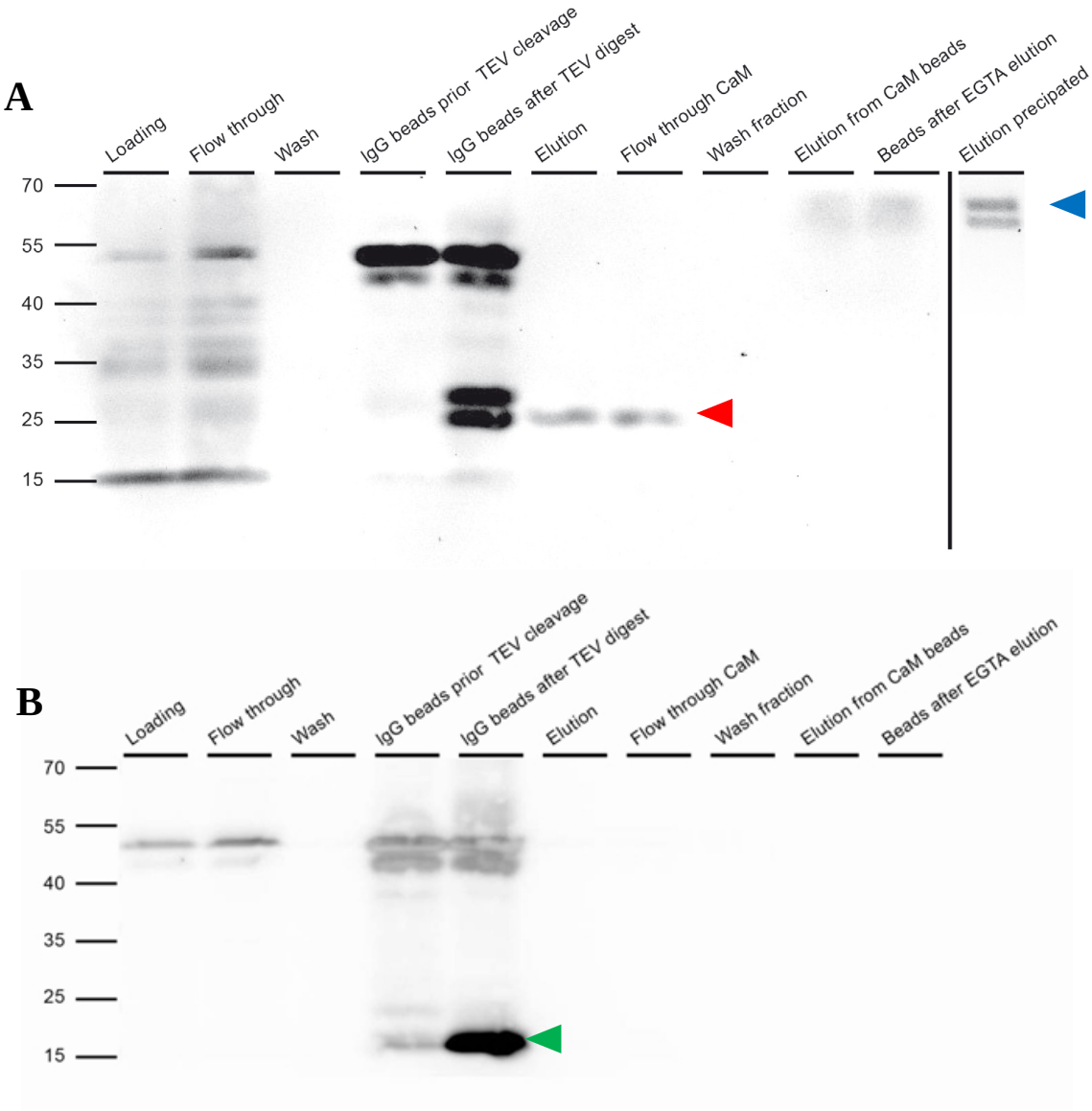

Figure 4.19 The Tandem Affinity Purification was successful as shown by SNB-1 signal in the elution fraction **A** Western blot of tandem affinity purification of ZX1592 (p*snb-1*::ProtA::2xTEV::*snb-1*::Bicis::*unc-64*::CBP::*unc-54* 3'UTR probed with SB1, the SNB-1 antibody. In the first two lanes two major bands are visible: the fusion construct at around 50 kDa and the SNB-1 wild type protein at 15 kDa. The beads loaded with the SNARE complex showed a specific signal at 50 kDa and after cleavage this signal was partially reduced to ~ 25 kDa . This band was found again in the elution fraction and in the flow through of CaM beads (red arrowhead). A faint band with a rather high size (~ 60 kDa; blue arrowhead) was detected in the elution of CaM and on eluted CaM beads. This SNB-1 signal was increased by precipitation and loading on a new SDS-PAGE. **B** After stripping of A) the blot was incubated with peroxidase antiperoxidase complex (PAP) that is bound by the ProtA moiety. ProtA is part of the ProtA::SNB-1 fusion construct (50 kDa) but released by TEV cleavage; ProtA is retained on the IgG beads (19 kDa signal; green arrowhead). Antibodies: A: anti-SNB-1(SB1, DSHB): B: peroxidase antiperoxidase complex (PAP, Sigma).

The tandem affinity purification analyzed by SDS PAGE and Western blotting, as shown in Figure 4.19, apparently worked, as suggested by the pattern of specific signals. TEV cleavage led to the expected decrease in size of the ProtA::SNG-1 fusion protein, i.e. from 50 kDa (doublet, characteristic for ProtA fusion proteins) to 30 kDa. The 30 kDa signal could be detected in the TEV elution fraction and in the CaM flow through. This could represent uncomplexed SNB-1, which cannot bind to CaM beads. The faint band at around 60 kDa in the CaM elution fraction could represent a formed SNARE complex (compare Figure 4.20). After stripping and reapplication of the blot with PAP complex displayed the ProtA at around 19 kDa on the eluted IgG beads and the presence of non-digested ProtA-SNB-1 on the beads.

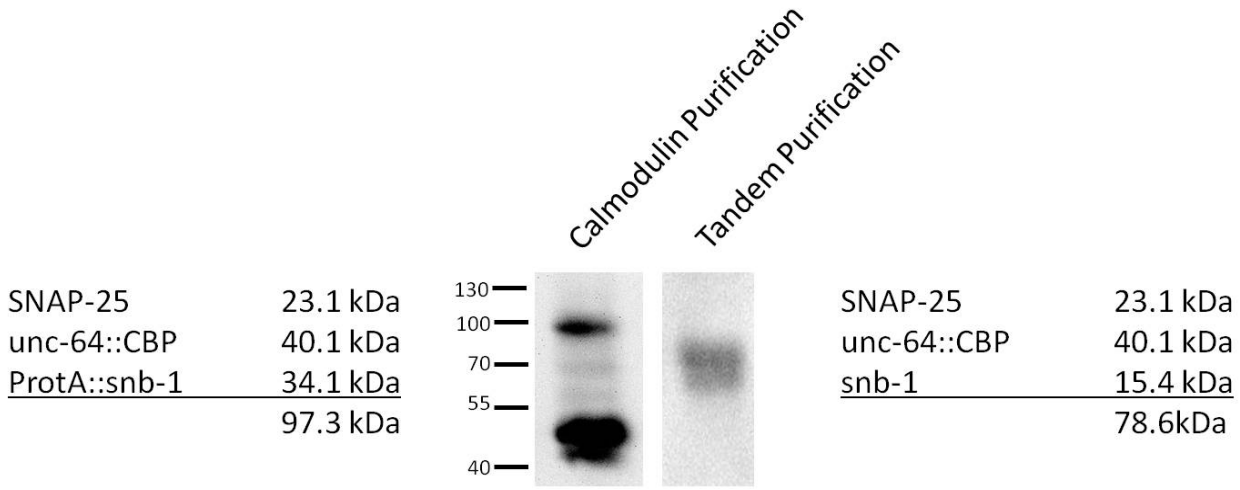

Figure 4.20 The calculation of the different sizes for SNARE complexes reflected the different purification steps After cleaving off the ProtA the complex resulted in a complex with a reduced size compared to ProtA::SNB-1 containing complexes. The bands are extracted from Figure 4.14 and Figure 4.19A. Antibodies: left: peroxidase antiperoxidase complex (PAP, Sigma); right: anti-SNB-1(SB1, DSHB).

Unlike its calculated size of 34 kDa the ProtA::SNB-1 fusion protein was always detect at 45-50 kDa (see Discussion in chapter 5.2), this could be due to several reasons e.g. SDS resistant interactions with other proteins or conformational changes, which reduce the migration speed in the SDS-PAGE (Fasshauer et al., 2002).

For a better understanding of the expression levels and purification properties two parallel purifications were performed (Figure 4.21). One strategy used a strain ZX1586 expressing the fusion construct transiently in an extrachromosomal array (chapter 3.2.2) and the other strain ZX1588 (zxIs72[bomb pFC07: pCFJ350 back bone; p*snb-1*::ProtA::2xTEV:::*snb-1*::Bicis::*unc-64*::CBP::*unc-54* 3'UTR, , Cbr *unc-119* Line 9.3]) was transformed via microparticle bombardment (chapter 3.2.3). Analyzing the elution fractions after precipitation showed a SNB-1 signal in the western blot of purifications originating from strains created by array formation and bombardment integration. Even if there should be an observable difference in the copy number between array and bombardment strain (compare chapter 3.2.3), only a minor difference was visible for the eluted beads. One possibility could be the regulation of expression, even for extrachromosomal arrays or the saturation of the IgG beads. In the CaM elution fractions a band was detectable at around 60 kDa, possibly reflecting formed SNARE complex (see chapter 5.2).

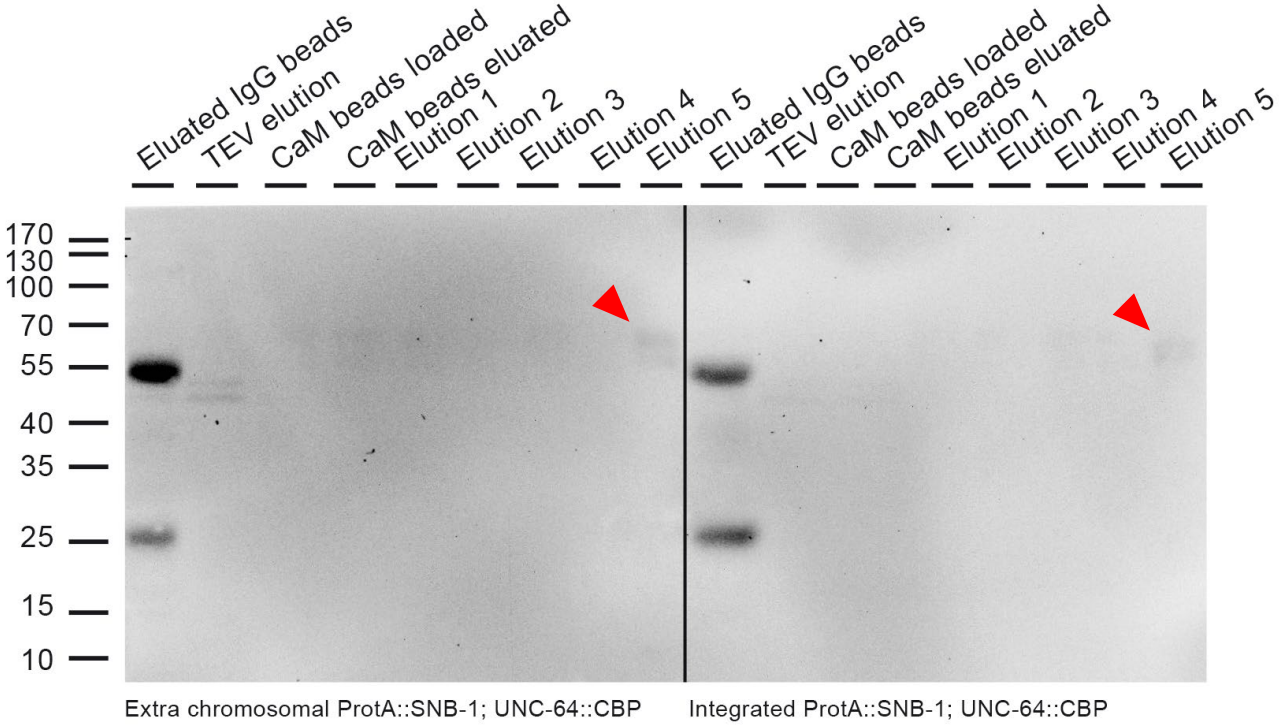

Figure 4.21 The strains ZX1586 (extrachr. array) and ZX1588 (integrated array) displayed a faint signal in the CaM bead elution fraction after tandem affinity purification The left part referred to the array purification whereas the right part displays an integrated strain via bombardment. A faint signal between 55 and 70 kDa (red arrowhead) in the different elution fractions can be detected. A clear difference between strains could not be observed, possibly due to the low quality of the western blot. ZX1586: (extrachr. array; p*snb-1*::ProtA::2xTEV:::*snb-1*::Bicis::*unc-64*::CBP::*unc-54* 3'UTR) and ZX1588 (integrated array; p*snb-1*::ProtA::2xTEV:::*snb-1*::Bicis::*unc-64*::CBP::*unc-54* 3'UTR) Antibody: anti-SNB-1(SB1, DSHB).

Whereas the western blot of the precipitated purification samples showed no distinct difference in the elution signal, the analysis with a general protein staining method (silver stain) showed a clear difference between the two purifications (Figure 4.22). The “array purification” showed more protein bands in the washing steps prior to TEV digest, but the washing steps of the CaM beads seem to have lower protein content. Even if the overall signals of the different elution fraction were in both cases rather weak, the elution fraction 3 of the bombardment purification displayed high protein content. Keeping in mind the precipitation of the washing fractions (50 times concentrated) and the CaM elution (5 times concentrated)(see Chapter 3.4), the signals of the unconcentrated TEV elution fraction, the bead samples and flow through were comparably intense. Interestingly, the protein distribution was rather different than expected from the western blot (compare Elution fraction 3 and 5 in Figure 4.21 and with elution fraction 3 and 5 in Figure 4.22). The reason could be an uneven resolubilization of the precipitated protein sample after TCA treatment or high protein content does not automatically correspond to a high SNB-1 concentration.

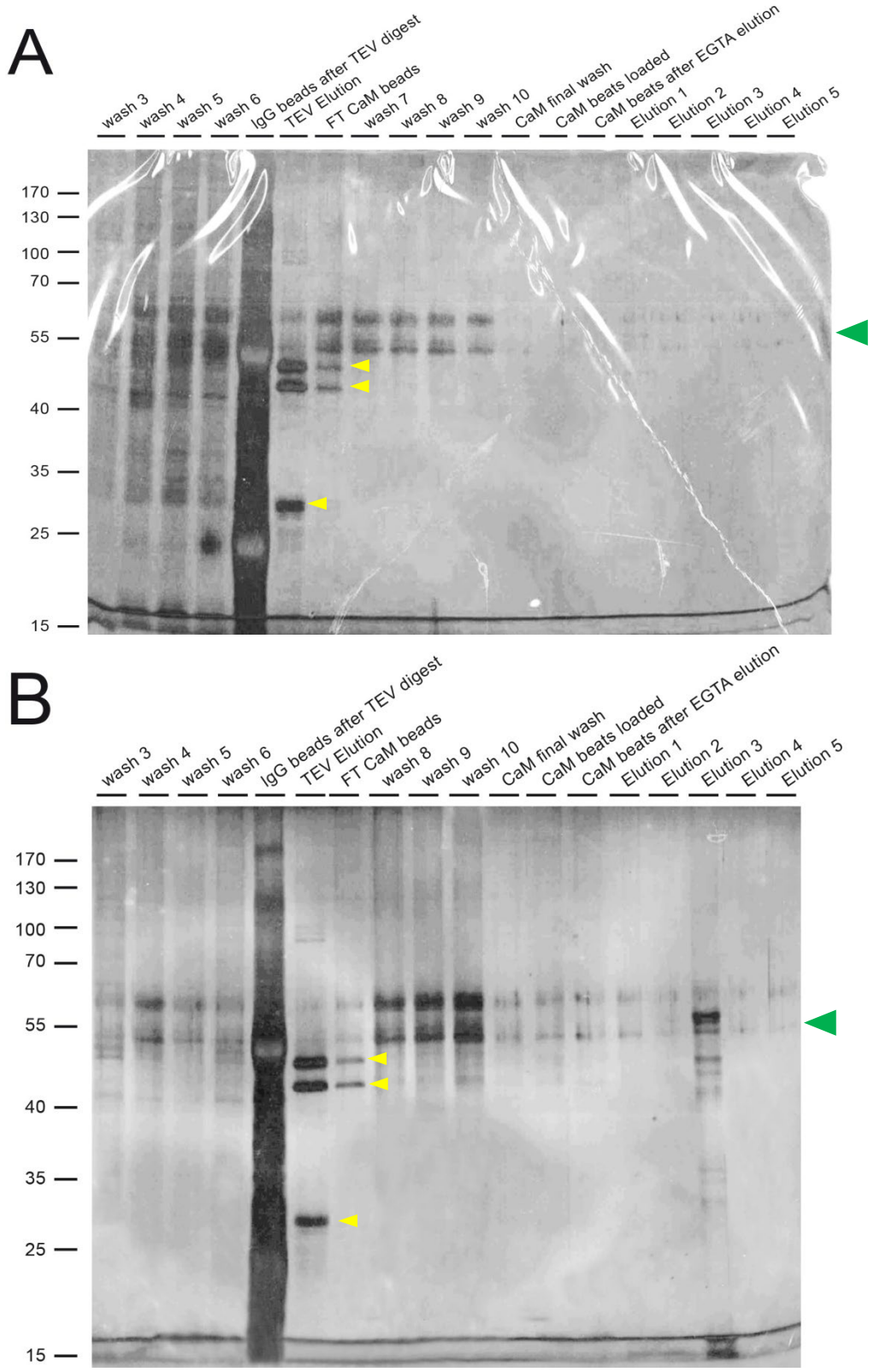

Figure 4.22 The elution in the microinjected (A) versus biolistic transformed strains (B) showed a successful purification for biolistic transformed strains The protein bands in the elution after TEV digest showed three strong reoccurring bands corresponding to turbo-TEV (double band at 45 kDa; yellow arrowhead and homemade TEV (25 kDa; yellow arrowhead) related signals. The regular occurring bands at 55 kDa (green arrowheads) were probably keratin contaminations. The elution in the bombardment purification showed a strong protein content in fraction 3.

Samples from several purifications with a SNB-1 signal in the CaM elution fraction in western blot and/or unspecifically detected proteins (silver stain) in the CaM elution fraction after clean washing steps were mass spectrometric analyzed.

4.2.2. Mass spectrometry analyses of purified SNARE complex preparations identified numerous potential SNARE-associated proteins

The mass spectrometry analyses were performed by the different collaborators: Heirich Heide (Wittig Lab, Frankfurt am Main), Ilka Wittig (Wittig lab, Frankfurt am Main) and Uwe Plessmann (Urlaub lab, Göttingen). In short protein samples were trypsin digested, the resulting peptides were separated by a reversed phase HPLC with LC-ESI-MS/MS performed on an Orbitrap XL mass spectrometer. The different databases were: uniprot *Caenorhabditis elegans* (Heirich Heide and Ilka Wittig), ws240 (most current worm peptide database from wormbase.org at that moment) and deposited sequences of the fusion constructs (Uwe Plessmann).
The samples included extrachromosomal arrays, bombardment strains, MosSCI strains and wild type N2 control. Several data sets were generated, but sets, which did not include SNARE complex proteins were regarded as unsuccessful purifications and were therefore excluded from further use.

In total 119 Proteins, which were identified in Datasets with SNARE proteins and had no appearance in wild type samples (N2) were detected (Table 13).

These proteins can be sorted into different functional groups. 5 SNARE (interacting) proteins were found (RIC-4, SNAP-29, SNB-1, UNC-64, VTI-1). 4 proteins belonged to chromosome interacting proteins (like histone 2a), 19 proteins were part of the cytoskeleton or motor protein family (like actin and kinesin-like protein), 18 ribosomal or translation-related proteins (ribosome subunit proteins and elongation factor) were detected, 6 identified proteins could be involved in signal transduction processes (e.g. guanylate cycles, cyclic nucleotide phosphodiesterase), 20 proteins were found as possibly linked to metabolic processes, as well as ATP synthesis and consumption (mitochondrial ATP synthase subunits ASB-2, ATP-4, vesicular H^+ ATPase), and 41 proteins with diverse or unknown function (e.g. calmodulin). The full list of identified proteins is given in chapter 6 (appendix to this thesis). The variety of protein families and the occurrence of proteins non-specifically pulled through the purification procedure even from wild type (un-tagged) extracts, and other purifications from different groups indicated that, as for most proteomic approaches (Morciano

et al., 2005; Takamori et al., 2006; Boyken et al., 2013), a 'background' of irrelevant proteins had to be distinguished from SNARE complex interactors (compare discussion in chapter 5.2.1.1).
Candidates for further analysis were selected, if they were identified in at least two purifications labelled as successful (presence of SNARE proteins), and were not present in negative control (from wild type samples) and if they had known neuronal function or homologies to known neuronal proteins in different species. Proteins from chromosomal origin and ribosomal subunits were regarded as contaminations, whereas proteins involved in metabolic processes were included. In previous purifications metabolic enzymes were found to be part of the synaptic vesicle (Takamori et. al, 2006; Morciano et al., 2005) and proteins involved in generation of ATP may be required for the high energy need of the synapse (Harris et al., 2012). Vesicular H^+ ATPases are required to establish a proton gradient, thus energizing the SV for subsequent loading with neurotransmitter (Lee et al., 2010). Additionally, they have been implicated in the generation of the fusion pore during neurotransmission (Bayer et al., 2003; Hiesinger et al., 2005). Phosphatases and kinases might be important for the plasticity of the synaptic complex to react to altered neuronal states (Jewell et al., 2011) and scaffold proteins are important for the generation of a protein network of the synapse (see Figure 2.2) (Südhof, 2012).

4.2.3. Selected candidates were analyzed for potential roles in synaptic transmission by RNAi knock down followed by aldicarb assays

The function of the gene, knock-out phenotype and localization were obtained from wormbase.org; the possible function was extrapolated by homologies with known proteins.

Table 11 Selected proteins from SNARE purifications for analysis with possible function in synaptic transmission

Gene	**Function/homologue**	**Knock out phenotype**	**Localization**
C33H5.8	Protein serine/threonine phosphatase with similarity to human phosphatase	NA	No clear localization
ekl-6	transmembrane and coiled-coil domain-containing protein; Transport and Golgi organization protein	lethal	No clear localization
F29G9.2	43 % homolog to Homo sapiens coiled-coil domain-containing protein	embryonic lethal	No clear localization
frm-2	anchoring proteins at PM/PDZ	NA	ventral cord neuron,

Gene	Function/homologue	Knock out phenotype	Localization
	protein scaffolds		nervous system, seam cell, intestine, uterine seam cell
klp-8	kinesin-like motor protein	no phenotype	Excretory cell, pharynx, pharyngeal neurons, and head neurons. Adult Expression: pharynx; anal sphincter; rectal epithelium; hypodermis; excretory cell; Nervous System; ventral nerve cord; head neurons; pharyngeal neurons; neurons along body; unidentified cells in head;
mca-3	plasma membrane Ca^{2+} ATPases - coelomocytic endocytosis, coordinated locomotion, recruitment of endcytotic machinery to PM	adult lethal, cell secretion variant, locomotion, nicotine hypersensitive	body muscle, the nervous system, the intestine and the coelomocyte secretory canal, all three isoforms localize to the plasma membrane
mdh-2	Probable malate dehydrogenase, mitochondrial; possible ATP production of fusion machinery	various	pharynx, intestine, body wall musculature
pfk-2	Probable 6-phosphofructokinase; energy metabolism on SVs	various	No clear localization
piki-1	Phosphatidylinositol 3-kinase - regulates apoptotic cell clearance - homolog in H.s. to second messenger in clathrin coated endocytosis	various	No clear localization
ric-4	SNAP-25	aldicarb resistant, backing uncoordinated, sluggish,	ventral nerve cord, nerve ring, dorsal nerve cord, mechanosensory neuron
snap-29	SNAP-29, 84 % homology to ric-4 isoform b	various, lethal	Excretory canal, gland cells, hypodermis, vulva, coelomocytes, intestine, gonad sheath cells and some neurons.
tag-241	homology to eea-1, a coiled-coil protein, *C. elegans* EEA-1 binds phosphatidylinositol 3-phosphate; EEA-1 reporter fusion proteins localize to early	lethal	No clear localization

Gene	Function/homologue	Knock out phenotype	Localization
	endosome.		
tax-6	Calcineurin	carbon dioxide avoidance variant, egg laying levamisole resistant, serotonin resistant	axon, cytoplasm, cilium, neuronal cell body, dendrite
unc-64	Syntaxin	aldicarb resistant, evoked postsynaptic current variant, locomotion variant	spermatheca, pharyngeal neuron, intestine, ventral nerve cord, nerve ring, dorsal nerve cord
vamp-8	Vesicle Associated Membrane Protein homolog	NA	pharynx, Nervous System, tail neurons
vha-10	vesicular H+ ATPase	neuron degeneration variant	No clear localization
vti-1	VTI (Vesicle Transport through t-SNARE Interaction) homolog	NA	No clear localization
W01B6.5	67 % homology to a Homo sapiens tyrosine-protein kinase	NA	No clear localization
W09C3.1	homology to tau-tubulin-kinase	lethal	No clear localization
Y116F11B.11	human Golgi subfamily A member 4 isoform 1; may play a role in delivery of transport vesicles	NA	No clear localization
NA = No data available			

These selected genes were addressed to RNAi knock-down. With the help of the RNAi producing bacterial strains from two commercially available libraries, inducing systemic RNAi in *C. elegans* through ingestion (one by Julie Ahringer (Kamath and Ahringer, 2003) (*mca-3*, W01B6.5, F29G9.2, PIKI-1, UNC-26, FRM-2, C33H5.8, MDH-2, PFK-2, SNAP-29), one by Mark Vidal (Rual et al., 2004) (VHA-10, VAMP-8, W09C3.1, KLP-8, RIC-4, ELK-6, TAG-241), and one bacterial strain that was generated by myself (Y116F11B.11), as well as using a specific worm strain generated by Sebastian Wabnig in our lab (ZX1513) (Wabnig et al., 2015), enabling cholinergic neuron specific feeding-RNAi, the appropriate mRNA was neuronally destroyed and consequently the expression of these genes in cholinergic neurons was reduced. After placing eggs onto RNAi bacteria, hatching and development according to Vashlishan et al. (Vashlishan et al., 2008), the transiently neuronal altered nematodes were transferred to aldicarb plates and analyzed according to their paralysis reaction (see chapter 3.2.4) after 100 min (Figure 4.23).

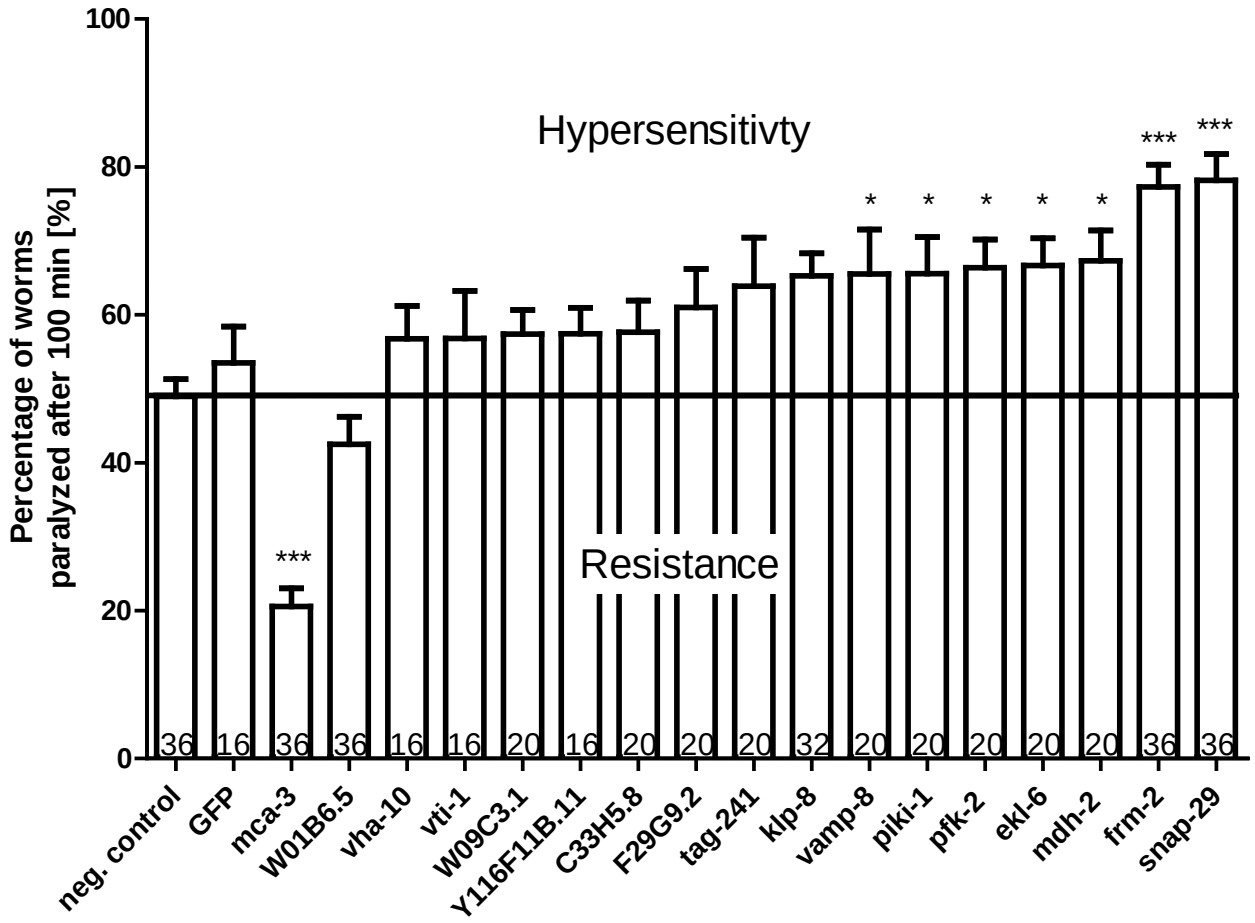

Figure 4.23 Knocking-down *mca-3* induced a resistance to aldicarb, whereas knocking-down *frm-2, snap-29, ekl-6, klb-8, mdh-2, pfk-2, piki-1* and *vamp-8* resulted in hypersensitivity. One-way ANOVA test related to negative control (L4440 empty vector) showed for several strains a significant alteration of aldicarb induced paralysis. Impeded *mca-3* expression resulted in a strong aldicarb resistance, whereas *frm-2* and *snap-29* knockdown animals displayed a strong hypersensitivity to aldicarb (all three showed statistical significance with a p-value of less than 0.001. *ekl-6, klb-8, mdh-2, pfk-2, piki-1* and *vamp-8* showed a statistically significant hypersensitivity to aldicarb with a p-value of less than 0.05 (one way analysis of variance (one-way ANOVA) in comparison to the negative control (L4440), due to Gaussian distribution, Dunnet comparison) (number in columns represent the number of independent experiments with 25 animals each).

Two positive controls for aldicarb resistance the SNARE complex proteins *ric-4* (*snap-25*) and *unc-64* (syntaxin) has been included. Unfortunately, *unc-64* has been erroneous annotated in the library (revealed by sequencing) and *ric-4* RNAi knock out did not display resistance. The missing effect of *ric-4* RNAi could not be explained by sequencing or corrected by re-inoculation of the corresponding bacterial strain. *mca-3, frm-2* and *snap-29* knock-out showed the most statistically significant alteration ($P<0.001$), whereas *ekl-6, klb-8, mdh-2, pfk-2, piki-1* and *vamp-8* showed a lower statistical significance ($P<0.05$) (Figure 4.23 and see discussion chapter 5.2.1).

4.2.4. Localization studies with the help of promoter fusion or functional fusion constructs of frm-2, snap-29, mca-3

To verify the neuronal role and the possible interaction with the SNARE complex co-localization experiments with the SNARE protein SNB-1 of the most statistically significant genes(*frm-2, snap-29, mca-3*) in the aldicarb assay were performed (KLP-8 has been analyzed by Huang et al. showing a partial neuronal expression: a transcriptional fusion drives expression of GFP in excretory cells, pharynx, pharyngeal neurons, and head neurons (see Figure 5.1)(Huang et al., 2007)). Different promoter GFP fusion constructs (transcriptional and translational) were generated and co-injected with a p*snb-1*::mCherry::*snb-1* construct (pFC23). An overlap of green and red fluorescence signals at neuronal structures would be in line with a neuronal role of the corresponding protein. The translational fusion constructs of FRM-2 and SNAP-29 were both available via the TransgeneOme project of the Max Planck Institute of Molecular Cell Biology and Genetics by Mihail Sarov (Sarov et al., 2012) and were microinjected in combination with mCherry::*snb-1* vector (pFC23) into *unc-119* animals (EG6699)(according to the injection protocol of Mihail Sarov) (Sarov, 2014).

FRM-2

frm stands for protein 4.1 (**f**our point one) of the ezrin-**r**adixin-**m**oesin family. Fürden et al. proposed for ERM proteins to link microfilaments to the plasma membrane and to have a role in scaffolding (van Fürden et al., 2004). But in their analysis they could not detect a specific phenotype upon RNA interference.

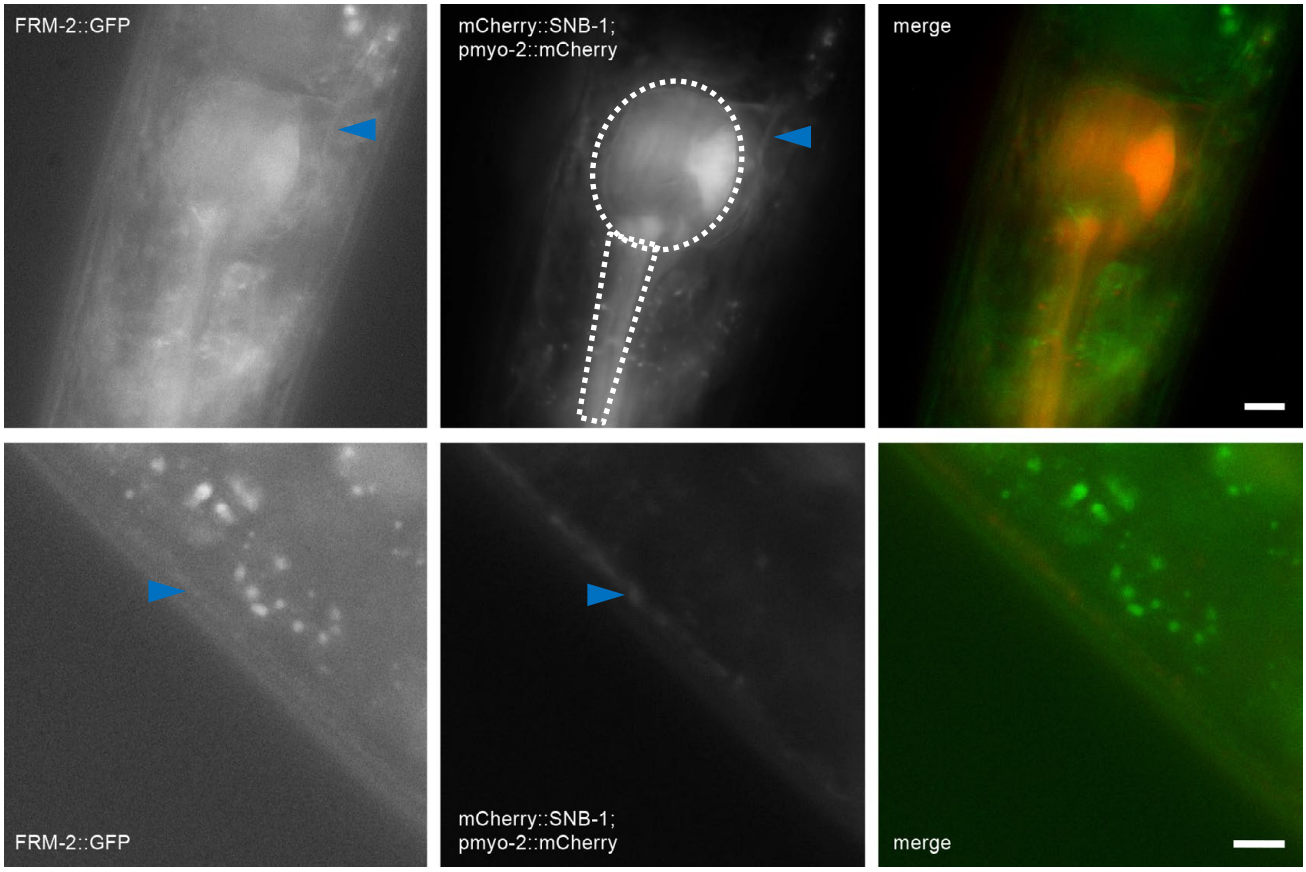

Figure 4.24 The FRM-2::GFP display a broad expression, not restricted to synapses or even neurons. The FRM expression is rather extensive and seems to be overlapping in some regions (blue arrowhead), but a distinct neuronal expression could not be observed. The *pmyo-2*::mCherry leads to an red fluorescent pharynx and therefore irrelevant (white dashed line) (scale bar, 10 µm).

SNAP-29

SNAP-29 is a homologue of the *ric-4* isoform b and interacts with proteins of the endosomal recycling (Rapaport et al., 2010; Sato et al., 2011). In humans a deletion of SNAP-29 leads to among others to neurological impairments (Sprecher et al., 2005) and has been proposed to inhibit synaptic transmission (Pan et al., 2005). SNAP-29 was discovered as a synaptic vesicle protein in the mouse (Takamori et al., 2006)

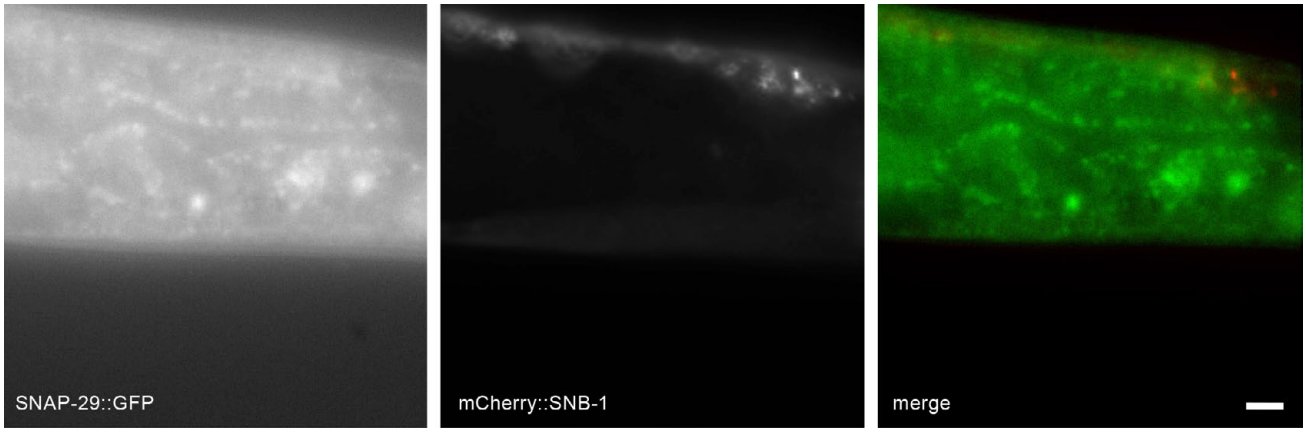

Figure 4.25 The SNAP::29 expression can be observed throughout the nematode. The expression of SNAP-29 seems to be ubiquitous and neuronal specific localizations were not detectable (scale bar, 10 µm).

Sato et al. reported that SNAP-29 has a role in membrane trafficking throughout the worm (Sato et al., 2011). The localization underlined this finding and I speculate the increased aldicarb response (hypersensitivity) was to be based on reduced body size (see chapter 5.2.1). Even if a change in aldicarb response due to RNA interference could be detected, FRM-2 and SNAP-29 did not show a neuronal or even a synaptic expression, compared to the mCherry::SNB-1 signal (Figure 4.24 and Figure 4.25).

MCA-3

The plasma membrane Calcium^{2+} ATPase *mca-3* has been described by Bednarek et al. primarily in the context of coelomocytes. Coelomocytes are scavenger cells responsible for the uptake of material from the pseudocoelom (the liquid filled body cavity). The coelomocytic uptake deficiency has been demonstrated by a GFP with a modified signal sequence (ssGFP) (Fares and Greenwald, 2001), which would be secreted into the pseudocoelom but finally incorporated by the coelomocytes, resulting in green fluorescent scavenger cells. The loss-of-function mutation of *mca-3* (ar492) induced an accumulation of GFP in the body cavity. Even when they saw a change in locomotion and a neuronal expression of a transcriptional fusion Bednarek et al. did not speculate about any role in neuronal function (Bednarek et al., 2007). In this work the *mca-3* knock-out displayed a profound aldicarb resistance and no obvious morphological changes were detectable (in contrast to the SNAP-29 RNAi worms, which were thinner than wild type controls).

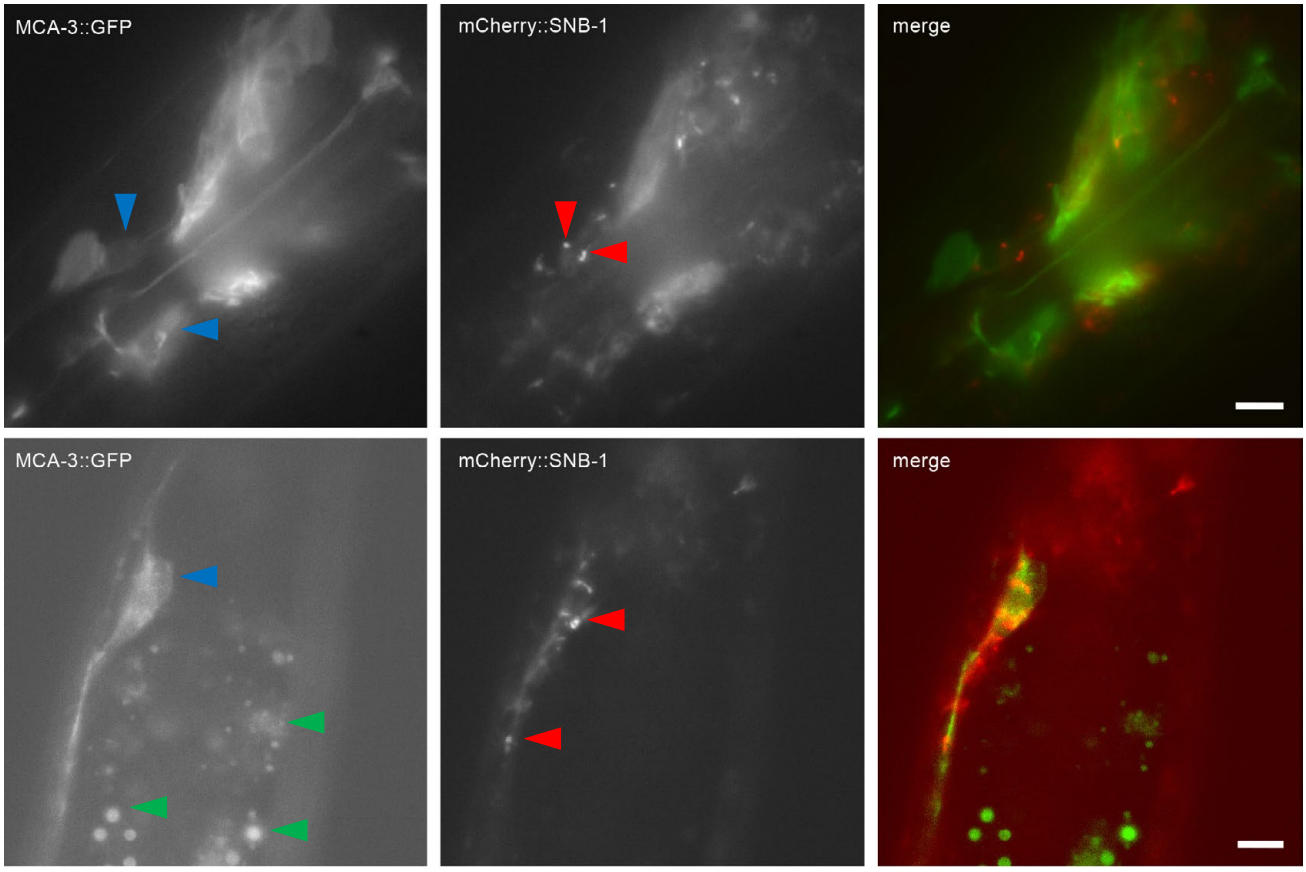

Figure 4.26 A clear neuronal expression of the MCA-3B::YFP could be observed A distinct co-localization of MCA-3B::YFP and mCherry::SNB-1 in cholinergic neurons is visible. But MCA-3B::YFP is localized to the plasma membrane (blue arrowheads) and SNB-1 concentrated at synaptic vesicles (red arrowheads). The tail images display some YFP fluorescence puncta localized to the gonads (green arrowheads) (scale bar, 10 µm).

The microinjection of pFC22 [p*unc-17::mca-3b* cDNA::YFP] in combination with pFC23 [p*snb-1*::mCherry::*snb-1*] displayed a neuronal co-localization of these two proteins on neuronal and plasma membrane level (Figure 4.27). As the fluorescent images displayed an potential neuronal co-localization, a further analysis of this expression pattern was performed with a confocal microscope (Figure 4.27).

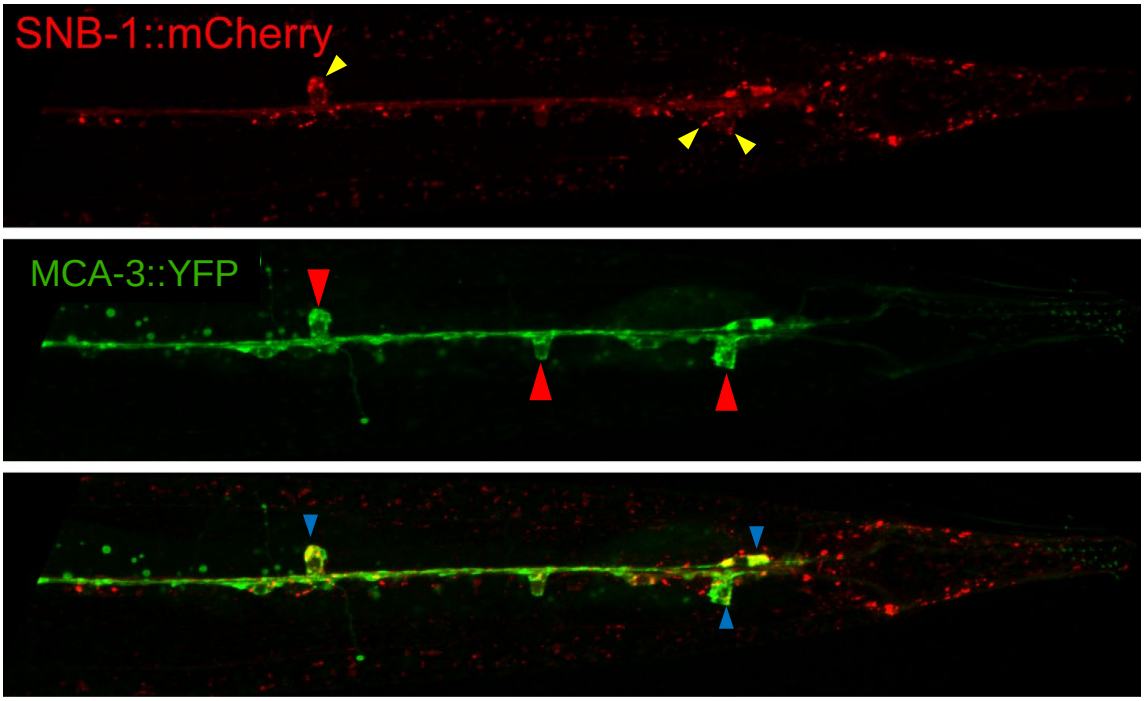

Figure 4.27 Confocal analysis of MCA-3B::YFP and mCherry::SNB-1 displayed the difference between plasma membrane localization of MCA-3 and vesicle localization of SNB-1 The neuronal plasma membrane localization of MCA-3::YFP could be observed (red arrowheads), whereas the expression of SNB-1::mCherry was concentrated into small spheres, which could be interpreted as synaptic vesicles (yellow arrowheads). The occurrence of yellow spots in the merge image (blue arrowheads) showed the co-localization and synaptic structures could be detected for both fusion constructs. The confocal images were prepared with the help of Christine Molenda.

The images demonstrated the plasma membranous localization of MCA-3B::YFP compared to the vesicular localization of mCherry::SNB-1, as proposed by Dittman et al. (Dittman and Kaplan, 2006). As MCA-3B::YFP showed a partial co-localization with mCherry::SNB-1 and could therefore hint to an interaction. This indicated that the previously by Bednarek et al. reported neuronal localization required an re-evaluation (Bednarek et al., 2007) and the role of *mca-3* in synaptic transmission was further investigated. To allow a comparison between a coelomocytic rescue and a rescue in a neuronal context *mca-3* knock-out worms were microinjected with a cholinergic neurons specific promoter p*unc*-17::*mca-3b*::YFP.

4.2.5. Phenotypic assessments of mca-3 mutants

4.2.5.1. mca-3 knock-out animals did not show a response in an aldicarb assay

To demonstrate the neuronal impairment by the *mca-3* mutation on the one hand and the rescuing effect of cholinergic mca-3 expression on the other hand an aldicarb assay was performed.

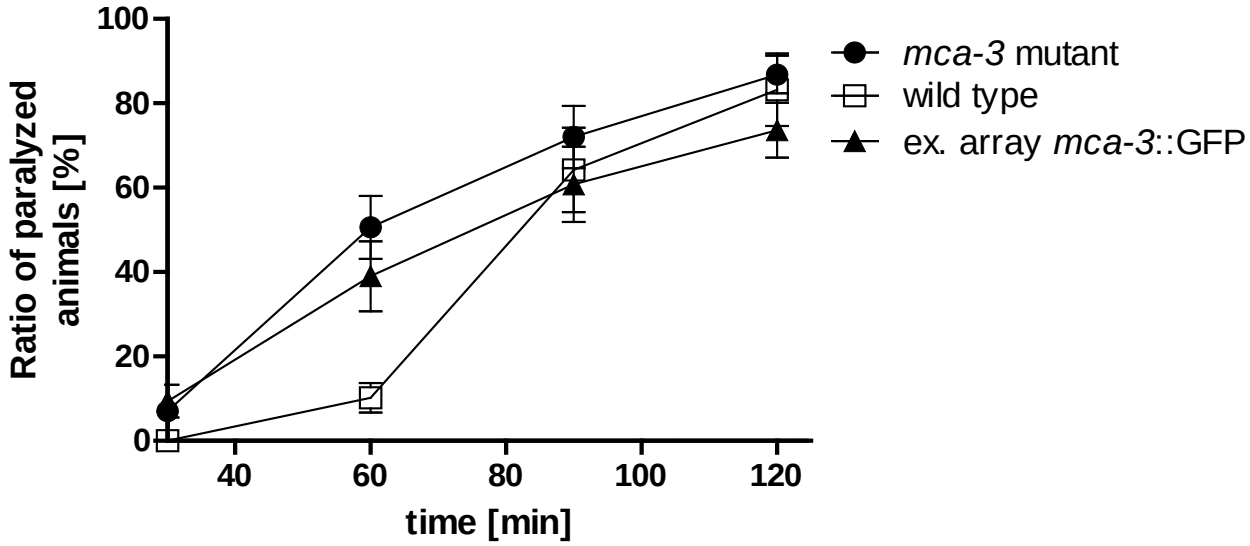

Figure 4.28 The aldicarb assay did not show a rescue phenotype after injection of with *punc-17::mca-3*
The wild type worms (N2) paralyzed at a later time point, but reached the same level as the *mca-3* mutant and its potential rescue. (N=5, 25 animals) 1 mM Aldicarb.

The aldicarb assay with the *mca*-3 mutant (GS2526 [arIs37 [pmyo-3::ssGFP; dpy-20] I; mca-3(ar492) dpy-20(e1282) IV]) could not repeat the previous results of the aldicarb assay. The mutant and microinjected strain paralyzed at 60 min already to 51 % and 39 % respectively, whereas the wild type showed only 10 % paralysis. The response compared to the previous aldicarb assay (Figure 4.13 and Figure 4.23) has been the same, but the rescuing effect of the p*unc*-17::*mca-3* transgene was not observed. Possible reasons are discussed in chapter 5.2.2.

4.2.5.2. mca-3 knock-out mutants had a trashing defect and could be partially rescued by MCA-3::YFP expression

To further analyze the behavior of the *mca-3* knock-out and its cholinergic rescue in alternative motor program, a swimming assay has been performed (compare chapter 3.2.5) (Kraemer et al., 2003) (Buckingham and Sattelle, 2009).

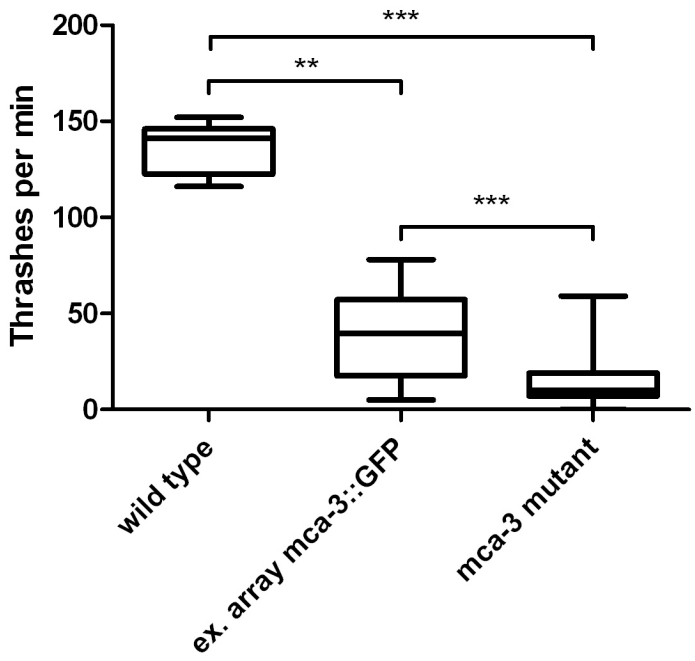

Figure 4.29 The *punc-17::mca-3* partially rescues the mca-3 mutant in the swimming assay The graph shows an obvious difference between the rescue and wild type (N2), but the rescuing effect of a p*unc*-17::*mca-3::*YFP was significant (P<0.001, Kruskal-Wallis test, due to non-Gaussian distribution of rescue and mutant) (N=36).

As a distinct phenotype for the mca-3 knock-down in the swimming assay could be observed and the injection of *punc-17::mca-3b::GFP* demonstrated a significant increase of thrashes (Figure 4.29) a synaptic role of *mca-3* can be assumed.

5. Discussion

5.1. Synaptic vesicle purification in *C. elegans* is more complex than expected

Purification of protein complexes utilizing tandem affinity purification (TAP) has been demonstrated by several groups (Rigaut et al., 1999; Puig et al., 2001; Gingras et al., 2005; Gottschalk et al., 2005; Li, 2010) and the purification of murine SVs with the help of fractionation of neuronal tissue, and capturing by specific antibodies immobilized on magnetic beads demonstrated its functionality by revealing many synaptic proteins (Morciano et al., 2005; Burré et al., 2006; Burré et al., 2007). In this work, attempting to purify SVs from crude *C. elegans* extracts via TAP, was not possible to obtain a sufficiently enriched and purified sample to enable mass spectrometric identification of SV associated proteins. As already described in the result section (4.1.1), many strategies were applied with the aim to improve the elution from IgG beads:

- The proteins synaptogyrin and synaptotagmin, which have a lower copy number per vesicle, were utilized to reduce the number of potential binding sites that are presented per SV to the affinity beads. They thus should have reduced the number of necessary TEV-cleavage events to eventually release the respective TAP-tagged synaptic vesicle, and should therefore have displayed an improved release of bound SV material from the affinity beads.
- The application of Mos1 single copy integration was supposed to reduce the amount of proteins to a native level. This should improve specificity of expressed fusion constructs and the elution of synaptic vesicles from the beads by a corresponding binding site reduction as in the previous attempt (Frøkjær-Jensen et al., 2008).
- Yvonne Füll introduced three additional TEV cleavage sites each separated by G_4S-linker between CBP and ProtA to increase the susceptibility for cleavage (Waugh, 2014).
- The elongation of the G4S-linker region between SNG-1 and CPB had the intension to increase the overall size of the TAP tag. This should reduce sterical hindrances and should therefore improve the binding capability during the second purification step (Arnau et al., 2006). The stated approaches did not lead to an improved elution of TAP signal for the magneto beads. A possible explanation is that during the first purification step crude protein/membrane debris, which were possibly only partially removed during the centrifugation steps bound to the beads. These debris would contain membrane bound SNG-1 (and SNB-1), but would not be accessible for any protease cleavage.

- To remove inaccessible debris and to allow the purification of synaptic vesicles, which were not bound to other structures a sucrose gradient was applied. The fractionation after the sucrose gradient was supposed to enrich free SVs, with the aim of a more homogenous starting material and to reduce the amount of cytoskeleton bound SV with reduced accessibility for the enteropeptidase (personal communication with Sandhya Padmanabhan Koushika, Koushika Lab, Bangalore, India). During several sucrose gradients it became apparent that the prepurification of SV could not be performed, as no fraction with a specifically high content of SV in the lower densities could be observed.
- The original TAP strategy was described by several publications as prone to technical difficulties (Rubio et al., 2005; Arnau et al., 2006; Schaffer et al., 2010, Gloeckner and Boldt, 2009): the rather large size of the tag with 21 kDa, the dependency on cleavage and the potential interference of CBP with the Ca^{2+}-signaling, especially in the neuronal context may induce further complications. Therefore, the Strep-/Flag-tag purification (using a Strep II-tag and a FLAG tag in a tandem tag, resulting in a 4.6 kDa construct) strategy has been attempted as an alternative (Gloeckner and Boldt, 2009). The FLAG tag did not show a specific signal and the specific OneStrep signal was lost during purification.

Even after several alterations of our purification strategy a satisfactory quality could not be obtained.

5.1.1. Challenges during synaptic vesicle purification

Possible reasons for technical difficulties were: a low ratio of fusion protein integrated in SV, as 30 % of the total amount of synaptobrevin were discovered to be bound to the presynaptic membrane (Dittman and Kaplan, 2006). The close organization of SV into the different vesicle pools could reduce the susceptibility of SVs for binding and later elution. The high performance strategy of TAP and using large amounts of worm material could not compensate the missing tissue with high SV content.

The magnetobeads were paramagnetic, polystyrene beads coated with a polyurethane layer and were coupled to the IgG-Antibodies with the help of the tosyl-group. These beads were incubated with an antibody and blocked with BSA/Tris 48 h prior to sample contact, still the incubation and protease cleavage process were time consuming, leaving the proteinaceous environment of the SV in close contact to the bead surface. Either further protein-bead covalent coupling could occur or the hydrophobic residues of the membrane could interact with the polyurethane layer of the beads.

I believe the main problem during purification was the accessibility of SVs for the following purification steps. Despite there are many examples of successful purifications of synaptic vesicles in rodents and the transmission structures a rather similar, the body composition including the cuticle and the distribution of neurons is quite divergent. Extensive experiments with different ways of homogenization, gradient fractionation and possible synaptosome lysis should be performed. As the experiments with SNG-1 revealed, the number of subunits on a synaptic vesicle is not responsible for elution. Therefore, it could be possible to utilize SNB-1 in combination with the SB-1 antibody with an intense signal during immunoblot analysis. It is still unclear, if this would lead to better results and if it is possible to natively purify synaptic vesicles from the nematode *C. elegans* due to SV interaction with the presynaptic membrane and the actin cytoskeleton.

5.2. **SNARE complex purification allows new insights to the synaptic machinery**

5.2.1. Understanding the transmission machinery

The detection of this large number of different proteins and different families by different groups (Morciano et al., 2009; Boyken et al., 2013) underlined the complexity of this machinery and of the different purification methods, which do not comprehensively reveal all important interaction partners. For example, Boyken et al. discovered in their docked SV fraction only low amounts of the SNARE complex, even if it would be expected as a dominating part of this purification. Next to chromosomal proteins and ribosomal subunits representing probably contaminations, metabolic proteins are feasible in the synaptic context as the high energy consumption of the transmission machinery needs to be sustained (Harris et al., 2012). Transport and cytoskeletal proteins could be related to the recuperation of SNARE complexes, vesicle pool organization and endosomal structures (Alabi and Tsien, 2013).

Knocking out proteins with expected essential functions does not block exocytosis completely (Imig et al., 2014) and knocking down the interesting genes is a multistep experiment with every step being essential for a correct outcome. So the aldicarb experiment with a high number of repetitions and with a strain prone to neuronal knock out was addressed to increase the specificity of our experimental setup. Unfortunately an aldicarb assay does not only report synaptic alterations, but reflect all neuronal impairments - even indirect ones e.g. metabolic stress.

5.2.1.1. Selected proteins and their probable role in the synaptic context

SNAP-29 has been an interesting candidate due to its homology to RIC-4 and it demonstrated a profound and regular hypersensitivity in the aldicarb assay (Figure 4.23). But looking at the phenotype, the animals displayed a small body diameter after RNAi incubation. The ubiquitous expression of the SNAP-29::GFP (Figure 4.25) demonstrated that a solitary neuronal role is doubtful. The reason for a higher number of paralyzed worms could be simply a higher surface area to volume ratio in small animals, resulting in a higher aldicarb uptake and a faster paralysis. As mentioned in the introduction, the SNARE motif is an extensively used mechanism and manipulations in the molecular sorting could down regulate cellular activity resulting in small worms. In 2011 Sato et al. demonstrated that SNAP-29 mediates fusion and is required for maintaining the organization and morphology of organelles (Sato et al., 2011), whereas Kang et al. observed an expression in addition to neuronal expression in several other tissues (Kang et al., 2011), so a neuronal role is improbable.

KLP-8, VTI-1 and MCA-3 were already analyzed for their expression by GFP-fusion constructs:

The Kinesin like motor protein KLP-8 has been analyzed by Huang et al. showing a partial neuronal expression: a transcriptional fusion drives expression of GFP in excretory cell, pharynx, pharyngeal neurons, and head neurons (see Figure 5.1B)(Huang et al., 2007). Fluorescent images of KLP-8 GFP fusion construct were published by Hunt-Newbury et al. on the www.gfpworm.org website (Hunt-Newbury et al., 2007).

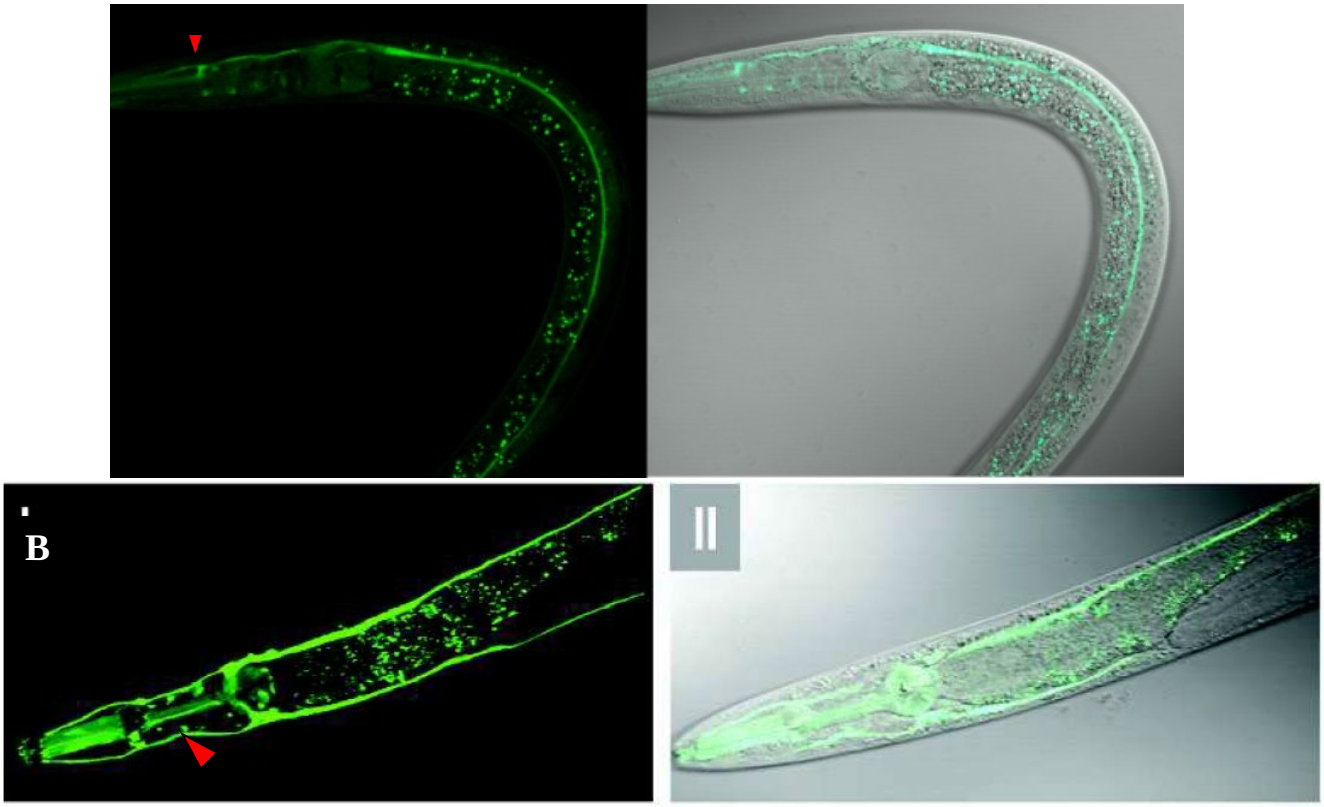

Figure 5.1 Fluorescent image of KLP-8::GFP fusion A The images were obtained from the gfpworm.org website (Hunt-Newbury et al., 2007); B Transcriptional fusion with GFP by Huang et al. displayed similar expression with a more intense fluorescent signal in the head neurons (red arrowheads)(Huang et al., 2007).

The name VTI-1 refers to a vesicle transport through the interaction with t-SNAREs 1 and has therefore been an interesting candidate as a SNARE interaction partner. Luo et al. demonstrated its function as part of the GARP (Golgi-associated retrograde protein) complex interacting with syntaxin-5, VPS-53, MEMB-2 and syntaxin-16 in motoneurons (Luo et al., 2011). Impairment of the Golgi apparatus of motorproteins could result in a reduced baseline secretion and therefore a reduced neuronal functioning.

The MCA-3 resistance to aldicarb in RNAi could be explained by two factors. A: The missing MCA-3 during development induced a compensatory reaction and the transmitter secretion is reduced. Bednarek et al. reported an important role in the clathrin mediated endocytosis (Bednarek et al., 2007). Or B) Impairing endocytosis could lead to a reduced number of neurotransmitter filled vesicles and could therefore reduce the secretion of acetylcholine. After microinjecting MCA-3 into knockout strains a hypersensitivity to aldicarb could be detected. This fact could be explained by the missing Ca^{2+}-transporter, which would probably result in elevated Ca^{2+} concentrations and could lead to an increased acetylcholine secretion. As the aldicarb assay of the *mca-3* mutant did not repeated the results of the RNAi knock-down/aldicarb assay, a swimming assay was performed where a

partial rescue for the cholinergic expressed MCA-3 could be observed. Possible reasons for the incomplete rescue are: a) the GFP fusion construct induced functional impairment, which could be solved by alterations of the linker length or exchange of the fusion terminus, b) a wrong or too few isoforms (five *mca-3* isoforms exist a-e, but specific functions for every isoforms are unknown in *C. elegans*, in mammals different isoforms are tissue specific expressed (Guerini et al., 1998; Brandt et al., 1992) could have been addressed, which could be altered by an alternative set of fusion constructs, c) microinjections are always prone to mosaicisms, reducing the overall performance, which could be corrected by an integration and d) addressing only cholinergic neurons leave GABAergic neurons with reduced functionality, which could be solved by using a pan-neuronal promoter (like p*rab-3*).

5.2.2. Proposed model of the SNARE/MCA-3 interaction

The plasma membrane Ca^{2+}-ATPases maintain a low intracellular calcium concentration which is needed for the functionality of many cellular processes, among others, synaptic transmission (Brandt et al., 1992). Morciano et al. and Boyken et al. discovered several Calcium ATPases in the mammalian docked vesicle proteome (Morciano et al., 2009; Boyken et al., 2013). In *C. elegans* MCA-3b has 63% identity to *Homo sapiens* MCA-3 (ATP2B3) and Bednarek et al. demonstrated a role in clathrin-mediated endocytosis in coelomocytes for MCA-3 (Bednarek et al., 2007). At the active zone of the synapse the primed synaptic vesicles are organized in scaffolds where interaction and localization between the regulatory partners is orchestrated (Südhof, 2012). A close interaction of syntaxin with Ca^{2+}-channels has already been demonstrated (Mochida et al., 1996; Li, 2004), therefore an important role of MCA-3 by reducing the Ca^{2+} concentration to a minimum could be speculated.

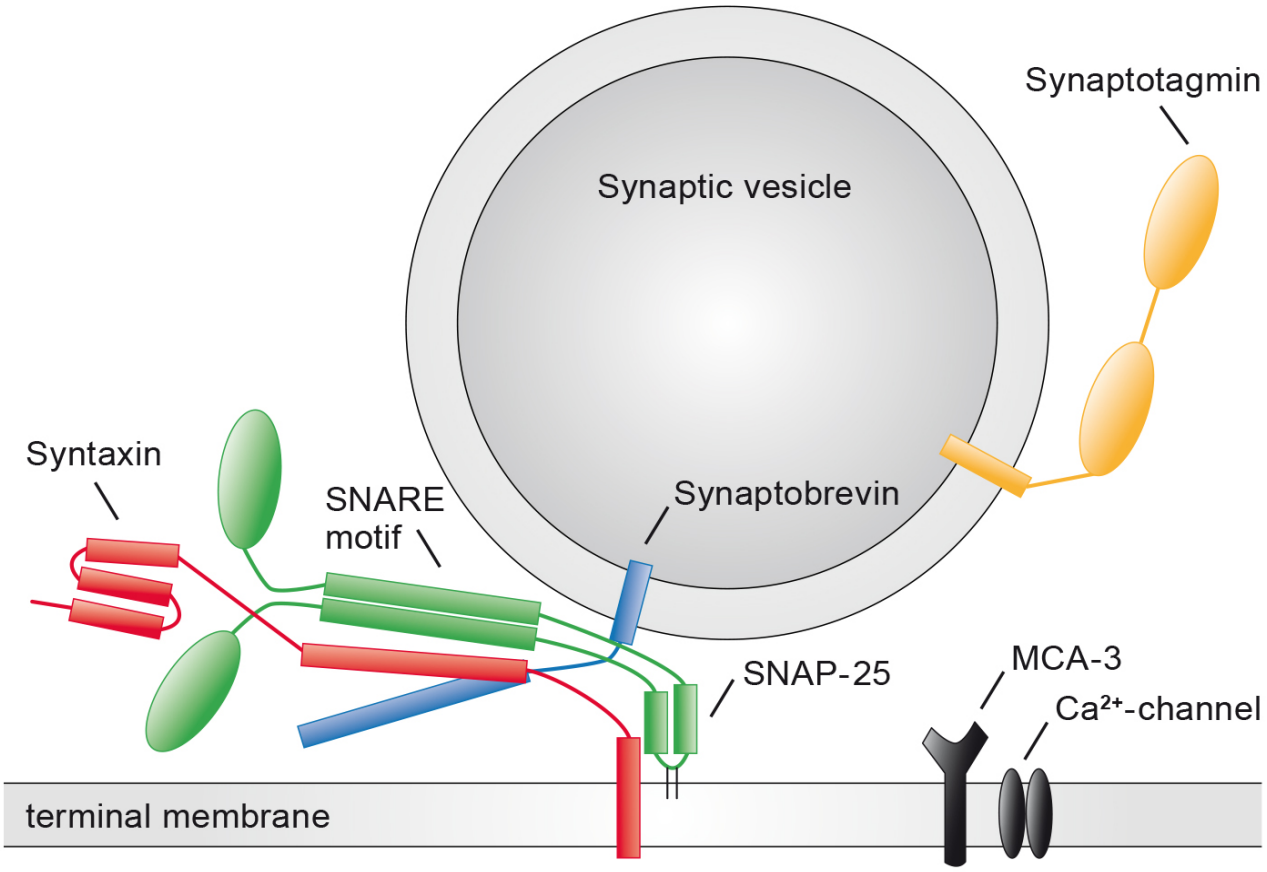

5.2 The MCA-3 has an important role in the functionality of Ca^{2+} induced vesicle fusion Our model proposes a link between SNARE complex proteins and Ca^{2+}-channels with MCA-3. Synaptotagmin (yellow) is activated by a local rise in Ca^{2+}-ions and triggers zippering of the primed SNARE complex (syntaxin red, SNAP-25 green, and synaptobrevin blue). The linked MCA-3 (black) reduces the local Ca^{2+}-concentration to a minimum and allows a fast recovery to the baseline Ca^{2+} concentration. By scaffolding all necessary proteins to one location, exocytosis could be more effective. The different molecules and structures are not in scale.

This could allow specific synaptotagmin activation: A reduction of Ca^{2+} concentration in the proximity of synaptotagmin to a minimum would allow the cell to generate (during evolution) a more susceptible synaptotagmin. This could reduce the amount of spontaneous exocytotic events and the refractory time. The exact mode of action requires further investigation, but could reveal a new class of proteins in the current model of the active zone.

5.2.3. Drawbacks during SNARE complex purification

Several drawbacks during purification were already addressed in the results chapter, but some facts require a theoretical discussion.

5.2.3.1. Only the UNC-64a was tagged with CBP and could therefore lead only to partial insights.

During vector development it became obvious that the CBP needed to be outside of the presynapse, due to possible alterations of Ca^{2+}-signaling and thus it had to be decided which splice variant to tag. Due to the better accessibility for cloning of UNC-64a (the isoforms a is the shortest) it was decided to use this isoform which might reduce some important factors during SNARE assembly (possible reason for incomplete rescue of the *unc-64* r-o-f mutant in the aldicarb assay, Figure 4.13). An alternative could be additional experiments with other isoforms of UNC-64, or using RIC-4 as the purification partner of SNB-1, or using different tags in conjunction with an N-terminal fusion or the tagging of every single isoform with CBP.

5.2.3.2. The purification of SNARE complexes from the microinjected and biolistic transformed strains did not show differences in the amount of purified SNB-1.

The fact that microinjected and biolistic transformed strains did not show different expression signals could be the result of several reasons: a) after several generations of overexpression the complex transcription and translation is down regulated/silenced. b) the combination of reduced transmission and mosaic expression results in an overall reduced production (Yochem, 2003; Frøkjær-Jensen et al., 2008). c) the purification of the complex is limited by the TAP characteristics/logistics, like TEV or IgG bead amount.

5.2.3.3. The number of hits in the sample and N2 purifications displayed a large background and many known interaction partners were not detected

As already mentioned, SNARE complex proteins were detected in some of the purified samples (compare chapter 4.2.2). The reason besides unsuccessful purifications and artificial bands during western blotting could be the resistance of SNARE complexes to trypsin digest, which is essential for mass spectrometric analysis. The SNARE complex, when fully coiled, is resistant to SDS (Fasshauer et al., 2002) and could be equally resistant to trypsin digest. To compensate this fact the different mass spec facilities (Urlaub lab/Wittig lab) were provided with the modified versions of the SNARE complex including linker regions, TEV cleavage sites (some could remain uncleaved) and the CBP-tag, but due to the complexity of sample preparation this data could not be analyzed (due to the high occurrence of G4S-linker and CBP motifs in the proteome).

Quetglas et al. showed a calmodulin binding ability of SNB-1 (Quetglas et al., 2000), which could result in a purification of SNB-1 alone during the process, due to the focus on SNB-1 antibodies.

Antibodies directed against the CBP-tag showed a considerable background in western analyses (Figure 4.14) and were not used for further analysis.

Many known interaction partners like synaptotagmin, mUNC-13/18, complexin, were not detected in the analysis. It might be possible that extensive washing steps with Triton X-100 during purification removed many interaction partners. The experiment shown in Figure 4.15 was performed to test alternative detergent strategies. Unfortunately, the substitute deoxycholate, despite good results in solubilization, did inhibit TEV cleavage.

5.2.4. Improvements of purification

Several improvements of the purification strategy are feasible. “Easily” performable alterations were addressed in the section “Modifications with moderate effort”, whereas more difficult changes in the purification strategy were discussion in the section “More complex modifications of the purification strategy”.

5.2.4.1. Modifications with moderate effort

Purification with exchange of the first and the second step would allow a TEV digest with lower endogenic proteases due to the second washing step already performed and the ability to use protease inhibitors during the first incubation and elution. Background of the affinity matrices still could be present, but the change of the sequence could result in a different and more elucidated dataset. Burré et al. stressed the fact that due to the complexity of the purification steps and sample preparation different groups identified different sets of proteins. 80 % of the neuronal proteins were discovered in solely one study (Burré and Volknandt, 2007).

Known and expected interaction partners like *unc*-18 and *unc*-13 and synaptotagmin (compare chapter 2.3.2.1.4) were not purified. The reason could be an alteration in the interaction due to the use of detergent (Edelmann et al., 1995), the formation of *cis*-SNARE complexes after detergent use (Jahn and Grubmüller, 2002) or extensive washing steps prior elution (personal communication with Ilka Wittig). Instead of having a rather pure sample with a reduced but definied number of interaction partners a different approach would be to perform less washing steps obtaining less pure samples, but more interaction partners. This approach stipulates a continuously available samples analysis (an MS analysis after the first purification step, for the presence of known interaction partners), which was not possible in the experimental setup.

The application of N-ethylmaleimide would render NSF, the AAA-ATPase for dissolving the *cis*-complex, non-functional and could induce a higher amount of *cis*-SNARE complexes.

Unfortunately, not only NSF, but many other proteins would be rendered non-functional and could therefore alter the interactome of the SNARE complex.

Prior to the application to IgG beads a size exclusion chromatography could be performed. With the help of fluorescence labeled SNB-1 fractions with SNARE complexes and interaction partners (higher molecular weight than uncomplexed SNB-1) could be isolated. The sample volume in the first purification step is of minor interest and the gel filtration could be a prepurification method to reduce non-specific proteins binding to the IgG motif. The washing could be reduced and a cleaner sample could be obtained. The risk would be to introduce another purification step in an already complex procedure and by increasing the sample volume to reduce the critical concentration of important partners over a relevant threshold.

5.2.4.2. More complex modifications of the purification strategy

In all samples a multitude of unspecific proteins were detected. As Burré et al demonstrated the same precipitated proteome showed different finding for different PAGE protocols (1d SDS/ESI-MS, 2d SDS/MaldiTOF-MS and 2d BAC/SDS/MaldiTOF-MS) and only 19 % of all discovered proteins were discovered in all analyses (Burré et al., 2006), underlining the complexity of purifications from multicellular organisms. Interaction moieties like IgG and CaM are commonly used motifs throughout cellular processes and are therefore prone to unspecific purifications. To reach a more favorable signal to noise ratio it is possible to either increase the expression of the fusion constructs by higher plasmid concentration during microinjection, which would result in a less native expression pattern (with a risk of purifying artificial complexes which are formed during ER translation and processing) or the use of a different TAP tag strategy e.g. Strep/FLAG (Gloeckner and Boldt, 2009). These motifs are less frequent, but could induce a different behavior of the SNARE complex. As this risk is always present for fusion constructs, the functionality of any manipulated protein must be analyzed (Arnau et al., 2006).

6. Supplements

Table 12 Excerpt of mass spectrometry results of CaM beads for SV purifications

SNG-1	integral synaptic protein
SNB-1	synaptobrevin
SNT-1	synaptic vesicle recycling
UNC-17	synaptic vesicle acetylcholine transporter
WDFY-2	WD40- and FYVE-domain, uncharacterized
SYD-2	differentiation of presynaptic active zones
RAB-1	intracellular vesicle trafficking
RAB-18	vesicular trafficking
UNC-116	kinesin
UNC-32	vesicular proton pump or transporter
EGL-3	proprotein convertase (neuropeptide processing)
EGL-21	carboxypeptidase (neuropeptide processing !)
EGL-30	g protein
UNC-36	calcium channel
PAR-5	Putative 14-3-3 protein
DYN-1	dynamin
DRP-1	dynamin-like
DHC-1	dynein heavy chain
CHC-1	clathrin heavy chain
GLT-5	excitatory aminoacid transporter
VPS-4	vacular transport proteins
NSF-1	vesicular fusion complex unwinding
KIN-3	casein kinase
VHA	vacuolar H+ ATPase

Table 13 Mass spectrometric analysis of several SNARE complex purifications

Gene/ Sequence name	Protein group	Function	Peptide hits	Found in different purifications	In which data set
Chromosomal proteins					
HIS-57	Chromosomal proteins	Histone H2A	2; 4	2	Elu3; N2 (Plessmann)
HMG-12	Chromosomal proteins	High mobility group	1	1	Elu3 (Heide)
HMG-5	Chromosomal proteins	High mobility group	1	1	Elu3 (Heide)
RSA-2	Chromosomal proteins	Regulator of spindle assembly	1	1	Elu3 (Wittig)
Cellular integrity and transport					
ACT-4	Cytoskeleton and structure	Actin	6; 5; 3; 14	4	Wittig
ACT-5	Cytoskeleton and structure	Actin	1; 1; 6	6	Elu3, Elu5, N2 Wittig und Plessmann
ACT-3	Cytoskeleton and structure	Actin	2; 2; 6	6	Elu3, Elu5, N2 Wittig und Plessmann
COL-9	Cytoskeleton and structure	Collagen	1	1	Elu2 (Plessmann)
CUTL-3	Cytoskeleton and structure	Cuticulin-like	2;1	2	Elu2, Elu 3 (Plessmann)
F48E3.8	Cytoskeleton and structure	Polysaccharide deacetylase	1	1	Heide
GEI-12	Cytoskeleton and structure	GEX interacting protein	1	1	Heide
LEV-11	Cytoskeleton and structure	Tropomyosin	2, 2	2	N2 (Wittig), Elu (Heide)
MLC-3	Cytoskeleton and structure	Myosin light chain	4	1	Elu (Heide)
PERM-2	Cytoskeleton and structure	Permable eggshell, sugar modifying enzyme to create eggshell barrier	1	1	Heide
TBA-1	Cytoskeleton and structure	Tubulin	2	1	Heide
TNT-2	Cytoskeleton and structure	Troponin T	1;1	2	Elu (Heide), N2 (Wittig)
UNC-15	Cytoskeleton and structure	paramyosin orthologue	3; 2	2	Elu (Heide), N2 (Wittig)
UNC-87	Cytoskeleton and structure	myofilaments in body wall muscle cells	1;1	2	Elu (Heide), N2 (Wittig)
RET-1	Cytoskeleton and structure	Reticulon protein	1	1	Elu 2 (Plessmann)
KAP-1	Motor protein	Kinesin associated	1	1	Heide

Gene/ Sequence name	Protein group	Function	Peptide hits	Found in different purifications	In which data set
		protein			
KLP-8	Motor protein	Kinesin-like motor protein	1	1	Elu3 (Wittig)
EKL-6	Transport protein	Enhancer of KSR-1 lethality	1	1	Elu2 (Plessmann)
KSR-1	Transport protein	Kinase suppressor of activated Ras	1	1	Elu2 (Plessmann)
Ribosome related					
TAG-17	Ribosome related	Cytidine Deaminase, mRNA editing	2	1	Elu2 (Plessman)
CEY-2	Ribosome related	C. elegans Y-box, RNA-binding protein	1	1	Heide
CEY-3	Ribosome related	C. elegans Y-box, RNA-binding protein	1	1	Heide
EEF-1A.2	Ribosome related	Elongation factor 1 alpha	7;1;1;2	4	Elu (Heide); Elu 5 bomb (Wittig), Elu 5 Array (Wittig), N2 (Wittig)
RBM-28	Ribosome related	RNA binding motif protein homolog	2	1	Elu 2 (Plessmann)
RPL-11.2	Ribosome related	Large ribosomal subunit	1	1	Heide
RPL-12	Ribosome related	Large ribosomal subunit	1	1	Heide
RPL-14	Ribosome related	Large ribosomal subunit	1	1	Heide
RPL-18	Ribosome related	Large ribosomal subunit	1;1	2	Elu2, N2 (Plessmann)
RPL-28	Ribosome related	Large ribosomal subunit	1;1;1	3	Elu2, N2 (Plessmann), N2 (Wittig)
RPL-36	Ribosome related	Large ribosomal subunit	1;1;2	3	Elu5, Elu3, N2 (Wittig)
RPS-0 40 S	Ribosome related	Small ribosomal subunit	15	1	Elu2 (Plessman)
RPS-10	Ribosome related	Small ribosomal subunit	2;2;5; 5; 3; 3	6	Elu2, Elu 3, N2 (Plessmann); Elu 2, Elu 3, N2 (Wittig)
RPS-17	Ribosome related	Small ribosomal subunit	2;1; 1; 1; 2	2	Elu2, N2 (Plessmann), Elu 2, Elu3; N2 (Wittig)
RPS-18	Ribosome related	Small ribosomal subunit	3	1	Heide
RPS-19	Ribosome related	Small ribosomal subunit	3; 1; 1	3	Elu2 (Plessman), Elu5, N2 (Wittig)
RPS-20	Ribosome related	Small ribosomal subunit	1; 1; 3; 2, 8; 2	6	Elu a 5, Elu b 3; Elu b 5, N2 (Wittig), Elu2, N2

Gene/ Sequence name	Protein group	Function	Peptide hits	Found in different purifications	In which data set
					(Plessmann)
RPS-22	Ribosome related	Small ribosomal subunit	5	1	Heide
Signal transduction					
GCY-6	Signal transduction	Guanylate cyclase	2	1	Elu2 (Plessmann)
IRLD-6	Signal transduction	Insulin/EGF-Receptor L domain protein	2	1	Elu2 (Plessmann)
PAR-5	Signal transduction	Abnormal embryonic Partitioning of cytoplasm	1, 1	2	Elu Heide; N2 (Wittig)
PDE-1	Signal transduction	Ca cyclic nucleotide phosphodiesterase	1	1	Elu b 3(Wittig)
PIKI-1	Signal transduction	Phosphoinoside-3-kinase, apoptotic cell clearance	1	1	Elu a 5 (Wittig)
W01B6.5	Signal transduction	67 % homology to H.s. Tyrosine-protein kinase FRK - proliferation	1	1	Elu 2 (Plessmann)
Energy homeostasis					
ASB-2	ATP synthase	Mitochondrial ATP synthase	1	1	Heide
ATP-4	ATP synthase	ATP synthase subunit	1	1	Heide
R05D3.6	ATP synthase	ATP synthase subunit	1	1	Elu 2 (Plessmann)
ALDO-2	Metabolism	Aldolase	1	1	Heide
COX-15	Metabolism	Cytochrome oxidase assembly protein	1	1	Heide
CTL-3	Metabolism	Catalase	1	1	Heide
CYC-1	Metabolism	Component of Cytochrome c reductase complex	10	1	Heide
CYP-13A4	Metabolism	Cytochrome P450	1	1	Elu b 5 (Wittig)
FLAD-1	Metabolism	Flavin Adenine Dinucleotide synthetase	1	1	Elu2 (Plessmann)
GDH-1	Metabolism	Glutamate	1	1	Heide

Gene/ Sequence name	Protein group	Function	Peptide hits	Found in different purifications	In which data set
		dehydrogenase			
MDH-2	Metabolism	Malate dehydrogenase	2	1	Elu 2 (Plessmann)
PFK-2	Metabolism	Phosphofructukinase	1	1	Elu 2 (Plessmann)
PME-5	Metabolism	Poly(ADP-ribose) Metabolism Enzyme	1	1	Elu a 5(Wittig)
UGT-18	Metabolism	UDP glucuronosyltransferase	1	1	Elu2 (Plessmann)
VHA-10	Transporter	Vesicular H+ ATPase	1	1	Elu2 (Plessmann)
MCA-3	Transporter	Plasma membrane Ca2+ ATPase	4; 1	2	Elu (Heide); Elu2 (Plessmann)
SFXN-1.5	Transporter	SideroFleXiN (mitochondrial iron transporter	1	1	Heide
ANT-1.1	Transporter	Mitochondrial nucleotide transporter	1; 2; 14	3	Elu2, N2 (Plessmann), Elu (Heide)
EEL-1	Ubiquitination related	Hect E3 ubiquitin ligase	1	1	Elu2 (Plessmann)
FBXC-39	Ubiquitination related	F-box c protein	1	1	Heide
SNARE complex proteins					
RIC-4	SNARE complex subunit	SNAP-25 homolog	4	1	Heide
SNAP-29	SNARE complex subunit	SNAP homolog, oocyte related	2	1	Elu 2 (Plessmann)
SNB-1	SNARE complex subunit	synaptobrevin	2; 1	2	Elu 2 (Plessmann); Elu a 5 (Wittig)
UNC-64	SNARE complex subunit	syntaxin	2	1	Elu 2 (Plessmann)
VTI-1	SNARE interaction	VTI (Vesicle Transport through t-SNARE Interaction) homolog	1	1	Heide
Diverse functions					
UNC-25	Neurotransmitter synthesis	Glutamic acid decarboxylase	1	1	Elu 2 (Plessmann)
VIT-2	Oocyte generation	VITellogenin structural genes (yolk protein	1	1	Heide

Gene/ Sequence name	Protein group	Function	Peptide hits	Found in different purifications	In which data set
		genes)			
F41C3.5	Peptidase	Serine Carboxypeptidase related to cathepsin A	2; 1	2	Elu 2; N2 (Plessmann)
PPW-1	RNAi related	PAZ/PIWI domain-containing	1	1	Elu b 3 (Wittig)
BRP-1	Signal protein	Bypass of Response to Pheromone in yeast	1	1	Heide
YAP-1	Transcription factor interaction	Yes-Associated Protein homolog	1	1	Elu 2(Plessmann)
CMD-1	Calcium binding	Calmodulin	2; 1; 1; 5; 4; 2; 3	7	Plessmann + Wittig
TAX-6	Calcium binding	Calcineurin homolog, protein phosphatase	2; 1; 1	2	Elu2, Elu3 (Plessmann), Elu (Heide)
Unknown function					
ARRD-15	Unknown function	Arrestin Domain Protein	1	1	Elu b 3 (Wittig)
B0464.2	Unknown function	Unknown function	1	1	Elua5 (Wittig)
B0563.6	Unknown function	Unknown function	1	1	Elu b 3 (Wittig)
C05C10.2	Unknown function	Unknown function	1	1	Heide
C06A8.3	Unknown function	Similarity to hypodermal antigen	1	1	Heide
C33D9.3A	Unknown function	Unknown function	1	1	Elu2 (Plessmann)
C33H5.8	Unknown function	Unknown function	1; 1	2	Elua5 (Wittig), Elu2 (Plessmann)
F01G4.6	Unknown function	Unknown function	6	1	Heide
F07F6.7	Unknown function	Unknown function	1	1	Elu2 (Plessmann)
F29G9.2	Unknown function	Unknown function	1	1	Heide
F36A2.7	Unknown function	Unknown function	1	1	Heide
F44E5.1	Unknown function	Unknown function	4;1	2	Heide, N2 (Wittig)
F55B12.10	Unknown function	Unknown function	1	1	Elu2 (Plessmann)
F57B10.4	Unknown function	Unknown function	1	1	Elu2 (Plessmann)

Gene/ Sequence name	Protein group	Function	Peptide hits	Found in different purifications	In which data set
FRM-2	Unknown function	FERM domain (protein4.1-ezrin-radixin-moesin) family, possible cytoskeletal re-arrangement, intracellular transport or signal transduction	1	1	Elu2 (Plessmann)
HPO-18	Unknown function	Hypersensitive to Pore forming toxin, possible GPCR, Signal transduction, Transcription factor or metabolism	1; 1; 1	2	Elu2, N2 (Plessmann), Elu (Heide)
K09H9.2	Unknown function	Unknown function	1	1	Heide
M05D6.6	Unknown function	Unknown function	2; 1	2	Elu (Heide); N2 (Wittig)
R04F11.2	Unknown function	Unknown function	2	1	Heide
RIL-1	Unknown function	RNAi induced longevity	2	1	Heide
T26E3.7	Unknown function	Unknown function	1	1	Heide
TAG-174	Unknown function	Temporarily Assigned Gene name	2	1	Elu2 (Plessmann)
TAG-241	Unknown function	Homology to eea-1 (encodes a coiled-coil protein that in yeast related to vesicle docking)	1	1	Elu2 (Plessmann)
TAG-278	Unknown function	Temporarily Assigned Gene name	1	1	Elu2 (Plessmann)
TAG-340	Unknown function	Temporarily Assigned Gene name	1	1	Elu b 3 (Wittig)
VAMP-8	Unknown function	VAMP (Vesicle Associated Membrane Protein) homolog	1	1	Heide
W04C9.2	Unknown function	unknown function	3	1	Heide
W05H9.1	Unknown	unknown	1;1	2	Elu2 (Plessmann); Elu

Gene/ Sequence name	Protein group	Function	Peptide hits	Found in different purifications	In which data set
	function	function			(Heide)
W09C3.1	Unknown function	unknown function	1	1	Elu b 3 (Wittig)
Y37E11B.1	Unknown function	unknown function	1	1	Elu2 (Plessmann)
Y69A2AR.18	Unknown function	unknown function	5; 2; 2; 7	4	Elu2; N2 (Plessmann), N2 (Wittig); Elu (Heide)
Y73B3A.18	Unknown function	unknown function	2; 2	2	Elu2 (Plessmann), Elu (Heide)
Y95B8A.6	Unknown function	unknown function	1	1	Heide
Y116F11B.11	Unknown function	human Golgin subfamily A member 4 isoform 1; May play a role in delivery of transport vesicles containing GPI-linked proteins	1	1	Elu2 (Plessmann)

7. References

Abbott, L.F., and Regehr, W.G. (2004). Synaptic computation. Nature *431*, 796-803.

Abraham, C., Bai, L., and Leube, R. (2011). Synaptogyrin-dependent modulation of synaptic neurotransmission in Caenorhabditis elegans. Neuroscience *190*, 75-88.

Abraham, C., Hutter, H., Palfreyman, M.T., Spatkowski, G., Weimer, R.M., Windoffer, R., Jorgensen, E.M., and Leube, R.E. (2006). Synaptic tetraspan vesicle membrane proteins are conserved but not needed for synaptogenesis and neuronal function in Caenorhabditis elegans. Proc Natl Acad Sci U S A 103, 8227-8232.

Akabas, M.H. (2004). GABAA receptor structure-function studies: a reexamination in light of new acetylcholine receptor structures. Int Rev Neurobiol 62, 1-43.

Alabi, A.A., and Tsien, R.W. (2013). Perspectives on Kiss-and-Run: Role in Exocytosis, Endocytosis, and Neurotransmission. Annu. Rev. Physiol. 75, 393-422.

Almedom, R.B., Liewald, J.F., Hernando, G., Schultheis, C., Rayes, D., Pan, J., Schedletzky, T., Hutter, H., Bouzat, C., and Gottschalk, A. (2009). An ER-resident membrane protein complex regulates nicotinic acetylcholine receptor subunit composition at the synapse. EMBO J 28, 2636-2649.

Altun, Z. and Hall D.H (2011). Nervous system. General description. http://www.wormatlas.org/hermaphrodite/nervous/Neuroframeset.html.

Antonin, W., Fasshauer, D., Becker, S., Jahn, R., and Schneider, T.R. (2002). Crystal structure of the endosomal SNARE complex reveals common structural principles of all SNAREs. Nat Struct Biol 9, 107-111.

Aravamudan, B., Fergestad, T., Davis, W.S., Rodesch, C.K., and Broadie, K. (1999). Drosophila UNC-13 is essential for synaptic transmission. Nat. Neurosci. 2, 965-971.

Archer, D.A. (2002). Complexin Regulates the Closure of the Fusion Pore during Regulated Vesicle Exocytosis. Journal of Biological Chemistry 277, 18249-18252.

Arnau, J., Lauritzen, C., Petersen, G.E., and Pedersen, J. (2006). Current strategies for the use of affinity tags and tag removal for the purification of recombinant proteins. Protein Expression and Purification 48, 1-13.

Barclay, J.W., Morgan, A., and Burgoyne, R.D. (2012). Neurotransmitter release mechanisms studied in Caenorhabditis elegans. Cell Calcium 52, 289-295.

Bargmann, C.I. (1998). Neurobiology of the Caenorhabditis elegans genome. Science 282, 2028-2033.

Bargmann, C.I., and Kaplan, J.M. (1998). Signal transduction in the Caenorhabditis elegans nervous system. Annu. Rev. Neurosci. 21, 279-308.

Barnard, R.J., Morgan, A., and Burgoyne, R.D. (1996). Domains of alpha-SNAP required for the stimulation of exocytosis and for N-ethylmalemide-sensitive fusion protein (NSF) binding and activation. Mol. Biol. Cell 7, 693-701.

Baumert, M., Maycox, P.R., Navone, F., Camilli, P. de, and Jahn, R. (1989). Synaptobrevin: an integral membrane protein of 18,000 daltons present in small synaptic vesicles of rat brain. EMBO J. 8, 379-384.

Bayer, M.J., Reese, C., Buhler, S., Peters, C., and Mayer, A. (2003). Vacuole membrane fusion: V0 functions after trans-SNARE pairing and is coupled to the Ca2+-releasing channel. J. Cell Biol. 162, 211-222.

Beesley, P., Kraus, M., and Parolaro, N. (2014a). The neuroplastins: multifunctional neuronal adhesion molecules--involvement in behaviour and disease. Adv Neurobiol 8, 61-89.

Beesley, P.W., Herrera-Molina, R., Smalla, K.-H., and Seidenbecher, C. (2014b). The Neuroplastin adhesion molecules: key regulators of neuronal plasticity and synaptic function. J Neurochem 131, 268-283.

Bednarek, E.M., Schaheen, L., Gaubatz, J., Jorgensen, E.M., and Fares, H. (2007). The plasma membrane calcium ATPase MCA-3 is required for clathrin-mediated endocytosis in scavenger cells of Caenorhabditis elegans. Traffic 8, 543-553.

Bennett, M.K., Calakos, N., Kreiner, T., and Scheller, R.H. (1992). Synaptic vesicle membrane proteins interact to form a multimeric complex. J. Cell Biol. 116, 761-775.

Benson, D.L., Colman, D.R., and Huntley, G.W. (2001). Molecules, maps and synapse specificity. Nat. Rev. Neurosci. 2, 899-909.

Beqollari, D., and Kammermeier, P.J. (2013). The interaction between mGluR1 and the calcium channel Cav(2).(1) preserves coupling in the presence of long Homer proteins. Neuropharmacology 66, 302-310.

Berezikov, E., Bargmann, C.I., Plasterk, R.H.A., and Berezikov, E. (2004). Homologous gene targeting in Caenorhabditis elegans by biolistic transformation. Nucleic Acids Res. 32, e40 // 40e–40.

Betke, K.M., Wells, C.A., and Hamm, H.E. (2012). GPCR mediated regulation of synaptic transmission. Progress in Neurobiology 96, 304-321.

Biederer, T., Sara, Y., Mozhayeva, M., Atasoy, D., Liu, X., Kavalali, E.T., and Südhof, T.C. (2002). SynCAM, a Synaptic Adhesion Molecule That Drives Synapse Assembly. Science 297, 1525-1531.

Blondeau, F., Ritter, B., Allaire, P.D., Wasiak, S., Girard, M., Hussain, N.K., Angers, A., Legendre-Guillemin, V., Roy, L., and Boismenu, D., et al. (2004). Tandem MS analysis of brain clathrin-coated vesicles reveals their critical involvement in synaptic vesicle recycling. Proc. Natl. Acad. Sci. U.S.A. 101, 3833-3838.

Bock, J.B., Matern, H.T., Peden, A.A., and Scheller, R.H. (2001). A genomic perspective on membrane compartment organization. Nature 409, 839-841.

Bono, M.d. (2003). Molecular approaches to aggregation behavior and social attachment. J. Neurobiol. 54, 78-92.

Bono, M.d., and Villu Maricq, A. (2005). Neuronal substrates of complex behavior in C. elegans. Annu. Rev. Neurosci. 28, 451-501.

Bowen, M., and Brunger, A.T. (2006). Conformation of the synaptobrevin transmembrane domain. Proc. Natl. Acad. Sci. U.S.A. 103, 8378-8383.

Boyken, J., Gronborg, M., Riedel, D., Urlaub, H., Jahn, R., and Chua, J.J.E. (2013). Molecular profiling of synaptic vesicle docking sites reveals novel proteins but few differences between glutamatergic and GABAergic synapses. Neuron 78, 285-297.

Brandt, P., Neve, R.L., Kammesheidt, A., Rhoads, R.E., and Vanaman, T.C. (1992). Analysis of the tissue-specific distribution of mRNAs encoding the plasma membrane calcium-pumping ATPases

and characterization of an alternately spliced form of PMCA4 at the cDNA and genomic levels. J Biol Chem 267, 4376-4385.

Brenner, S. (1974). The genetics of Caenorhabditis elegans. Genetics 77, 71-94.

Bretou, M., Jouannot, O., Fanget, I., Pierobon, P., Larochette, N., Gestraud, P., Guillon, M., Emiliani, V., Gasman, S., and Desnos, C., et al. (2014). Cdc42 controls the dilation of the exocytotic fusion pore by regulating membrane tension. Mol Biol Cell 25, 3195-3209.

Brose, N., Petrenko, A., Sudhof, T., and Jahn, R. (1992). Synaptotagmin: a calcium sensor on the synaptic vesicle surface. Science 256, 1021-1025.

Brose, N., Rosenmund, C., and Rettig, J. (2000). Regulation of transmitter release by Unc-13 and its homologues. Curr. Opin. Neurobiol. 10, 303-311.

Brownlee, D.J., and Fairweather, I. (1999). Exploring the neurotransmitter labyrinth in nematodes. Trends Neurosci. 22, 16-24.

Bruns, D., and Jahn, R. (1995). Real-time measurement of transmitter release from single synaptic vesicles. Nature 377, 62-65.

Bryant, N.J., and James, D.E. (2001). Vps45p stabilizes the syntaxin homologue Tlg2p and positively regulates SNARE complex formation. The EMBO Journal 20, 3380-3388.

Buckingham, S.D., and Sattelle, D.B. (2009). Fast, automated measurement of nematode swimming (thrashing) without morphometry. BMC Neurosci 10, 84.

Burdina, A.O., Klosterman, S.M., Shtessel, L., Ahmed, S., Richmond, J.E., and McCabe, B.D. (2011). In Vivo Analysis of Conserved C. elegans Tomosyn Domains. PLoS ONE 6, e26185.

Burré, J., Beckhaus, T., Schägger, H., Corvey, C., Hofmann, S., Karas, M., Zimmermann, H., and Volknandt, W. (2006). Analysis of the synaptic vesicle proteome using three gel-based protein separation techniques. Proteomics 6, 6250-6262.

Burré, J., and Volknandt, W. (2007). The synaptic vesicle proteome. J Neurochem 101, 1448-1462.

Burré, J., Zimmermann, H., and Volknandt, W. (2007). Immunoisolation and subfractionation of synaptic vesicle proteins. Analytical Biochemistry 362, 172-181.

Cesca, F., Baldelli, P., Valtorta, F., and Benfenati, F. (2010). The synapsins: Key actors of synapse function and plasticity. Progress in Neurobiology 91, 313-348.

Chen, Y.A., Scales, S.J., and Scheller, R.H. (2001). Sequential SNARE Assembly Underlies Priming and Triggering of Exocytosis. Neuron 30, 161-170.

Christian Frøkjær-Jensen. www.wormbuilder.org/.

Cohen, F.S., and Melikyan, G.B. (2004). The energetics of membrane fusion from binding, through hemifusion, pore formation, and pore enlargement. J. Membr. Biol. 199, 1-14.

Curtis, D.R., and Ryall, R.W. (1964). Nicotinic and muscarinic receptors of Renshaw cells. Nature 203, 652-653.

Denker, A., Bethani, I., Kröhnert, K., Körber, C., Horstmann, H., Wilhelm, B.G., Barysch, S.V., Kuner, T., Neher, E., and Rizzoli, S.O. (2011). A small pool of vesicles maintains synaptic activity in vivo. Proceedings of the National Academy of Sciences of the United States of America 108, 17177-17182.

Denker, A., and Rizzoli, S.O. (2010). Synaptic vesicle pools: an update. Frontiers in Synaptic Neuroscience 2.

Diamond, J., and Huxley, A.F. (1968). The activation and distribution of GABA and L-glutamate receptors on goldfish Mauthner neurones: an analysis of dendritic remote inhibition. J Physiol 194, 669-723.

Dittman, J.S., and Kaplan, J.M. (2006). Factors regulating the abundance and localization of synaptobrevin in the plasma membrane. Proc. Natl. Acad. Sci. U.S.A. 2006, 11399-1104.

Duerr, J.S., Han, H.-P., Fields, S.D., and Rand, J.B. (2008). Identification of major classes of cholinergic neurons in the nematodeCaenorhabditis elegans. J. Comp. Neurol. 506, 398-408.

Dulubova, I., Khvotchev, M., Liu, S., Huryeva, I., Südhof, T.C., and Rizo, J. (2007). Munc18-1 binds directly to the neuronal SNARE complex. Proc. Natl. Acad. Sci. U.S.A. 104, 2697-2702.

Dulubova, I., Sugita, S., Hill, S., Hosaka, M., Fernandez, I., Südhof, T.C., and Rizo, J. (1999). A conformational switch in syntaxin during exocytosis: role of munc18. EMBO J. 18, 4372-4382.

Dulubova, I., Yamaguchi, T., Arac, D., Li, H., Huryeva, I., Min, S.-W., Rizo, J., and Sudhof, T.C. (2003). Convergence and divergence in the mechanism of SNARE binding by Sec1/Munc18-like proteins. Proc. Natl. Acad. Sci. U.S.A. 100, 32-37.

Dun, A.R.C., and Duncan, R.R. (2010). The t-SNARE Complex: A Close Up. Cell Mol Neurobiol 30, 1293-1294.

Edelmann, L., Hanson, P.I., Chapman, E.R., and Jahn, R. (1995). Synaptobrevin binding to synaptophysin: a potential mechanism for controlling the exocytotic fusion machine. EMBO J. 14, 224-231.

Edgley, M.L., Baillie, D.L., Riddle, D.L., and Rose, A.M. (2006). Genetic balancers. WormBook, 1-32.

Eisenstein, M. (2006). A look back: adventures in the matrix. Nat Meth 3, 410.

Eshkind, L.G., and Leube, R.E. (1995). Mice lacking synaptophysin reproduce and form typical synaptic vesicles. Cell Tissue Res. 282, 423-433.

Evans, T. (2006). Transformation and microinjection. WormBook.

Fares, H., and Greenwald, I. (2001). Genetic analysis of endocytosis in Caenorhabditis elegans: coelomocyte uptake defective mutants. Genetics 159, 133-145.

Fasshauer, D., Antonin, W., Subramaniam, V., and Jahn, R. (2002). SNARE assembly and disassembly exhibit a pronounced hysteresis. Nat. Struct Biol. 9, 144-151.

Fasshauer, D., Bruns, D., Shen, B., Jahn, R., and Brünger, A.T. (1997). A structural change occurs upon binding of syntaxin to SNAP-25. J. Biol. Chem. 272, 4582-4590.

Fasshauer, D., Eliason, W.K., Brünger, A.T., and Jahn, R. (1998a). Identification of a minimal core of the synaptic SNARE complex sufficient for reversible assembly and disassembly. Biochemistry 37, 10354-10362.

Fasshauer, D., and Margittai, M. (2004). A Transient N-terminal Interaction of SNAP-25 and Syntaxin Nucleates SNARE Assembly. Journal of Biological Chemistry 279, 7613-7621.

Fasshauer, D., Sutton, R.B., Brunger, A.T., and Jahn, R. (1998b). Conserved structural features of the synaptic fusion complex: SNARE proteins reclassified as Q- and R-SNAREs. Proc. Natl. Acad. Sci. U.S.A. 95, 15781-15786.

Fatt, P., and Katz, B. (1952). Spontaneous subthreshold activity at motor nerve endings. J. Physiol. (Lond.) 117, 109-128.

Fernández-Busnadiego, R., Zuber, B., Maurer, U.E., Cyrklaff, M., Baumeister, W., and Lucic, V. (2010). Quantitative analysis of the native presynaptic cytomatrix by cryoelectron tomography. J. Cell Biol. 188, 145-156.

Fiebig, K.M., Rice, L.M., Pollock, E., and Brunger, A.T. (1999). Folding intermediates of SNARE complex assembly. Nat. Struct Biol. 6, 117-123.

Frei, J.A., Andermatt, I., Gesemann, M., and Stoeckli, E.T. (2014). The SynCAM synaptic cell adhesion molecules are involved in sensory axon pathfinding by regulating axon-axon contacts. J Cell Sci 127, 5288-5302.

Frøkjær-Jensen, C., Davis, M.W., Ailion, M., and Jorgensen, E.M. (2012). Improved Mos1-mediated transgenesis in C. elegans. Nat Meth 9, 117-118.

Frøkjær-Jensen, C., Wayne Davis, M., Hopkins, C.E., Newman, B.J., Thummel, J.M., Olesen, S.-P., Grunnet, M., and Jorgensen, E.M. (2008). Single-copy insertion of transgenes in Caenorhabditis elegans. Nat Genet 40, 1375-1383.

Giles, A.C., Rose, J.K., and Rankin, C.H. (2005). Investigations of Learning and Memory in Caenorhabditis elegans. In The Neurobiology of C. elegans (Elsevier), pp. 37–71.

Gingras, A.-C., Aebersold, R., and Raught, B. (2005). Advances in protein complex analysis using mass spectrometry. The Journal of Physiology 563, 11-21.

Gloeckner, C.J., and Boldt, K. (2009). Strep/FLAG Tandem Affinity Purification (SF-TAP) to Study Protein Interactions. Current Protocols in Protein Science 2009.

Goda, Y., and Südhof, T.C. (1997). Calcium regulation of neurotransmitter release: reliably unreliable? Curr. Opin. Cell Biol. 9, 513-518.

Grabner, C.P., Price, S.D., Lysakowski, A., Cahill, A.L., and Fox, A.P. (2006). Regulation of large dense-core vesicle volume and neurotransmitter content mediated by adaptor protein 3. Proc Natl Acad Sci U S A 103, 10035-10040.

Gracheva, E.O., Maryon, E.B., Berthelot-Grosjean, M., and Richmond, J.E. (2010). Differential Regulation of Synaptic Vesicle Tethering and Docking by UNC-18 and TOM-1. Front. Syn. Neurosci. 2.

Grey, E.G. (1963). Electron microscopy of presynaptic organelles of the spinal cord. J. Anat. 97, 101-106.

Guerini, D. (1998). The significance of the isoforms of plasma membrane calcium ATPase. Cell Tissue Res. 292, 191-197.

Hadwiger G, Dour S, Arur S, Fox P, and Nonet ML (2010). A Monoclonal Antibody Toolkit for C. elegans. PLoS ONE 2010, 1-6.

Hammarlund, M., Palfreyman, M.T., Watanabe, S., Olsen, S., and Jorgensen, E.M. (2007). Open Syntaxin Docks Synaptic Vesicles. Plos Biol 5, e198.

Harris, J.J., Jolivet, R., and Attwell, D. (2012). Synaptic Energy Use and Supply. Neuron 75, 762-777.

Hata, Y., Slaughter, C.A., and Südhof, T.C. (1993a). Synaptic vesicle fusion complex contains unc-18 homologue bound to syntaxin. Nature 366, 347-351.

Hatsuzawa, K., Lang, T., Fasshauer, D., Bruns, D., and Jahn, R. (2003). The R-SNARE motif of tomosyn forms SNARE core complexes with syntaxin 1 and SNAP-25 and down-regulates exocytosis. J. Biol. Chem. 278, 31159-31166.

Hess, D.T., Slater, T.M., Wilson, M.C., and Skene, J.H. (1992). The 25 kDa synaptosomal-associated protein SNAP-25 is the major methionine-rich polypeptide in rapid axonal transport and a major substrate for palmitoylation in adult CNS. J. Neurosci. 12, 4634-4641.

Hiesinger, P.R., Fayyazuddin, A., Mehta, S.Q., Rosenmund, T., Schulze, K.L., Zhai, R.G., Verstreken, P., Cao, Y., Zhou, Y., and Kunz, J., et al. (2005). The v-ATPase V0 subunit a1 is required for a late step in synaptic vesicle exocytosis in Drosophila. Cell 121, 607-620.

High, B., Cole, A.A., Chen, X., and Reese, T. (2015). Electron Microscopic Tomography Reveals Discrete Transcleft Elements at Excitatory and Inhibitory Synapses. Frontiers in Synaptic Neuroscience 7.

Hirano, S., and Takeichi, M. (2012). Cadherins in brain morphogenesis and wiring. Physiol Rev 92, 597-634.

Hobson, R.J., Liu, Q., Watanabe, S., and Jorgensen, E.M. (2011). Complexin Maintains Vesicles in the Primed State in C. elegans. Current Biology 21, 106-113.

Hochbaum, D., Ferguson, A.A., and Fisher, A.L. (2010). Generation of Transgenic C. elegans by Biolistic Transformation. JoVE.

Hollmann, M., and Heinemann, S. (1994). Cloned glutamate receptors. Annu Rev Neurosci 17, 31-108.

Hoover, C.M., Edwards, S.L., Yu, S.-C., Kittelmann, M., Richmond, J.E., Eimer, S., Yorks, R.M., and Miller, K.G. (2014). A novel CaM kinase II pathway controls the location of neuropeptide release from Caenorhabditis elegans motor neurons. Genetics 196, 745-765.

Huang, P., Pleasance, E.D., Maydan, J.S., Hunt-Newbury, R., O'Neil, N.J., Mah, A., Baillie, D.L., Marra, M.A., Moerman, D.G., and Jones, S.J.M. (2007). Identification and analysis of internal promoters in Caenorhabditis elegans operons. Genome Res. 17, 1478-1485.

Hua, Y., and Scheller, R.H. (2001). Three SNARE complexes cooperate to mediate membrane fusion. Proc Natl Acad Sci U S A 98, 8065-8070.

Hu, Y., Qu, L., and Schikorski, T. (2008). Mean synaptic vesicle size varies among individual excitatory hippocampal synapses. Synapse 62, 953-957.

Hübner, K., Windoffer, R., Hutter, H., and Leube, R.E. (2002). Tetraspan vesicle membrane proteins: synthesis, subcellular localization, and functional properties. Int. Rev. Cytol. 214, 103-159.

Hui, E., Gaffaney, J.D., Wang, Z., Johnson, C.P., Evans, C.S., and Chapman, E.R. (2011). Mechanism and function of synaptotagmin-mediated membrane apposition. Nat Struct Mol Biol 18, 813-821.

Hunt-Newbury, R., Viveiros, R., Johnsen, R., Mah, A., Anastas, D., Fang, L., Halfnight, E., Lee, D., Lin, J., and Lorch, A., et al. (2007). High-Throughput In Vivo Analysis of Gene Expression in Caenorhabditis elegans. Plos Biol 5, e237.

Huttner, W.B., Schiebler, W., Greengard, P., and Camilli, P. de (1983). Synapsin I (protein I), a nerve terminal-specific phosphoprotein. III. Its association with synaptic vesicles studied in a highly purified synaptic vesicle preparation. J. Cell Biol. 96, 1374-1388.

IBA GmbH (2008). Purification of One-STrEP-tag fusion proteins. Protocol 6 Purification of One-STrEP-tag fusion proteins using gravity flow columns One-STrEP™ Kit, 22-25.

Imig, C., Min, S.-W., Krinner, S., Arancillo, M., Rosenmund, C., Südhof, T.C., Rhee, J., Brose, N., and Cooper, B.H. (2014). The Morphological and Molecular Nature of Synaptic Vesicle Priming at Presynaptic Active Zones. Neuron 84, 416-431.

Jahn, R., and Grubmüller, H. (2002). Membrane fusion. Curr. Opin. Cell Biol. 14, 488-495.

Jahn, R., and Scheller, R.H. (2006). SNAREs — engines for membrane fusion. Nat Rev Mol Cell Biol 7, 631-643.

Jahn, R., and Südhof, T.C. (1994). Synaptic vesicles and exocytosis. Annu. Rev. Neurosci. 17, 219-246.

Jang, S., Oh, D., Lee, Y., Hosy, E., Shin, H., van Riesen, C., Whitcomb, D., Warburton, J.M., Jo, J., and Kim, D., et al. (2015). Synaptic adhesion molecule IgSF11 regulates synaptic transmission and plasticity. Nat Neurosci.

Jewell, J.L., Oh, E., Ramalingam, L., Kalwat, M.A., Tagliabracci, V.S., Tackett, L., Elmendorf, J.S., and Thurmond, D.C. (2011). Munc18c phosphorylation by the insulin receptor links cell signaling directly to SNARE exocytosis. The Journal of Cell Biology 193, 185-199.

Jin, Y. (2005). Synaptogenesis. WormBook.

Kamath, R.S., and Ahringer, J. (2003). Genome-wide RNAi screening in Caenorhabditis elegans. Methods 30, 313-321.

Kang, J., Bai, Z., Zegarek, M.H., Grant, B.D., and Lee, J. (2011). Essential roles of snap-29 in C. elegans. Dev Biol 355, 77-88.

Kantamneni, S. (2015). Cross-talk and regulation between glutamate and GABAB receptors. Front Cell Neurosci 9, 135.

Keller, J.E., Cai, F., and Neale, E.A. (2004). Uptake of botulinum neurotoxin into cultured neurons. Biochemistry 43, 526-532.

Kenyon, C. (1988). The nematode Caenorhabditis elegans. Science 240, 1448-1453.

Kim, S., Atwood, H.L., and Cooper, R.L. (2000). Assessing Accurate Sizes of Synaptic Vesicles in Nerve Terminals. Brain Res. 877, 209-217.

Kittelmann, M., Liewald, J.F., Hegermann, J., Schultheis, C., Brauner, M., Steuer Costa, W., Wabnig, S., Eimer, S., and Gottschalk, A. (2013). In vivo synaptic recovery following optogenetic hyperstimulation. Proc Natl Acad Sci U S A 110, E3007-16.

Kozlovsky, Y., and Kozlov, M.M. (2002). Stalk Model of Membrane Fusion: Solution of Energy Crisis. Biophysical Journal 82, 882-895.

Kraemer, B.C., Zhang, B., Leverenz, J.B., Thomas, J.H., Trojanowski, J.Q., and Schellenberg, G.D. (2003). Neurodegeneration and defective neurotransmission in a Caenorhabditis elegans model of tauopathy. Proceedings of the National Academy of Sciences 100, 9980-9985.

Krishnakumar, S.S., Kümmel, D., Jones, S.J., Radoff, D.T., Reinisch, K.M., and Rothman, J.E. (2013). Conformational Dynamics of Calcium-Triggered Activation of Fusion by Synaptotagmin. Biophysical Journal 105, 2507-2516.

Lee, S.-K., Li, W., Ryu, S.-E., Rhim, T., and Ahnn, J. (2010). Vacuolar (H+)-ATPases in Caenorhabditis elegans: what can we learn about giant H+ pumps from tiny worms? Biochim. Biophys. Acta 1797, 1687-1695.

Li, F., Pincet, F., Perez, E., Giraudo, C.G., Tareste, D., and Rothman, J.E. (2011). Complexin activates and clamps SNAREpins by a common mechanism involving an intermediate energetic state. Nat Struct Mol Biol 18, 941-946.

Lin, R.C., and Scheller, R.H. (2000). Mechanisms of synaptic vesicle exocytosis. Annu. Rev. Cell Dev. Biol. 16, 19-49.

Li, Q. (2004). A Syntaxin 1, G o, and N-Type Calcium Channel Complex at a Presynaptic Nerve Terminal: Analysis by Quantitative Immunocolocalization. Journal of Neuroscience 24, 4070-4081.

Li, Q., Dai, X.-Q., Shen, P.Y., Cantiello, H.F., Karpinski, E., and Chen, X.-Z. (2004). A modified mammalian tandem affinity purification procedure to prepare functional polycystin-2 channel. FEBS Letters 576, 231-236.

Littleton, J.T., Barnard, R.J.O., Titus, S.A., Slind, J., Chapman, E.R., and Ganetzky, B. (2001). SNARE-complex disassembly by NSF follows synaptic-vesicle fusion. Proceedings of the National Academy of Sciences 98, 12233-12238.

Liu, H., Dean, C., Arthur, C.P., Dong, M., and Chapman, E.R. (2009). Autapses and networks of hippocampal neurons exhibit distinct synaptic transmission phenotypes in the absence of synaptotagmin I. J. Neurosci. 29, 7395-7403.

Li, Y. (2010). Commonly used tag combinations for tandem affinity purification. Biotechnol. Appl. Biochem. 55, 73-83.

Luo, L., Hannemann, M., Koenig, S., Hegermann, J., Ailion, M., Cho, M.-K., Sasidharan, N., Zweckstetter, M., Rensing, S.A., and Eimer, S. (2011). The Caenorhabditis elegans GARP complex contains the conserved Vps51 subunit and is required to maintain lysosomal morphology. Mol. Biol. Cell 22, 2564-2578.

Ma, C., Su, L., Seven, A.B., Xu, Y., and Rizo, J. (2013). Reconstitution of the Vital Functions of Munc18 and Munc13 in Neurotransmitter Release. Science 339, 421-425.

Madison, J.M., Nurrish, S., and Kaplan, J.M. (2005). UNC-13 interaction with syntaxin is required for synaptic transmission. Curr. Biol. 15, 2236-2242.

Mahoney, T.R., Luo, S., and Nonet, M.L. (2006). Analysis of synaptic transmission in Caenorhabditis elegans using an aldicarb-sensitivity assay. Nat Protoc 2006, 1772-1777.

Margeta, M.A., Shen, K., and Grill, B. (2008). Building a synapse: lessons on synaptic specificity and presynaptic assembly from the nematode C. elegans. Current Opinion in Neurobiology 18, 69-76.

Martens, S., Kozlov, M.M., and McMahon, H.T. (2007). How synaptotagmin promotes membrane fusion. Science 316, 1205-1208.

Martin, R., Vaida, B., Bleher, R., Crispino, M., and Giuditta, A. (1998). Protein synthesizing units in presynaptic and postsynaptic domains of squid neurons. J. Cell. Sci. 111 (Pt 21), 3157-3166.

McEwen, J.M., Madison, J.M., Dybbs, M., and Kaplan, J.M. (2006). Antagonistic Regulation of Synaptic Vesicle Priming by Tomosyn and UNC-13. Neuron 2006, 303-315.

McIntire, S.L., Reimer, R.J., Schuske, K., Edwards, R.H., and Jorgensen, E.M. (1997). Identification and characterization of the vesicular GABA transporter. Nature 389, 870-876.

McMahon, H.T., Bolshakov, V.Y., Janz, R., Hammer, R.E., Siegelbaum, S.A., and Südhof, T.C. (1996). Synaptophysin, a major synaptic vesicle protein, is not essential for neurotransmitter release. Proc. Natl. Acad. Sci. U.S.A. 93, 4760-4764.

Meriney, S.D., and Dittrich, M. (2013). Organization and function of transmitter release sites at the neuromuscular junction. J Physiol 591, 3159-3165.

Miledi, R. (1960). Junctional and extra-junctional acetylcholine receptors in skeletal muscle fibres. J Physiol 151, 24-30.

Miljanich, G.P., Brasier, A.R., and Kelly, R.B. (1982). Partial purification of presynaptic plasma membrane by immunoadsorption. The Journal of Cell Biology 94, 88-96.

Miller, K.G., Alfonso, A., Nguyen, M., Crowell, J.A., Johnson, C.D., and Rand, J.B. (1996). A genetic selection for Caenorhabditis elegans synaptic transmission mutants. Proc. Natl. Acad. Sci. U.S.A. 93, 12593-12598.

Mochida, S., Sheng, Z.H., Baker, C., Kobayashi, H., and Catterall, W.A. (1996). Inhibition of neurotransmission by peptides containing the synaptic protein interaction site of N-type Ca2+ channels. Neuron 17, 781-788.

Montecucco, C., Schiavo, G., and Pantano, S. (2005). SNARE complexes and neuroexocytosis: how many, how close? Trends Biochem Sci 30, 367-372.

Morciano, M., Beckhaus, T., Karas, M., Zimmermann, H., and Volknandt, W. (2009). The proteome of the presynaptic active zone: from docked synaptic vesicles to adhesion molecules and maxi-channels. Journal of Neurochemistry 108, 662-675.

Morciano, M., Burré, J., Corvey, C., Karas, M., Zimmermann, H., and Volknandt, W. (2005). Immunoisolation of two synaptic vesicle pools from synaptosomes: a proteomics analysis. J Neurochem 2005, 1732-1745.

Nagy, A., Baker, R.R., Morris, S.J., and Whittaker, V.P. (1976). The preparation and characterization of synaptic vesicles of high purity. Brain Res. 109, 285-309.

Nguyen, M., Alfonso, A., Johnson, C.D., and Rand, J.B. (1995). Caenorhabditis elegans mutants resistant to inhibitors of acetylcholinesterase. Genetics 140, 527-535.

Nichols, B.J., Ungermann, C., Pelham, H.R.B., Wickner, W.T., and Haas, A. (1997). Homotypic vacuolar fusion mediated by t- and v-SNAREs. Nature 387, 199-202.

Nix, P., Hammarlund, M., Hauth, L., Lachnit, M., Jorgensen, E.M., and Bastiani, M. (2014). Axon Regeneration Genes Identified by RNAi Screening in C. elegans. Journal of Neuroscience 34, 629-645.

Nobelprize.org (2013). The 2013 Nobel Prize in Physiology or Medicine - Press Release.

Nonet, M.L. (1999). Visualization of synaptic specializations in live C. elegans with synaptic vesicle protein-GFP fusions. J. Neurosci. Methods 89, 33-40.

Nonet, M.L., Saifee, O., Zhao, H., Rand, J.B., and Wei, L. (1998). Synaptic transmission deficits in Caenorhabditis elegans synaptobrevin mutants. J. Neurosci. 18, 70-80.

Pan, P.-Y., Cai, Q., Lin, L., Lu, P.-H., Duan, S., and Sheng, Z.-H. (2005). SNAP-29-mediated modulation of synaptic transmission in cultured hippocampal neurons. J. Biol. Chem. 280, 25769-25779.

Park, Y., and Kim, K.-T. (2009). Short-term plasticity of small synaptic vesicle (SSV) and large dense-core vesicle (LDCV) exocytosis. Cellular Signalling 21, 1465-1470.

Peng, R., and Gallwitz Dieter (2002). Sly1 protein bound to Golgi syntaxin Sed5p allows assembly and contributes to specificity of SNARE fusion complexes. The Journal of Cell Biology 157, 645-655.

Pettitt, J. (2005). The cadherin superfamily. WormBook, 1-9.

Phillips, G.R., Huang, J.K., Wang, Y., Tanaka, H., Shapiro, L., Zhang, W., Shan, W.-S., Arndt, K., Frank, M., and Gordon, R.E., et al. (2001). The Presynaptic Particle Web. Neuron 32, 63-77.

Polanowska, J., Martin, J.S., Fisher, R., Scopa, T., Rae, I., and Boulton, S.J. (2004). Tandem immunoaffinity purification of protein complexes from Caenorhabditis elegans. BioTechniques 36, 778-80, 782.

Praitis, V., Casey, E., Collar, D., and Austin, J. (2001). Creation of Low-Copy Integrated Transgenic Lines in Caenorhabditis elegans. Genetics 2001, 1217-1226.

Puig, O., Caspary, F., Rigaut, G., Rutz, B., Bouveret, E., Bragado-Nilsson, E., Wilm, M., and Séraphin, B. (2001). The Tandem Affinity Purification (TAP) Method: A General Procedure of Protein Complex Purification. Methods 24, 218-229.

Purcell, A.L., and Carew, T.J. (2003). Tyrosine kinases, synaptic plasticity and memory: insights from vertebrates and invertebrates. Trends Neurosci 26, 625-630.

Quetglas, S., Leveque, C., Miquelis, R., Sato, K., and Seagar, M. (2000). Ca2+-dependent regulation of synaptic SNARE complex assembly via a calmodulin- and phospholipid-binding domain of synaptobrevin. Proc. Natl. Acad. Sci. U.S.A. 97, 9695-9700.

Qu, L., Akbergenova, Y., Hu, Y., and Schikorski, T. (2009). Synapse-to-synapse variation in mean synaptic vesicle size and its relationship with synaptic morphology and function. J Comp Neurol 514, 343-352.

Rapaport, D., Lugassy, Y., Sprecher, E., Horowitz, M., and Hotchin, N.A. (2010). Loss of SNAP29 Impairs Endocytic Recycling and Cell Motility. PLoS ONE 5, e9759.

Rathore, S.S., Bend, E.G., Yu, H., Hammarlund, M., Jorgensen, E.M., and Shen, J. (2010). Syntaxin N-terminal peptide motif is an initiation factor for the assembly of the SNARE–Sec1/Munc18 membrane fusion complex. Proc. Natl. Acad. Sci. U.S.A. 2010, 22399-22406.

Reim, K., Mansour, M., Varoqueaux, F., McMahon, H.T., Südhof, T.C., Brose, N., and Rosenmund, C. (2001). Complexins regulate a late step in Ca2+-dependent neurotransmitter release. Cell 104, 71-81.

Rey, S.A., Smith, C.A., Fowler, M.W., Crawford, F., Burden, J.J., and Staras, K. (2015). Ultrastructural and functional fate of recycled vesicles in hippocampal synapses. Nature Communications 6, 8043.

Richard C. Lin, and Richard H. Scheller (2000). Mechanisms of synaptic vesicle exocytosis. Annu. Rev. Cell Dev. Biol. 2000, 19-49.

Richmond, J. (2006). Synaptic function. WormBook.

Richmond, J.E., and Broadie, K.S. (2002). The synaptic vesicle cycle: exocytosis and endocytosis in Drosophila and C. elegans. Current Opinion in Neurobiology 2002, 499-507.

Richmond, J.E., Weimer, R.M., and Jorgensen, E.M. (2001). An open form of syntaxin bypasses the requirement for UNC-13 in vesicle priming. Nature 412, 338-341.

Rickman, C., Medine, C.N., Dun, A.R., Moulton, D.J., Mandula, O., Halemani, N.D., Rizzoli, S.O., Chamberlain, L.H., and Duncan, R.R. (2010). t-SNARE protein conformations patterned by the lipid microenvironment. J. Biol. Chem. 285, 13535-13541.

Rigaut, G., Shevchenko, A., Rutz, B., Wilm, M., Mann, M., and Séraphin, B. (1999). A generic protein purification method for protein complex characterization and proteome exploration. Nature Biotechnology 1999, 1030-1032.

Rizo, J., Chen, X., and Araç, D. (2006). Unraveling the mechanisms of synaptotagmin and SNARE function in neurotransmitter release. Trends in Cell Biology 16, 339-350.

Rizzoli, S.O., and Betz, W.J. (2005). Synaptic vesicle pools. Nature Reviews 2005, 57-69.

Robertis, E.d., and Franchi, C.M. (1956). Electron microscope observations on synaptic vesicles in synapses of the retinal rods and cones. J Biophys Biochem Cytol 2, 307-318.

Rohila, J.S., Chen, M., Chen, S., Chen, J., Cerny, R.L., Dardick, C., Canlas, P., Fujii, H., Gribskov, M., and Kanrar, S., et al. (2009). Protein-Protein Interactions of Tandem Affinity Purified Protein Kinases from Rice. PLoS ONE 4, e6685.

Rohrbough, J., Rushton, E., Woodruff, E., Fergestad, T., Vigneswaran, K., and Broadie, K. (2007). Presynaptic establishment of the synaptic cleft extracellular matrix is required for post-synaptic differentiation. Genes Dev. 21, 2607-2628.

Rolls, M.M. (2002). Targeting of Rough Endoplasmic Reticulum Membrane Proteins and Ribosomes in Invertebrate Neurons. Molecular Biology of the Cell 13, 1778-1791.

Rual, J.-F., Ceron, J., and Koreth, J. (2004). Toward Improving Caenorhabditis elegans Phenome Mapping With an ORFeome-Based RNAi Library. Genome Research 14, 2162-2168.

Rubio, V., Shen, Y., Saijo, Y., Liu, Y., Gusmaroli, G., Dinesh-Kumar, S.P., and Deng, X.W. (2005). An alternative tandem affinity purification strategy applied to Arabidopsis protein complex isolation. The Plant Journal 41, 767-778.

Sabatini, B.L., and Regehr, W.G. (1996). Timing of neurotransmission at fast synapses in the mammalian brain. Nature 384, 170-172.

Sakmann, B., Bormann, J., and Hamill, O.P. (1983). Ion transport by single receptor channels. Cold Spring Harb Symp Quant Biol 48 Pt 1, 247-257.

Saifee, O., Wei, L., and Nonet, M.L. (1998). The Caenorhabditis elegans unc-64 locus encodes a syntaxin that interacts genetically with synaptobrevin. Mol. Biol. Cell 9, 1235-1252.

Sanes, J.R., and Lichtman, J.W. (2001). Induction, assembly, maturation and maintenance of a postsynaptic apparatus. Nat. Rev. Neurosci. 2, 791-805.

Sarov, M. (2014). FAQ - Manual. https://transgeneome.mpi-cbg.de/transgeneomics/manuals.html#.

Sarov, M., Murray, J.I., Schanze, K., Pozniakovski, A., Niu, W., Angermann, K., Hasse, S., Rupprecht, M., Vinis, E., and Tinney, M., et al. (2012). A Genome-Scale Resource for In Vivo Tag-Based Protein Function Exploration in C. elegans. Cell 150, 855-866.

Sato, M., Saegusa, K., Sato, K., Hara, T., Harada, A., and Sato, K. (2011). Caenorhabditis elegans SNAP-29 is required for organellar integrity of the endomembrane system and general exocytosis in intestinal epithelial cells. Mol. Biol. Cell 22, 2579-2587.

Schafer, W.R. (2006). Neurophysiological methods in C. elegans: an introduction. WormBook.

Schaffer, U., Schlosser, A., Muller, K.M., Schafer, A., Katava, N., Baumeister, R., and Schulze, E. (2010). SnAvi - a new tandem tag for high-affinity protein-complex purification. Nucleic Acids Research 38, e91.

Schaub, J.R., Lu, X., Doneske, B., Shin, Y.-K., and McNew, J.A. (2006). Hemifusion arrest by complexin is relieved by Ca2+-synaptotagmin I. Nat. Struct. Mol. Biol. 13, 748-750.

Schoch, S., Deák, F., Königstorfer, A., Mozhayeva, M., Sara, Y., Südhof, T.C., and Kavalali, E.T. (2001). SNARE function analyzed in synaptobrevin/VAMP knockout mice. Science 294, 1117-1122.

Schultheis, C., Liewald, J.F., Bamberg, E., Nagel, G., and Gottschalk, A. (2011). Optogenetic Long-Term Manipulation of Behavior and Animal Development. PLoS ONE 6, e18766.

Shen, C., Rathore, S.S., Yu, H., Gulbranson, D.R., Hua, R., Zhang, C., Schoppa, N.E., and Shen, J. (2015). The trans-SNARE-regulating function of Munc18-1 is essential to synaptic exocytosis. Nat Commun 6, 8852.

Shi, L., Shen, Q.-T., Kiel, A., Wang, J., Wang, H.-W., Melia, T.J., Rothman, J.E., and Pincet, F. (2012). SNARE Proteins: One to Fuse and Three to Keep the Nascent Fusion Pore Open. Science 335, 1355-1359.

Siebert, A., Lottspeich, F., Nelson, N., and Betz, H. (1994). Purification of the synaptic vesicle-binding protein physophilin. Identification as 39-kDa subunit of the vacuolar H(+)-ATPase. Journal of Biological Chemistry 269, 28329-28334.

Sieber, J.J., Willig, K.I., Kutzner, C., Gerding-Reimers, C., Harke, B., Donnert, G., Rammner, B., Eggeling, C., Hell, S.W., and Grubmüller, H., et al. (2007). Anatomy and Dynamics of a Supramolecular Membrane Protein Cluster. Science 317, 1072-1076.

Sieburth, D., Ch'ng, Q., Dybbs, M., Tavazoie, M., Kennedy, S., Wang, D., Dupuy, D., Rual, J.-F., Hill, D.E., and Vidal, M., et al. (2005). Systematic analysis of genes required for synapse structure and function. Nature 436, 510-517.

Sloniowski, S., and Ethell, I.M. (2012). Looking forward to EphB signaling in synapses. Semin Cell Dev Biol 23, 75-82.

Söllner, T., Bennett, M.K., Whiteheart, S.W., Scheller, R.H., and Rothman, J.E. (1993a). A protein assembly-disassembly pathway in vitro that may correspond to sequential steps of synaptic vesicle docking, activation, and fusion. Cell 75, 409-418.

Söllner, T., and Rothman, J.E. (1994). Neurotransmission: harnessing fusion machinery at the synapse. Trends Neurosci. 17, 344-348.

Söllner, T., Whiteheart, S.W., Brunner, M., Erdjument-Bromage, H., Geromanos, S., Tempst, P., and Rothman, J.E. (1993b). SNAP receptors implicated in vesicle targeting and fusion. Nature 362, 318-324.

Sprecher, E., Ishida-Yamamoto, A., Mizrahi-Koren, M., Rapaport, D., Goldsher, D., Indelman, M., Topaz, O., Chefetz, I., Keren, H., and O'Brien, T.J., et al. (2005). A Mutation in SNAP29, Coding for a SNARE Protein Involved in Intracellular Trafficking, Causes a Novel Neurocutaneous Syndrome Characterized by Cerebral Dysgenesis, Neuropathy, Ichthyosis, and Palmoplantar Keratoderma. The American Journal of Human Genetics 77, 242-251.

Stevens, R.J., Akbergenova, Y., Jorquera, R.A., and Littleton, J.T. (2012). Abnormal Synaptic Vesicle Biogenesis in Drosophila Synaptogyrin Mutants. The Journal of Neuroscience 32, 18054-18067.

Stevens, D.R., Wu, Z.-X., Matti, U., Junge, H.J., Schirra, C., Becherer, U., Wojcik, S.M., Brose, N., and Rettig, J. (2005). Identification of the Minimal Protein Domain Required for Priming Activity of Munc13-1. Current Biology 15, 2243-2248.

Stiernagle, T. (2006). Maintenance of C. elegans. WormBook.

Stigloher, C., Zhan, H., Zhen, M., Richmond, J., and Bessereau, J.-L. (2011). The presynaptic dense projection of the Caenorhabiditis elegans cholinergic neuromuscular junction localizes synaptic vesicles at the active zone through SYD-2/liprin and UNC-10/RIM-dependent interactions. The Journal of neuroscience : the official journal of the Society for Neuroscience 31, 4388-4396.

Stofko-Hahn, R.E., Carr, D.W., and Scott, J.D. (1992). A single step purification for recombinant proteins. Characterization of a microtubule associated protein (MAP 2) fragment which associates with the type II cAMP-dependent protein kinase. FEBS Lett. 302, 274-278.

Südhof, T.C. (1995). The synaptic vesicle cycle: a cascade of protein-protein interactions. Nature 375, 645-653.

Südhof, T.C. (2008). Neuroligins and neurexins link synaptic function to cognitive disease. Nature 455, 903-911.

Südhof, T.C. (2004). The Synaptic Vesicle Cycle. Annu. Rev. Neurosci. 27, 509-547.

Südhof, T.C. (2012). The Presynaptic Active Zone. Neuron 75, 11-25.

Südhof, T.C., and Rothman, J.E. (2009). Membrane Fusion: Grappling with SNARE and SM Proteins. Science 2009 // 323, 474-477.

Sulston, J.E., Schierenberg, E., White, J.G., and Thomson, J.N. (1983). The embryonic cell lineage of the nematode Caenorhabditis elegans. Dev. Biol. 100, 64-119.

Sutton, R.B., Fasshauer, D., Jahn, R., and Brunger, A.T. (1998). Crystal structure of a SNARE complex involved in synaptic exocytosis at 2.4 A resolution. Nature 395, 347-353.

Takamori, S., Holt, M., Stenius, K., Lemke, E.A., Grønborg, M., Riedel, D., Urlaub, H., Schenck, S., Brügger, B., and Ringler, P. (2006). Molecular Anatomy of a Trafficking Organelle. Cell 127, 831-846.

Tanaka, H., Miyazaki, N., Matoba, K., Nogi, T., Iwasaki, K., and Takagi, J. (2012). Higher-order architecture of cell adhesion mediated by polymorphic synaptic adhesion molecules neurexin and neuroligin. Cell Rep 2, 101-110.

Tarr, T.B., Dittrich, M., and Meriney, S.D. (2013). Are unreliable release mechanisms conserved from NMJ to CNS? Trends Neurosci 36, 14-22.

Toonen, R.F.G., and Verhage, M. (2003). Vesicle trafficking: pleasure and pain from SM genes. Trends Cell Biol. 13, 177-186.

Trimble, W.S., Cowan, D.M., and Scheller, R.H. (1988). VAMP-1: a synaptic vesicle-associated integral membrane protein. Proc. Natl. Acad. Sci. U.S.A. 85, 4538-4542.

van den Bogaart, G., Holt, M.G., Bunt, G., Riedel, D., Wouters, F.S., and Jahn, R. (2010). One SNARE complex is sufficient for membrane fusion. Nat. Struct. Mol. Biol. 17, 358-364.

van Fürden, D., Johnson, K., Segbert, C., and Bossinger, O. (2004). The C. elegans ezrin-radixin-moesin protein ERM-1 is necessary for apical junction remodelling and tubulogenesis in the intestine. Dev. Biol. 272, 262-276.

Varshney, L.R., Chen, B.L., Paniagua, E., Hall, D.H., Chklovskii, D.B., and Sporns, O. (2011). Structural Properties of the Caenorhabditis elegans Neuronal Network. PLoS Comput Biol 7, e1001066.

Vashlishan, A.B., Madison, J.M., Dybbs, M., Bai, J., Sieburth, D., Ch'ng, Q., Tavazoie, M., and Kaplan, J.M. (2008). An RNAi Screen Identifies Genes that Regulate GABA Synapses. Neuron 58, 346-361.

Verhage, M., Maia, A.S., Plomp, J.J., Brussaard, A.B., Heeroma, J.H., Vermeer, H., Toonen, R.F., Hammer, R.E., van den Berg, T.K., and Missler, M., et al. (2000). Synaptic assembly of the brain in the absence of neurotransmitter secretion. Science 287, 864-869.

Völkel, P., Le Faou, P., and Angrand, P.-O. (2010). Interaction proteomics: characterization of protein complexes using tandem affinity purification–mass spectrometry. Biochem. Soc. Trans 38, 883.

Wabnig, S., Liewald, J.F., Yu, S.-C., and Gottschalk, A. (2015). High-Throughput All-Optical Analysis of Synaptic Transmission and Synaptic Vesicle Recycling in Caenorhabditis elegans. PLoS ONE 10, e0135584.

Walch-Solimena, C., Blasi, J., Edelmann, L., Chapman, E.R., Mollard, G.F. von, and Jahn, R. (1995). The t-SNAREs syntaxin 1 and SNAP-25 are present on organelles that participate in synaptic vesicle recycling. J. Cell Biol. 128, 637-645.

Wang, C.-T., Lu, J.-C., Bai, J., Chang, P.Y., Martin, T.F.J., Chapman, E.R., and Jackson, M.B. (2003). Different domains of synaptotagmin control the choice between kiss-and-run and full fusion. Nature 424, 943-947.

Wang, J., Bello, O., Auclair, S.M., Coleman, J., Pincet, F., Krishnakumar, S.S., Sindelar, C.V., and Rothman, J.E. (2014). Calcium sensitive ring-like oligomers formed by synaptotagmin. Proc. Natl. Acad. Sci. U.S.A.

Watanabe, S. (2015). Slow or fast? A tale of synaptic vesicle recycling. Science 350, 46-47.

Watanabe, S., Rost, B.R., Camacho-Pérez, M., Davis, M.W., Söhl-Kielczynski, B., Rosenmund, C., and Jorgensen, E.M. (2013). Ultrafast endocytosis at mouse hippocampal synapses. Nature 504, 242-247.

Watanabe, S., Trimbuch, T., Camacho-Perez, M., Rost, B.R., Brokowski, B., Sohl-Kielczynski, B., Felies, A., Davis, M.W., Rosenmund, C., and Jorgensen, E.M. (2014). Clathrin regenerates synaptic vesicles from endosomes. Nature 515, 228-233.

Waugh, D.S. TEV FAQ. http://mcl1.ncifcrf.gov/waugh_tech/faq/tev.pdf.

Weimer, R.M. (2003). Controversies in synaptic vesicle exocytosis. Journal of Cell Science 116, 3661-3666.

Weimer, R.M., Gracheva, E.O., Meyrignac, O., Miller, K.G., Richmond, J.E., and Bessereau, J.-L. (2006). UNC-13 and UNC-10/rim localize synaptic vesicles to specific membrane domains. J. Neurosci. 26, 8040-8047.

Weimer, R.M., Richmond, J.E., Davis, W.S., Hadwiger, G., Nonet, M.L., and Jorgensen, E.M. (2003). Defects in synaptic vesicle docking in unc-18 mutants. Nat. Neurosci. 6, 1023-1030.

Weninger, K., Bowen, M.E., Choi, U.B., Chu, S., and Brunger, A.T. (2008). Accessory proteins stabilize the acceptor complex for synaptobrevin, the 1:1 syntaxin/SNAP-25 complex. Structure 16, 308-320.

Weninger, K.R. (2011). Complexin arrests a neighbor. Nat Struct Mol Biol 18, 861-863.

White, J.G., Southgate, E., Thomson, J.N., and Brenner, S. (1976). The structure of the ventral nerve cord of Caenorhabditis elegans. Philos. Trans. R. Soc. Lond., B, Biol. Sci. 275, 327-348.

White, J.G., Southgate, E., Thomson, J.N., and Brenner, S. (1986). The structure of the nervous system of the nematode Caenorhabditis elegans. Philos. Trans. R. Soc. Lond., B, Biol. Sci. 314, 1-340.

Wilm, T., Demel, P., Koop, H.U., Schnabel, H., and Schnabel, R. (1999). Ballistic transformation of Caenorhabditis elegans. Gene 229, 31-35.

Wisden, W., and Seeburg, P.H. (1993). Mammalian ionotropic glutamate receptors. Curr Opin Neurobiol 3, 291-298.

Xue, M., Craig, T.K., Xu, J., Chao, H.-T., Rizo, J., and Rosenmund, C. (2010). Binding of the complexin N terminus to the SNARE complex potentiates synaptic-vesicle fusogenicity. Nat Struct Mol Biol 17, 568-575.

Yang, L., Biswas, M., and Chen, P. (2003). Study of Binding between Protein A and Immunoglobulin G Using a Surface Tension Probe. Biophysical Journal 84, 509-522.

Yang, X., Hou, D., Jiang, W., and Zhang, C. (2014). Intercellular protein-protein interactions at synapses. Protein Cell 5, 420-444.

Yochem, J.H.R. (2003). Investigating C. elegans development through mosaic analysis. Development 130, 4761-4768.

Zhao, M., Wu, S., Zhou, Q., Vivona, S., Cipriano, D.J., Cheng, Y., and Brunger, A.T. (2015). Mechanistic insights into the recycling machine of the SNARE complex. Nature 518, 61-67.

8. List of Abbreviations

°C degree Celsius
A Ampère
ACh Acetylcholine
APS Ammonia persulphate
ATP Adenosine 5'-triphosphat
BSA Bovine Serum Albumin
CBP Calmodulin Binding Peptide
cDNA complementary DNA
C. elegans Caenorhabditis elegans
CGC Caenorhabditis Genetics Center
dATP Deoxyadenosine 5'-triphosphat
DC Dorsal nerve cord
dCTP Deoxycytidine 5'-triphosphat
ddNTP 2',3'-Didesoxyribonukleosidtriphosphat
dGTP Deoxyguanosine 5'-triphosphat
DMEM Dulbecco's Modified Eagle Medium
DMSO Dimethyl sulfoxide
DNA Deoxyribonucleic acid
dNTP Deoxyribonucleoside triphosphat
dsRNA double strand RNA
DTT 1,4-dithiothreitol
ECFP Enhanced cyan-fluorescent protein
EDTA Ethylendiamintetra acetic acid
ER Endoplasmatic Reticulum
EtOH Ethanol
GABA Gamma amino butyric acid
GFP Green fluorescent protein
h hours
HRP Horse radish peroxidase
Hz Hertz
IgG Immunoglobulin G
kb Kilobases

kD kilo Dalton
L Liter
LB Lysis Broth
M Molar
µ mikro
m Milli
MCS Multiple cloning site
min Minutes
µg microgram
µL microliter
mL milliliter
mM millimolar
MN Motorneuron
mRNA Messenger Ribonucleic acid
MosSCI Mos1 Single Copy Integration
MS Mass spetrometry
n.s. not significant
N2 Wild type C. elegans
nAChR nicotinic Acetylcholine receptor
NGM Nematode growth medium
NMJ Neuromuscular junction
nt Nukleotide
OD Optic Density
PAGE Polyacrylamide gel elektrophoresis
PBS Phosphate buffered saline
PFA Paraformaldehyd
pH Potentia hydrogenii
PCR polymerase chain reaction
PNK Polynucleotide kinase
RNA Ribonucleic acid
RNase Ribonuclease
RT Room temperature
s Seconds
SDS Sodium Dodecylsulphate
s.e.m. Standard error of the mean

SEWLB Single egg or worm lysis buffer
SNARE Soluble N-ethylmaleimide-sensitive-factor attachment receptor
SV Synaptic vesicle
TAE Tris-Acetate-EDTA solution
TAP Tandem affinity purification
Taq Thermophilus aquaticus (referring to the polymerase)
TBS Tris buffered saline
TBS-T Tris buffered saline - Triton X-100
TEMED N,N,N',N'-Tetramethyl-ethylendiamine
TEV Tobacco Etch Virus (referring to the Protease)
U Unit
UTR Untranslated region
V Volt
v/v volume per volume
W Watt
w/v weight per volume
wt Wild type
YFP yellow-fluorescent protein
zxEx systematic label of an extrachromosomal transgene
zxIs systematic label of a genomic integration of a transgene
ZX systematic label of a *C. elegans* strain (originating from the Gottschalk lab)